Dissertation

submitted to the

Combined Faculty of Natural Sciences and Mathematics

of the Ruperto Carola University Heidelberg, Germany

for the degree of

Doctor of Natural Sciences

presented by
M.Sc. Ali Seleit
born in: Giza, Egypt
Oral examination: 19.07.2019

On the Development and Evolution of the Lateral Line

Referees: Jun.-Prof. Dr. Lazaro Centanin
Prof. Dr. Joachim Wittbrodt

Table of Contents

Abstract

At its core, developmental biology can be reduced to the study of three overarching processes; axiation, pattern formation and induction. By exploiting the formation of the lateral line system during embryogenesis in Medaka fish, I was able to contribute novel insights to each of these fundamental processes. The lateral line system is a sensory module present in fish and amphibians and is composed of individual neuromast organs. Its main function is to sense the direction of water flow and relay the information back to the brain. A fantastic diversity of lateral line patterns exists in the wild, the basis of which remains largely unknown. By live-imaging the polarized migration (axiation) of tissue during development I was able to demonstrate how the formation of the posterior lateral line in Medaka fish occurs. This led to a reassessment of the prevailing view held in the field, as it for the first-time placed changes in pattern construction occurring during development as a major contributor to the diversity of lateral line patterns. It also led to the discovery that the same molecular players can result in the formation of different posterior lateral line patterns in different teleost species, simply by modulating their temporal and spatial expression profiles. This modulation has been repeatedly spotted by developmental biologists studying a variety of organisms, and thus can be regarded as a common principle driving evolutionary novelty.

Using a variety of available and newly generated mutants I delved deeper into the guiding logic/principles behind posterior lateral line pattern formation. A process revealed to harbour a high degree of plasticity and self-organization. Specifically, I was able to show that precursor clusters of the migrating primordium can act as autonomous units, demonstrating the plasticity of the developmental tissue of origin for neuromasts (the primordium). In fact, within the same animal the left and right posterior lateral lines have varying outputs, reinforcing the idea of an inherent plasticity of primordia and strongly suggesting the presence of a low-range Waddingtonian developmental buffering system. Along the same lines, I was

able to show that changes in the immediate environment surrounding the primordium (for e.g. epithelial morphology) can have a direct effect on the posterior lateral line pattern being formed. And postulate that these properties of the system might have constituted a fault-line that evolution could have exploited to generate the kaleidoscopic variety of lateral line patterns we observe in the wild. Going from tissue level dynamics to individual organs, I focus on the differentiation of neuromasts and provide strong evidence for the location and potency of the stem cells that maintain them. I also report that during development neural stem cell precursors induce the formation of their own niches, which in turn are used to maintain the stem cells life-long. A finding that could have important implications in fields like tissue engineering and stem cell biology. Lastly, I focused my efforts on the cellular level by studying the post-embryonic formation of neuromasts, a process that re-utilizes axiation, is highly stereotypical and driven by individual cell behaviour. I characterize in detail the cells participating in post-embryonic organogenesis and reveal early molecular heterogeneities within the stem cells that seem to contribute to the differential behaviour they undergo later on. All in all, traversing tissue to organ and finally cellular scales in the lateral line led to novel insights into how this system is built and maintained all whilst being constantly remodelled. Surprisingly this approach even led to initial insights on the evolution of lateral lines. As with the nature of all scientific progress no matter how miniscule, more questions have been conjured that need to be answered in due time.

Zusammenfassung

Im Wesentlichen kann die Lehre der Entwicklungsbiologie in drei übergreifende Prozesse aufgespalten werden: Achsenbildung, Entstehung von Strukturen, und Induktion. Durch das Studium der Entstehung des Seitenlinienorgans während der Embryogenese des Medakafisches konnte ich neue Erkenntnisse bezüglich dieser fundamentalen Prozesse gewinnen. Das Seitenlinienorgan ist ein sensorisches Modul, das in allen Fischen und aquatischen Amphibien vorhanden ist und von einzelnen Organen, genannt Neuromasten, gebildet wird. Die Hauptfunktion des Seitenlinienorgans ist es die Richtung der Wasserströmung zu detektieren und diese Information an das Gehirn zu vermitteln. In der freien Wildbahn existiert eine beträchtliche Vielfalt an unterschiedlichen Strukturen des Seitenlinienorgans, deren Ursprung größtenteils unbekannt ist. Mit Hilfe von Lebendmikroskopie konnte ich die Abläufe der gerichteten Gewebsmigration (Achsenbildung) und der damit verbundenen Entwicklung des posterioren Seitenlinienorgans im Medakafisch beschreiben. Die daraus gewonnen Erkenntnisse führten zu einem Überdenken der bisherigen Einschätzung: Zum ersten Mal werden Veränderungen in der Strukturbildung während der Embryonalentwicklung als Hauptverantwortlicher für die Strukturvielfalt von Seitenlinienorganen benannt. Die Ergebnisse führten außerdem zur Erkenntnis, dass die gleichen molekularen Akteure, die sich lediglich in ihrer zeitlichen und räumlichen Expression unterscheiden, an der Bildung des posterioren Seitenlinienorgans verschiedener Teleosten beteiligt sind. Die Modulation der Genexpression wurde wiederholt von Entwicklungsbiologen in einer Vielzahl an Organismen beobachtet und kann daher als ein übergreifendes Prinzip betrachtet werden, das evolutionäre Neuheit hervorbringt. Mit Hilfe bestehender und neu generierter Mutantenlinien vertiefte ich mich in die zugrundeliegenden Prinzipien der Strukturbildung der Neuromasten des posterioren Seitenlinienorgans, ein hochgradig plastischer und von Selbstorganisation getriebener Prozess. Speziell konnte ich zeigen, dass Vorläufercluster, hervorgegangen aus dem migrierenden Primordium, als autonome Einheiten agieren. Dies zeigt die Plastizität des Gewebes (Primordium) während der Entwicklung der Neuromasten. Die Idee einer dem Primordium eigenen Plastizität wird zusätzlich gestützt durch die Tatsache, dass die rechte und linke Seite des Seitenlinienorgans innerhalb eines Fisches unterschiedlich sind. Dies deutet auf die Existenz eines niederschwelligen waddingtonartigen Puffersystems während der Entwicklung des Seitenlinienorgans hin. Ebenso konnte ich zeigen, dass Veränderungen in der unmittelbaren, das Primordium umgebenden Umwelt (z.B. in der Epithelmorphologie) einen direkten Einfluss auf die Struktur des posterioren Seitenlinienorgans haben. Weiterhin ist anzunehmen, dass diese Eigenschaften des Systems ein Trittbrett darstellen, das die Evolution genutzt haben könnte, um die kaleidoskopische Strukturvielfalt an Seitenlinienorganen zu generieren, die in freier Wildbahn zu beobachten ist.

Von der Gewebsebene übergehend auf die Ebene der einzelnen Organe studierte ich die Differenzierung der Neuromasten und liefere starke Hinweise auf die Lokalisierung und auf die Potenz der Stammzellen, die die Neuromasten

aufrechterhalten. Weiterhin beschreibe ich, dass neurale Stammzellvorläufer während der Entwicklung die Bildung ihrer eigenen Nische induzieren, die im Gegenzug dazu benutzt wird, die Stammzellen lebenslang zu erhalten. Diese Erkenntnisse könnten wichtige Einflüsse auf die Bereiche des Tissue Engineering und der Stammzellbiologie haben.

Schließlich konzentrierte ich mich auf zellulärer Ebene auf das Studium der post-embryonalen Bildung von Neuromasten, ein Vorgang, der den Prozess der Achsenbildung beinhaltet. Post-embryonale Bildung von Neuromasten ist in hohem Maße stereotyp und angetrieben durch individuelles (und aller Wahrscheinlichkeit nach binärem) Zellverhalten. Im Detail charakterisierte ich die Zellen, die an der post-embryonalen Organogenese beteiligt sind und entdeckte eine frühe molekulare Heterogenität innerhalb der Stammzellen, die zu dem späteren unterschiedlichen Verhalten beizutragen scheint.

Das übergreifende Studium des Seitenlinienorgans auf Gewebs-, Organ- und zuletzt Zellebene führte zu neuen Erkenntnissen bezüglich der Frage wie das System aufgebaut und aufrechterhalten wird während es konstanter Veränderung ausgesetzt ist. Überraschenderweise führte dieser Ansatz sogar dazu, dass erste Einsichten in die Evolution des Seitenlinienorgans gewonnen werden konnten. Wie es in der Natur jedes wissenschaftlichen Fortschritts liegt, wenn er auch noch so klein ist, wurden neue Fragen aufgeworfen, die zur rechten Zeit beantwortet werden müssen.

Abbreviations

Abbreviation	Full name
%	Percent
C°	Degrees Celsius
3D	3-Dimensional
4D	4-Dimensional
Amp	Ampicillin
µ	Micro
AP	Alkaline phosphatase
ATP	Adenosine Triphosphate
arrdc3a	Arrestin-domain containing 3a
aLL	Anterior lateral line
BBW	Brainbow
Bp	Base pair
BrdU	Bromdesoxyuridin
BSA	Bovine serum albumin
CFP	Cyan Flourescent protein
cmlc2	cardiac myosin light chain
Cre	Cre recombinase
Cre^{ERT2}	Tamoxifen inducible Cre recombinase
Cas	CRISPR associated protein
CRISPR	Clustered Regularly Interspaced Short Palindromic repeats
cDNA	Complementary DNA
CDS	Coding sequence
Ccl25b	Chemokine ligand 25b
Ccr9a	Chemokine receptor 9a
Cxcr4b	Chemokine receptor 4b
Cxcr7	Chemokine receptor 7
CNC	Caudal neuromast cluster
DAPI	2-(4-amidinophenyl)-1H-indole-6-carboxamidine
DA	Double anal mutant
DiAsp	4-Di-2-ASP
DKK	Dickkopf
DNA	Deoxyribonucleic acid
dH_2O	Distilled water
Dpf	Days post fertilization
Dph	Days post hatch
dpi	Days post injury
DTT	Dithiotheritol
DMSO	Dimethyl sulfoxide
DNA	Deoxyribonucleic aic
dNTPs	Deoxynucleoside triphosphates
DSB	Double strand break
dox	Doxycycline
E. coli	Escherichia coli
EB	Elution Buffer
EDTA	ethylenediaminetetraacetic acid
eGFP	enhanced Green fluorescent protein
eCFP	enhanced cyan
ERM	embryo rearing medium
Eya1	eyes absent 1
EtBr	Ethidium Bromide
FCS	Fetal Calf Serum
Fat1a	Fat cadherin 1 a
FGF	Fibroblast growth factor
g	Grams
gRNA	Guide RNA
$Gaudi^{RSG}$	Gaudi Red Switch Green
Gaudi ^{NSG}	Null-switch-Green
GG	Golden Gate

h	hour
H2A	Histone H2A
H2B	Histone H2B
H_2O	water
H_2O_2	Hydrogen Peroxide
HCl	Hydrogen Chloride
HC	Hair cell
Hsp70	70 kilodalton heat shock protein
Hsp70::Cre	heat-shock inducible Cre recombinase
HDR	Homology Directed Repair
IPTG	Isopropyl β-D-1-thiogalactopyranoside
IHC	Immunohistochemistry
I-SceI	meganuclease I-SceI
INC	Inter neuromast cells
ICN	Intercalary neuromasts
Kb	kilobases
Kcnk6	potassium two-pore omain channel subfamily k6
KOH	Potassium Hydroxide
KO	Knock-out
K15	Keratin 15
LA-HF	Left Arm Homology Flank
l	Litre
LB	lysogeny broth
M	Molar
MC	Mantle cell
m	milli
mCherry	Monomeric cherry fluorescent protein
MeOH	Methanol
mYFP	Membrane yellow flourescent protein
$MgCl_2$	magnesium chloride
Min	Minute
mRNA	Messenger RNA
MuVi-SPIM	Multi-view single plane illumination microscope
n	nano
N	Number
nm	nanometers
nBCs	Neuromast border cells
NICD	Notch intracellular domain
NSCs	Neural stem cells
NaCl	Sodium Chloride
NEB	New England Biolabs
NBRP	National Bioresource Project Medaka
NGS	Natural Goat Serum
nls	Nuclear localization signal
NHEJ	Non-homologus end joining
Oca2	Oculocutaneous albinism II
ON	overnight
PAM	Protospacer adjacent motifs
PBS	phosphate buffered saline
PCR	Polymerase Chain Reaction
PGCs	Primordial germ cells
PFA	paraformaldehyde
pLL	Posterior lateral line
pmp22b	Peripheral myelin protein 22b
PolyA	polyadenylation signal
PTW	Phosphate buffered saline plus Tween 20
RNA	Ribonucleic acid
rNTPs	Ribonucleotide triphosphate
RPM	Rotations per minute
RT	Room temperature
S	Second
SC	Support cell

SDS	Sodium dodecyl sulphate
SSC	saline sodium citrate
SSCT	saline sodium citrate plus Tween 20
Sox10	sex determining region Y-Box 2
TAE	Tris-acetate-EDTA
TB	Terrific broth
TE	Tris-EDTA
Tet	Tetracycline
tRFP	Tag-RFP
TRIS	Tris hydroxymethyl aminomethane
U	Unit
UAS	Upstream Activating Sequence
Ubi	Ubiquitous
V	Volt
vgll2b	Vestigial like-family member 2b
wt	Wild type
x	Times
X-Gal	5-bromo-4-chloro-3-indolyl- beta-D-galactopyranoside

"the course of a developmental reaction is the resultant of a large number of mutually interacting influences. if one plots a developmental process against time one must regard the line as occupying a position of equilibrium, determined by a number of processes which tend to push it upwards and a number which tend to push it downwards. This notation might seem to be merely our old friend dialectical materialism rearing its head out of the shifting seas of metaphysical controversy. But it is more than that..."
(Waddington, 1941)

Prologue

I have struggled to place the major findings of this thesis under a unified theoretical framework. That is primarily due to two reasons, the first being the broad range of experiments performed that did not aim to answer one specific question but rather to understand how the system is behaving as a whole. And the second is the lack of any suitable theoretical model in the current literature on the topic that could account for the rather intriguing results obtained. Briefly the problem can be crystalized in the following way; in nature, we know there is a breath-taking diversity of lateral line patterns generated in teleost fish, we do not know how or why this is the case. What it does mean though is that the system must be highly evolvable, that is, it must be able to produce the variety of patterns we observe in the wild. One recognized way of doing so is to change the genetic code or the reading of the code, that is to change the temporal and spatial pattern of gene expression during development. To prove this could be happening necessitates the use of a comparative approach and indeed by following one I have found evidence of this modulation of gene expression influencing the lateral line patterns in different teleosts during embryogenesis. However, it is also clear that this alone could not account for the observed diversity. Specifically, I have found evidence that even with the same genotype (Isogenic inbred medaka Cab line) the output (phenotype) in terms of numbers of organs produced in the posterior lateral line of each fish is

different. Even more surprising is the fact that within one organism the output of the system does vary between left and right posterior lateral lines in the vast majority of cases. What this means is that the genotype does not necessarily equal the phenotype. In addition, changing the immediate environment surrounding the primordium does lead to a modulation in lateral line patterns. These findings strongly suggest a degree of plasticity and self-organization built into the system itself.

It is here that I found it of great use to resurrect some rather old theoretical ideas from Conrad Waddington. His epigenetic landscape metaphor is currently in vogue once more among biologists (and for good reason), however it is a lesser known idea that I am proposing to use as a theoretical framework for the results obtained studying the lateral line patterns in fish, namely that of developmental buffering systems (Waddington 1941, 1942, 1968). Put succinctly, Waddington believed in the existence and operation of developmental buffering systems whose chief function is to canalize developmental processes, that is, to ensure the arrival at the same output even though there might be slight genetic and non-genetic (environmental) differences present in the initial starting conditions. This 'robustness' would ensure in turn the reproducibility of and lessen the variability in the outcome of developmental processes. Waddington immediately realized that this meant two things a) these buffering systems must themselves have a genetic component and must be heritable if they are to be passed-on to the next generations and b) there should exist different buffering capacities in different developmental processes depending on the need. In Waddington's own words

"in general it seems likely that the optimum response to the environment will involve some degree of proportionality and some restriction of this canalization, the most favorable picture of the two tendencies will presumably differ for different characters" (Waddington, 1942).

Indeed, a system with a high buffering capacity will be able to internalize a bigger difference in initial conditions and still produce the same output, while that with a low buffering capacity will be highly susceptible to small changes in the initial conditions. The latter will by definition be more plastic and so could respond more malleably to external influences and 'evolve' more easily than the former. In other words; highly evolvable systems most probably have a low developmental buffering capacity. One other idea is important to mention here before getting into how this all fits within the frame-work of the lateral line, that being the fact that for Waddington the environment acts on the phenotype (defined as a process) and not the genotype (Waddington, 1968).

I am proposing to think of the posterior lateral line system as a developmental module operating with a low-range buffering capacity. Meaning that small changes (genetic or non-genetic) in initial conditions are not thoroughly buffered and can easily lead to differences in output. This not only can explain a wide range of puzzling experimental data, but also makes useful predictions on the fast evolvability of the posterior lateral line system in different teleost fish. Below I outline a number of points which highlight first the probable presence of this developmental buffering capacity and second, different ways of reaching the (rather low) limits of the posterior lateral line buffering capacity and what this can teach us about the system.

A) Compared to the anterior lateral line (neuromasts around the head region), the posterior lateral line (neuromasts in the trunk) exhibits a much larger variability in numbers between and within fish of the same genotype and between different species of fish. This argues for the presence of distinct developmental buffering capacities in the two systems even though they are essentially building the same organs.

B) Comparing the variability of organ numbers in the posterior lateral line between the *wild-type* condition and that of mutants reveals that the mutants consistently have a wider variability. As if the presence of the mutation unhinges the capacity of the system to buffer. This was predicted to happen by Waddington and is used as evidence for the existence of the developmental buffering system in this case on the genetic level. In the words of Waddington

> (The) "wild type of an organism, that is to say the form which occurs in nature under the influence of natural selection is much less variable in appearance than the majority of the mutant races....in drosophila the phenomenon is extremely obvious; there is scarcely a mutant which is comparable in constancy with the wild type...the constancy of the wild type must be taken as evidence of the buffering of the genotype against minor variations not only in the environment...the genotype can as it were absorb a certain amount of its own variation without exhibiting any alteration in development" (Waddington, 1942)

C) The outcome in terms of numbers of organs between the left and right posterior lateral lines of the same fish (identical genotype) is in the majority of cases different. This strongly argues that some non-genetic subtle external differences can lead to different outputs. This plasticity was further confirmed in the case of patterns formed in the *Da* mutants which strongly suggested that even within the same side (left or right) the precursors building the posterior lateral line pattern can act as autonomous units and

behave differently according to highly local changes in their immediate environment.

D) If the above is true, then one can design experiments with the explicit aim to test the limits of the developmental buffering capacity. One such experiment I proposed that was carried out by a master's student in the lab (Jana Roeder 2018 Master's thesis) is to test the effect of temperature modulation on lateral line patterns. The idea being one can amplify the small differences already observed at regular conditions by challenging the system to operate under harsher ones. So, while eye morphogenesis is able to buffer extreme temperature modulation to produce two essentially identical eyes, the variability of output between the left and right side of the posterior lateral line in the same fish is further amplified under high temperature conditions (Jana Roeder 2018 Master's thesis). This argues that we can reach the limits of the rather low developmental buffering system in the posterior lateral line simply by modulating the immediate (external in this case) environment.

E) Indeed, by modulating the immediate environment the primordium travels through (epithelial cell morphology) without (knowingly) changing any intrinsic properties of the primordium itself also led to significant changes in the patterns of lateral lines obtained and a wider variability in organ numbers as compared to *wild-types*. Both results again argue that changes in the immediate environment can have a direct and noticeable effect on the patterns being built by essentially the same primordium.

The picture that emerges from all this is that we now have a relatively simple process to dissect the effects of genetic and non-genetic changes on a system with a low-range developmental buffering capacity. This promises to further our understanding of the plasticity of development, the robustness of biological systems, the capacities of these developmental buffering systems, how they are built and what are their limits. It also introduces an important conceptual shift in our understanding of the relationship between genotype, phenotype and environment. What seems to be clear from these experiments is that as Waddington proposed a long time ago, the phenotype must be understood as the output of a developmental process and cannot (and should not) be simply reduced to a particular genotype, and that the environment can and does act directly on the phenotype to shape that process. This is where things do get murky and I want to purposefully avoid getting into any "Lamarckian" discussions about adaptive trait acquisition. But I do believe that the challenge now is to better understand how this environmental modulation can eventually feed-back to the genetic level under a strong selective pressure. That is, the mechanistic link from environment to phenotype modulation to genotype fixing is still not completely worked out. Neither is how one can change the developmental buffering capacity of a particular process. However, what is clear is that all the data seem to fit quite well the general picture we observe in nature; that is; the vast diversity of posterior lateral line patterns and organ numbers necessitates having a system that is highly evolvable and one way to achieve this is by having a low-range developmental buffering capacity.

Introduction

'A sense of touch at a distance' Dijkgraaf 1963

Historical currents shaping early lateral line studies

For over two centuries the lateral line system of fish and Amphibia has been an active area of research (Parker 1905; Dijkgraaf 1963). The early days were mostly concerned with morphological descriptions and a fascination with structure and patterns. This however quickly gave rise to more pertinent questions about function. It was recognized early on that this must be a sensory module, what it was sensing though was heavily debated in the scientific community (Dercum, 1880; Lee F S., 1893; Parker, 1905). The issue was more or less settled by Harvard researchers who were able to show that the lateral line responded to low-frequency water current changes (Parker 1905). The following decades witnessed a plethora of studies concerned with detailed neuromast organ descriptions and electro-physiological experiments to try and identify what kind of and how signals are perceived and propagated from the environment to the brain of teleosts (Dijkgraaf 1963). Concurrently, embryologists (the forefathers of modern developmental biologists) have been trying to understand how the system is set up during development (Stone 1933). They relied heavily on three experimental approaches that surprisingly have survived up to this day and are heavily utilized throughout this thesis. Those being: tissue labelling (in their case with vital dyes), live-imaging (in their case repeated direct observation) and transplantations (in their case tissue grafting) (Stone 1933). What emerged from these meticulous approaches is

a detailed description of the developmental origin of neuromast organs. A migrating primordium that delaminates from the head region deposits rosette clusters from its trailing end that in turn mature to become neuromast organs consisting of morphologically distinct cell types (Stone 1933). With the advent of the molecular era biologists of all flavours have reutilized the lateral line as the simplicity of the system and its superficial location (directly under the overlying skin epithelium) (Dijkgraaf 1963) made it an excellent model to answer fundamental biological questions.

"the molecular explanation must constitute the core of understanding biological systems" Sydney Brenner, 2010

The modern era: merging observation with genetics in the posterior lateral line

Pioneering work by George Streisinger established zebrafish as a model organism amenable to genetic manipulation (Streisinger et al., 1981; Meyers 2018), this endeavour was aided by huge advances in microscopy and tissue labelling. Since then, Zebrafish has been exploited heavily to study the origin and genetic underpinnings of a variety of developmental processes, including lateral line development. In many cases with the explicit aim of arriving at general principles driving and controlling highly conserved morphogenetic processes (for e.g. collective cell migration) (Friedl & Gilmour, 2009). We now know in great detail the genetic and morphological underpinnings driving the development of the posterior lateral line in Zebrafish. It initially begins by a delamination event near the otic vesicle of a lateral line placode consisting of around 120-140 cells (known as a primordium) that start a process of collective cell migration (Ghysen and Dambly-Chaudieŕe, 2007; Kimmel et al., 1995 Piotrowski & Baker, 2014). This

migration occurs along the horizontal myoseptum of the embryo, where the primordium will deposit from its trailing edge clusters of cells that will differentiate into mature neuromast organs (Ghysen and Dambly-Chaudiere, 2007; Lecaudey et al., 2008; Nechiporuk and Raible, 2008). These precursor clusters are connected to one another by a trail of interneuromast cells (Ghysen & Dambly-Chaudiere, 2007; Whitfield, 2005). Within the primordium it has been shown that there are compartments with distinct roles for *wnt* and *fgf* signalling (Lecaudey et. al, 2008; Aman & Piotrowski, 2008; Ghysen&Dambly-Chaudiere, 2007; Chitnis et al., 2012) that keep the overall numbers within the tissue stable despite the regular loss of clusters from the trailing edge during migration. What occurs after the primordium (primI) terminates near the tail is that a second primordium (primII) starts the same process of migration and follows the same path of (primI) while depositing neuromast organs from its trailing edge (Ghysen and Dambly Chaudiere,2007; Ledent,2002; Sapede et al., 2002). This marks the end of Zebrafish embryogenesis yet the lateral line system still keeps on developing. What occurs next is that organs deposited by primI and primII will move ventrally (Ghysen and Dambly-Chaudière, 2007; Ledent, 2002; Whitfield, 2005) and new neuromasts arising from the inter-neuromast cells will form (Grant et al., 2005; López-Schier and Hudspeth, 2005; Lush and Piotrowski, 2014; Whitfield, 2005).

The huge migratory path the primordium has to undertake during Zebrafish development is even more astounding when one considers how reproducible and controlled this event is. This led researchers to look for the genetic underpinnings of this highly accurate and stereotypic migratory route. A variety of groups were able to show that this depended on the action of chemokine ligands and receptors

(David et al., 2002; Haas and Gilmour, 2006; Valentin et al., 2007). Briefly it was shown that the receptor *cxcr4b* locates primarily to the leading edge of the migrating primordium where it is able to perceive its cognate ligand *sdf1a* located on the horizontal myoseptum (Donà et al., 2013; Venkiteswaran et al., 2013). The action of another receptor *cxcr7* located on the trailing end of the primordium ensures the directionality of travel by allowing *cxcr4b* to constantly perceive higher levels of *sfd1a* (Donà et al., 2013; Venkiteswaran et al., 2013). In this way, the system ensures an ordered collective cell migration. Mutants for all of the above-mentioned chemokines produce fish with no (or massively reduced) *pLLs* (posterior lateral line). In a beautifully crafted experiment researchers at EMBL were able to show that a few transplanted *wildtype* cells can rescue a *cxcr4b* mutant primordium, this proves that a limited number of leading cells can drive the entire coordinated tissue migration (Haas & Gilmour, 2006). However, with the almost exclusive focus of lateral line studies on Zebrafish (Aman and Piotrowski, 2008; David et al., 2002; Grant et al., 2005; Haas and Gilmour, 2006; Hernández et al., 2006; Lecaudey et al., 2008; López-Schier and Hudspeth, 2005, 2006; Lush and Piotrowski, 2014; Ma and Raible, 2009; McGraw et al., 2014; Nechiporuk and Raible,2008; Sánchez et al., 2016) our understanding of how the *pLL* system is shaped or has evolved in other teleosts remains highly limited. This is important to address as it will shed light on the evolution of morphogenetic processes and highlight common principles of operation that promise to reveal the guiding logic behind lateral line morphogenesis.

"It has been clear at least since von Baer's day [1830s] that a theory of evolution requires, as a fundamental part of it, some theory of development" Waddington 1941

The plot thickens: the diversity of lateral line patterns

Teleosts are the most abundant class of vertebrates on the planet (Nelson, 2006; Moriyama et al., 2012) and as such have evolved a boundless variety of body shapes and sizes. This diversity is matched by the kaleidoscopic lateral line patterns that exist in the wild (Ghysenetal.,2012 ,2010; Pichon and Ghysen,2004; Sapede et al., 2002). It is currently largely unclear what the basis of this diversity in patterns is and if it has any functional relevance. But it has been suggested that it could relate to the body shapes of the different fish (Coombs et al., 2014, 1988), this would in theory make sense for a peripheral nervous system to adapt to different morphologies (Ghysen & Dambly-Chaudière, 2016). Initial comparative work in the *pLLs* of different teleosts strongly suggested that the embryonic patterns are highly conserved (Ghysen et al., 2012, 2010; Pichon and Ghysen,2004; Sapede et al., 2002) in terms of primordium migration, number of organs, their positions and even the number of *pLL* primordia (two, in all studied cases). This has led to the belief that most of the observed diversity of posterior lateral lines in adult fish must be produced post-embryonically (Nuñez et al., 2009; Pichon and Ghysen, 2004). In other words, embellishments on an essentially unified rudimentary pattern. The results obtained on *pLL* development in Medaka (Wittbrodt 2002) (and other teleosts) presented in this thesis challenges this assumption by showing fundamental differences in how *pLL* patterns are built during development. I present data that argues that these differences partly stem from different temporal and spatial expression of conserved genes that play important roles during primordium migration in different teleosts. In addition, I

will show how plastic the development of the *pLL* is even within one species (Medaka) and will reveal common principles that might explain the fast evolvability of *pLL* patterns in teleosts.

"I believe very strongly that the fundamental unit, the correct level of abstraction, is the cell and not the genome"
Sydney Brenner, Columbia lecture 2003

Cell behaviour in the spotlight: neuromast organization, resilience and iteration

After the patterns of *pLLs* are established during embryogenesis, neuromast organs start differentiating to fulfil their main function; the detection of water flow and relaying of information back to the brain (Ghysen and Dambly- Chaudiere, 2007). Considerable attention has been given to this process as it was recognized that the differentiated cell type of the neuromasts, the hair cell bundles, are morphologically equivalent to inner hair cells in the ears of humans (Nicolson, 2005; Whitfield, 2002). With the fundamental difference that in humans hair cells are lost due to injury/trauma or aging and are not replaced, which in turn can result in deafness (Cox et al., 2014; Furness 2015). While Zebrafish has shown an enviable life-long ability to replenish lost hair cells under homeostatic and injury paradigms (Cruz et al., 2015; Williams and Holder, 2000; Hernandez et al., 2007; Lopez-Schier and Hudspeth, 2006; Pinto- Teixeira et al., 2015). A variety of groups have shown quite convincingly that a supporting cell population sitting directly underneath the hair cell bundles are able to proliferate and differentiate into hair cells in response to injury and hair cell loss (Hernandez et al., 2007; Lopez-Schier and Hudspeth, 2006; Ma et al., 2008; Romero-Carvajal et al., 2015; Wibowo et al., 2011; Williams and Holder, 2000). However, where the stem cells of neuromast

organs reside is still not completely clear (Pinto-Teixeira et al., 2015). It has been reported that a ring of mantle cells surrounding the support and hair cells can act as the cellular source of new neuromasts during post-embryonic organogenesis (Dufourcq et al., 2006; Jones and Corwin, 1993; Stone, 1933; Wada et al., 2013). This has led to the suggestion that mantle cells are the true stem cells of neuromasts capable of producing support and hair cell populations and building new organs *de novo* (Ghysen and Dambly-Chaudiere, 2007). However, this proposition has never been experimentally proven. In this thesis, I show that mantle cells act as neuromast neural stem cells in Medaka under regenerative conditions, and that they are able to induce the formation of their own niches during development. This highlights self-organization principles operating in the *pLL* of Medaka and shows the appearance of an emergent property (induction) that depends on the presence of clusters of neuromast precursors and their interaction with the overlying epithelium. Additionally, I show that mantle stem cells undergo individual cell migration post-embryonically to participate in new neuromast organogenesis in a highly stereotyped and reproducible fashion. I show the robustness of this process and how early molecular heterogeneities of mantle stem cells *in vivo* can predict their behavioural differences. All in all, the results highlight how both stereotyped cellular behaviour and emergent properties from collectives of cells can influence morphogenesis.

The future is here: the death of model organisms

I believe that a comparative-species approach will be essential to drive the field of developmental biology forward in the coming decades. This is essentially because it offers an insight into how evolutionary processes have tinkered with

development to produce the variety of novelties and peculiarities we observe in different (and sometimes closely related) organisms. What this means is that even with a highly reductionist rudimentary model we can attempt to reconstruct evolutionary processes that took millions of years in a matter of a few months of lab-work. The level of insight gained by these approaches cannot be overstated. With the advent and ease of use of CRISPR technologies to precisely modify the genome of (in theory) any organism, in combination with the massive reduction in sequencing and bioinformatics costs, developmental biologists must make use of the already existing diversity in the natural world to drive the field into a post-model organism era. The types of questions that one can address using this approach are unique and essentially unexplored territory and as such can add meaningful knowledge instead of the enormous (& largely vacuous) data-gathering expeditions one often sees happening in today's technique-driven high-octane scientific environment. Whether you are studying regeneration capacities, gastrulation strategies, pattern formation or the segmentation clock a comparative approach is essential to distil the operational logic governing these highly conserved processes and to illuminate the fault-lines evolution could have exploited to tinker with them.

Aims

Uncovering some of the guiding principles and operational logic behind *pLL* pattern construction and post-embryonic neuromast organogenesis. Initial insights into the evolution of lateral lines (see prologue for more details).

Results

The following figures (1,3,4,5, 6) and figure legends are adapted directly from (Seleit et al., 2017a) and have been written by myself. All experiments are carried out by myself unless otherwise specified.

Labeling Medaka neuromasts reveals species-specific *pLL* pattern

Medaka has a particular and divergent posterior lateral line pattern at the end of embryogenesis than previously characterized teleosts (Figure 1 A). With two parallel lines of neuromast organs; one at the horizontal myoseptum (*mpLL*) and the other in a ventral position (*vpLL*). This pattern was assessed by DAPI stainings on fixed fish and *in situ* hybridization using the pan neuromast marker *eya1* (Figure 1 B-C). Based on the pre-existing line in the lab Tg(Eya1:GFP) and the described results above, I generated an Eya1:mCFP transgenic line that allowed the visualization of the *pLL* and *aLL* of Medaka in live fish, in addition to labelling the *pLL* nerve and all neuromasts at the end of embryogenesis. The medaka *pLL* pattern always has one *mpLL* in between two *vpLLs* except at the most anterior and most posterior positions where an *mpLL* is regularly absent. It was still unclear how this pattern comes to being during development and whether two primordia or one primordium is responsible for building it.

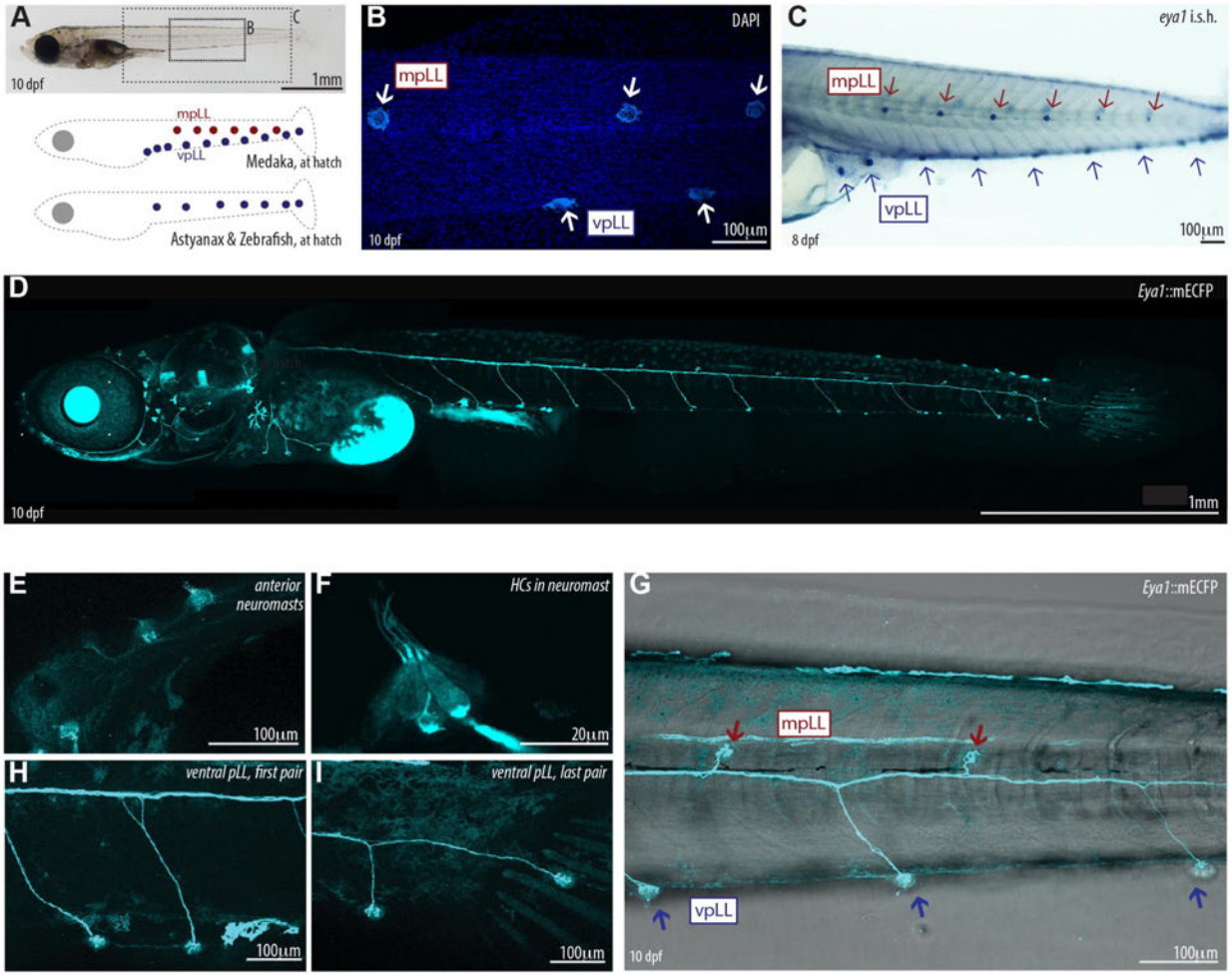

Figure (1) The Medaka lateral line at the end of embryogenesis. "(A) Whereas Astyanax and zebrafish have a single ventral pLL at the end of embryonic development, medaka shows an additional line at the horizontal myoseptum – the mpLL. (B) Neuromasts are easily identified by DAPI staining on fixed embryos. (C) In situ hybridisation shows strong expression in mpLL and vpLL neuromasts in a stage 39 medaka embryo. (D) Tg(Eya1:mECFP) labels neuromasts and their neural connections in vivo. Composite of seven individual frames stitched together using a Fiji macro. (E,F) Detail of neuromasts in the anterior lateral line (E), and hair cells (HCs) (F). (G-I) Alternating distribution of midline and ventral pLL neuromasts (G) along the trunk of a medaka larva, with exceptions of the first two pairs (H) and the last pair (I) of ventral pLL neuromasts." Figure and Figure legend adapted directly from (Seleit et al., 2017a)

Sequential organogenesis sets two parallel posterior lateral lines in Medaka

By relying on a 4D live-imaging approach during development on the newly generated transgenic lines (Eya1:GFP and Eya1:mCFP), I was able to follow the morphogenetic steps leading to the establishment of the *pLL* of medaka. This would be the first teleost other than Zebrafish that the process could be observed in live-fish and with a high temporal and spatial resolution. To my surprise the process

involved a series of well-defined steps that were clearly divergent from those reported in other teleosts. Initially the primordium migrates from anterior to posterior along the horizontal myoseptum and deposits neuromasts from its trailing edge (Figure 2 A). But unlike Zebrafish where deposited organs remain in the midline, Medaka neuromast clusters start moving ventrally as soon as they are deposited. This creates a slope-like pattern of neuromast deposition (Figure 2 B). In between primary deposited organs by the primordium small clusters of inter-neuromast cells (INCs) start to coalesce (Figure 2B). These clusters grow in number and start migrating dorsally towards the horizontal myoseptum while the primary organs continue their ventral movement (Figure 2 C). As this occurs connections of INCs hold the primary organs to the secondary ones, what is consistently observed at this stage is cell recruitment and migration from primary organs towards secondary organs that helps the developmentally younger neuromasts grow in size (Figure 2 C). At the end of embryogenesis, the connections between primary and secondary organs are lost and we end with two lines of parallel organs, one at the horizontal myoseptum (secondary organs) and one at the ventral end (primary organs) (Figure 2 D). These highly reproducible morphogenetic steps rely on the action of one *pLL* primordium, as ablating it results in no *pLL* neuromasts in Medaka (Seleit et al., 2017a). This is another major difference Medaka has compared to other teleosts since all other reported species have two posterior lateral line primordia, medaka has only one, yet the number of organs it forms at the end of development is higher than that of Zebrafish and the pattern more elaborate.

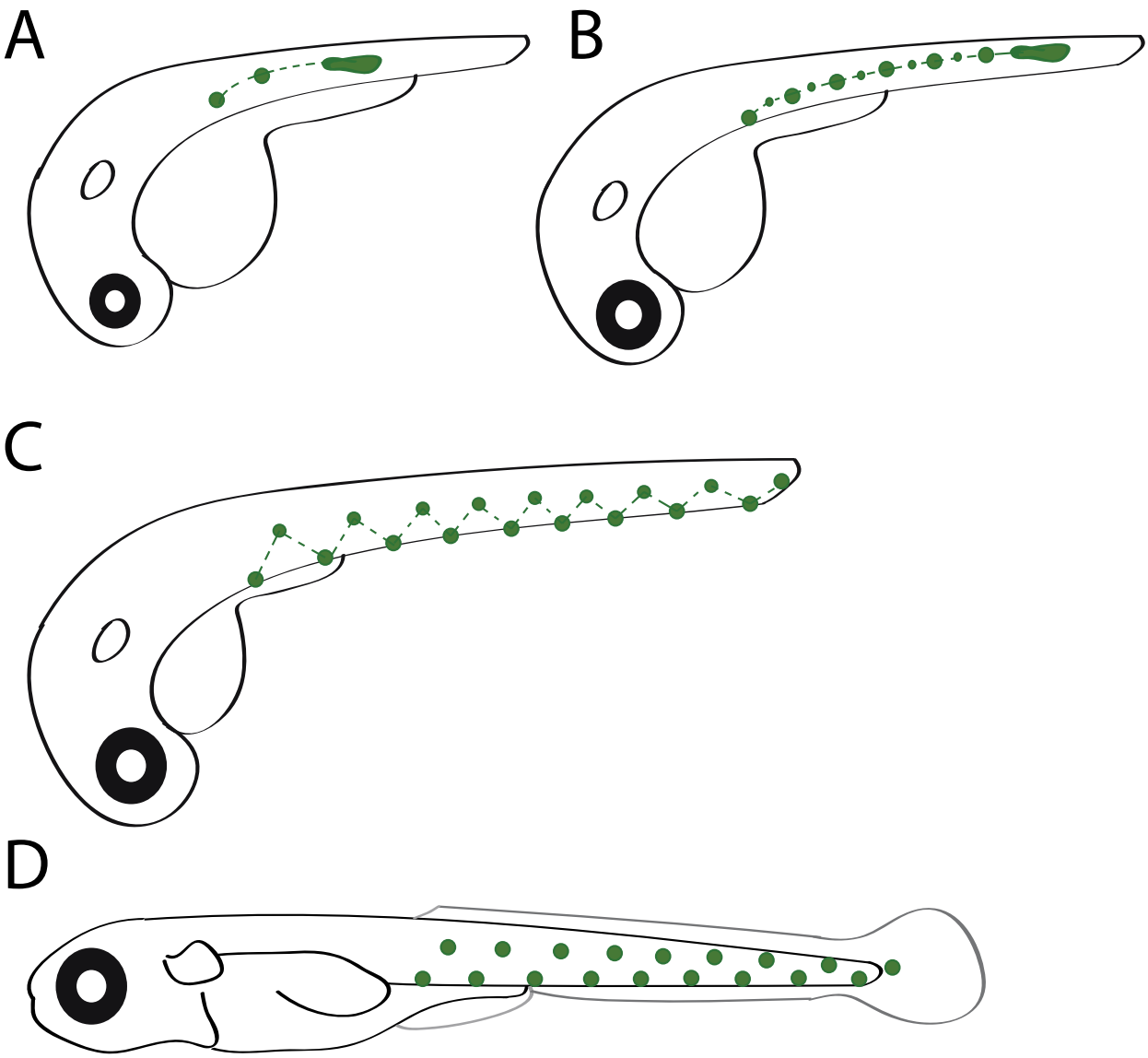

Figure (2) Schematic summary of posterior lateral line development in Medaka. Scheme done by Julian Stolper. A combination of live-imaging and ablation experiments indicate that there is only one posterior lateral line primordium in medaka that travels from anterior to posterior along the horizontal myoseptum and deposits organs from its trailing end. These primary organs start ventral movement as soon as they are deposited and new organs start forming by coalescence of inter neuromast cells in between the two primary organs (with always only 1 secondary organ forming in between the two primaries). Secondary organs move dorsally towards the horizontal myoseptum while primary organs continue their ventral movement. By the end of embryogenesis two parallel lines of sensory neruomasts are present in stage 42 Medaka embryos, one at the horizontal myoseptum (formed from secondary organs) and at the ventral end (formed from primary organs). Both lines are not connected to one another.

Medaka primordium migration depends on conserved chemokine receptors/ligand

The described morphogenetic movements undertaken to build the *pLL* of Medaka are significantly different from that of Zebrafish. This raises the spectre that the molecular machinery driving the process might be divergent between the two species. To test this directly I relied first on *in situ* hybridizations of chemokine ligand/receptor pairs that are known to drive primordium migration in Zebrafish. This revealed the high expression of *cxcr4b* chemokine receptor in the migrating primordium, deposited organs and INCs in Medaka (Figure 3A &C). A transgenic line I generated of a partial promoter of Medaka *cxcr4b* driving eGFP showed strong expression in the migrating primordium as well (Figure 3B). Next I checked the expression of *sdf1a* (also known as *cxcl12a*) the main known ligand of *cxcr4b* and found that it is expressed as a trail along the horizontal myoseptum as reported in Zebrafish (Figure 3 D-E). This chemokine interaction where *cxcr4b* perceives and travels towards the source of the *sdf1a* ligand is known to be responsible for primordium migration in Zebrafish (Ghysen & Dambly-Chaudiere 2007). The last piece of conserved machinery was the expression of another chemokine receptor *cxcr7* in the trailing end of the migrating primordium (Figure 3 F) that acts as a sink for *sdf1a*, this is exactly what has been reported to happen in Zebrafish (Ghysen & Dambly-Chaudiere 2007; Dona et al., 2013). *Cxcr7* expression remains in primary deposited organs but is not present in INCs or secondary organs in Medaka (Figure 3G). All in all, there is a highly conserved expression of the machinery driving primordium migration in Zebrafish and Medaka, two distantly related teleosts (Wittbrodt, 2002).

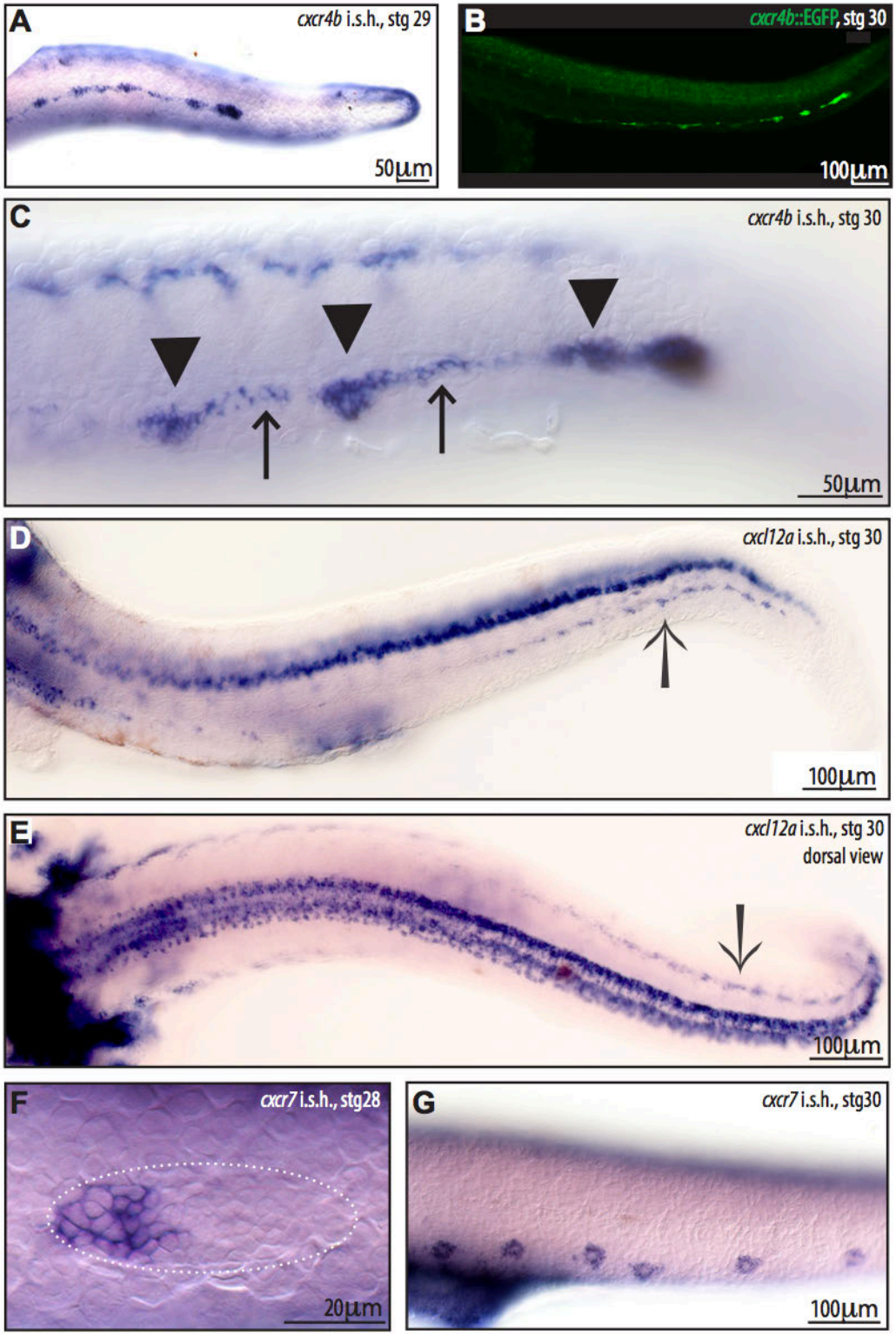

Figure (3) "*in-situ* hybridisation for *cxcr4b, sdf1a* and *cxcr7* in medaka. (A-C) cxcr4b is expressed in the migrating primordium and in the deposited neuromasts (A). The Tg(cxcr4b:EGFP) recapitulates the endogenous expression of cxcr4b (B). cxcr4b is also expressed in IC cells (C, arrows) between deposited organs (C, -lled arrowheads). (D, E) cxcl12a can be detected along the myoseptum (arrow) in a lateral (D) and a dorsal (E) view, as well as along the spinal cord. (F, G) cxcr7 is more abundant at the rear of the migrating primordium (F) and is expressed in the deposited organs (G), but could not be detected in ICs." Figure and Figure legend adapted directly from (Seleit et al., 2017a)

Reutilization of *cxcr4b/cxcr7* during secondary organ formation in Medaka *pLL*

Unlike the conserved initial movements involved in *pLL* pattern formation in Medaka, the formation of secondary organs in Medaka involves morphogenetic movements that do not occur in Zebrafish. What I realized is that *cxcr4b* mRNA remains expressed in primary deposited organs (even as they move ventrally), in INCs connecting primary to secondary organs and to secondary organs traveling towards the horizontal myoseptum (Figure 4A). At later stages *cxcr4b* expression persists only in secondary (developmentally younger) organs and is undetectable in INCs and primary organs (Figure 4B). Using the *cxcr4b*:GFP transgenic line I was able to observe that the cells migrating from primary organs towards the secondary ones have an upregulated expression of GFP (Figure 4 C-C'''). This raised the possibility that *cxcr4b* could play a role in secondary organ formation. Indeed, *cxcr4b kazura* mutants in Medaka reproducibly show failure of *pLL* primordium migration, consistent with the role of this chemokine in driving the migratory behaviour of the primordium. However, within the *kazura* mutants there were always 'escapers' that were able to form a number of primary organs before the primordium stopped migrating, in these cases no secondary organs were ever observed (Figure 4D). We have shown that the expression of *cxcr7* is restricted to primary organs and is not present in INCs or secondary organs (Figure 4 E-F), but it was still unclear whether this chemokine plays a role during secondary organ formation. The *cxcr7 yanagi* mutants in Medaka showed perturbed lateral line primordium migration, but 'escapers' consistently had the full cohort of primary organs but no secondary organs were able to form (Figure 4

G). These results strongly argue for a specific role for *cxcr4b* and *cxcr7* during secondary organ formation.

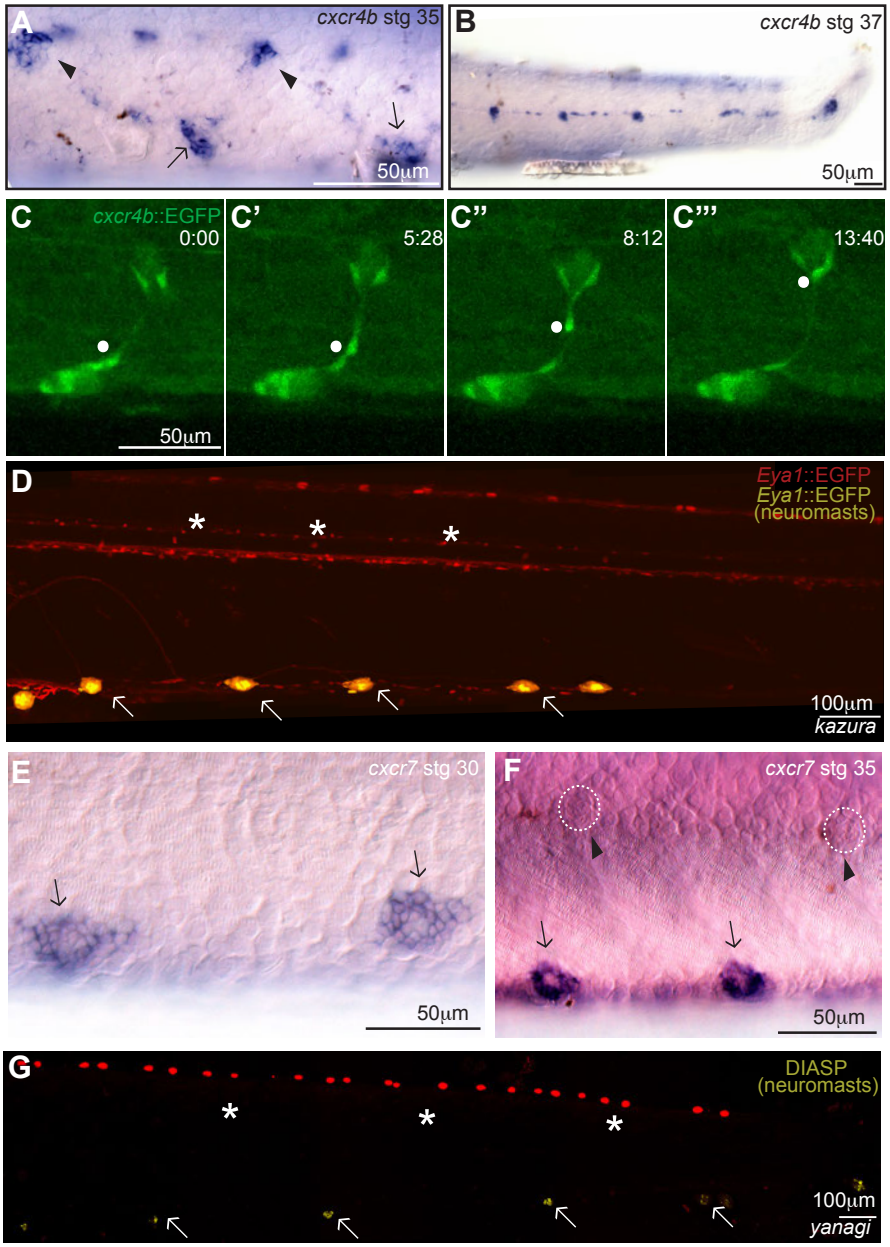

Figure (4) Chemokine receptors cxcr4b and cxcr7 are required for secondary organ formation. "(A,B) In situ hybridisation using a cxcr4b antisense probe indicates expression of the chemokine receptor in primary neuromasts (arrows in A), forming secondaries (arrowheads in A) and ICs (n=2, stage 35). Expression of cxcr4b is detected only in secondary organs at late embryonic stages (B) (n=3, stage 37).(C-C''') Time lapse of Tg(cxcr4b:EGFP) showing an $EGFP^+$ cell migrating from a ventral to a midline neuromasts (white dot). (D) kazura mutants that display primary organs (arrows) do not generate secondary organs (asterisks). (E,F) cxcr7 is expressed in the deposited organs (arrows in E). Expression is still detectable after ventral migration (arrows in F), but not in ICs nor in secondary organs (arrowheads and dotted circles in F). (G) yanagi mutants that display primary organs (arrows) do not generate secondary organs (asterisks). Neuromasts were detected either with DiAsp staining (G) or using Tg(Eya1:EGFP) embryos (D). Images in D and G were stitched and psuedocoloured to highlight neuromasts. Pigmented background (G) or total expression pattern of Tg(Eya1:EGFP) (D) are depicted in red, and $DiAsp^+$ (G) or $EGFP^+$ (D) neuromasts are shown in yellow" Figure and Figure legend adapted from (Seleit et al., 2017a)

Presence of *wt* cells rescues secondary organ formation in *cxcr4b, cxcr7* mutants

In addition to relying on published mutants I generated two gRNAs to target the *cxcr4b* locus in medaka by CRISPR. This led to a recapitulation of known phenotypes in the F0 injected generation. Where I consistently observed fish with a reduced number of secondary organs forming (Figure 5 A-B). To further prove the involvement of c*xcr4b* and *cxcr7* in secondary organ formation transplantation experiments were performed where *wildtype* (GFP labelled cells) were transplanted into *kazura* and *yanagi* mutants. It has been previously shown that the presence of a few *wt* cells can rescue primordium migration entirely in *cxcr4b* mutants in zebrafish (Haas & Gilmour, 2006). I therefore generated mosaic primordia and rescued primordium migration in Medaka *kazura* mutants. I was then able to focus on whether the presence of *wt* cells can rescue secondary organ formation per se. And the results strongly argue that a rescue of secondary organ formation only occurs if *wt* green cells are present (Figure 5 C & F arrowheads), while organs were missing in areas that did not contain primordium derived GFP+ cells (Figure 5 C asterisk). The same rescue transplantation was performed in *yanagi* mutants and there the presence of *wt* green cells was able to rescue secondary organ formation (Figure 5 D& E white arrowheads), however this required that the majority of the migrating primordium be of *wt* origin (since *cxcr7* localizes exclusively at the trailing edge of the migrating primordium). These results demonstrate that *cxcr4b* and *cxcr7* signalling are required for secondary organ formation.

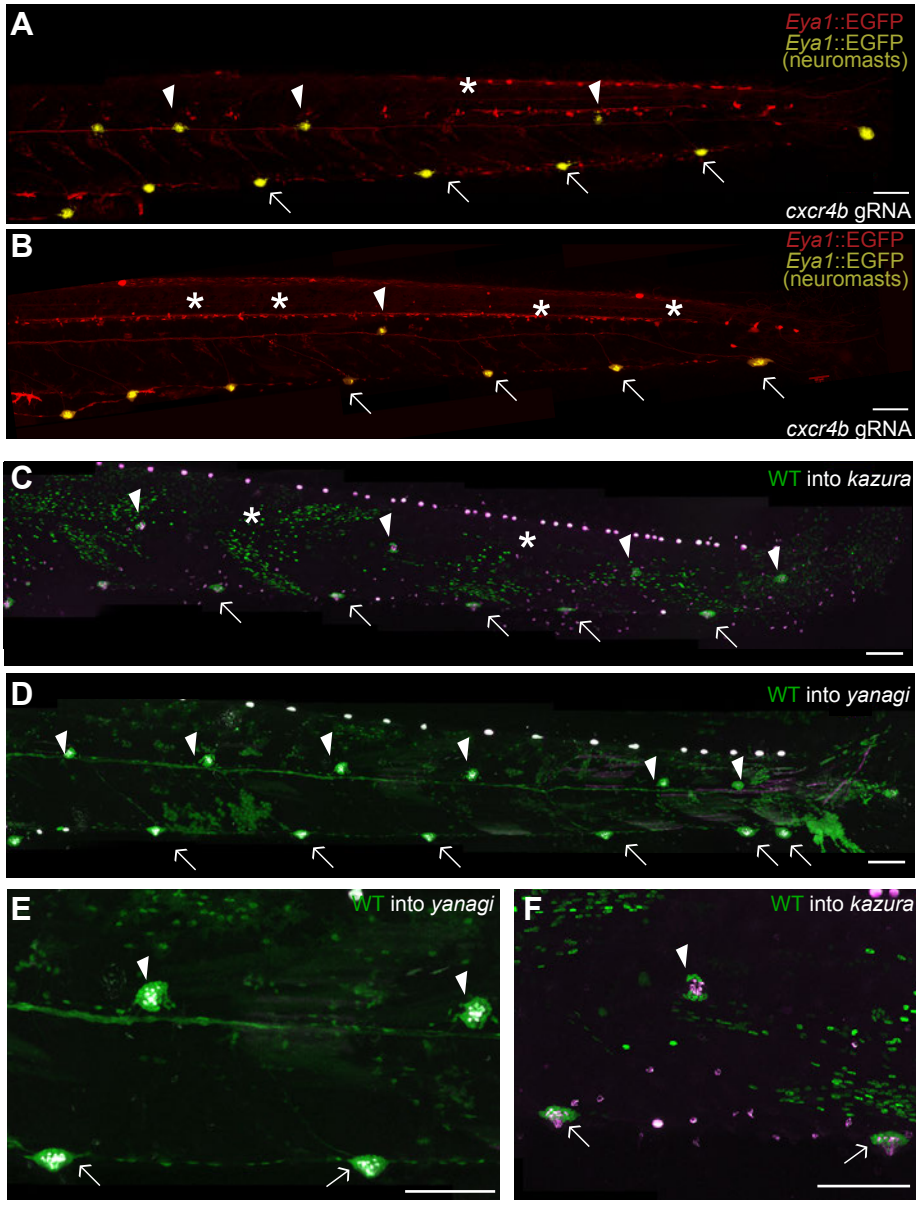

Figure (5) Transplantation of wild-type cells into *cxcr4* and *cxcr7* mutants rescues secondary organ formation. "(A,B) Injection of gRNAs against cxcr4b results in Tg(Eya1:EGFP) larvae lacking some (A, asterisk) or many (B, asterisks) secondary neuromasts. (C-F) When wild-type $EGFP^{+}$ cells are transplanted to kazura (C,F) or yanagi (D,E) mutants, they can rescue secondary organs (arrowheads in C-F) that contain functional hair cells as seen by DiAsp staining (magenta). All rescued secondary organs contain $EGFP^{+}$ cells (E,F). Images were treated as in Fig. 6. Arrows indicate primary organs, arrowheads secondary organs and asterisks missing secondary organs." Figure and Figure legend adapted from (Seleit et al., 2017)

Plasticity of neuromast numbers in different Medakas contrasts to constancy in *pLL* pattern

I noticed that while the one-between-two (one secondary organ in between two primary organs) pattern of neuromasts in the *pLL* of Medaka fish is highly

reproducible in different fish, the number of organs (primordium output) can vary quite considerably between different fish (Figure 6). This variation was puzzling since the Medaka *wt* line we use in the lab is highly inbred, this genetic isogenicity would argue against genetic differences being the source of this different output of the primordium. But while there seems to be an inherent plasticity in the number of organs produces by the migrating primordia the pattern was highly fixed and reproducible.

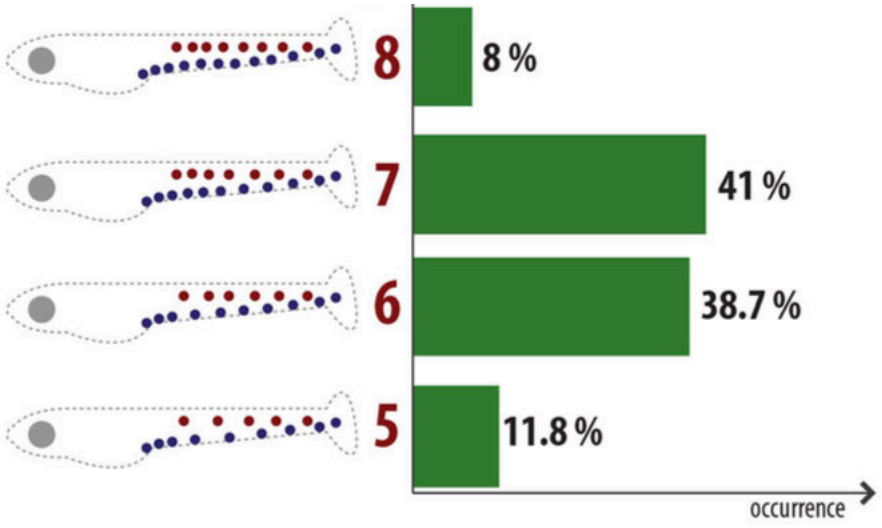

Figure (6) Schematic representation and graph showing the different number of secondary posterior lateral line organs at the end of embryogenesis in isogenic in-bred Medaka Cab line. Figure adapted from (Seleit et al., 2017a)

pLL of Medaka as a developmental process with low buffering capacity

The above observation argues that there must be a non-genetic aspect to the output of the *pLL* primordium of Medaka. Realizing this is an interesting avenue for further study I looked at the left and right *pLL* primordium output within the same Medaka fish. Surprisingly 73% of all fish (N=90 fish) (Seleit et al., 2017a) had different number of organs on the left and right side of their *pLLs*. This further strengthens the argument for A) high plasticity of the primordium as a

developmental tissue and B) non-genetic cause for the differences in primordium output. This sounded quite similar to old theoretical ideas from Conrad Waddington (see prologue section) about developmental buffering systems. We reasoned that the behaviour of the primordium would suggest it is has a low developmental buffering capacity (high plasticity and influence by surrounding environment and probably a lower genetic determinism). To test this experimentally we decided to modulate the environmental conditions (temperature) to check the limits of the buffering capacity of the system. Briefly we reasoned that a highly robust developmental process (eye formation) will have a high noise buffering capacity so challenging the system with different temperatures will still produce fish with two eyes at the end of development. While for the *pLL* we hypothesized that since the system appears to be plastic, temperature changes might impinge on it more forcefully and lead to a further decoupling of left right asymmetry in output of the *pLL* primordium (Figure 7). The experiment was carried out by (Jana Roeder Master's thesis 2018) and the results clearly show that at extreme temperatures one can decouple further the asymmetry of lateral line outputs (percentage of left/right identical organ numbers in *pLLs* of the same fish: 18°C= 20%, 28°C= 16.7%, 32°C=11.1%). These results argue that the *pLL* of Medaka could be a system operating under a low developmental buffering capacity.

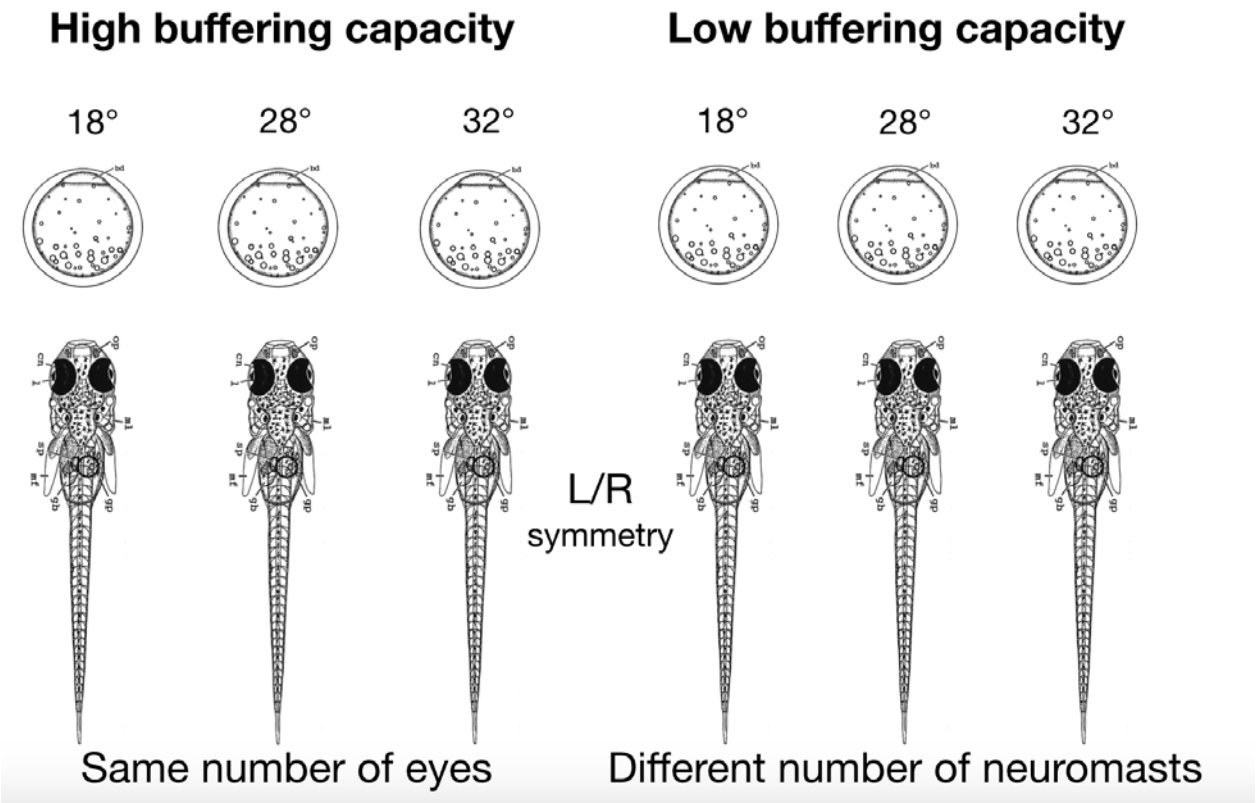

Figure (7) High and low developmental buffering systems. Raising medaka embryos at 18, 28 and 32 degrees produces fish with the same number of eyes (high buffering capacity), while raising the same fish on these temperatures produces a more different number of organs on the left and right posterior lateral lines. This asymmetry is specific to the pLL and is not observed in the aLL. Suggesting that the pLL operates at a low developmental buffering capacity. Figure adapted from (Iwamatsu et al., 2004)

Diversity of embryonic *pLL* patterns in different teleosts

The fact that in Medaka the *pLL* output seems highly plastic and with a low developmental buffering capacity would predict that in different species this plasticity will be exploited and might lead to a high evolvability and differences in number and pattern of neuromasts at the end of development. To test this directly I analysed the embryonic *pLL* pattern in a variety of fish both by DiAsp and DAPI stainings (Figure 8). This led to the realization that the system is indeed highly evolvable as we report not only differences in number of organs between the different species but also major pattern changes (Figure 8). These results put the low buffering capacity and high plasticity of the *pLL* as a possible reason for its very rapid and diverse evolvability in teleost fish. I then focused my efforts on trying to interfere with the *pLL* pattern and organ numbers in Medaka

fish by a variety of different mechanisms, with the aim of furthering our understanding of the guiding principles of pattern formation and the interaction of developmental processes with their immediate environment as shapers of 'phenotypes.'

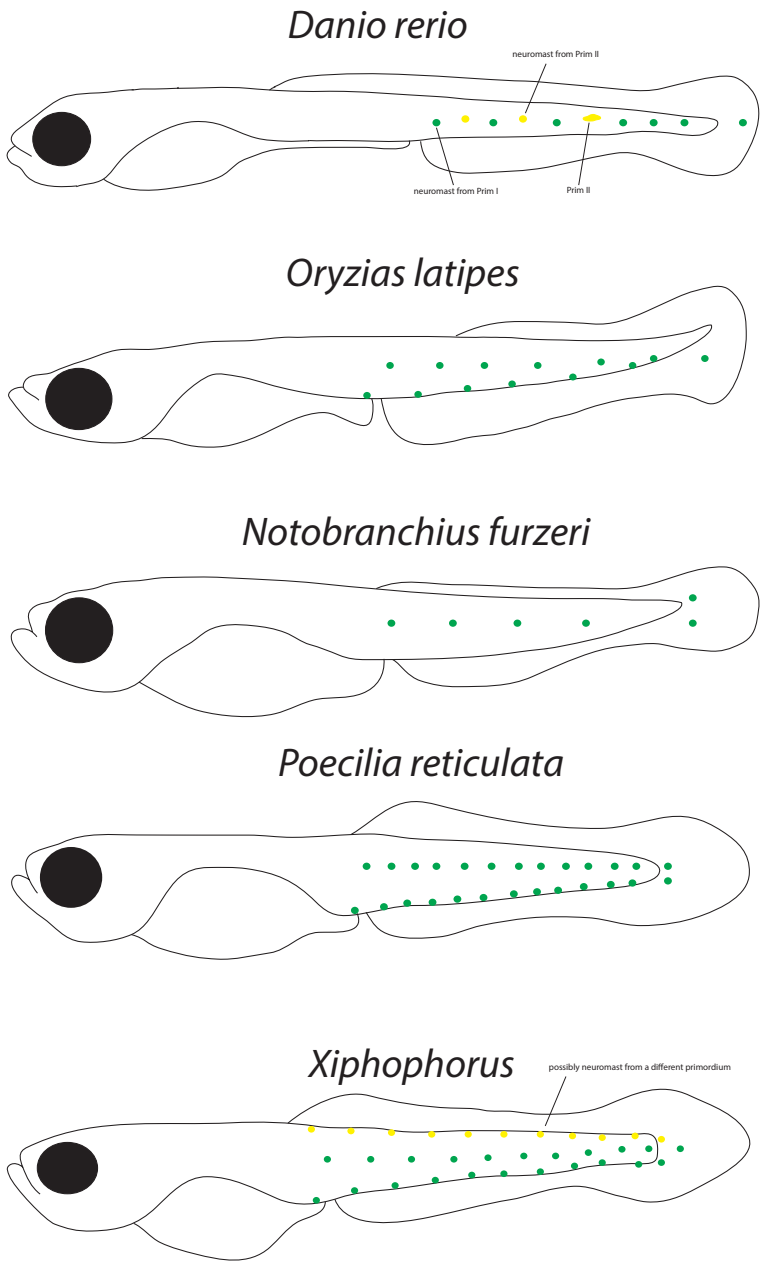

Figure (8) The diversity of pLL patterns at the end of embryogenesis in a variety of teleosts. I discovered that the pattern of neuromast at the end of development is not only different between medaka and Zebrafish but also a number of other teleosts. Scheme showing the distribution and relative approximation of organ numbers in a variety of teleost fish that were DAPI stained and imaged or DiAsp stained and imaged. N=4 for all species but zebrafish and medaka N>20. Fish embryos are not drawn to scale. Both organ numbers and positions differ between the different species. Schemes by Karen Gross.

***Keratin 15* CRIPSR mutant shows a perturbed *pLL* pattern in Medaka**

I decided to target our newly identified mantle cell and epithelial marker *keratin* 15 with CRISPR by designing 2 gRNAs targeting exonic regions of its CDS. Injecting the two guides along with the xCas9 led to a massive phenotype in the *pLL* of stage 42 embryos of a variety of transgenic lines (around 20% of all fish showed strong defects). Precisely the pattern of neuromast deposition was heavily altered with most organs located on the midline and very few found on the ventral end (Figure 9 A-B). In addition, the distribution and morphology of epithelial cells appear highly perturbed in the injected fish compared to controls (Figure 9 A-B). Looking more carefully I realized that there are consistent organ orientation defects in the injected F0 mutants (Figure 9 C-D'). I was able to raise a stable F2 CRIPSR line (that contains a composite allelic KO) that recapitulated all the phenotypes of the strongest injected generation fish (Figure 9 E-G) (Figure 35 A). What was also clear from these fish is the prevalence of epithelial cell lesions (magenta arrows Figure 9 F-G). All in all, *k15* mutants show a highly perturbed *pLL* pattern at the end of embryogenesis in Medaka in addition to organ orientation defects and prevalence of epithelial cell lesions with incorrectly shaped and positioned epithelial cells. I then compared more systematically and quantitatively organ positioning between *wt* and *k15* mutants on the left and right *pLLs* (Graph 1). And what became apparent are two things, there is a complete inversion of the pattern of neuromasts with more organs present at the midline in the mutant than in the *wildtype*, while the number of organs that were at the ventral side of mutants was almost equivalent to the number of secondary organs at the midline in the *wildtype* situation. The second interesting finding was that the mutant was a lot more

variable in terms of organ numbers than the *wildtype* situation (it is possible this could be due to the composite allelic combinations of the mutants). I next checked whether the output of the primordium in terms of the total number of organs in the *pLL* is divergent between *wildtype* and mutant conditions. Surprisingly primordium output was highly comparable between the mutant and the *wildtype* (Graph 2). This means that the major phenotype in the *k15* mutant is organ positioning and not total organ numbers, the primordium in both cases produces a similar number of overall organs. This also suggests that secondary organ formation in *k15* mutants is most probably not compromised.

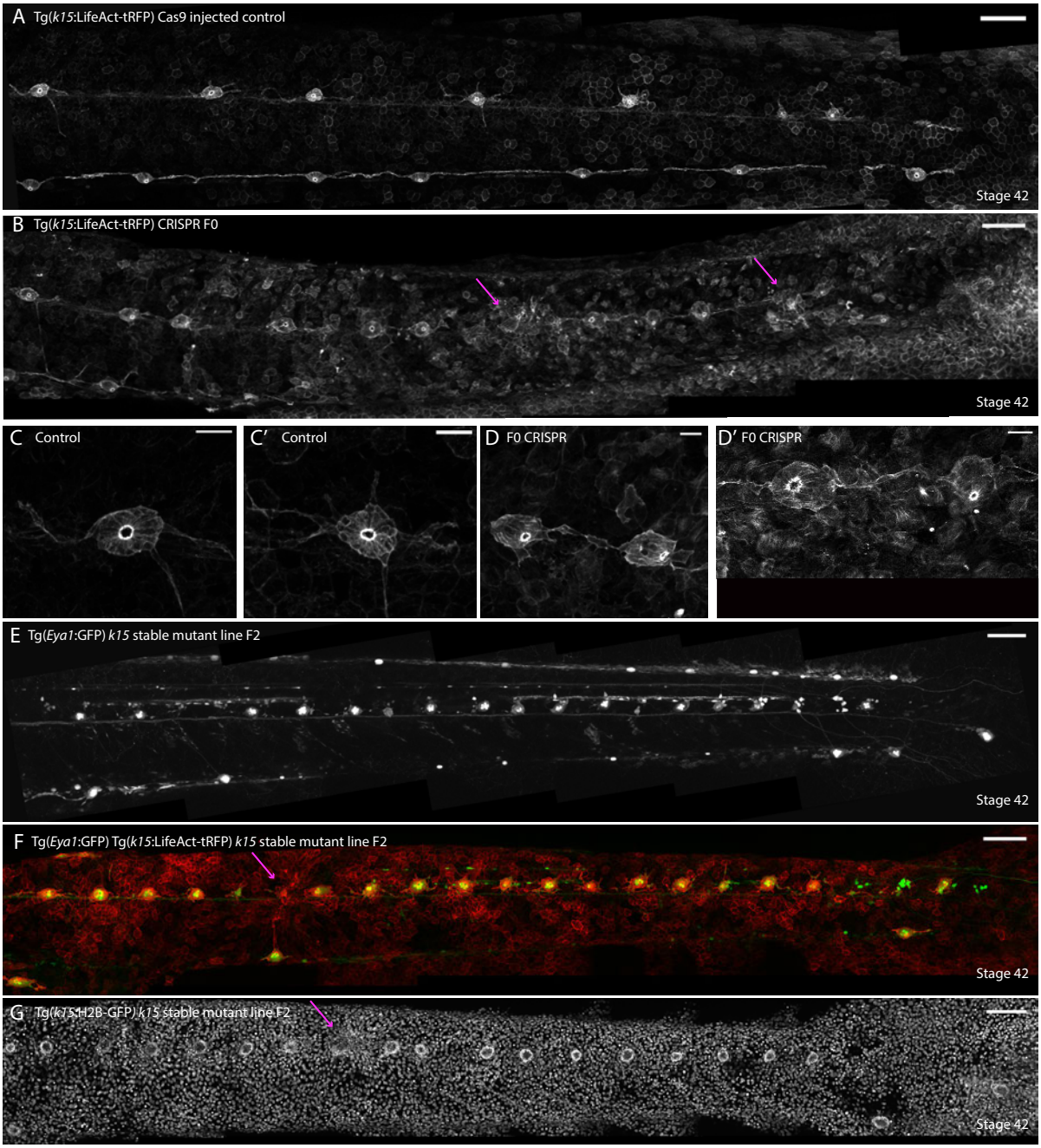

Figure (9) *K15* crispants and stable mutants show perturbed pLL pattern, epithelial lesions and neuromast mis-orientation defects (A) Cas9 injected control Tg(*K15*:LifeAct-tRFP) stage 40 medaka embryo shows normal pLL pattern, number of organs, organ orientation and normal epithelial cell morphology and cohesion. Scalebar=100 microns. (B) F0 Cas9 + gRNA1,2 against k15 locus injected Tg(*K15*:LifeAct-tRFP) shows epithelial disorganization and lesions (purple arrow) disturbed pLL patterns with most organs stuck at the midline Scalebar=100microns. (C-D') Zoom-in panels on *wildtype* and mutant neuromasts notice the mis-orientation of mutant organs compared to the wild-type scale bars=20 microns. (E, G) stable CRISPR F2 *K15* mutant line recapitulates F0 phenotypes and shows majority of organs stuck at the mid-line. Notice in (F and G) the presence of epithelial lesions indicated by purple arrows. Scale bar=100microns. N>10 for all panels. Anterior is to the left, posterior is to the right. Dorsal is up and ventral is down.

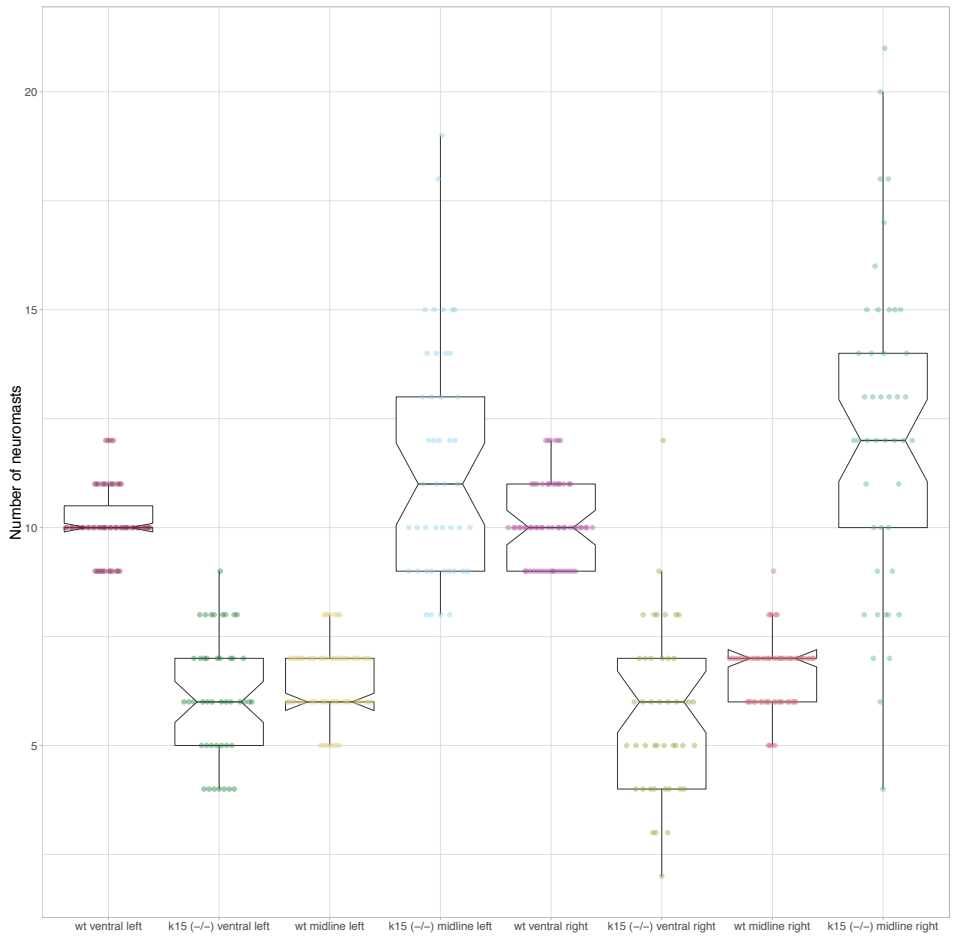

Graph (1) Boxplot showing number of organs present at the midline and ventral sides of wildtype and *k15* mutant fish. Notice the complete inversion of number of organs in each line (midline and ventral) in *k15* mutants compared to *wildtype*. In addition, the variability of number of organs is more widespread in *k15* mutants compared to *wild-type*. Overall pattern of organs is massively disturbed in *k15* mutant fish.

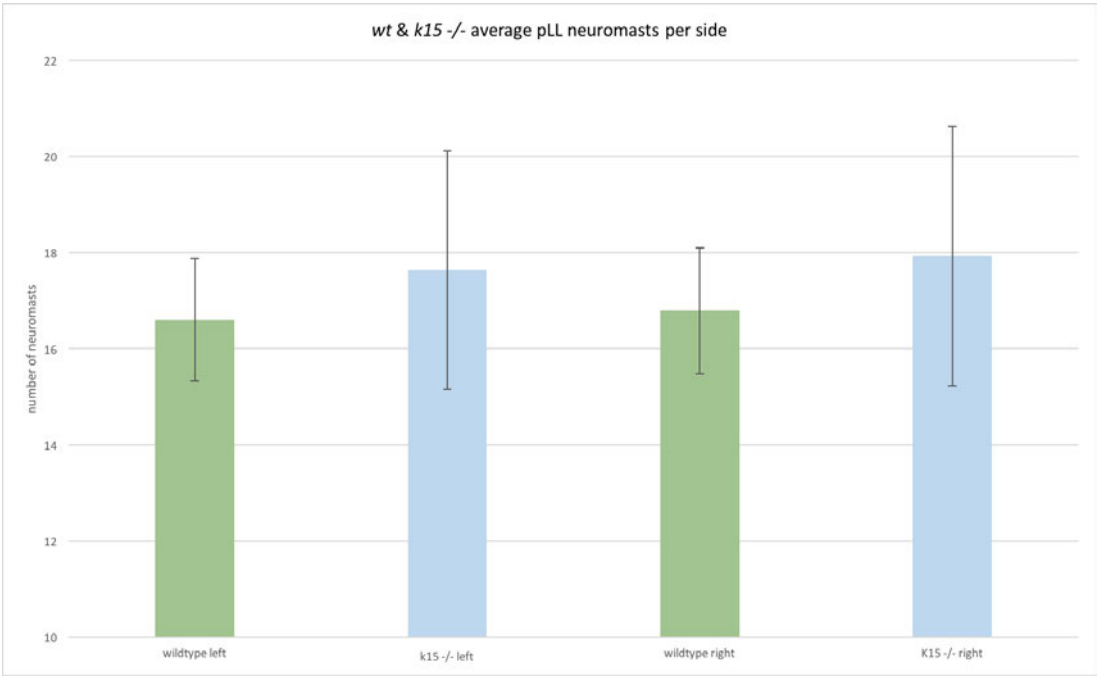

Graph (2) While pattern is perturbed in *k15* mutants, average overall organ numbers are similar to the *wildtype* suggesting the defect is not in primordium output but rather organ positioning (N=63 larvae and 126 pLLs for *wt* and 45 larvae and 90 pLLs in *k15* mutants). Standard deviation are black bars with capped ends.

Epithelial cell extrusion and cell death in *keratin 15* mutants

Already at 11dpf when one observes *k15* mutants under bright-field conditions one can clearly see epithelial cell lesions and epithelial cell extrusion along with a disorganized epithelium (Figure 10 A-B). Epithelial cell extrusion is a known consequence of epithelial cell death and turnover (Gudipaty et al., 2017) and I wondered whether evidence for excess cell death can be observed in *k15* mutants. Indeed, evidence for epithelial cell death as shown both in live samples and DAPI stained fixed ones was apparent (Figure 10 C-H). Specifically, it was quite obvious the high prevalence of small condensed nuclei surrounded by very small cellular membranes (an indication of nuclear fragmentation and apoptosis) (Figure 10 C arrows, G arrows). In addition, DAPI staining showed the presence of the same small condensed nuclei (Figure 10 F and H yellow arrows). All in all, it seems a majority of *k15* mutants do exhibit a higher rate of epithelial cell death and this leads to higher epithelial turnover that becomes apparent by the increased extrusion present in the mutant.

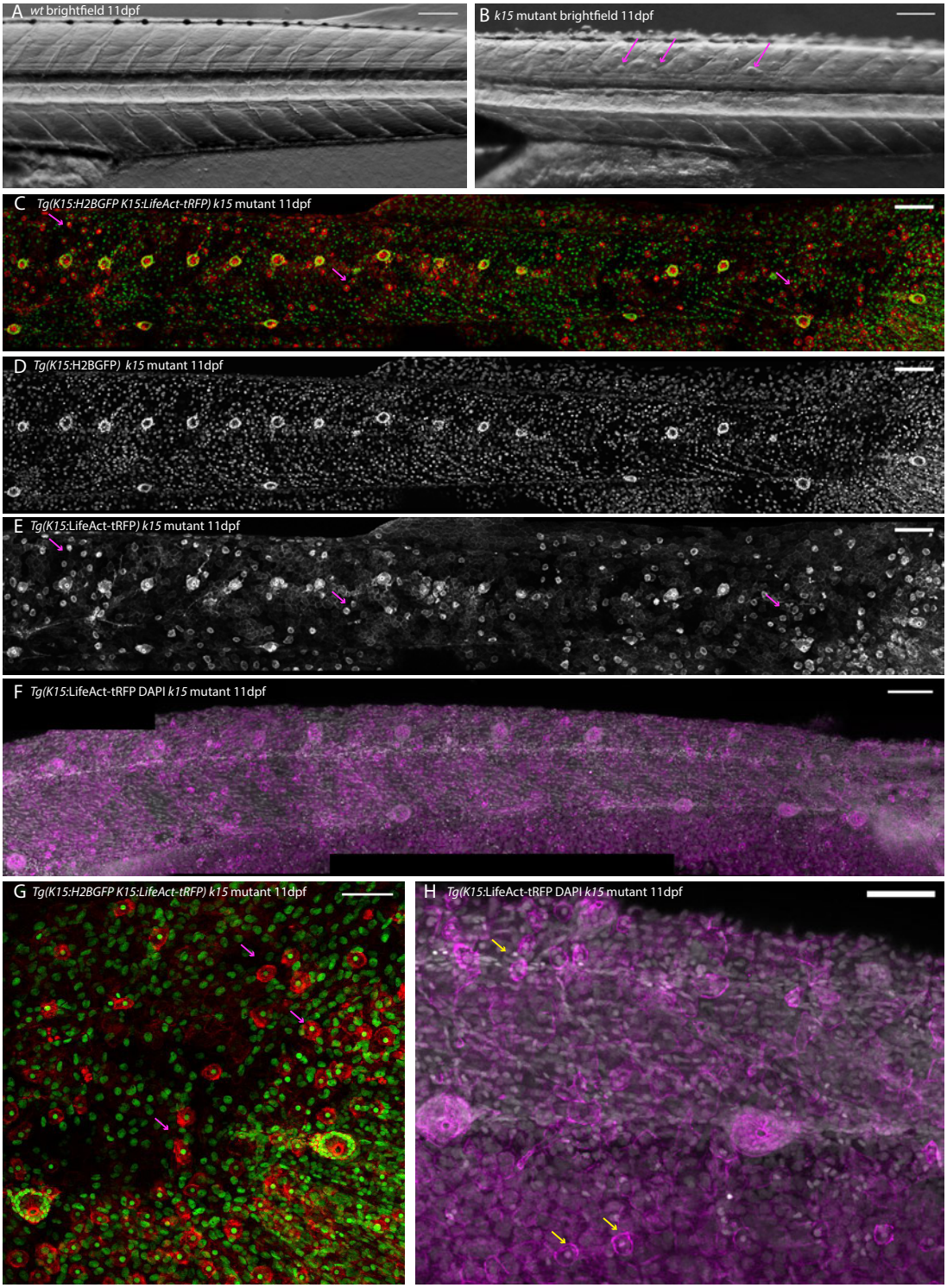

Figure (10) Epithelial cell extrusion and death in *k15* mutants (A) 11dpf bright-field imaging of *wildtype* embryo, notice normal epithelium Scale bar 100 microns. (B) Same imaging on *k15* mutant embryo notice the presence of extruding cells from the epithelial cell layer. Scale bar=100 microns. (C) 11dpf Tg(K15:H2BGFP K15:LifeAct-tRFP) *k15* mutant embryos notice the presence of fragmented and very small nuclei an indication of cell death (magenta arrows) Scalebar 100 microns. (D-E) individual channels showing K15:H2bGFP and K15:LifeacttRFP from (C) Notice the presence of compacted epithelial cells an indication of cellular death. (F) DAPI and immunostaining on *k15* mutants reveals the presence of the same phenomenon. Scale bar 100 microns (G-H) Zoom in panels on live and fixed samples reveals the prevalence of small nuceli in both cases Scale bar =50 microns Magenta and yellow arrows point at epithelial cells with condensed nuclei and cellular membrane shrinkage. Anterior is to the left, posterior is to the right. Dorsal is up and ventral is down.

Perturbed epithelia in *k15* mutants linked to neuromast mis-positioning

All the above discussed phenotypes seem to suggest there is a major problem with the epithelial cell layers in *keratin 15* mutants. To dissect these defects more closely I decided to manually segment the suprabasal epithelial layer (which is negative for *k15* transgenic line(s) expression but apparent in bright-field images) in *wildtype* and *k15* mutant 9dpf embryos. This revealed the massive disorganization of the mutant epithelium, with a huge variety in cellular shape and a perturbed structural integrity of the epithelium (Figure 11 A-B). This combined with previously described *k15+* epithelial cell defects points to the fact that both epithelial cell layers are heavily affected in *k15* mutants. Since the primordium and deposited organs have to interact and travel through the overlying epithelium this could be the source of organ mis-positioning. To investigate this in finer detail I made use of stable *k15* mutants where the *pLL* nerve was labelled by Eya1:mCFP. The nerve connection in this case can act as a tracer for neuromast trajectory (or lack thereof) in the mutant compared to *wt* fish. This led to the consistent observation that neuromast organs in *k15* mutants seem to be initially correctly specified (i.e they do move ventrally) as revealed by the nerve connection, but at some point the organs revert to the midline once more and stay there (Figure 11 C-E magenta arrows). Indeed by 4D time-lapse imaging the Eya1:mCFP *k15* mutants during *pLL* formation one can clearly observe two behaviors A) primary organs that start moving ventrally (correctly) and then stall and revert back dorsally (Figure 11 F-F' yellow dots) and B) primary organs that are not able to move ventrally and remain stuck at the midline (Figure 11 F-F' yellow dots). These results strongly suggest that the interaction between the heavily disturbed

epithelial cell layers and the primordium (and deposited neuromasts) could be the basis of the pattern defect observed in the *pLL* of *k15* Medaka mutants.

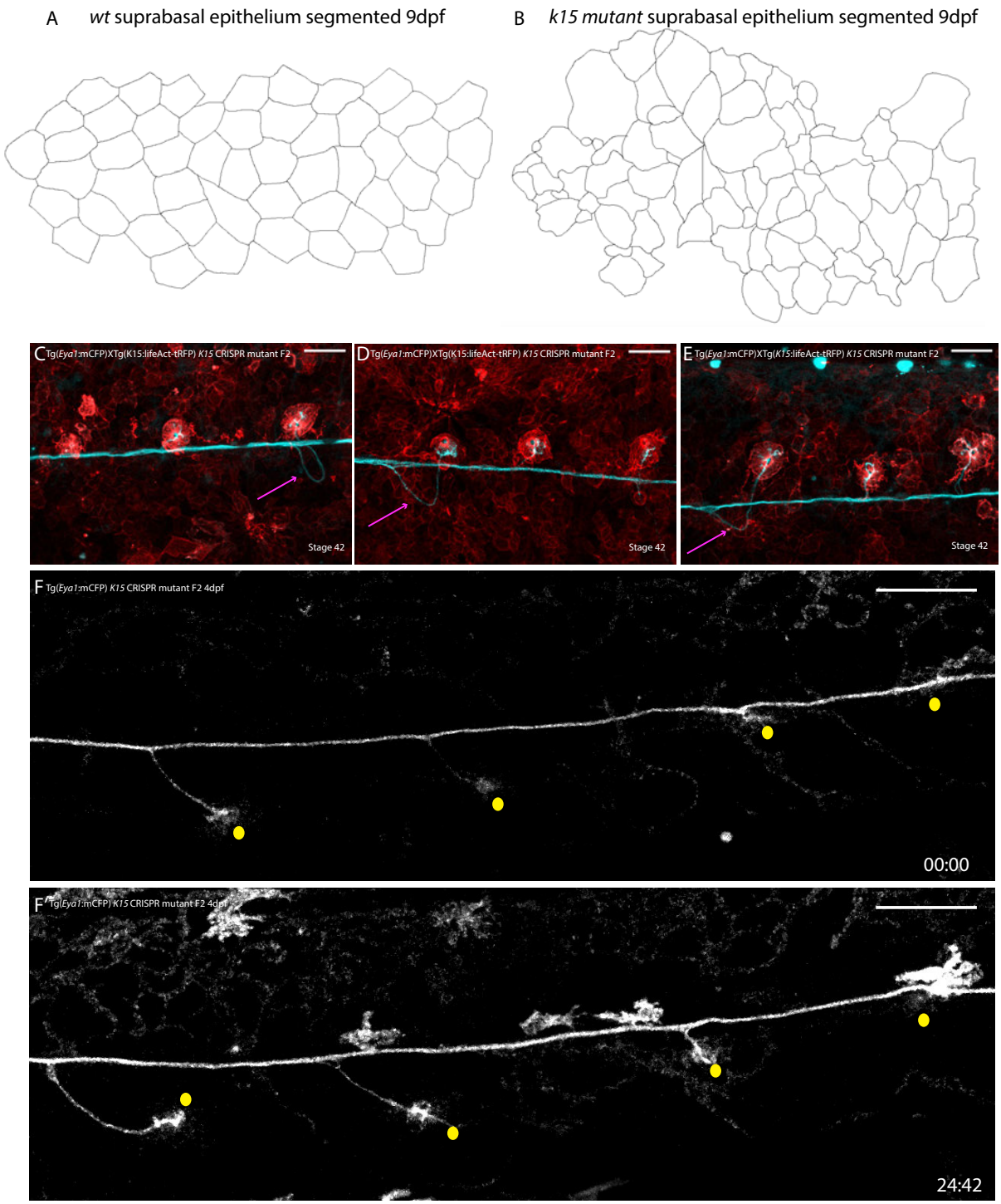

Figure (11) Perturbed epithelia linked to neuromast mis-positioning in *k15* mutants (A) Segmentation of *wt* suprabasal epithelial layer in 9dpf embryos, notice the regular packing and conserved shape of epithelial cells. (B) Segmentation of *k15* mutant suprabasal epithelial layer reveals massive disorganization loss of structural packing and loss of uniform cell size N=>100 cells segmented in *wt* and *k15* mutants number of fish 5 control and 15 *k15* mutants. (C-E) *K15* mutant Tg(Eya1:mCFP) Tg(K15LifeAct-tRFP) 9dpf shows the pLL nerve connection of the neuromasts notice (magenta arrow) the

correct initial specification of neuromast positioning, downward nerve movement, which consistently is followed by an upward shift, suggests organs are initially receiving the right cues and are specified correctly but somehow are blocked from proceeding Scale bar=50 microns. (F-F') Time-lapse imaging on *k15* mutant Tg(Eya1:mCFP) shows a number of neuromast organs being correctly specified but failing to continue downward movement and getting blocked, yellow dots indicate organ poitions, some revert direction majority remain stalled throughout movie Time in hours scale bar=50 microns N= 6 fish. Anterior is to the left, posterior is to the right. Dorsal is up and ventral is down.

Primordium migration defects and stalling in *k15* mutants

In addition to the previously described defects in organ positioning in *k15* mutants I was wondering whether the primordium migration as such is also affected in the mutants. This seemed probable since the epithelial cell layers the primordium has to migrate directly underneath for huge distances are heavily perturbed in the mutants. I therefore relied on a highly resolved 4D imaging of *k15* mutant and wildtype migrating primordia. Results (Figure 12 A-D) show that while mutant primordia travel a very short distance in a 15-hour time period (as revealed by the position of the yellow dot relative to the leading edge of the migrating primordium), its *wildtype* counterpart was able to cover a considerably longer distance in the same time interval (Figure 12 E-H). This strongly argues that primordium stalling occurs in *k15* mutants, presumably because the mutant primordium has to break-through forming epithelial lesions that can block its movement. Indeed, quantitatively assessing both velocity and overall distance covered by *k15* mutant and *wildtype* fish revealed that the average velocity and distance covered in three 5 hour intervals of mutant primordia is significantly lower than the *wildtype* (Graph 3 A-B). I was also interested in assessing overall primordium velocity in *wt* Medaka, *k15 mutants*, dorso-ventral patterning *Da* mutants (duplicated ventral side) and Zebrafish. Interestingly this revealed that primordium velocity in Zebrafish (around 50μm/hour, comparable to Lecaudey et al., 2008, 60-70 μm/hour, Knutsdottir et al., 2017 report 1-2μm/min) is more than double that of

wt Medaka. *Da* mutant primordia travel with the same velocity as the *wt* & only *k15* mutant primordia are significantly slower than both (Graph 3C).

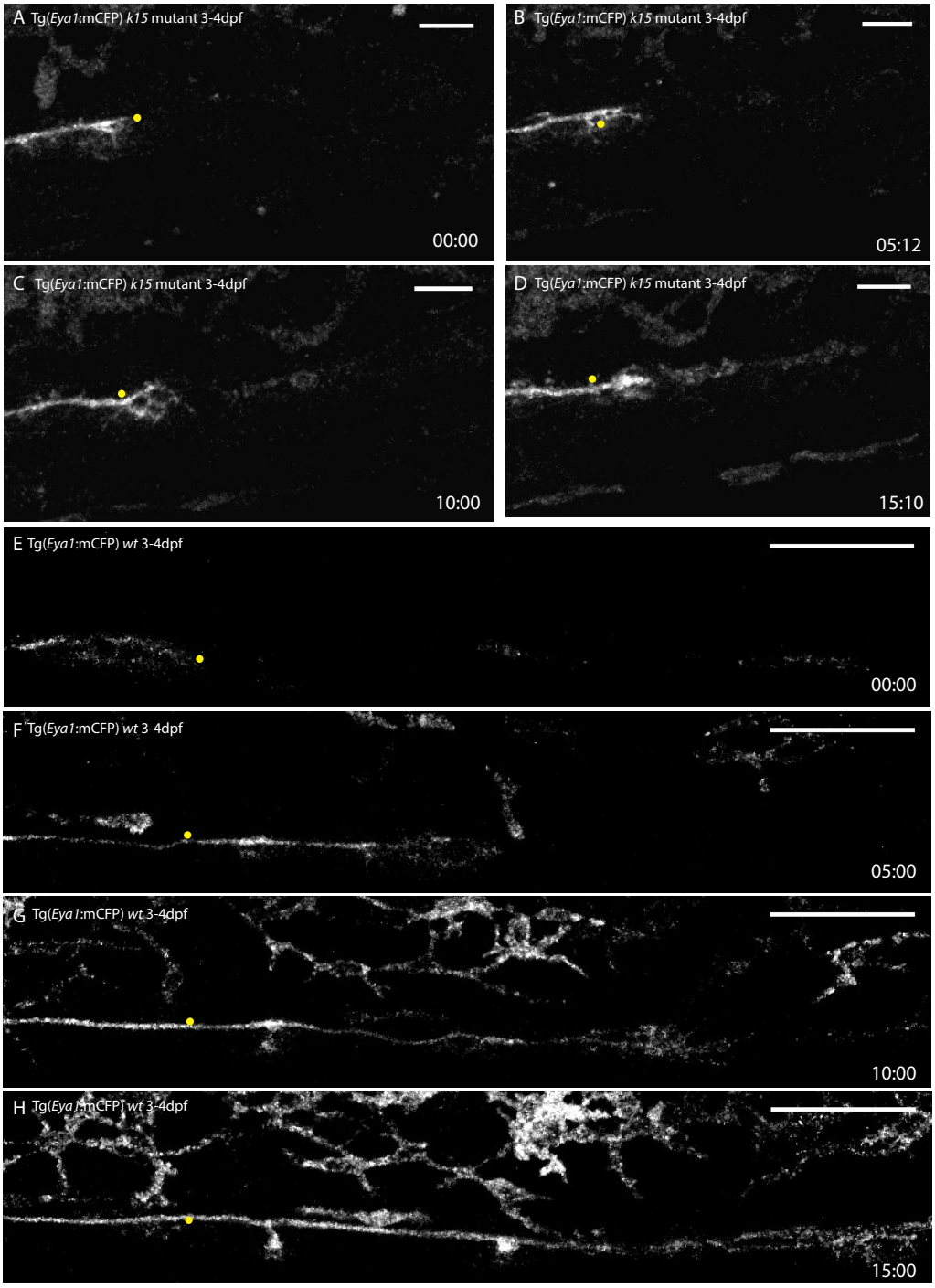

Figure (12) *K15* mutant primordium stalls (A) live-imaging on Tg(Eya1:mCFP) primordium during organ deposition. Yellow dot depicts the position of the extending tip of the migrating primordium timepoint=0. Time in hours. Scalebar=20microns. (B) Same primordium in (A) 5 hours 12 minutes later, position of yellow dot unchanged from (A) notice the very little displacement that occurred, indicates primordium is stalled Time in hours. Scalebar=20microns. (C) 10 hours of the same primordium, displacement is minimal, primordium is still stalled Time in hours. Scalebar=20microns

(D) 15 hours 10 minutes after, total displacement in 15 hours can be computed from the distance of the leading edge of the migrating primordium to the yellow dot Time in hours. Scalebar=20microns. (E-H) live-imaging on control *wildtype* Eya1:mCFP primordium during organ deposition. Yellow dot depicts the position of the leading edge of the migrating primordium timepoint=0, 5h, 10h and 15h time in hours scalebar 50 microns. Notice the large displacement of the yellow dot over time indicating the *wt* primordium traversed a considerable distance over the same time than *k15* mutant.

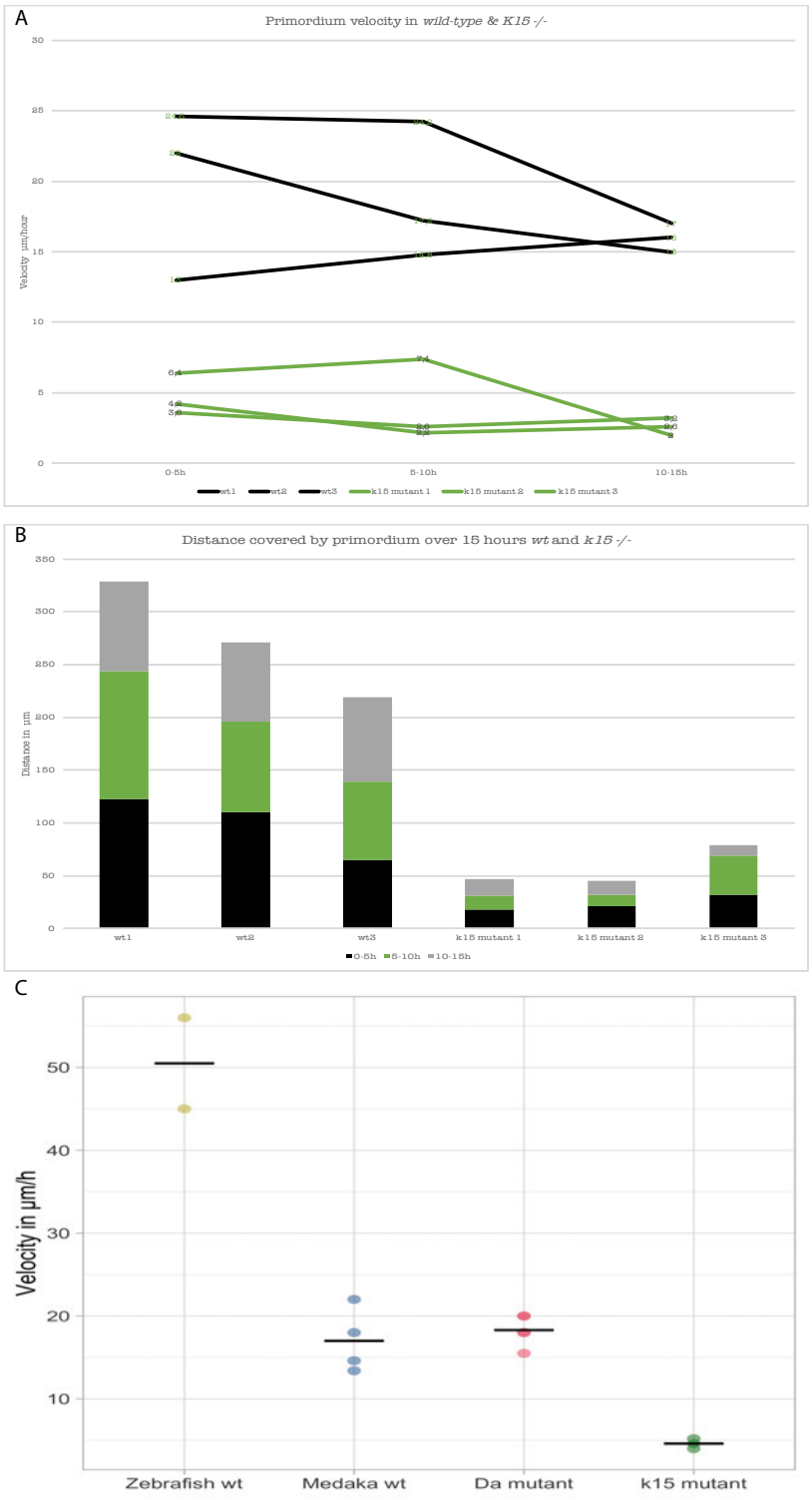

Graph (3) (A) Differences in primordium velocity between wild-type and *k15* mutants over 3 5 hour intervals. Notice the overall velocity is slower in *k15* mutant fish. (B) Distance covered by primordium over 3 5 hour intervals in *wt* and *k15* mutant embryos. Notice the massive difference with *k15* mutants covering a much smaller overall distance that their *wt* counterparts. (C) overall velocity in different teleosts and different genetic backgrounds for Medaka. Notice the almost double velocity of zebrafish primordia compared to Medaka, in addition both primordia are much faster than *K15* mutant primordia.

Pattern defects are extrinsic to the primordium and deposited organs

To definitively prove that defects within the primordium itself or the deposited organs themselves are not accounting for the observed perturbation in *pLL* pattern formation in *k15* mutants I decided to perform transplantation of *k15* mutant cells in *wildtype* fish and vice-versa. These transplantations show that the presence of a majority of *k15* mutant cells in a deposited organ does not prevent its proper positioning, arguing that the defect observed cannot be due to the presence of mutant cells within the deposited organs (Figure 13 A-B'' this transplantation was performed by Oui Pui Hoang a rotation student in the lab at the time and imaged by myself). The opposite transplantation of *wt* cells in a *k15* mutant background revealed that the presence of a vast majority of *wt* cells in a deposited organ is not able to rescue the positioning defect (Figure 12 C-E). Both transplantations provide strong evidence that the observed defects in *pLL* pattern are extrinsic to the primordium or deposited organs and in all probability come as a consequence of mutant epithelial layers. This places epithelial layer structural integrity and mechanical tension as important candidates in the possible modulation of lateral line patterns.

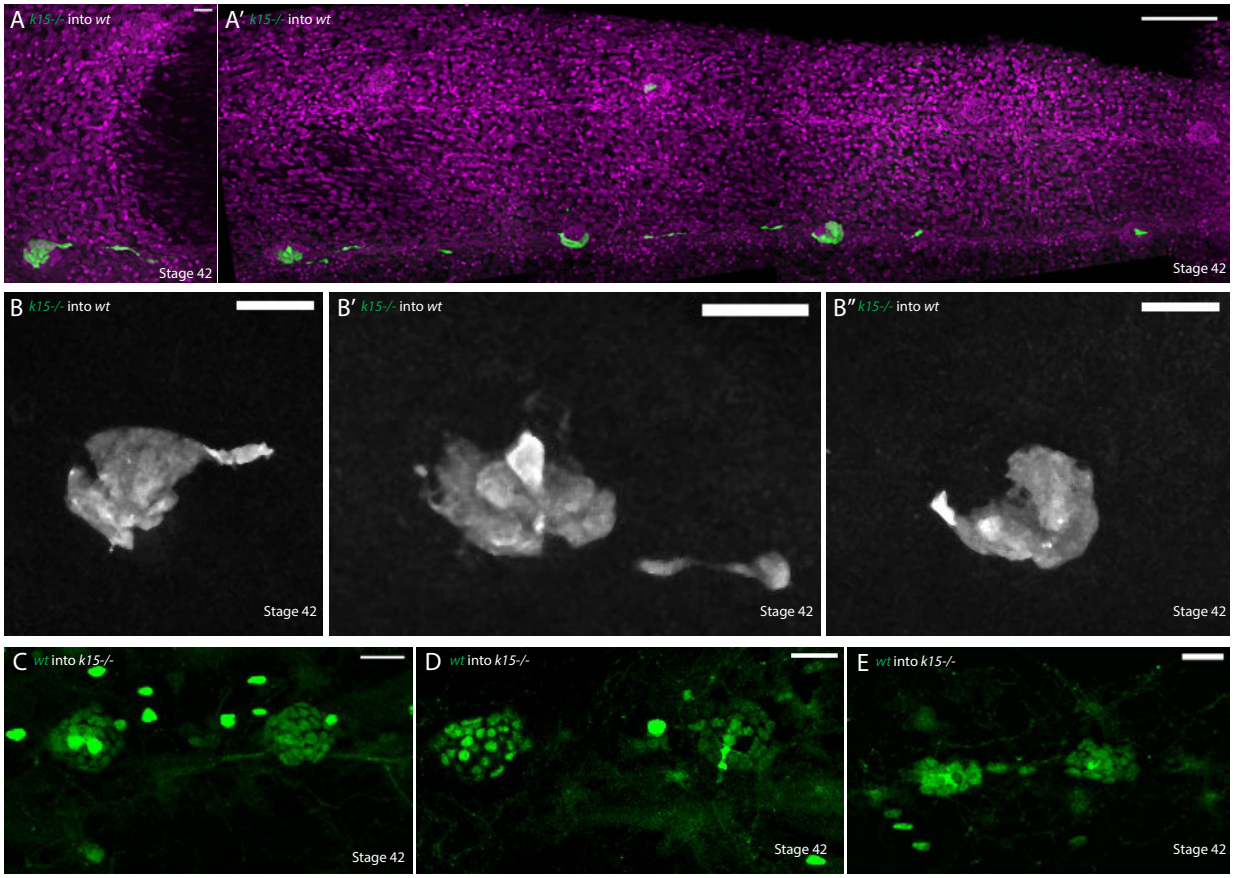

Figure (13) neuromast organ mis-positioning defect caused by mutant epithelium(A) *K15* mutant Tg(Eya1:GFP) cells transplanted into a cab *wild-type* background. Notice that even in organs where the majority of cells are mutant the organ is still able to specify correctly to the ventral side. Immunostaining GFP in green, DAPI in magenta. N=6 fish in total n>12 mosaic organs, zigzag pattern largely normal, mosaic organs can migrate normally to ventral side, transplanted secondary organs localize to correct place and overall neuromast positioning and numbers are as in *wts.* Confocal imaging for figure done by myself, in this particular transplantation was performed by a rotation student in the lab Oui Pui. Scale bar= 20 microns A' 100microns A'. (B-B") Zoom in on organs from (A) where the majority of cells in the neuromast are mutant for K15 (Eya1:GFP) Organs specify correctly to ventral side. Scale bar 20 microns. (C-E) opposite transplantation of wt H2B-GFP cells from LoxPout donors into *k15* mutant hosts (some hosts are positive for Eya1:GFP) reveals that the presence of *wt* cells in the majority of cells of the neuromast organ cannot rescue the migration defect, all organs remain stuck in the midline. Strongly arguing that *k15* is not sufficient in primordium or neuromasts to rescue phenotype this strongly points for the defect being caused by the mutant epithelium. N= 3 transplanted fish, 6 neuromast organs with a majority of *wt* cells stuck at midline. Scale bar 20 microns. Anterior=left, posterior= right. Dorsal is up and ventral is down.

Eya1 CRISPR mutant recapitulates known phenotypes & reveals new *pLL* & sarcomere defects

I then turned my attention to other possible mutants that can lead to a perturbation of lateral line pattern formation in Medaka. It has been reported that mutations in *eya1* in Zebrafish lead to a reduced migratory potential of the primordium and a lower number of deposited organs (Kozlowski et al., 2005), but since the pattern in Zebrafish is all organs located at the midline at the end of

embryogenesis I wondered whether *eya1* might play a role in both organ numbers and positioning in Medaka. I therefore generated 3 gRNAs targeting the CDS of *eya1* and injected them in a variety of transgenic lines. I was able to maintain a stable heterozygous *eya1+/-* line. *eya1-/-* mutants are not viable as they die at the end of embryogenesis primarily from failure to swim properly and heart edemas. The *eya1-/-* CRISPR F2 mutants (Figure 15 B) recapitulated known phenotypes from Zebrafish, including otic vesicle mal-formation and patterning defects (Figure 14 A-C magenta arrows for otic vesicle). Crucially the overall size of the embryos was massively reduced compared to *wildtypes* (Figure 14 A). In addition, I was able to observe gross phenotypes not described in the Zebrafish *eya1* mutant but reported to occur in other models. Those included major cranio-facial defects (Abdelhak et al., 1997) , clear sarcomere defects in shape and orientation of muscle fibers (Y.-H. Liu et al., 2009) as shown both in the bright-field overview and by injection of a ubiquitous cyan label mosaically in *eya1* mutants and *wildtype* fish (Figure 14 D-E and H to J). In the context of the *pLL* I observed phenotypes that were unreported in Zebrafish. In the stable mutant line no primordium migration or neuromasts were observed in the *pLL*, therefore it is very likely that *eya1* is involved in correct primordium specification and/or early migration in Medaka. Interestingly, in the injected generation a range of phenotypes was observed in the *pLL*, the strongest of which recapitulated the defects observed in the stable mutants (Figure 14 G). But among the milder effects were failure of primordium migration to the tail and a mis-localization of primordium migration (below mid-line and observed U-turns) (Figure 14 F magenta arrows highlight neuromast organs). This was consistently seen in the initial steps of migration (more

anteriorly) where I could trace the path of the primordium by following the *pLL* nerve. It is possible that the primordium itself is mis-localized and the nerve follows or there is a decoupling of nerve and primordium migration in the *eya1* F0 milder phenotypes. All in all, these results suggest that *eya1* could also be involved in correct primordium migration and sensing directionality as in its mosaic absence the primordia veer ventrally and even lose orientation. With regards to the stable *eya1* mutant, the phenotypes are much more severe than those reported in Zebrafish and include the complete absence of all neuromasts in the *pLL,* massive cranio-facial defects, sarcomere patterning defects and heart edemas, the mutant fish are non-viable.

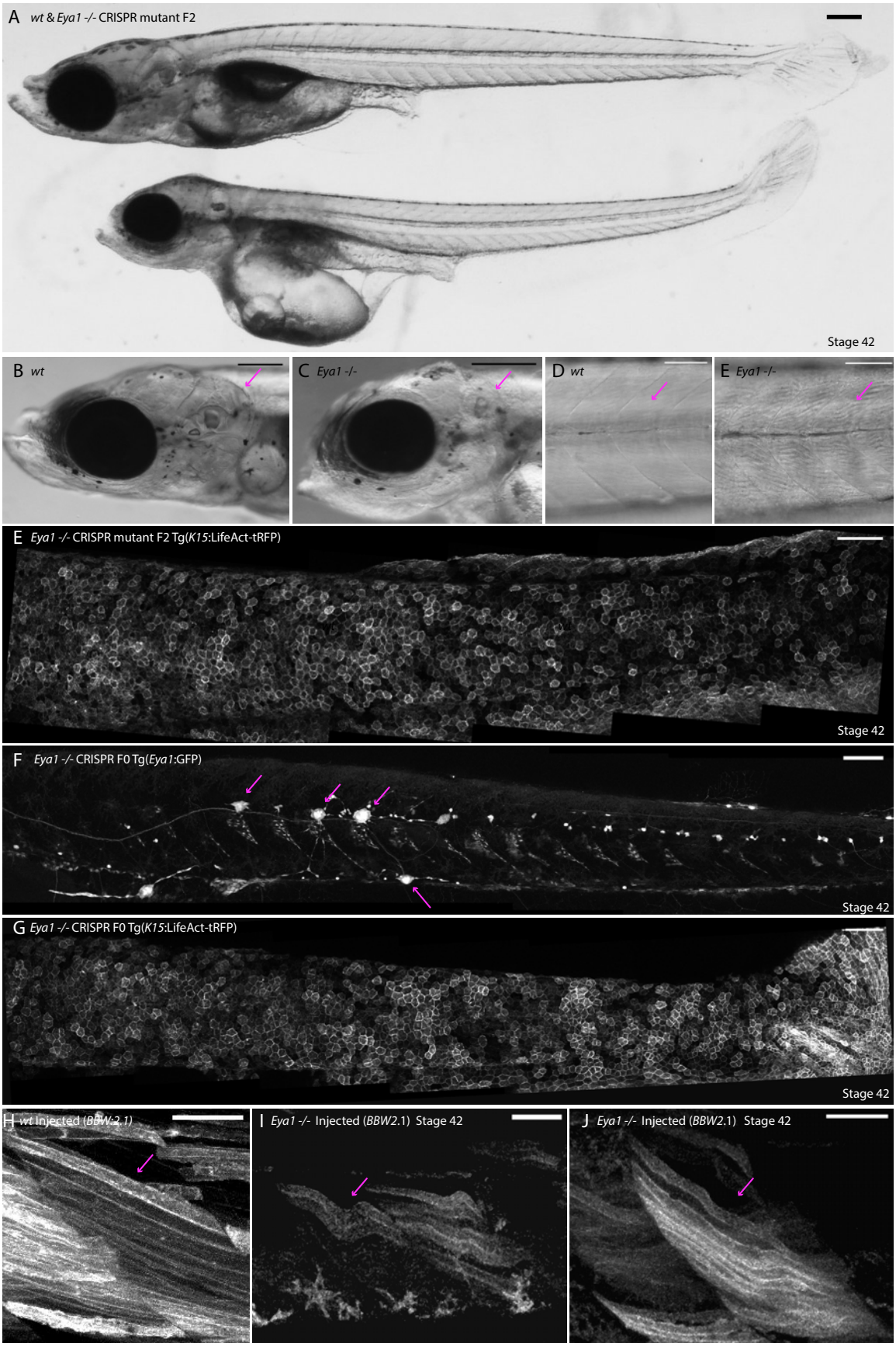
A wt & Eya1 -/- CRISPR mutant F2
Stage 42
B wt
C Eya1 -/-
D wt
E Eya1 -/-
E Eya1 -/- CRISPR mutant F2 Tg(K15:LifeAct-tRFP)
Stage 42
F Eya1 -/- CRISPR F0 Tg(Eya1:GFP)
Stage 42
G Eya1 -/- CRISPR F0 Tg(K15:LifeAct-tRFP)
Stage 42
H wt Injected (BBW2.1)
I Eya1 -/- Injected (BBW2.1) Stage 42
J Eya1 -/- Injected (BBW2.1) Stage 42

Figure(14) Eya1 CRISPR mutants show cranio-facial, sarcomere alignment, pLL migration and overall size defects (A) Above *wildtype* stage 42 embryo, below *Eya1* CRIPSR F2 mutant stage 42. Notice the overall size difference, the smaller craniofacial development of the mutant, Scale bar=200microns. N>20 (B-C) *wt* and mutant cranio-facial zoom in shows the difference in organization, notice the massive reduction of the otic vesicle (magenta arrows). Scale bars 200 microns. N>20 (D-E) *wt* and *Eya1* CRSIPR mutant notice the straight sarcomere organization in the *wt* as compared to the massively perturbed and crooked sarcomere organization in the mutant (magenta arrows). Scale bars 50 microns. N>20 (E) stable *Eya1* CRIPSR mutant line Tg(K15:LifeAct-tRFP) shows the complete absence of all pLL neuromasts and no evidence of primordium migration Scale bar=100microns N>20. (F) Weaker phenotypes in the F0 injected generation consistently showed primordium stalling and interestingly mis-migration (ie not in the midline) magenta arrows for positions of neuromasts Scale bar 100 microns. Tg(Eya1:GFP) n>10 (G) Strong phenotypes in F0 CRISPR injected embryos Tg(K15:LifeAct-tRFP) show complete lack of pLL neuromasts mirroring the stable mutant line. Scale bar 100 microns. N>10 (H-J) Sarcomere defects evident in shape and organization in mosaic brainbow2.1 injected embryos (labels sarcomeres in cyan) . Notice differences in shape and organization of sarcomeres between *wt* and mutant fish (magenta arrows). Scale bar 20 microns. N= 5 mutant fish and 5 *wild-type* fish. Anterior= left, posterior= right. Dorsal= up and ventral is down.

Pattern defects in the *pLL* linked to defective glial cells in a variety of F0 CRISPR models

Looking for more ways to perturb the lateral line pattern in medaka fish I focused my efforts on the known role of glial cells in maintaining organ numbers in the *pLL* in check. Absence of glia leads to major increases in neuromast organ numbers in Zebrafish (Lush & Piotrowski, 2014; Lopez-Schier & Hudspeth, 2005) but nothing is known about pattern modulation. I decided to target known regulators of glial cell development and/or maintenance (Lyons & Talbot 2015; Jessen & Mirsky 2005) via CRISPR. The following genes were selected, *ngn1*: responsible for specifying sensory ganglia that glial cells depend on for migration (Andermann et al., 2002; Gilmour et al.,2002), *foxd3*: an early marker of glial cells (Gilmour et al., 2002) and *erbb3a/3b*: essential genes for Schwann cell development and migration (Lyons et al., 2005). The designed gRNAs were only injected in F0 fish due to time and space limitations for raising mutant lines (as such the analysis should be treated with caution) and the results obtained were quite interesting. For the *ngn1* F0 CRIPSR this led to a massive increase in organ numbers but interestingly a consistently observed phenotype was organs stuck in the mid-line (Figure 15A). *foxd3* CRISPRed fish showed a similar phenotype however there was no increase in organ numbers, only that the majority of organs were stuck in the midline

(Figure 15 B). For *erbb3a/3b* CRISPR F0 fish showed strong phenotypes (almost 40% of all injected fish) in the *pLL*, where it was common to observe failure of primordium migration to the tail and organs stuck in the midline (Figure 15 C). The strongest phenotype of the *erbb3a/3b* injections included a complete failure of primordium migration (Figure 15 D), this is quite surprising as Zebrafish mutants do not show similar phenotypes (Lush & Piotrowski, 2014) and *erbb* signaling is not known to be important for primordium specification or migration. The results strongly argue for a role of glial cells in correct organ positioning in Medaka, since the shared phenotype among all different regulators was that primary organs were stuck in the midline. I also decided to make use of the dorso-ventral patterning *Da* mutant in medaka that has "a mirror-image duplication across the lateral midline in the dorsal trunk-tail region" (Ohtsuka et al., 2004) due to the inactivation of zic genes (Ohtsuka et al., 2004; Moriyama et al., 2012), this results in viable fish with two mirror-imaged ventral sides. And I wondered whether there could be a perturbation of lateral line pattern formation in these fish as well. Indeed, by analyzing fish at stage 42 I could observe that primary organs can end up in the induced ventral side or the normal ventral side (Figure 15 E yellow arrows) but that in 80% of all lateral lines analyzed one or more primary organs remained stuck in the midline (Figure 15 E magenta arrows). To investigate the role of glial cells in correct organ positioning and numbers further I generated a new transgenic line using the Zebrafish *sox10* promoter driving mCherry. This led to the labeling of glial cells not only in the *pLL* (Figure 15 F magenta arrows) but all over the peripheral nervous system of Medaka. And I aimed to further use this line to study the role of glia in the context of *pLL* pattern formation in Medaka.

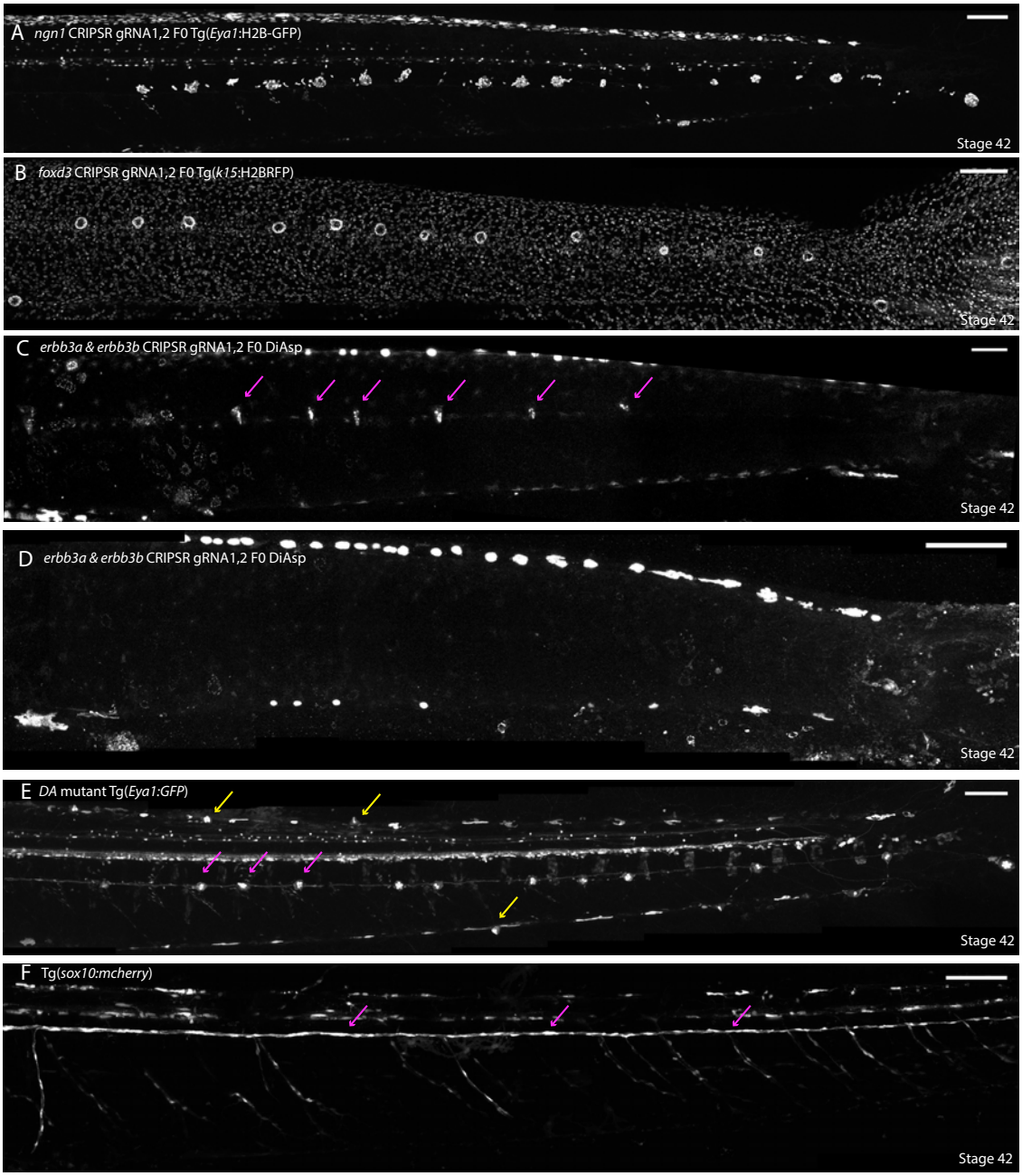

Figure (15) perturbing glial cell migration and differentiation leads to pLL organ positioning defects. (A) F0 CRIPSR on *ngn1* using 2 gRNAs injected in Eya1:H2BGFP fish leads to an increase in number of organs in the pLL but crucially organs also fail to properly locate and remain in the midline. Phenotype with *ngn1* crispants is rare 10/100 injected fish exhibit pLL defects of increased numbers or organ mis-positioning. Scale bar 100microns. (B) F0 CRISPR on *foxd3* using 2 gRNAS injected into k15:H2B-RFP leads to organs failing to locate properly but no apparent increase in organ numbers, phenotype is rare only around 5/100 injected fish show defects in pLL pattern scale bar =100 microns. (C) *erbb3a,3b* CRISPR 4 gRNAs injected into cabs followed by DiAsp staining to locate neuromasts, around 40% of all injected fish show defects in pLL pattern with most common phenotype being organs stuck in the midline (magenta arrows) and failure of primordium migration to caudal fin (C) and in stronger phenotypes (D) primordium fails to deposit any organ scale bar 100 microns. (E) *Da* mutant with duplicated ventral side shows organs locating to normal and induced ventral sides (yellow arrowheads) whilst most organs remain stuck in the midline (magenta arrows). Scale bar 100 microns. (F) Tg (*sox10*:mcherry) labels glial cells at the end of embryogenesis along the pLL nerve (magenta arrowheads) scale bar =100 microns n>10. Anterior is to the left, posterior is to the right. Dorsal is up and ventral is down.

Normal number & pattern of *pLL* neuromasts despite loss of nerve & glia

Since it is known that glial cells migrate on the lateral line nerve and concurrently with the primordium (Lush & Piotrowski, 2014) I aimed to decouple primordium migration from glial cell migration this time using non-genetic laser ablation tools. I reasoned that removing the *pLL* nerve might prevent glial migration, since it was shown in Zebrafish that the presence of the nerve is essential for glial cell migration (Gilmour et al., 2002). I therefore ablated *pLL* nerves in 3-4 dpf embryos during primordium migration using the Eya1:mCFP line (Figure16A-B). The first surprise came after observing that the *pLL* nerve fails to regenerate or regrow in Medaka unlike the situation in Zebrafish. Even more unexpectedly both organ numbers & positions were completely normal in the absence of the pLL nerve (Figure 16 C-D). This is particularly strange since similar experiments in Zebrafish lead to massive increases in *pLL* neuromasts precisely because of the failure of glial cell migration. The results suggest that either glial cells can migrate independently of the nerve in Medaka or they are dispensable for correct organ numbers and positions in the *pLL* (this would argue that defects in the genetic backgrounds described previously could be due to indirect developmental problems or earlier effects of these genes). To test whether glial cells can migrate in the absence of the *pLL* nerve in Medaka, I ablated the nerve in *sox10*:mcherry fish, however glial cells cannot migrate further than the tip of the *pLL* nerve as is the case in Zebrafish (Figure 16 E). These results are contradictory but could point to the presence of an undescribed cell-type that is *sox10* negative in Medaka & that is able to maintain organ numbers and positions, the alternative explanation is that glial cells are dispensable for correct organ numbers and positions in the *pLLs* of Medaka.

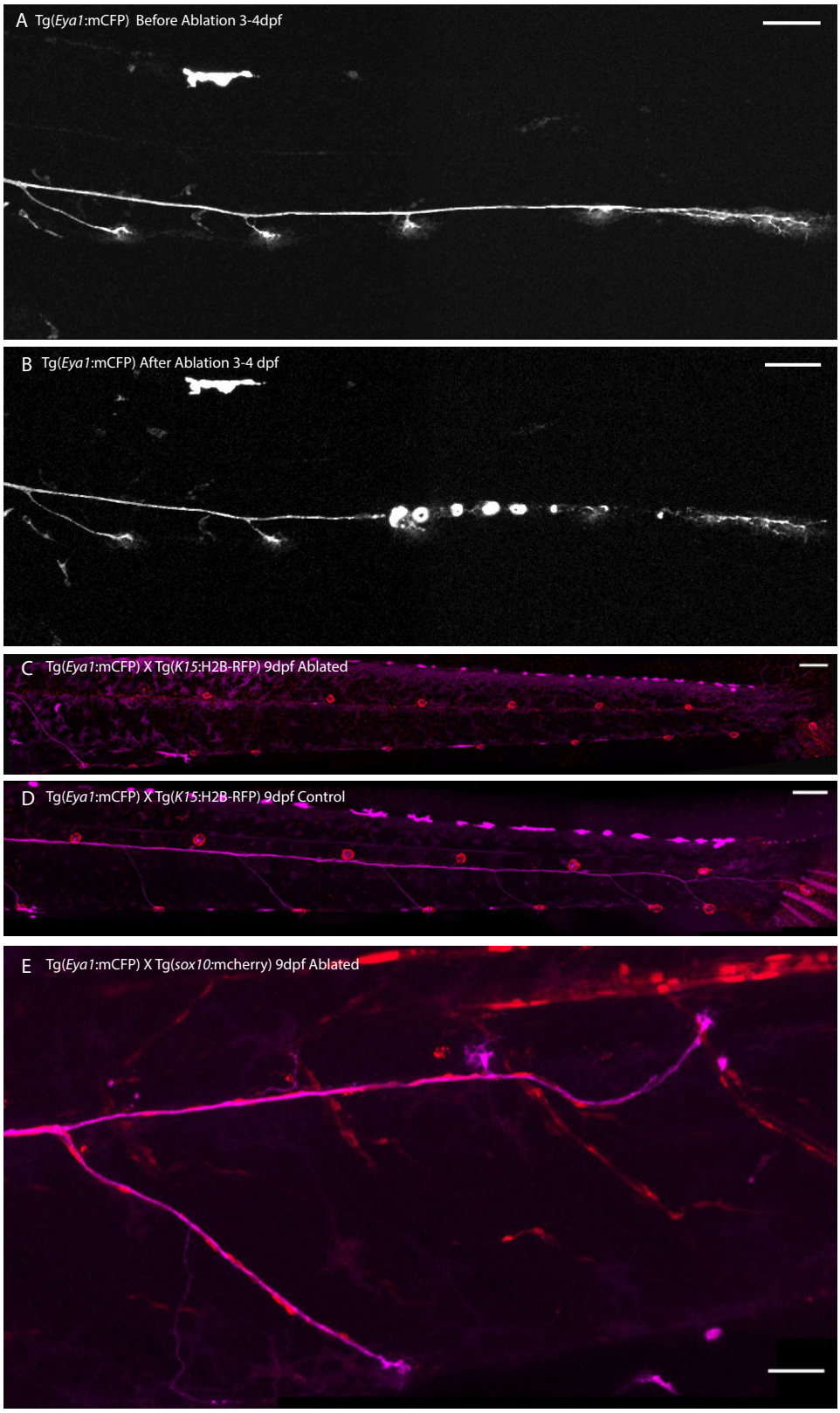

Figure (16) Normal pattern and number of neuromast despite loss of nerve and glia (A) 3-4dpf Eya1:mCFP medaka embryo before MP ablation, primordium is migrating and a few organs have been deposited Scalebar=100microns. (B) 3-4dpf Tg(Eya1:mCFP) medaka embryo after MP ablation, pLL nerve ablated while neuromasts are maintained intact and uninjury Scalebar=100microns (C) Pattern and number of neuromast organs are normal despite failure of pLL nerve to regrow Tg(Eya1:mCFP)X Tg(k15:H2B-RFP) 9dpf Scalebar=100microns. (D) control unablated Tg(Eya1:mCFP)X

Tg(k15:H2B-RFP) 9pdf embryo Scalebar=100microns. 11 fish ablated during embryogenesis and studied at hatch (and 9 days post hatch) (E) Tg(Eya1:mCFP) X Tg(Sox10:mcherry) 9dpf embryo notice that the glial cells are only present where the nerve is present, glial cells do not seem to be able to travel without the nerve connection. Scalebar=100microns. Anterior is to the left, posterior is to the right. Dorsal is up and ventral is down.

Organ and glial cell behavior in *Da* mutants during *pLL* pattern formation

I was interested in the behaviour of individual organs in the case of the *Da* mutants and therefore decided to take a 4D live-imaging approach to understand better the organ level decisions and how they are made in these mutants. This led to the realization that within the same side of the fish deposited neuromast organs can behave as autonomous units going to the new ventral side, the normal ventral side or getting stuck in the midline (Figure 17 A-C'''). These results suggest the presence of either a chemokine attractive signal on ventral sides or an exclusionary signal from the midline, these possibilities will be dealt with in further detail in the discussion section. On organs that remain stuck in the midline they usually undergo 'yo-yo' like movements (initially specifying ventrally then moving dorsally then moving ventrally again ending up in the midline) suggesting their position is being 'fought over' (Figure 17 C-C''') and ruling out the possibility of a passive ventral movement of primary organs occurring in the *wt.* I next wondered whether the *Da* mutant could harbour some defects in glial cell positioning or numbers and this might explain the contradictory movements of primary organs, for this I live-imaged *wt* and *Da* mutant fish with glial cells labelled by the *sox10*:mcherry. This led to the observation that while glial cells consistently travel with the primary organ nerve connections (Figure 17 D magenta arrows) the situation in the *Da* is more varied with some primary organs showing no concomitant glial cell migration on their nerves (Figure 17 E) (it should be pointed out that I have observed a number of primary organs in *Da* mutants that did

contain glial cells migrating with the nerve 2/7 organs). These results suggest that glial cell distribution differences between *wt* and *Da* mutants during organ formation could be of functional relevance in the positioning of neuromast organs, alternatively this could also not be a causal relationship but simply a correlation that goes awry in the *Da* mutant. Next I checked the overall number and distribution of glial cells in *Da* mutants and *wt* at stage 42. And while overall glial cell numbers are comparable (Graph 4), the distribution of *sox10+* cells appeared to be different in the *Da* mutants with glial cell clusters a common phenotype (Figure 17 F-G magenta arrows). This is an interesting observation but whether it is of any functional relevance in terms of neuromast organ positioning (*i.e* linking glial cells clusters to primary organs stuck in the midline) remains to be investigated and will require iterative live-imaging of both processes (neuromast positioning and glial cell clustering) with an earlier glial cell marker.

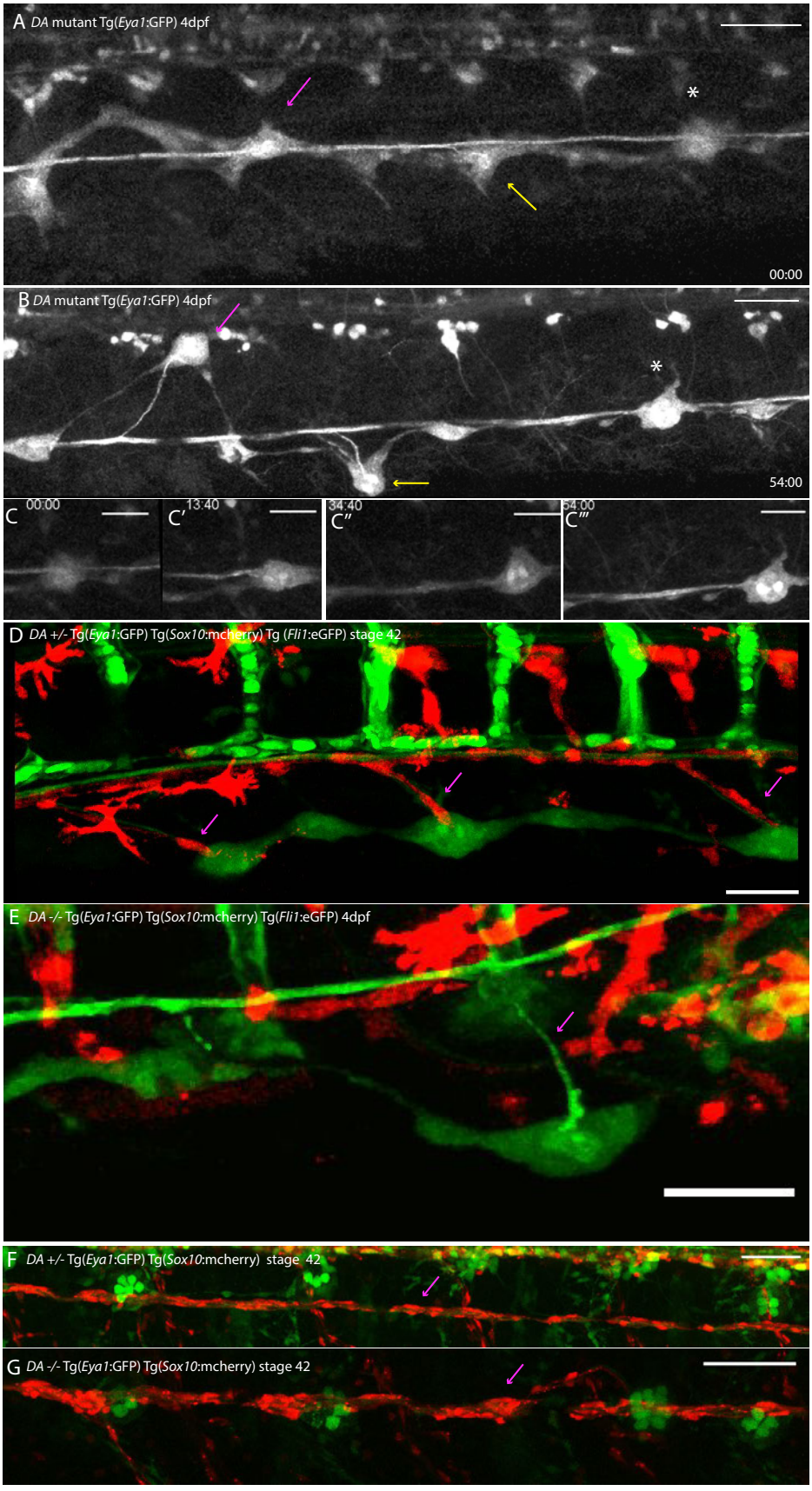
A DA mutant Tg(Eya1:GFP) 4dpf
00:00
B DA mutant Tg(Eya1:GFP) 4dpf
54:00
C 00:00
C′ 13:40
C″ 34:40
C‴ 54:00
D DA +/- Tg(Eya1:GFP) Tg(Sox10:mcherry) Tg (Fli1:eGFP) stage 42
E DA -/- Tg(Eya1:GFP) Tg(Sox10:mcherry) Tg(Fli1:eGFP) 4dpf
F DA +/- Tg(Eya1:GFP) Tg(Sox10:mcherry) stage 42
G DA -/- Tg(Eya1:GFP) Tg(Sox10:mcherry) stage 42

Figure(17) *DA* mutant live-imaging reveals plasticity of precursors and differences In glial cell clustering(A-B) Live-imaging on *DA* mutant Tg(Eya1:GFP) during pLL organ deposition 4dpf reveals the autonomous nature of precursor clusters, notice the difference in behavior with organs moving to the induced ventral side (magenta arrow) the regular ventral side (yellow arrow) and crucially organs that remain stuck in the midline (white asterisk) scale bar 50 microns time in hours. N=5 fish (7 confocal 2 spim (C-C''') Zoom-in on neuromast stuck in the midline (white asterisk in A,B) shows the initial ventral specification followed by dorsal movement of the organ followed by a ventral movement once more to settle in the mid-line, this yo-yo like behavior is common in the majority of stuck organs. Scale bar 30 microns.(D) *DA* heterozygote Eya1:GFP Sox10:mcherry Fli1:eGFP 4dpf shows that *sox10+* glial cells are present on the pLL nerve and also on the ventral connections of primary organs (magenta arrowheads) scalebar=30 microns. (E) DA mutant shows a lack of *sox10+* glial cells on the migrating primary organ (magenta arrow). This phenotype was commonly observed in *DA* mutant organsN=3 fish 5 organs, however in a few cases migrating glial cells following the nerve can be observed in *DA* mutant primary organs. (F-G) *sox10+* glial cell distribution between heterozygote carriers and *DA* mutants at stage 42 reveals that the clustering of cells is different, with more pronounced clusters consistently observed in *DA* mutants Scale bar =100 microns. N= 5 heterozygotes and 7 *DA* mutants. Anterior is to the left, posterior is to the right. Dorsal is up and ventral is down.

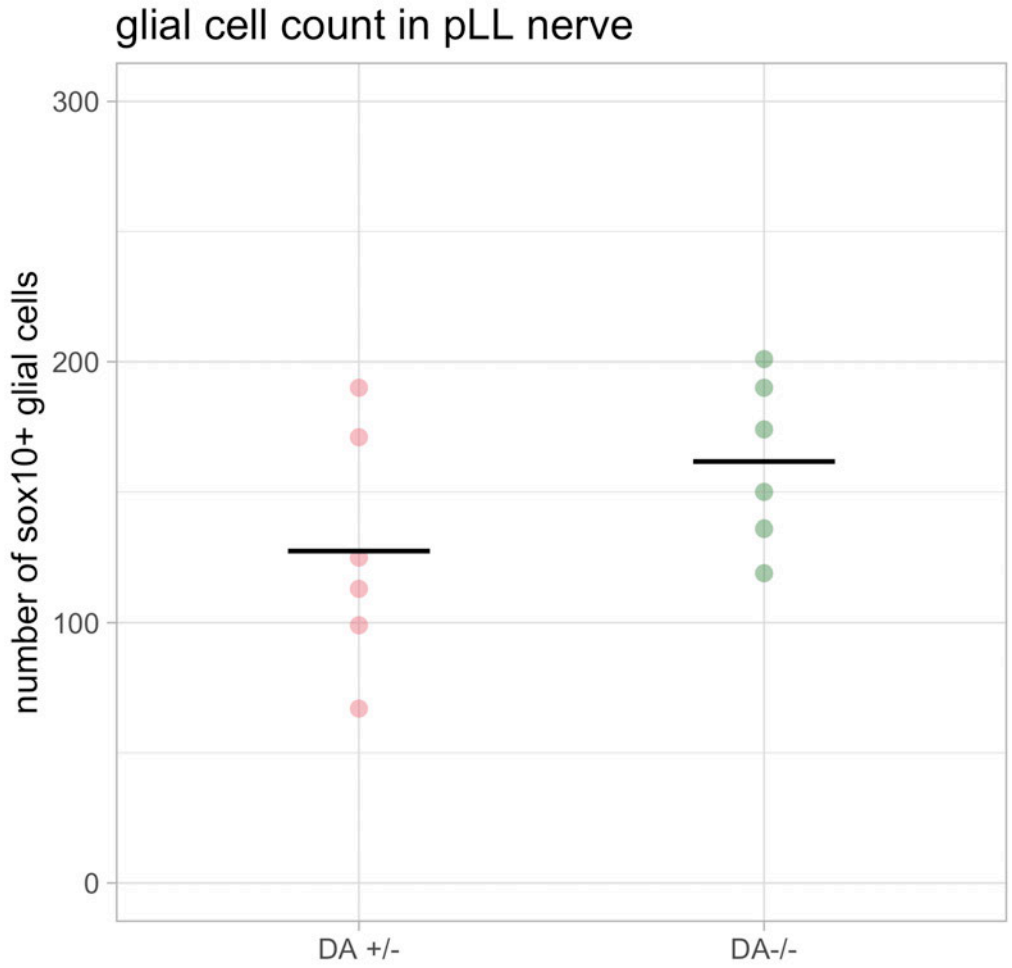

Graph (4) No significant difference in total numbers of *sox10* glial cells between heterozygotes *&* *DA* mutants . Two tailed t-test assuming unequal variance =0,16 no significant difference in numbers of *sox10* cells.

Primordium output not significantly altered in *k15* & *Da* mutants despite strong pattern defects

To close this section of the results I wanted as a last experiment to assess whether both *k15* and *Da* mutants had a difference in overall output of neuromasts in the

pLL at the end of development from the *wildtype*. (Graph 5) shows that while there are slight differences, these are not significant between both mutants and the *wildtype*. What is also obvious is that the variance in organ numbers in the mutants is consistently wider than in the *wildtype* (for the *k15* mutant this might be due to the composite allelic nature of the mutant). These results strongly suggest that neuromast positioning is a distinct feature that does not depend on organ numbers or primordium output. Interestingly it seems there is a range of outputs of Medaka *wildtype* primordia that gets even more varied in both mutants.

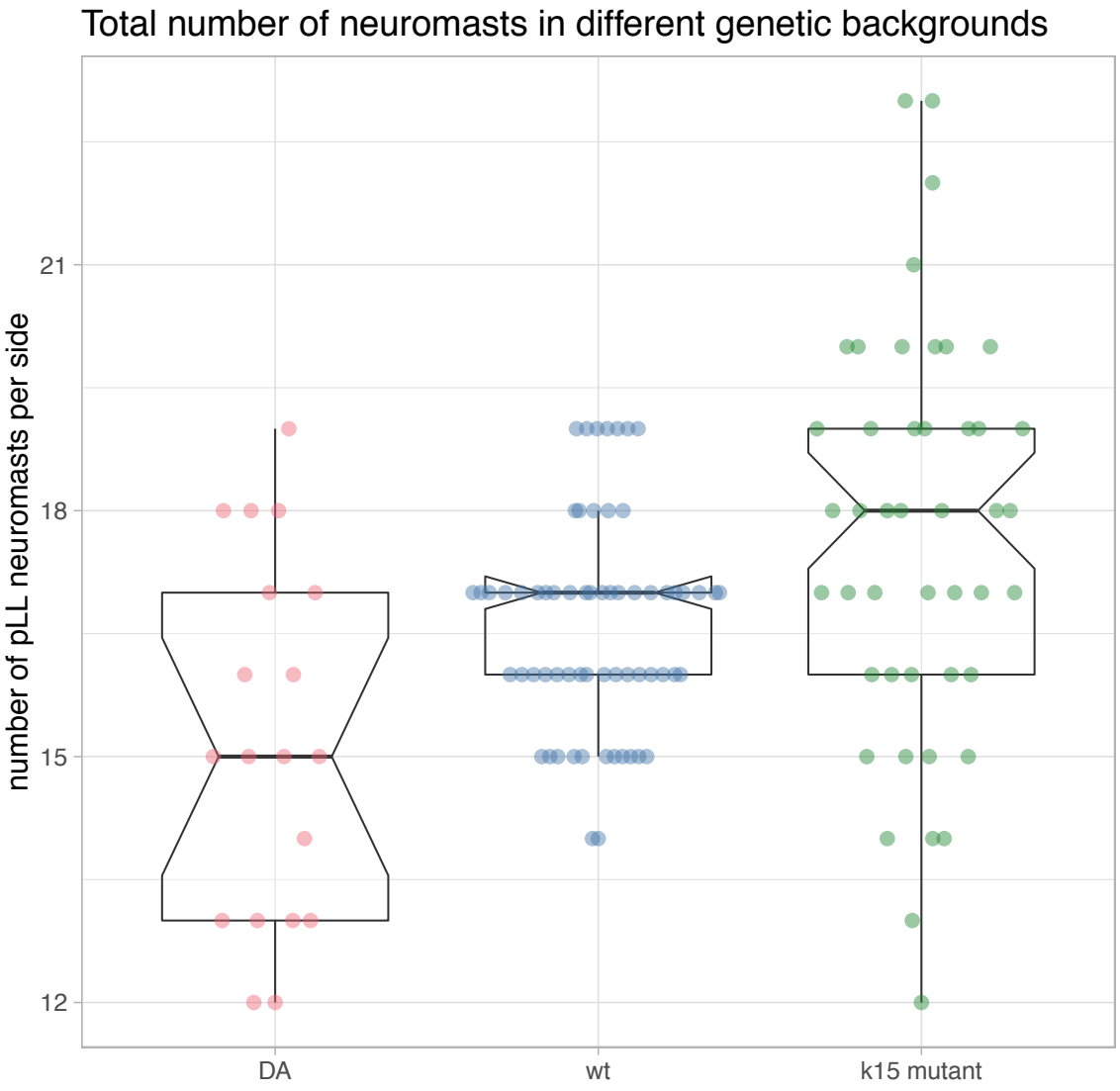

Graph (5) Total number of neruomasts in different genetic backgrounds reveals no big differences despite very strong organ positioning differences between all 3 genotypes. Notice also the increase in variability of organ numbers in the mutant conditions compared to the more constancy of the wild-type, a feature predicted to happen by Conrad Waddington.

The next section deals with post-pattern formation, namely neuromast organ differentiation and maintenance. The following figures and figure legends are directly adapted from (Seleit et al., 2017b) and were written by myself. Any panels or experiments carried out by students under my supervision or other members of the Lab are duly noted at the end of the figures

Tissue-specific labels for different cell types in mature neuromast organs

In order to characterize the stem cells in charge of long-term maintenance of neuromasts it was imperative to generate cell type specific labels. I have been directly involved in generating and characterizing the following lines that label hair cells and inner support cells (Eya1:EGFP) (Figure 18A), mantle and support cells in addition to the suprabasal epithelium (neurom K8:H2B-EGFP) (Figure 18B) and specific mantle cell label in addition to basal epithelium (K15:H2B-RFP) (Figure 18C). With these tools at hand, double and triple transgenic fish were generated to understand the 3D dimensionality of the organ and its constituent cell organization (Figure 19). This revealed the highly organized bundle of hair cells projecting towards the outside are protected by the cell membranes of mantle cells, while the support cell population sits directly underneath the hair cells. All cell-types were recognized both by known markers and known location and morphology from previous work in a variety of model organisms.

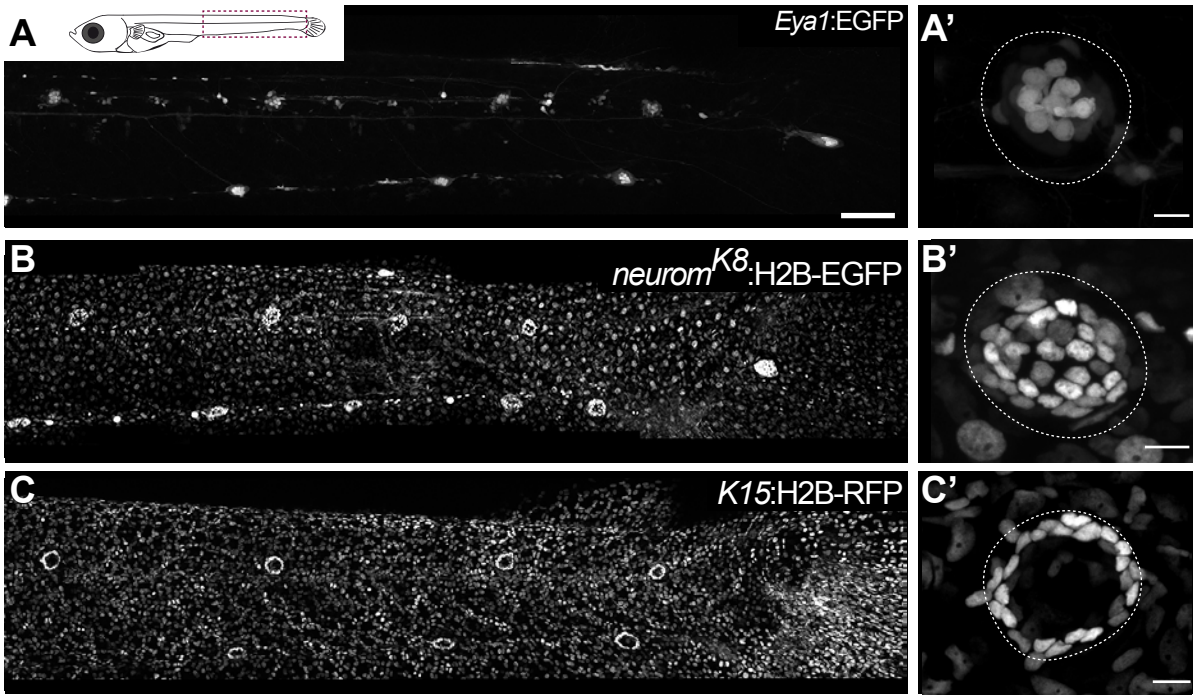

Figure (18) Specific transgenic lines label mantle, support and hair cells in mature medaka neuromasts. (Seleit et al., 2017b)"Tg(Eya1:EGFP) allows visualisation of all neuromasts along the pLL (A), and labels hair cells and internal support cells (A') (N=>20 neuromasts in >10 larvae). The enhancer trap neurom^{K8} line labels skin epithelia (B) and mantle and support cells of a mature neuromast (B') (N=>20 neuromasts in >10 larvae). Tg(K15:H2B-RFP) also labels skin epithelia all over the body surface (C), but RFP expression in mature neuromasts is restricted to mantle cells (C') (N=>10 neuromasts in >10 larvae)." Figure and figure legend adapted from (Seleit et al.,2017b. The K8 transgenic line (B) was injected by Elizabeth Amborosio. Anterior is to the left, posterior is to the right. Dorsal is up and ventral is down.

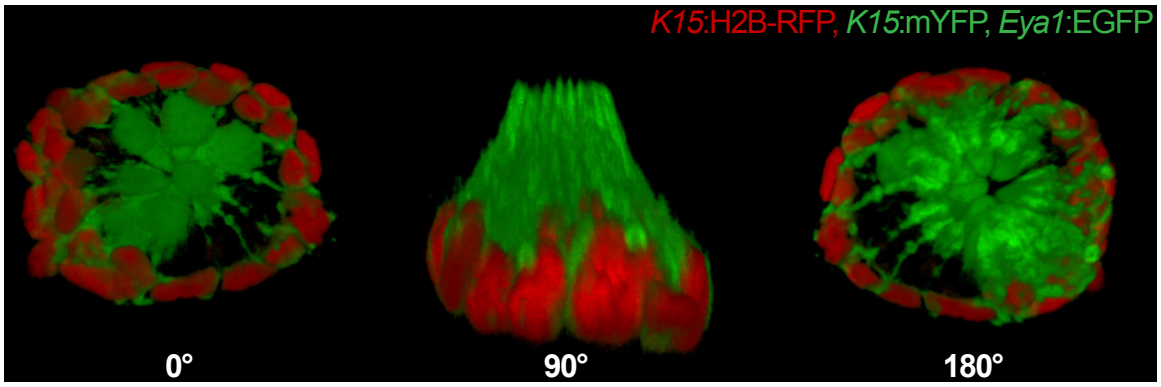

Figure(19) "A 3D reconstruction of a mature neuromast (E) of the triple transgenic line Tg(K15:mYFP)Tg(Eya1:EGFP)Tg(K15:H2B-RFP) of an early juvenile. Six neuromast hair cells (green bundles) project outwards, surrounded by a ring of mantle cells (red nuclei and green membranes) that encapsulate the hair cell bundles in a cupula-like structure (N = 6 neuromasts in two larvae). Scalebars are 100 mm for entire trunks (A, B, C) and 10 mm in neuromast close-ups." Figure and figure legend adapted from (Seleit et al.,2017b).

nBCs surround the neural lineage of Medaka neuromasts

While performing immunohistochemistry stainings on neuromasts of the K15:H2B-eGFP we noticed the consistent presence of a ring of elongated DAPI

stained nuclei that tightly wrap around the mantle cell layer (Figure 20 A-B). These cells had been undescribed before in the literature but appear both by organization and shape to be part of the neuromast organ, we termed them nBCs (neuromast border cells). To understand the structural relationship between the nBCs and the rest of the neuromast organ better we performed electron microscopy on fixed neuromasts. This showed the direct connection of nBCs to mantle cells of the neuromasts, and the presence of cellular protrusions both from the nBCs to the mantle cells and vice-versa (Figure 20 B-C''). When we looked at developmentally younger neuromasts that had just formed we were able to observe that nBCs were *k15+* and that only as the neuromast matures do nBCs lose their *k15* expression (Figure 20D). This suggested that the origin of nBCs could have been either from the *k15+* epithelium or the *k15+* mantle cell population or their precursors. All in all, this discovery led to a new proposed neuromast organ model where hair cells were surrounded by support cells which were in turn en-sheathed by a layer of mantle cells, and those mantle cells were tightly connected to the nBCs (Figure 20E).

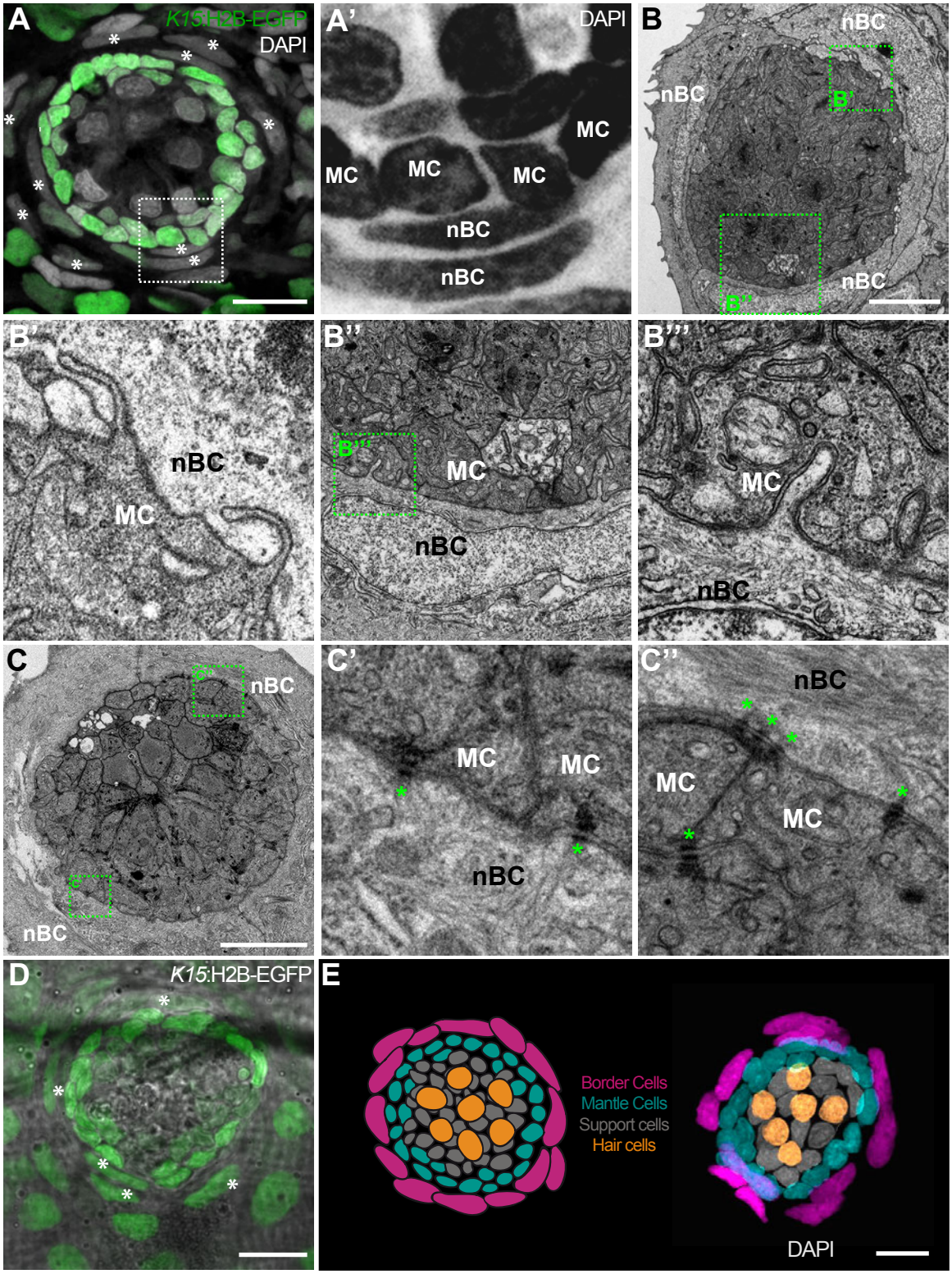

Figure (20) nBCs surround mantle cells in mature neuromasts.(Seleit et al.,2017b) "Early juvenile neuromasts from Tg(K15:H2B-GFP) show mantle cells (green in A, 'MC' in A') that are closely surrounded by elongated nuclei (border cells, nBCs) visualised by DAPI (white asterisks in A, 'nBC' in A') (N=>10 neuromasts in >5 larvae). DAPI is shown in grey (A) and black (A') to enhance contrast. Electronmicroscopy reveals that nBC and K15 +mantle cells are in close contact (B–C") (N = 6 neuromasts in four fish). (B) Overview of a mature neuromast where mantle cells are surrounded by three

nBCs. (B'–B''') Zoom-in panels from figure (B) reveal a close association between MCs and nBCs that includes cytoplasmic protrusions of each cell type into the other (B'–B''') (N = 6 neuromasts in four fish). (C) An upper section on a neuromast where mantle cells are surrounded by two nBCs. The darker dots (green asterisks) are cytoplasmic plaques of desmosomes formed between mantle cells and nBCs (C', C'') (N = 2 neuromasts in one fish). (D) A younger neuromast than the one depicted in (A) from Tg(K15:H2B-GFP) shows that nBCs are also labelled with GFP (white asterisks in D) (N=>10 neuromasts in >5 larvae). (E) Pseudo-coloured DAPI neuromast and scheme depicting the four cell types observed in every mature neuromast organ. Hair cells are shown in yellow, support cells in grey, mantle cells in green and border cells in magenta. Scalebars are 10 mm." Figure and figure legend adapted from (Seleit et al.,2017b). The panel in (A) was generated by Lazaro Centanin on a transgenic line I formed and characterized. All EM data panels were generated by the EM facility at the university of Heidelberg. Panel in (D) was generated by Lazaro Centanin in a transgenic line created and characterized by myself. (E) the pseudo-colored neuromast was generated by Elizabeth Amborosio a co-author on the manuscript.

Mantle cells are neural stem cells under regenerative conditions

With the double and triple transgenic ready I now had the tools to address and characterize where the stem cells of neuromast organs reside. Specifically, I exploited a regenerative approach to understand whether mantle cells (which were proposed to be the stem cells but never formally proven to be in other neuromast models) (Ghysen and Dambly-Chaudiere, 2007; Pinto-Teixeira et al., 2015) can act as neural stem cells. To do this I relied on a laser ablation model with the help of Nico Dross from the Nikon imaging facility using K15-H2BRFP X Eya1:GFP fish. There we were able to ablate all cells within the neuromast with the exception of a few mantle cells (Figure 21 A-B') and asked whether these cells will be sufficient to regenerate all the neural lineage cell types within a neuromast organ. But initially I wanted to probe whether an efficient regenerative response can even be triggered in Medaka neuromasts, since it has been recently shown that the regenerative potential of Medaka is more limited than that of Zebrafish in a variety of tissues (Lust & Wittbrodt, 2018 ; Ito et al. 2014; Lai et al. 2017). Medaka efficiently regenerated all the injured neuromasts in a short time frame (Figure 21 C-D). Already 48-hours post injury one can observe the coalescence of surviving mantle cells (Figure 21 C), this resembles closely what I report happening during

secondary organ formation of neuromasts under physiological conditions. These *k15+* mantle cells are weakly positive for *eya1* and could as such be reverting to an earlier developmental stage (possibly inter-neuromast cell-like). 6-days post ablation mantle, support and hair cells are regenerated and the neuromast grows in size, the patterning and organization within the organ appears to be normal (Figure 21 D). Since this happens in a relatively short period of time support cells still are positive for k15:H2BRFP (this could also be due to the rather long half-life of H2B-RFP). In conclusion with as few as 4 surviving mantle cells after injury, neuromasts can regenerate efficiently in Medaka. This proves that under regenerative conditions mantle cells can act as neural stem cells. This combined with long-term lineage tracing data from Isabel Kraemer (Seleit et al., 2017b) proves that mantle cells are stem cells both during regeneration and under homeostatic conditions.

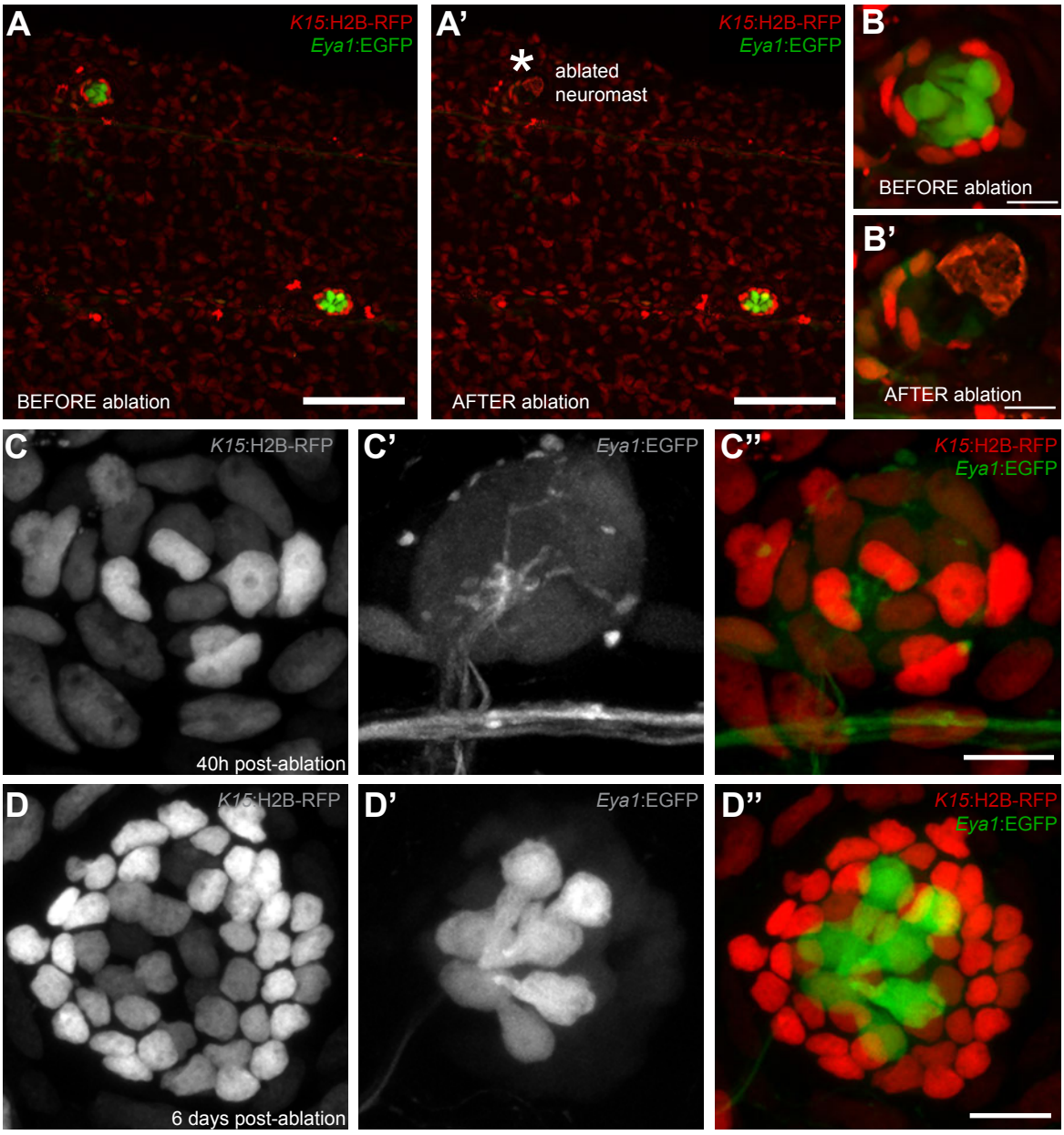

Figure (21) Mantle cells regenerate support and hair cells and act as stem cells under regenerative condtions(Seleit et al.,2017b) "Two photon ablation on neuromasts of the double transgenic Tg(K15:H2B-RFP), Tg(Eya1:EGFP) at 12 dpf. (A–B'). Ablations were done to remove most cells in the neuromasts, sparing a few $K15^{+}$ cells (B'). The same neuromast shown 40 hr post- ablation reveals a small cluster of RFP +cells that have coalesced around the site of injury without any apparent differentiation (C–C''). Six days post-injury all cell types within the neural lineage have been reconstituted (D–D''). Mantle and support cells can be observed in K15:H2B-RFP (D, D''), while hair cells and internal support cells are evident in the Eya1:EGFP (D', D''). (N = 18 neuromasts in four larvae for Tg(K15:H2B-RFP), Tg(Eya1:EGFP)), N = 8 neuromasts in four larvae for Tg(K15:H2B-RFP)($neurom^{K8}$:H2B-EGFP)) Scalebars are 100 mm for trunks (A, A') and 10 mm for neuromasts (B–D'')." Figure and figure legend adapted from (Seleit et al.,2017b).

Epithelial cells induced by the arrival of neural stem cells to become nBCs

We had previously described the existence of a new cell-type (nBCs) in mature neuromasts but their developmental origin remained unclear. The two realistic possibilities were that they were derived from the migrating primordium tissue or that they had a primordium independent origin. To address the cellular source of nBCs I relied on a highly spatially and temporally resolved 4D SPIM imaging approach. Almost 3 days of continuous imaging on K15:H2B-GFP transgenic embryos during secondary neuromast formation revealed the step-by-step process of nBC induction by the neural stem cell precursors (Figure 22 A). Briefly what occurs is that the neural stem cell precursors migrate towards the overlying epithelial cell layer, once in contact this triggers a tight association between the neural stem cell precursors and the overlying epithelial cells. This process continues for almost two days and progressively a number of epithelial cells start a major transformation in shape (elongation) and tightly wrap around the differentiating neuromast organ. Epithelial cells undergoing the induction event can divide to produce two cells with elongated nuclei. At the end of imaging the induced cells highly resemble the nBCs. Therefore, the origin of nBCs is from normal epithelial cells that are induced to become nBCs by the arrival of neural stem cells (Figure 22 A). Mosaic injection of both K15:H2BRFP and K15:mYFP allowed the simultaneous labelling of nuclei and cellular membranes. This combined with immunohistochemistry to amplify the signal allowed us to observe freshly induced nBCs and show that in addition to changes in nuclear shape there are concomitant changes in membrane organization, with membranes becoming highly elongated and showing small protrusions (Figure 22B-B').

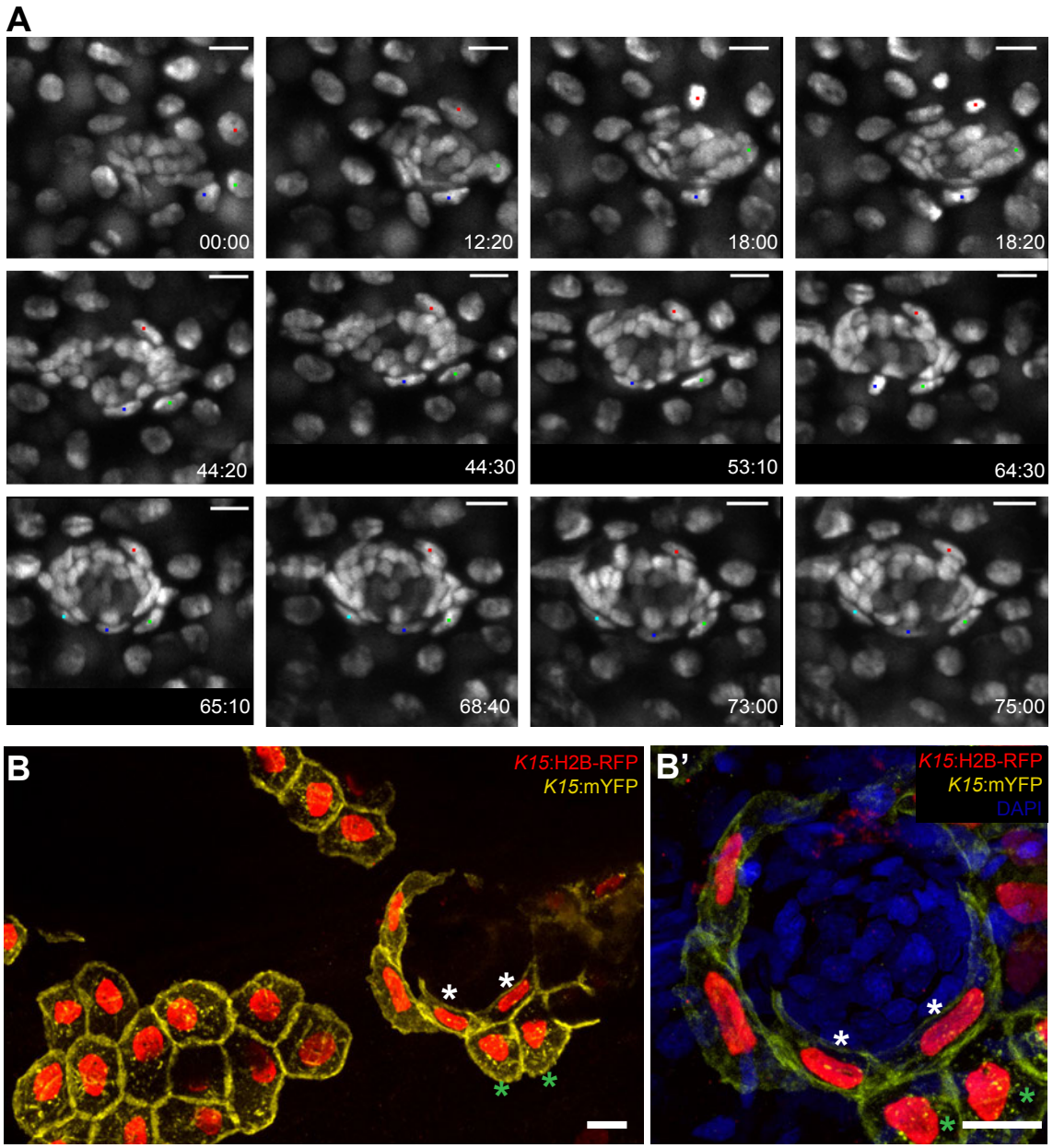

Figure (22) Developmental origin of nBCs by induction from skin epithelial cells. (Seleit et al.,2017b) "(A) Time-lapse imaging of a stage 35 Tg(K15:H2B-EGFP) embryo during secondary organ formation, where three epithelial cells (blue, green and red dots) dynamically associate with the arriving neural stem cells precursors. The red cell divides (18:00 hr to 18:20 hr) to generate one skin epithelial daughter and another daughter that will become a nBC (64:00 hr to 75:00 hr). The green cell transitions into a nBC without dividing, and the blue cell first becomes a nBC (18:20 hr to 43:00 hr) and then divides to generate two nBCs (64:30 hr to 65:10 hr) that stay in the neuromast. The images in (A) are selected time-points from three consecutive movies of the same developing neuromast (five ventral neuromasts and four midline neuromasts in the pLL and two neuromasts in the aLL, N = 5 embryos). (B–B') Immunostaining of a double injected (mosaic) K15:mYFP, K15:H2B-RFP embryo shows that nBC induction involves a drastic remodelling of both nuclear and cellular morphologies (B) (N=12 neuromasts in six larvae). Compare skin epithelial cells (green asterisks in B, B') with their sibling nBCs (white asterisks in B,B') included in the neuromast. Scalebars are 10 mm." Figure and figure legend adapted from (Seleit et al.,2017b). The immunostaining on B-B' was generated by Elizabeth Amborosio in the lab a co-author of the manuscript.

Arrival of neural stem cells is necessary & sufficient for induction of nBCs

At this point it was still unclear whether there were 'hotspots' of epithelial transformation, in other words whether certain epithelial cells were 'primed' to be transformed into nBCs or whether the arrival of neural stem cell precursors was necessary and sufficient to induce the transformation event. To answer this question I generate an *ngn1* CRSIPR F0 mosaic mutant by injecting two guide RNAs and xCas9 into Tg(Eya1:GFP) embryos targeting the endogenous *ngn1* CDS. *ngn1* is known to block the specification of all cranial sensory ganglia (Andermann et al., 2002). Perturbation of the concurrent glial cell migration as the *pLL* primordium is migrating leads to an over proliferation of inter-neuromast cells and a higher number of neuromast organs (Lopez-Schier & Hudspeth, 2005; Lush & Piotrowski, 2014). My injections led to the formation of an ectopic number of neuromast organs in ectopic locations (Figure 23 A) all of which were able to induce their immediate epithelial environment to form nBCs (Figure 23 B-H). This experiment (along with ablation experiments on the primordium) prove that neural stem cell precursor arrival is necessary and sufficient for induction of nBCs.

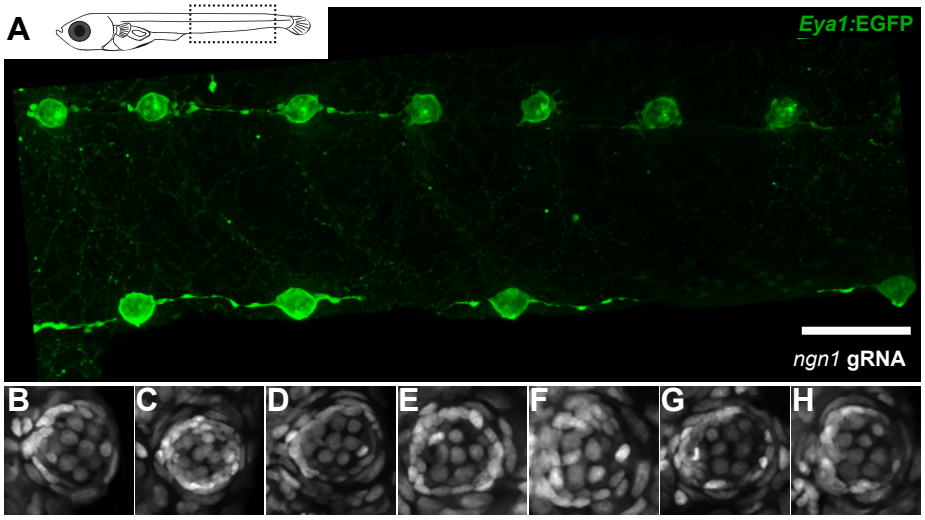

Figure (23) *ngn1* mosaic CRISPR leads to ectopic number of neural stem cells and an ectopic number of neuromast organs. All extra neuromasts do contain induced nBcs as revealed by DAPI stainings. "(A) Anti-GFP staining of a Tg(*Eya1*:EGFP) embryo at stage 42 that was injected with *CAS9* mRNA and *ngn1* gRNAs reveals the formation of ectopic pLL midline neuromasts (N = 58 pLL neuromasts in two larvae). (B–H) DAPI images of seven consecutive midline neuromasts show that all of them contain nBCs." Figure and figure legend adapted from (Seleit et al.,2017b). Anterior is to the left, posterior is to the right. Dorsal is up and ventral is down.

nBCs are conserved in distantly related teleost fish

The discovery of nBCs in Medaka could be a species-specific trait that is of no relevance in neuromasts of other fish species. To check evolutionary conservation of this newly discovered cell-type we performed DAPI stainings on mature neuromast organs in distantly related teleosts (Zebrafish and *Poecilia formosa*). This revealed the presence of nBCs surrounding the mantle cell layer of neuromasts of both species (Figure 24 A-D). Injecting the Medaka K15:H2B-GFP construct in Zebrafish lead to the labelling of the same cell-types as in Medaka, crucially developmentally younger Zebrafish neuromasts contained *k15+* nBCs exactly as I reported for Medaka (Figure 24 E-F). Raising the K15:H2BGFP stable line in Zebrafish allowed dynamic live-imaging which revealed the same induction event of nBCs from the overlying epithelium by the action of neuromast precursor cells. This proves the high evolutionary conservation of this induction event and strongly argues for a presence of a functional role for the nBCs.

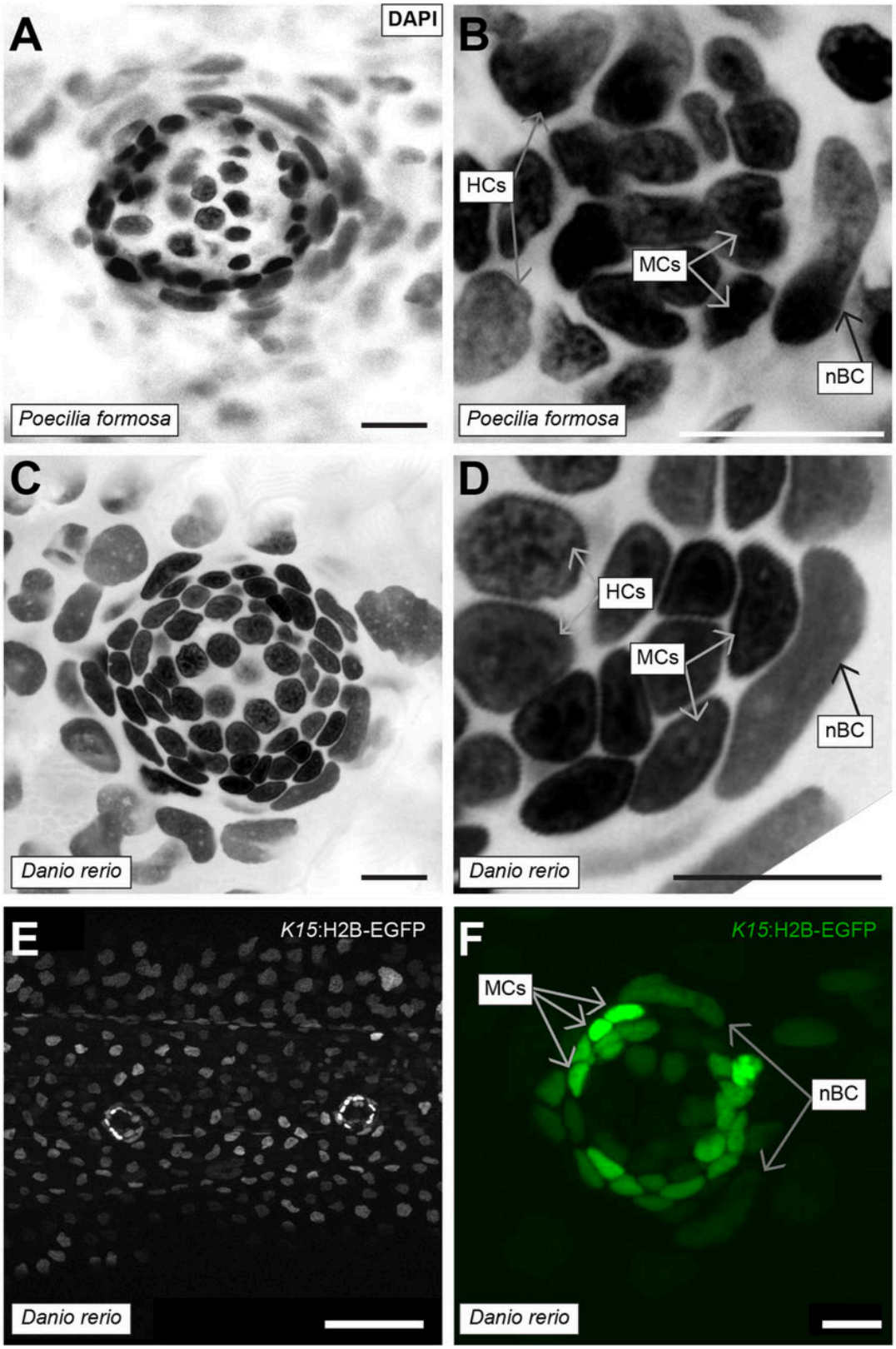

Figure (24) nBCs are evolutionarily conserved. (Seleit et al.,2017b) "(A) DAPI-stained neuromast Peocilia formosa, a close relative of medaka, reveals the presence of nBCs as assessed by their distinct morphology and relative location (N = 10 neuromasts in a single 1 month old fish). (B) Close-up on a Peocilia formosa neuromast reveals that nBCs are immediately adjacent to mantle cells (N = 10 border cells in four neuromasts). (C) DAPI-stained neuromast of Danio rerio, a distant

relative of medaka, reveals the presence of nBCs as assessed by their distinct morphology and location (N=>5 neuromasts in three larvae). (D) Close-up of a zebrafish neuromast reveals that nBCs intimately associate with mantle cells (N=>5 neuromasts in three larvae). (E) Tg(ol.K15::H2B-eGFP) shows labelling of the skin epithelium and mantle cells in a 5 dph zebrafish larvae. (F) Close-up of a Tg(ol.K15::H2B-eGFP) zebrafish neuromast shows labelling of cells within the neural lineage and nBCs (N= 5 neuromasts in three larvae). Scalebars = 10 mm, except in panel E, Scalebar = 100 mm." Figure and figure legend adapted from (Seleit et al.,2017b). Anterior is to the left, posterior is to the right. Dorsal is up and ventral is down.

Ablation of nBCs leads to strong structural integrity defects in neuromasts

To check for a functional role for nBCs within neuromasts was difficult since we did not have a cell-type specific label. Nevertheless, I attempted to address this question on developmentally younger neuromasts in which the majority of nBCs were still *k15+*. I decided to pursue two approaches, one would be to ablate one or 2 nBCs and see the reaction of the neuromast tissue (this was done in parallel by Isabel Kraemer as well), the other was to ablate the majority of nBCs and see the effect on neuromast architecture, regenerative potential and structural organization. Ablating a single nBC led to an immediate recoil of the remaining neuromast suggesting the tissue is held at high tension (Figure 25 A-A'''). The structural organization of the neuromast was affected directly in the area where the nBC was ablated. Ablating the majority of nBCs led to massive defects in the structural organization of neuromasts (Figure 25 B). Six days post injury the regenerating neuromast regained its shape and new nBCs can be seen surrounding the organ (Figure 25 B), their source could have been from surviving nBCs that proliferate or from a new induction event.

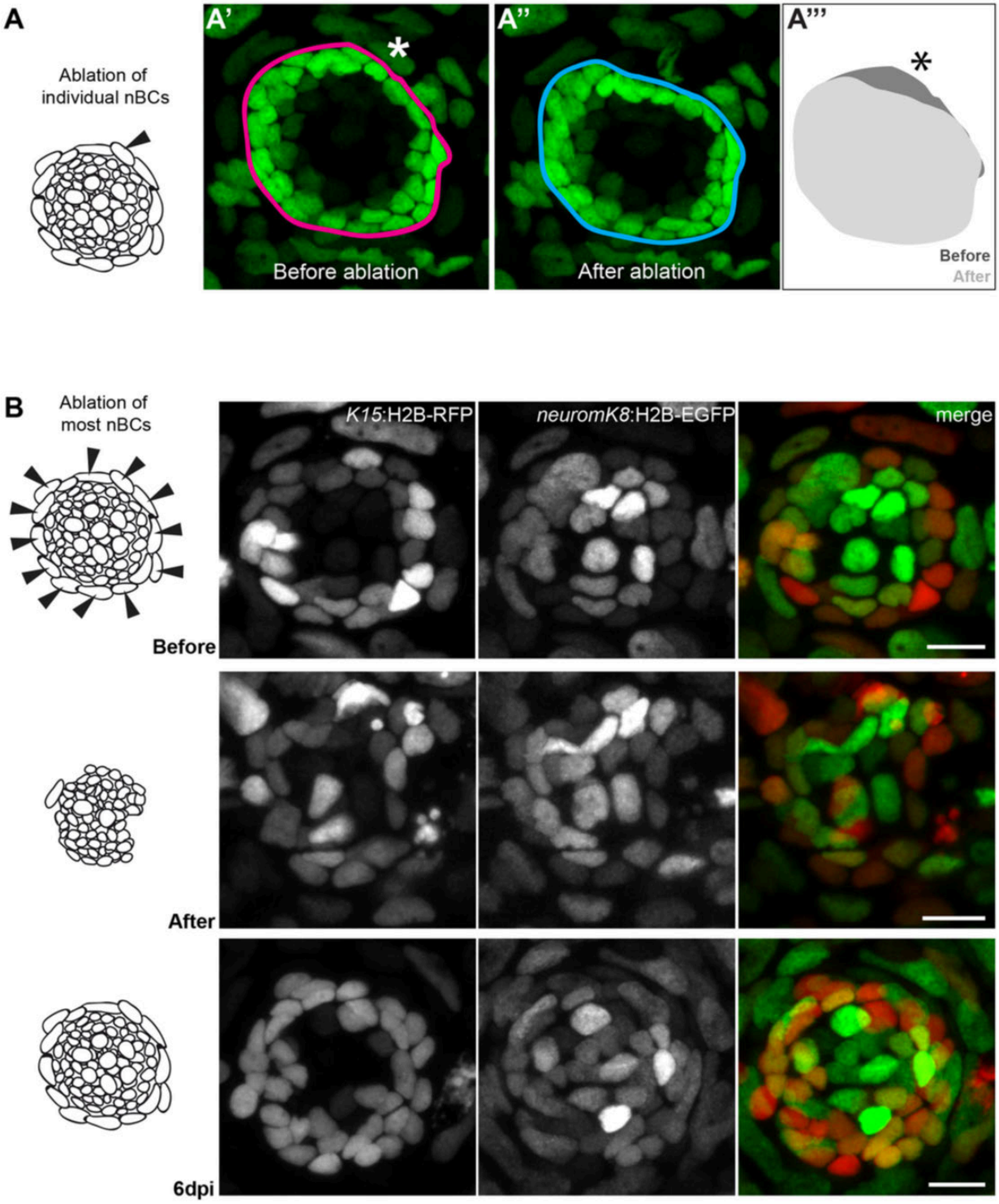

Figure (25) "Ablation of nBCs disrupts organ architecture." (Seleit et al.,2017b) "(A–A'") Ablation of single nBCs in mature neuromasts (stage 39) of Tg(K15:H2B-EGFP) results in a local disruption of the organ architecture near the injury site. Mantle cells retract inwards towards the center of the neuromas resulting in a shape change of the organ (A'") (N = 10 neuromasts in seven larvae.) (B) Ablation of most nBCs in an immature neuromast of a stage 36 double Tg(K15::H2BRFP) (neurom^{K8}:H2B-EGFP) results in a severe disruption of organ architecture. Iterative imaging reveals that new nBCs appear by 6 days post injury and organ architecture is re-established (N = 8 neuromasts in four fish). Scalebars = 10 mm." Figure and figure legend adapted from (Seleit et al.,2017b) A-A'" performed by Isabel Kraemer.

The next section deals with cellular and molecular behavior during post-embryonic neuromast organogenesis, principally in the caudal neuromast cluster (CNC) of Medaka.

Individual cell migration drives post-embryonic neuromast organogenesis in the CNC of Medaka

As fish grow life-long scaling of organs becomes a major issue, since organs need to constantly grow whilst still being functional. Neuromasts have been known to increase number of organs as fish grow (Wada et al., 2008). Here we use the caudal neuromast cluster (CNC) as a minimal model to study post-embryonic organogenesis in Medaka. A mature neuromast consists of three neural lineage cell types (Mcs, Scs and Hcs) that are clonally related (Figure 26 A-A') (Seleit et al., 2017b). At 9dpf the caudal fin neuromast (also known as founder P0 organ) is already differentiated, at this point there is no evidence of any organogenesis (Figure 26B). Observing the same K15:H2BGFP neuromast 10 days later one can clearly see two things A) the original organ has grown considerably in size by adding more cells and B) a new smaller organ appears anterior to the original and is connected to it by *k15+* cells (Figure 26B'). Looking at the same growing cluster 10 days later one can observe that the cluster now contains 3 neuromasts (Figure 26B''). To trace the original steps leading to new organ formation I utilized a more time-resolved approach in which I could observe the polarized migration of individual *k15+* mantle cells outside of the original founder CNC organ at a stereotypic place (Figure 26C). The migrating cells clearly up-regulate *eya1* (as has been previously reported by Isabel Kraemer) and always travel on the *pLL* nerve connection (Figure 26D). One can therefore conclude that new organogenesis (from the founder to the second neuromast organ) depends on individual cellular migratory behaviour that is highly stereotypic and involves

molecular changes to stem cells. This is one of the first reported examples of heterogeneities among stem cells of Medaka neuromasts.

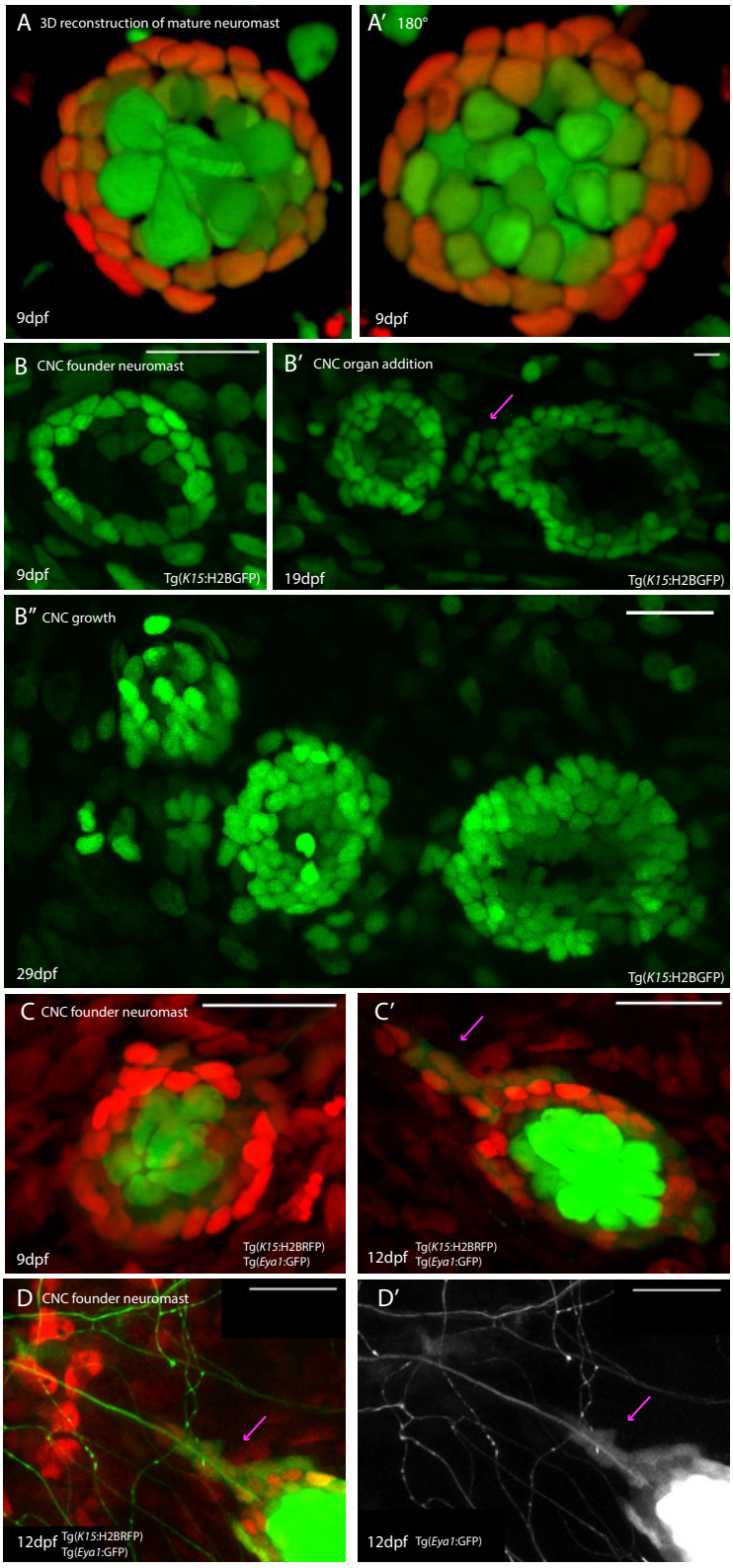

Figure (26) Post-embryonic neuromast organogenesis; building the caudal fin cluster (A-A') A 3D reconstruction of the three neural lineage cell types within a mature neuromast organ in a 9dpf embryo Tg(*Eya1*:GFP) labels hair cells in green, Tg (*K15*:H2BRFP) labels mantle cells in red and Tg(*K8*:H2B-GFP) Labels a proportion of mantle cells and all support cells in green. (B-B') formation of caudal fin cluster (CNC), initial founder neuromast labelled with Tg (*K15*:H2BGFP) prior to any new organ formation. B' Same neuromast organ 1- days later notice the growth in size of the founder neuromast and the addition of a new organ more anterior to it, the new organ is connected by *k15+* cellular bridges to the founder neuromast (magenta arrow) scale bar 20 microns.(B'') same CNC cluster one month later reveals a new addition of an organ more anterior, in total the cluster contains 3 neuromast organs scale bar 50 microns, the cluster will continue to grow as the fish grows, it is typically to see between 6-7 organs in the cluster in an adult 1 year old fish. (C-C') initial steps on new organ formation involves the polarized migration of individual k15+ cells that upregulate *Eya1* expression and start migrating anteriorly Tg (*k15*H2BRFPX *Eya1*:GFP). Scale bar 20 microns N>10. (D-D') in addition to the upregulation of *Eya1* expression the migrating cells invariably migrate on the pLL nerve connection laid down during the initial primordium migration (magenta arrows). Scale bar= 20 microns. N>10. Anterior = left, posterior= right.

Tg(*fat1a*:GFP) is a specific & stable label of interneuromast & mantle cells in mature organs

While trying to molecularly characterize the process of post-embryonic neuromast organogenesis better, I came across an RNA-seq data-set from Zebrafish that showed the cadherin *fat1a* to be highly expressed in Mantle cells (Steiner et al., 2014). I therefore cloned a 2.2kb fragment of the promoter region of the Medaka *fat1a* and cloned it under GFP. The stable line Tg(fat1a:eGFP) labels the migrating primordium, interneuromast cells, primary and secondary organs during the development of the *pLL* (Figure 27 A-C). Interestingly as the organs differentiate I consistently observed what I termed 'exploratory cells' outside but connected to neuromast organs (Figure 27 D), these cells are highly dynamic and continue to 'probe' their immediate environment (their origin could be in part from INCs). As the organs terminally differentiate the *fat1a* expression becomes restricted to the mantle cell population as assessed by morphology and position (Figure 27 E-H). This new transgenic line therefore constitutes a specific label for mantle cells within Medaka neuromasts.

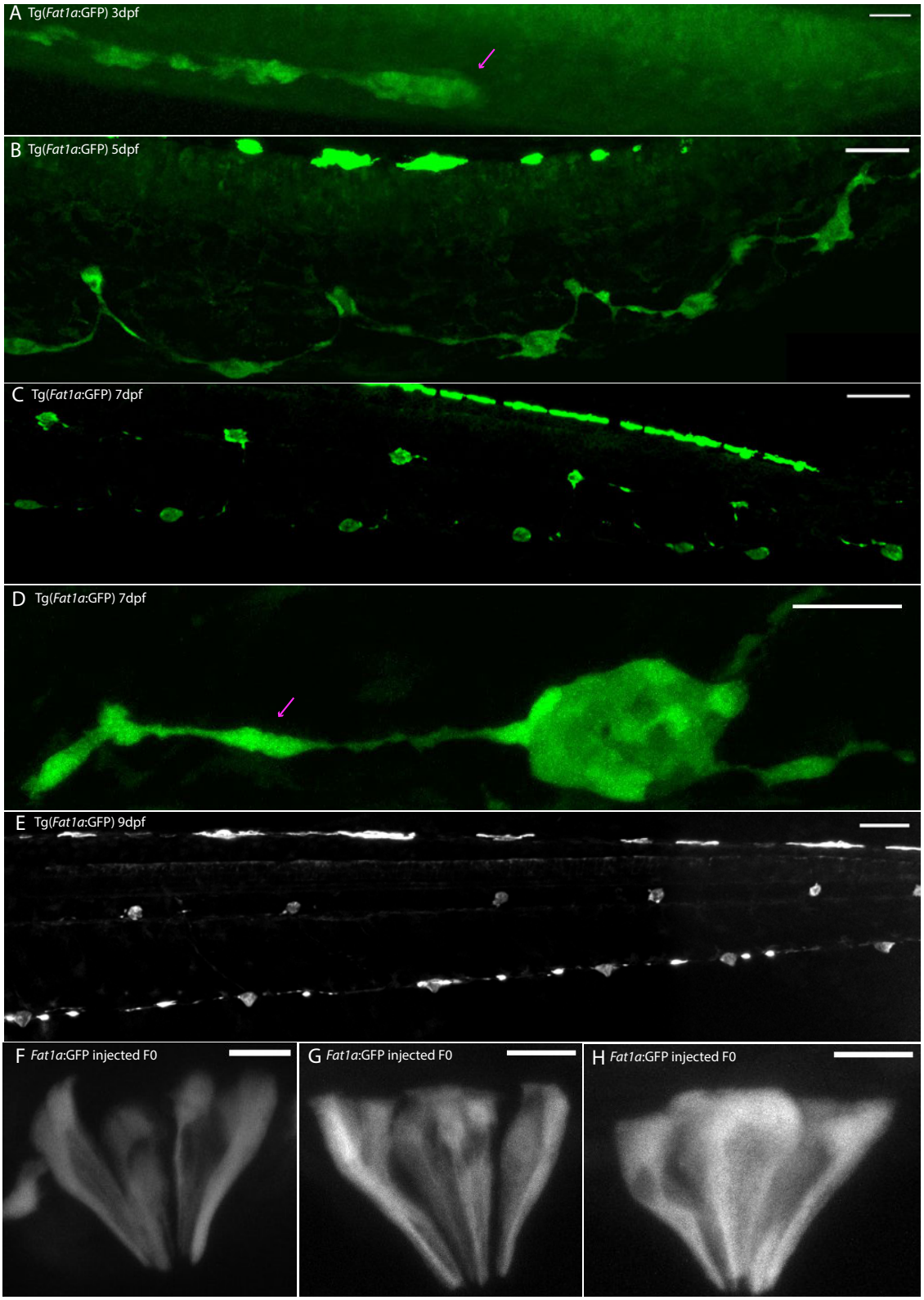

Figure (27) Characterization of fat1a:GFP transgenic line (A) Tg(Fat1a:GFP) labels the migrating primordium and deposited neuromasts at 3 dpf. Scale bar=50 microns. N=6 (B) Tg(Fat1a:GFP) labels primary and secondary organs and inter neuromast celllsat 5 dpf. Scale bar 50 microns n=6. (C) Tg(Fat1a:GFP) labels primary and secondary organs at 7dpf scale bar= 100 microns n=6. (D) at this stage secondary organs extend massive protrusions of individual *fat1a+* high cells

probing in all directions magenta arrows still connected to neuromast scale bar =20 microns. (E) Tg(Fatla:GFP) stably labels primary and secondary neuromasts in 9dpf embryos. Scale bar = 100 microns n>10. (F-G-H) Fatla:GFP injected mosaics show labelled mantle cells as reveal by morphology and position. Scale bar= 10 microns. Ant=left post=right

Heterogeneities in *fatla*:GFP co-relate with differential behavior of neuromast exploratory cells

I was very intrigued by the behavior of the newly identified exploratory cells outside of mature neuromast organs and decided to follow them over time. The first observation is that even as the neuromasts differentiate these exploratory cells remain probing and interestingly have a much higher expression of f*atla:*GFP than cells within the neuromast (Figure 28A-A'). These features are maintained if one looks 7 days later, where *fatla* high exploratory cells are still seen to dynamically move outside the neuromast organ (Figure 28 B-B''). To try to understand better whether there is a preferred positional location of these exploratory cells I looked 10 days later, this time labelling the nerve connection of neuromasts by the Eya1:mCFP line. This led to the realization that *fatla+* high cells specifically coalesce around the nerve connections of neuromasts (Figure 28C-C''). To sum up it seems that *fatla* high exploratory cells outside but connected to mature neuromasts are a stable feature of the organs, these cells start out probing more dynamically and eventually stabilize around the nerve connections over time. The results suggest A) that these cells can sense nerve vs non-nerve and are probably attracted to the nerve connection B) they might be sensing antennas for correct position and conditions for neuromast organogenesis, since new organs must be formed on existing or new nerve connections.

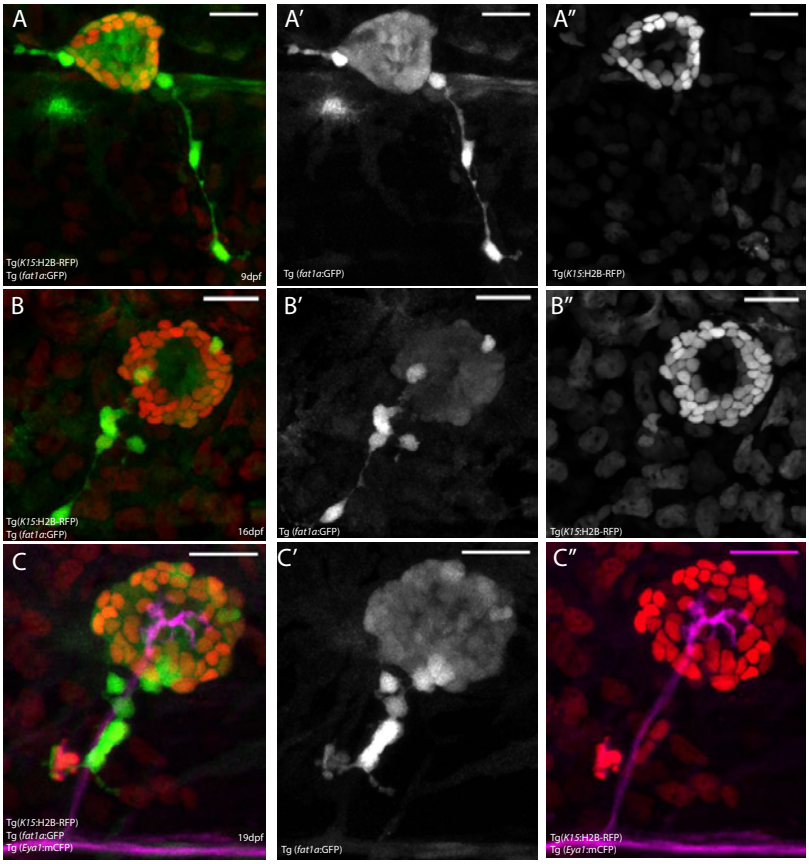

Figure (28) *Fat1a+* high exploratory cells, a stable feature of neuromasts (A-A'') secondary neuromast at 9dpf double labelled with Fat1a:GFP and K15:H2B-RFP. Mantle cells within the neruomasts are labelled with both reporters, notice the high level of expression of exploratory cells that remain outside of the organ but still directly connected to it. Scale bar= 20 microns N>10 (B-B'') same genotype at 14dpf, *fat1a+* high exploratory cells can still be seen outside but connected to the neuromast. Scale bar 20 microns N=4. (C-C'') 19dpf same genotype in addition to Eya1:mCFP notice the presence of *fat1a+* high exploratory cells preferentially where the nerve connection is located. Scale bar=20 microns N=4.

Fat1a:GFP high cells participate in new organ formation in the CNC of Medaka

To investigate whether these newly identified *fat1a* high exploratory cells participate in post-embryonic organogenesis in the context of the caudal fin neuromast cluster (CNC) in Medaka I undertook a time-resolved live-imaging approach to the formation of the first additional organ in the CNC. By following double and triple transgenic fish, I was able to observe that *fat1a* high exploratory cells are already probing outside of the founder neuromast in the absence of any individual cell migration of mantle cells within the organ at this time point (Figure 29 A-A''). At 12dpf one can clearly observe the coordinated individual mantle cell

migration out of the founder organ in an anterior direction. The migrating cells highly upregulate *fat1a* expression and send out protrusions in the direction of migration arguing for an active and guided migratory process. At 19dpf one can clearly observe the formation of a new neuromast more anterior to the founder organ that is still in the process of differentiation as seen by the spread of the *fat1a+* and *k15+* cells to encompass the majority of cells within the organ (Figure 29 C-C''). Since I had already observed that *fat1a* high exploratory cells exist before cell migration begins and that they exist around nerve connections, and since the migratory path of the individual mantle cells that form the new organ is always around the nerve, I decided to ablate all *fat1a* high exploratory cells outside the founder neuromast prior to any cellular migration (Figure 29 D-E). This was done without any injury to the nerve itself or the founder neuromast. The idea was to test whether these *fat1a+* high cells are required for post-embryonic organogenesis in the CNC of Medaka. However, the results showed that these cells are entirely dispensable since correct organogenesis occurred in their absence (Figure 29 F-F''). It is a possibility that the neuromast was able to regenerate lost *fat1a+* exploratory cells or that other *fat1a-* exploratory cells might have aided the process.

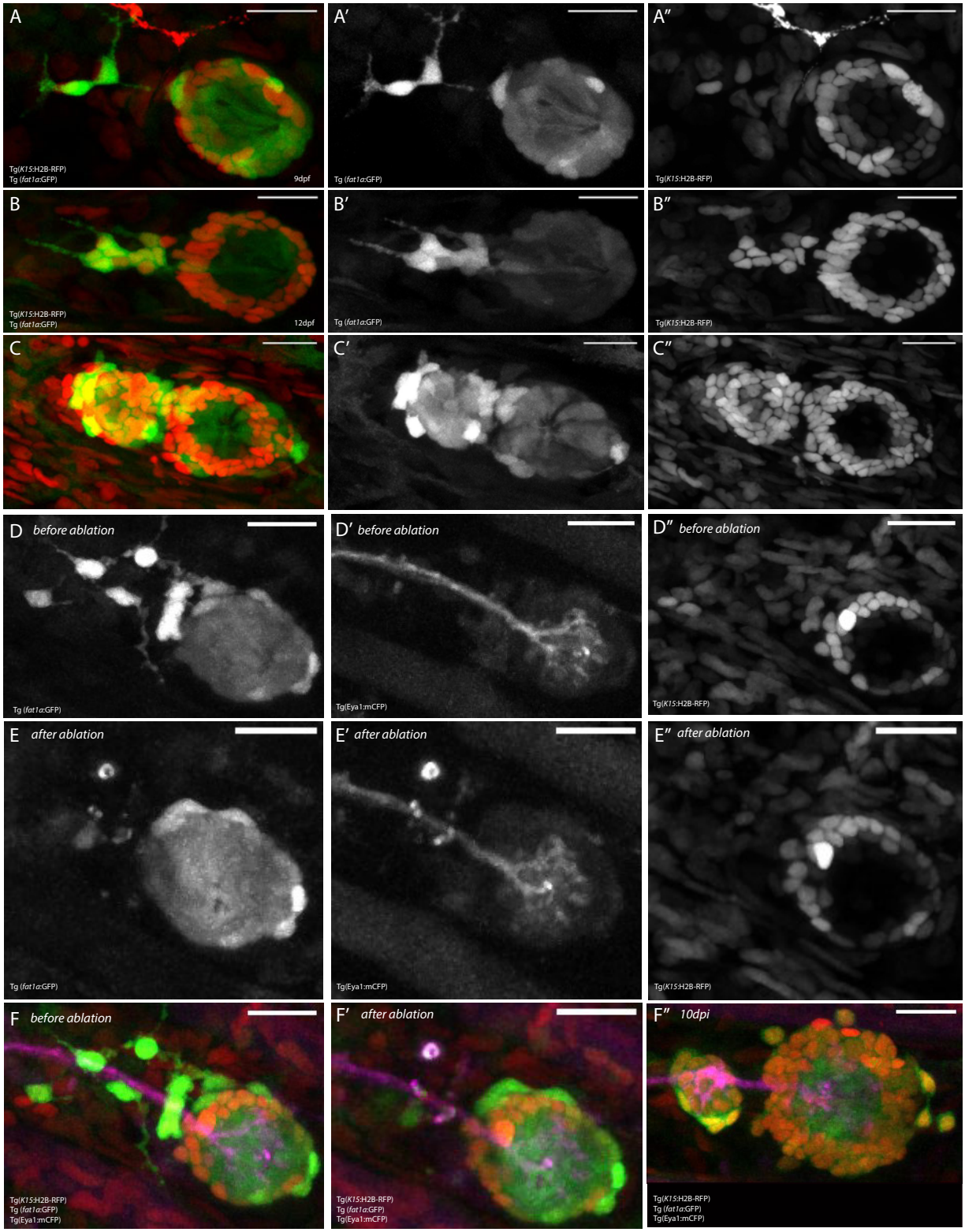

Figure (29) *fat1a* high exploratory cells participate in post-embryonic organogenesis (A-A'') caudal fin neuromast at 9dpf double Tg line fat1a:GFP X K15:H2BRFP. Prior to any cell migration for new organ formation notice the upregulation of *fat1a* in exploratory cells on the anterior edge of the neuromast. Scale bar 20 microns N=5. (B-B'') 12dfp same genotype notice the polarized individual cell migration of *k15+ fat1a* high exploratory cells anterior to start the process of new neuromast organogenesis. Scale bar=20 microns N=5. (C-C'') same genotype 19dpf new organ formation is evident anterior to migration site, notice the presence of high *fat1a* in the new immature organ compared to the founder and the spread of the *k15* label. Scale bar 20 microns N=5.(D-E'') Laser ablation of *fat1a* high exploratory cells before new neuromast

organogenesis begins removes all *fat1a* high cells and leave neuromast and nerve connection intact. Notice the presence of the *fat1a* high cells around the nerve connection. Scale bar 20 microns N=6. (F-F'') despite loss of all exploratory cells a new organ is still able to form in the correct position 10dpi and at the correct time anterior to the founder neuromast Scale bar=20 microns. N=6. Anterior is to the left, posterior is to the right. Dorsal is up and ventral is down.

Robustness of individual cell migration driven organogenesis despite absence of nerve and injury of founder neuromast

At this point I was interested in trying to think of other methods to perturb new organ formation in the posterior cluster CNC. To understand better the guiding principles involved in the highly reproducible and stereotypic trajectories traversed by the cells forming a new neuromast. Since the nerve connection was the position both of individual mantle cell migration and new organ formation I decided to ablate the *pLL* nerve during primordium migration (Figure 30 A-A'). This led to the formation of an entire *pLL* pattern at the end of embryogenesis that was normal in number and organ position (including the CNC founder organ) despite the loss of the nerve (Figure 30 B *&* C-C''). Interestingly and unlike the situation in Zebrafish(Gilmour et al., 2002; Wada et al., 2013) the *pLL* nerve in Medaka never is able to re-grow or regenerate pointing at a deficiency in the regenerative potential of parts of the peripheral nervous system in Medaka. At 19dpf one can clearly observe that the non-innervated organs are still present although they are significantly smaller in size than their innervated counter-parts (Figure 30 B'). This argues for the stabilizing role of the nerve connection on neuromast organization and cellular number distribution. Interestingly the CNC founder organ, despite not being innervated at any point during its formation is able to correctly form hair cells (Figure 30 C-C''). Even more surprisingly the original organ is able to form a completely new neuromast that is both correctly localized and contains hair cells at the right timing (Figure 30 D-D''), meaning that

the nerve connection is entirely dispensable for the formation and positioning of the new neuromasts in the CNC of Medaka. This is in complete contrast to the situation in zebrafish where innervation is essential for new neuromast organogenesis (Wada et al., 2013a). The decision to form a new organ therefore could be intrinsically driven, to test this possibility I decided to challenge a founder neuromast already containing polarized individual cells migrating to form a new organ by ablating its posterior half. The idea was to observe whether we can influence the cellular behavior of the individual migrating mantle cells, in other words will they participate in regenerating the founder neuromast they originally came from or will they continue organogenesis regardless. The results (Figure 3OE-E'') clearly show that the decision to form a new organ seems to be not readily reverisble since even after ablating half of the founder neuromasts, individual cells continue migrating outwards and do not contribute to the regeneration of the original founder neuromast. This founder neuromast 'fixes' the situation by scaling down in size (and presumably will then grow further once more). These results demonstrate how robust the correct formation of neuromasts post-embryonically is despite a variety of challenges, the system seems heavily 'coded' to produce this outcome, and I could not stop it from occurring. The results suggest that cells can take certain trajectories that in some cases are not easily reversible.

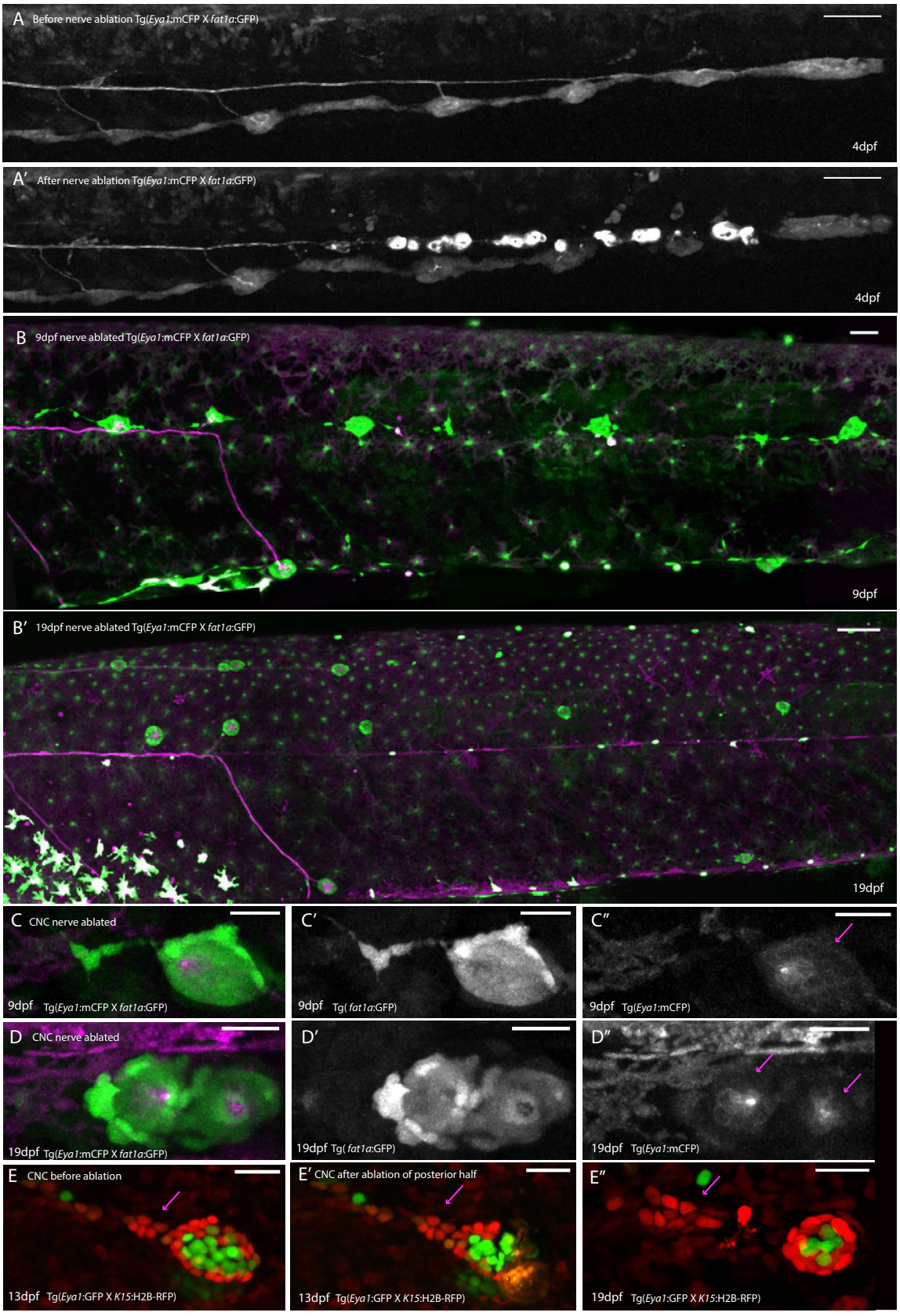

Figure (30) New and correct organ formation in the absence of any nerve connection (A-A') Before and after nerve ablation images on 4dpf Tg (fat1a:GFP)X(Eya1:mCFP) shows the specific loss of nerve during primordium migration but not affecting the underlying neuromasts n=8 fish. Scale bar= 50 microns (B-B') despite the absence of any nerve

innervation the *pLL* pattern and organ numbers and positions are unaffected. 10 days later scale bar 30 microns (B') uninnervated organs appear to be smaller in size than their innervated counter-parts, *pLL* nerve does not re-grow and uninnervated neuromast organs seem to become progressively smaller. Scale bar 50 microns n=5 fish (C-C'') posterior CNC founder neuromast at 9dpf, notice that the organ seems normal and hair cells are present despite the lack of nerve innervation. (D-D'') 10 days later same neuromast shows the correct addition of a new organ that contains hair cells (magenta arrows) despite the lack of any nerve innervation. Scale bar 20 microns n=5 fish. (E-E'') ablation of posterior half of founder caudal neuromast in Tg (k15:H2BRFPX Eya1:GFP) while individual cells have started migrating outwards to form a new organ does not lead to a change in cellular behaviour, instead a smaller founder neuromast is regenerated and cells continue migrating outwards (magenta arrows) to participate in new organ formation n=3 fish. Scalebar 20 microns. Anterior is to the left, posterior is to the right. Dorsal is up and ventral is down.

K15 CRIPSR mutants exhibit defects in post-embryonic organ positioning

While neither ablation of *pLL* nerve, *fat1a+* cells or injury to founder neuromasts could affect new organ formation in the CNC of Medaka fish, the *k15* mutant showed some interesting phenotypes. It must be noted however that these phenotypes were not fully penetrant (this could be due to the composite alleles I reported earlier for these mutants). By looking at juvenile and adult *k15* mutants I was able to observe what appear to be permissive paths for neuromasts to undertake. Precisely a recurring phenotype is the appearance of neuromasts near or in the dorsal fin (Figure 31 A-B). These neuromasts seem to be following a path that we never observe them following in the *wt* situation (magenta arrowheads A). In terms of phenotypes in the CNC I consistently observed that the positioning of new organs was dorso-ventral instead of anterior-posterior as in the *wildtype* (Figure 31C-E). In addition, there appeared many more exploratory cells located in dorso-ventral positions than in the *wildtype*. These results suggest that it is possible a correctly specified and maintained epithelium might be providing instructive cues for neuromast positioning and that this might be perturbed in some *k15* mutants. These phenotypes are the only ones I report that affect CNC pattern building in Medaka.

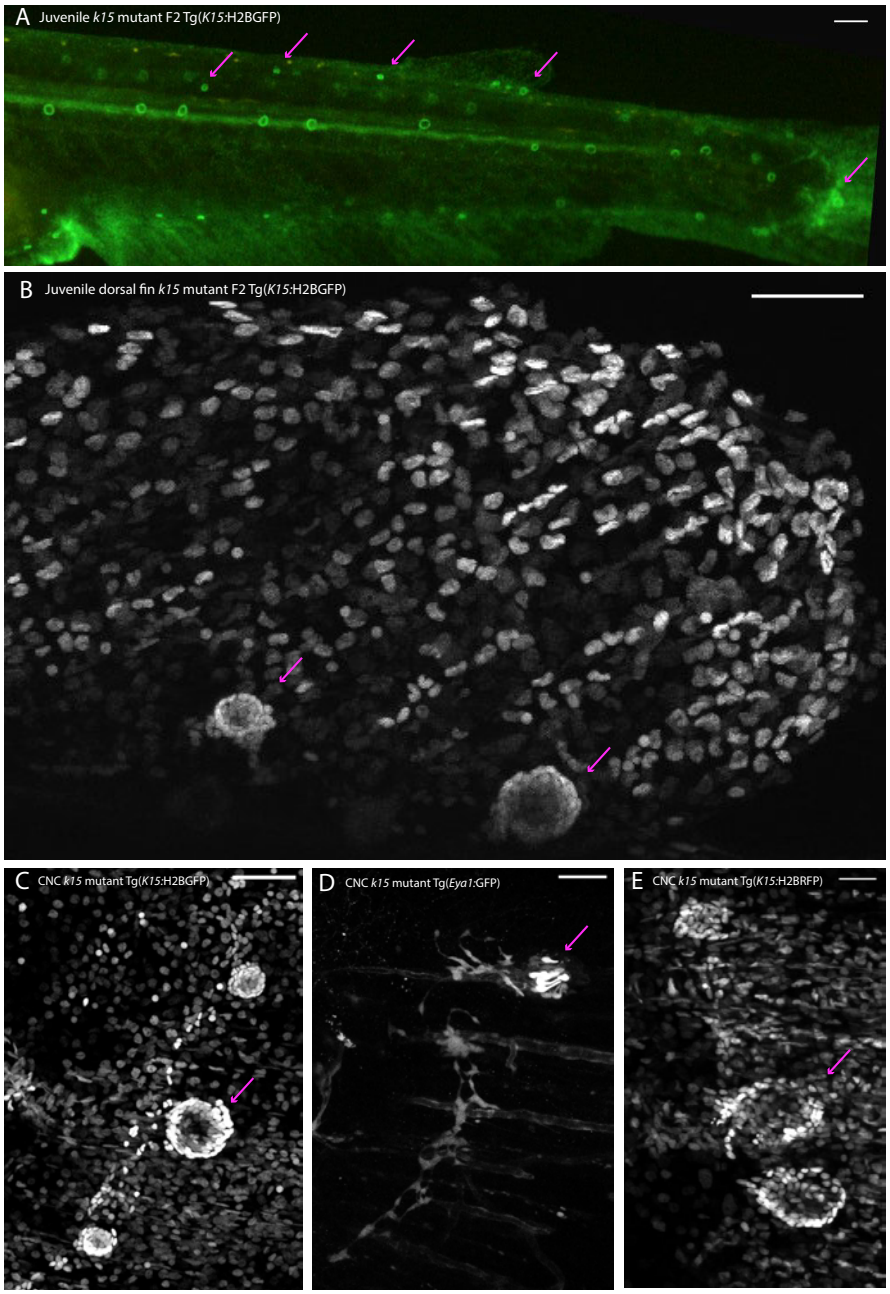

Figure (31) Juvenile *k15* mutants show permissive paths of neuromasts (A) Juvenile *k15* mutant F2 Tg(K15H2BGFP) showing the presence on neuromasts in the dorsal fin, and permissive paths for neuromasts elsewhere that are not seen in the wildtype (magenta arrows), posterior CNC organ composition and pattern is dorso-ventral and is thus different from the wild-type. Scale bar=100microns. N=6 fish (B) Zoom in on neuromasts in dorsal fin (magenta arrows) scale bar= 50 microns. N=3. (C-E) Organ number and position in CNCs of *k15* mutants notice the dorso-ventral position of organs, the excessive individual cell migration and huge size differences between the organs. Magenta arrows indicate likely position of founder organ. N=10 CNCs.

Conserved embryonic *aLL* pattern & *aLL* post-embryonic organogenesis in Medaka

To address whether principles of post-embryonic neuromast organogenesis are specific to the CNC or more widely used in other contexts I decided to look at the anterior lateral line (*aLL*). Despite the formation of essentially the same organs *aLL* and *pLL* formation operate on quite distinct principles (Nikaido et al., 2017). The initial observation is that at 9df there is a strong left/right symmetry within the same fish in number and position of organs (Figure 32 A-B, appendix Figure 36). Within different fish this symmetry is maintained (N=8), this argues that the dorsal *aLL* system is much more deterministic than the *pLL* of Medaka. By following the same neuromasts over time (white asterisk) I was able to observe the initial steps of new organ formation as the system adds more organs (Figure 32 A-D''). This relied on the same individual cell migration observed in the CNC and this can be regarded as a general mechanism of neuromast organogenesis. Interestingly the direction of new organ formation can occur either anteriorly or posteriorly in the *aLL* (Figure 32 C-D'') unlike the CNC where new organs always form more anteriorly. The general principles involve mantle cell migration and an upregulation of *eya1 & fat1a* expression. Seeing the highly conserved organ position & numbers in the *aLL* of medaka I wondered whether the *aLL* will be more stable and conserved in distantly related teleosts, I therefore assessed the overall *aLL* pattern in Zebrafish at the end of embryogenesis using the K15:H2BGFP line (Figure 32E). Initial results (in addition to published data Ledent et al., 2002; Owens et al., 2007; Ishikawa et al., 1994; Raible & Kruse 2000) suggests a high degree of similarity between the overall *aLL patterns* of Zebrafish and Medaka.

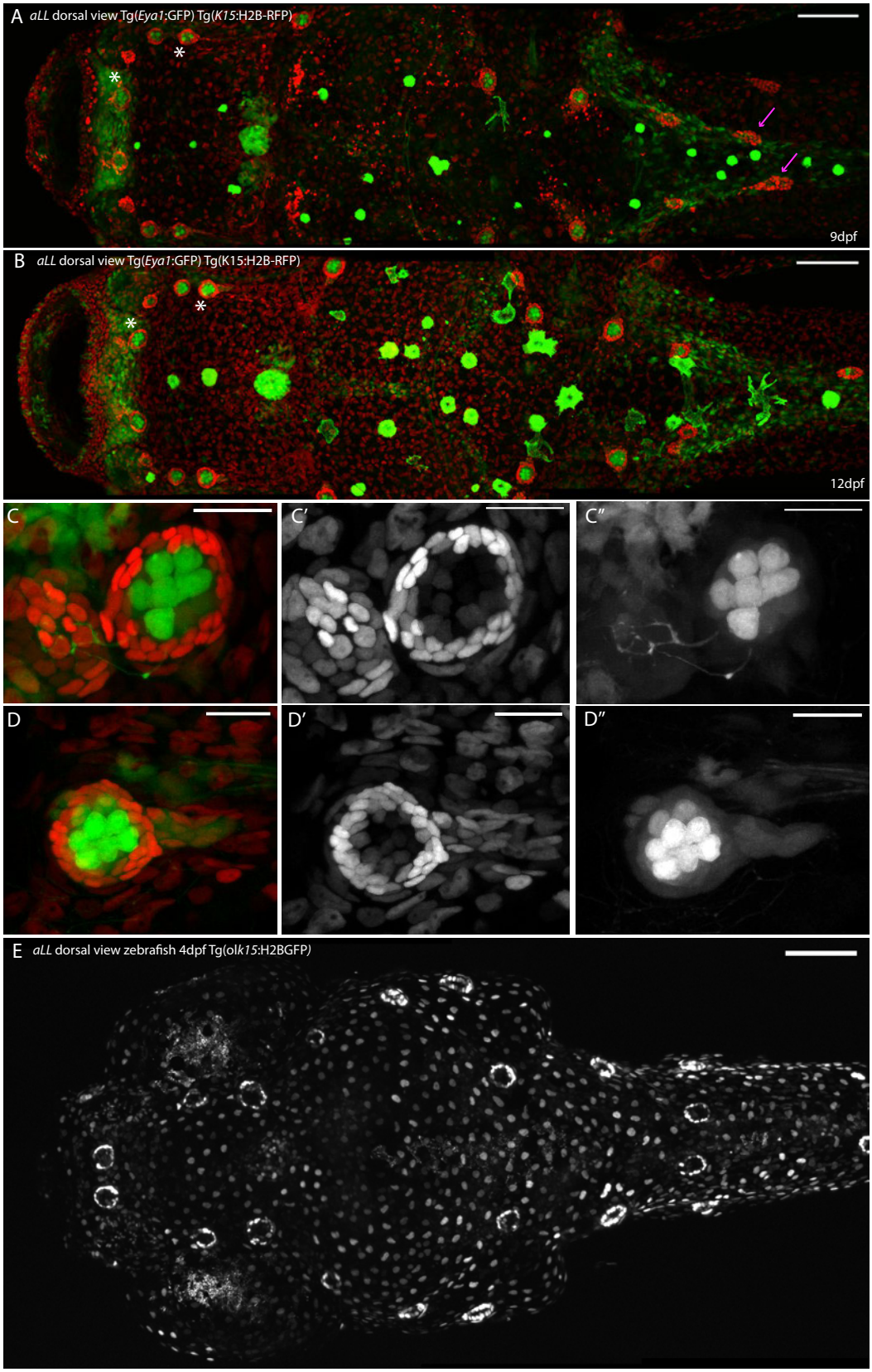

Figure (32) *aLL* pattern of organs and new organ addition (A) anterior lateral line dorsal view in a Tg (Eya1:GFP) Tg(K15:H2B-RFP) 9dpf embryo, notice the high degree of symmetry between the left and right side of the embryo, individual organs highlighted in white asterisk and traveling primordia with magenta arrows Scale bar=100 microns N= 8 embryos. (B) Same embryo 12dpf. Notice the beginning of new organ formation at the same neuromasts as in (A) overall

symmetry of pattern is maintained Scale bar=100microns N=8 embryos. (C-D") Zoom-ins on organs with white asterisks in (A) and (B) notice the individual cell migration both anterior and posterior to the original neuromast, this involves axiation of individual cells and an up-regulation of eya1GFP in migrating cells, process looks similar to CNC neuromast addition scale bar 20 microns. (E) *aLL* pattern in Zebrafish olK15:H2B-GFP 4dpf embryo shows a high degree of conservation to pattern found in Medaka N=10 embryos. Scale bar=100 microns. Anterior = left, posterior =right.

Eya1 CRIPSR mutants show strong *aLL* pattern and organ number defects

The robustness of the *aLL* was further demonstrated by the fact that the *k15* CRIPSR mutant line showed no obvious phenotype in *aLL* despite the very strong effects on the *pLL* (data not shown). I therefore assessed *aLL* pattern and organ numbers in the *eya1* CRISPR mutant from the ventral and lateral angles. I reasoned since the *eya1* mutant I generated has major cranio-facial defects in addition to otic vesicle organization and size problems we should be able to observe an effect in the *aLL*. And indeed, when one compares the ventral *aLL* patterns in *wt* and *eya1* mutant fish there are major differences in organ numbers and positions (Figure 33A-B). However, some organs are still clearly formed in the mutant (magenta arrows) arguing that a complete organ loss (like what happens in the *pLL*) does not occur. The situation on the lateral side is even more pronounced with a strong loss of organ numbers (Figure 33C-D). But once again some organs do form in the mutant still (magenta arrows D). It is therefore possible that the initial specification of organs occurs in the mutant but any migratory ability or new organ formation is perturbed. That said the *eya1* mutant here is the first described mutant that heavily perturbs both the *aLL* and *pLL* patterns and as thus *eya1* can be regarded as essential for correct neuromast pattern formation and maintenance during development.

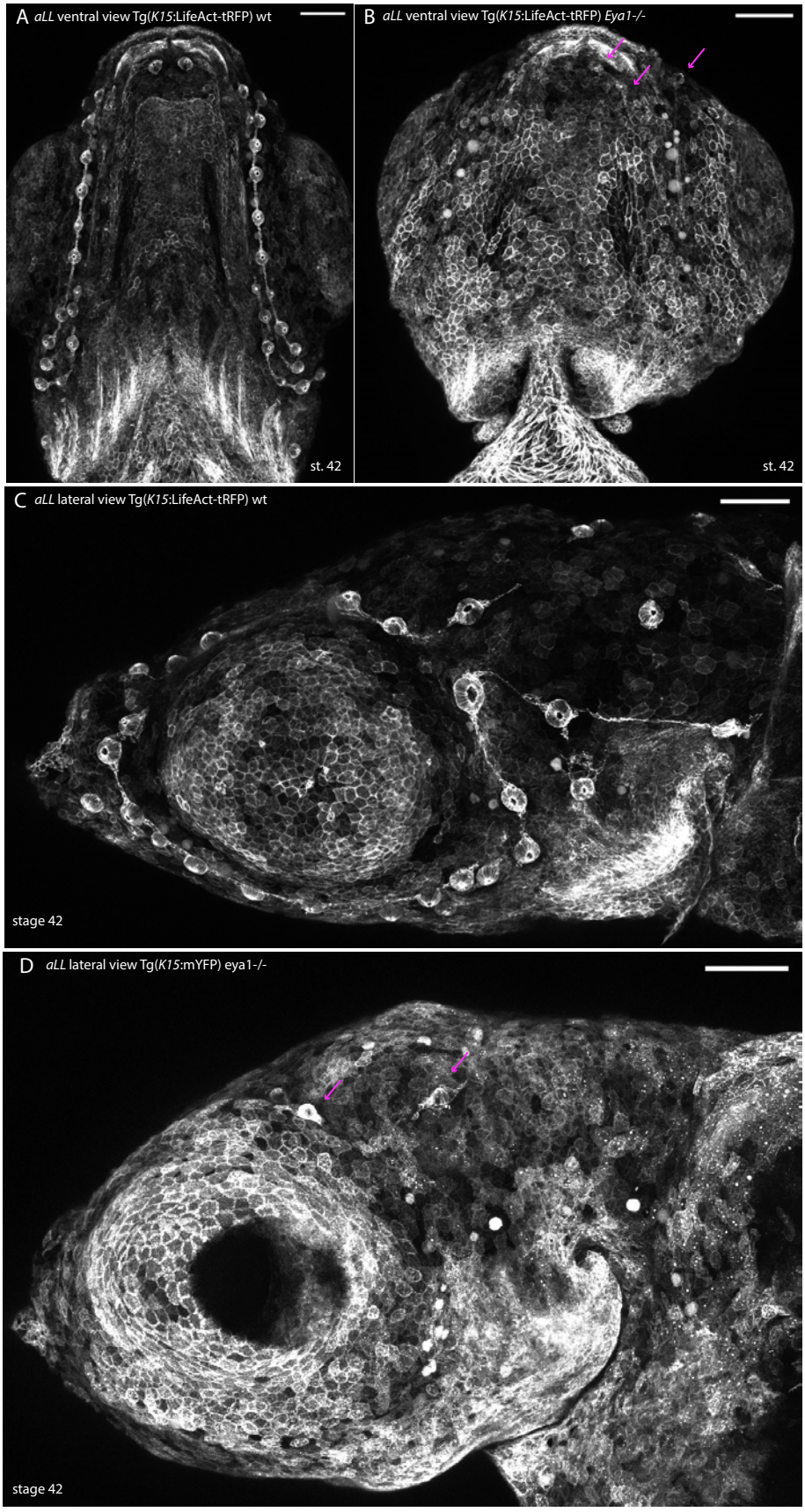

Figure (33) *aLL wt* and *eya1* mutant (A) aLL ventral view in a wildtype Tg(K15:LifeAct-tRFP) stage 42 embryo notice the

high regularity of neuromast numbers and positions N=5 embryos scale bar 100 microns. (B) *aLL* Ventral view in Tg (k15:LifeAct-tRFP) *eya1* CRIPSR mutant notice the high degree of cranio-facial abnormalities and the missing neuromasts. Some neuromasts on the ventral side can still be detected (magenta arrows) but pattern and numbers largely reduced compared to wildtype. N=5 Scale bar =100 microns. Anterior=up posterior=down (C) *aLL* lateral view Tg(K15:LifeAct-tRFP) *wildtype* view around the eye, notice the position and numbers of neuromast organs scale bar =100 microns. N=5. (D) same view on K15:mYFP *eya1* CRISPR mutants notice the massively reduced neuromast numbers although a number of organs can still be recognized (magenta arrows), numbers of organs and overall cranio-facial development highly perturbed in mutants scale bar = 100 microns. N=5. Anterior to the left, posterior to the right.

Organ growth and organ addition drive post-embryonic lateral line embellishment

As Medaka fish grow life-long organs cope by growing in size to maintain proportionality or by adding more functional units (more organs). What we have discovered in the case of neuromasts in the Medaka is that both processes occur. As the fish grows neuromasts also grow in size by constituent cell addition (Figure 34 A-D) this does not happen in zebrafish(Wada et al., 2013a) where neuromasts do not grow in size. I have previously described how individual cell migration drives post-embryonic organogenesis of neuromasts, this occurs in the *aLL* and in the context of the CNC in the *pLL*(C-D). However, we have also observed another method of neuromast formation post-embryonically that is utilized for primary and secondary neuromasts. This has been described before in the literature and involves a budding/stitching process. It is unclear still what the steps are that lead to this type of organ formation (Figure 34 E). By following neuromasts over-time I was able to catch juvenile fish in the process of neuromast budding/stitching (Figure 34F-F''). This process involved the upregulation of *k15* in all neuromast cell types and the formation of a second center for hair cells, eventually these two centers will separate and a new neuromast organ will form that is distinct from the founder organ (Figure 34 E). Once this occurs *k15* expression becomes restricted once more to the mantle cell population. It is highly intriguing that this process

happens while presumably maintaining organ functionality. To sum up there are two ways in which organs can cope with a constantly growing body; either scale-up in size or form new functional units. In the case of Medaka neuromasts both processes occur, it is unclear still how this is coordinated but could be related to constituent cell quorum sensing. With regards to new organ formation post-embryonically there are two distinct mechanisms. One relies on individual cell migration and occurs in the *pLL* CNC cluster and the early *aLL*, the other involves organ budding/stitching and occurs at least in primary and secondary organs of the *pLL* and involves molecular changes in the neuromast during the process of budding.

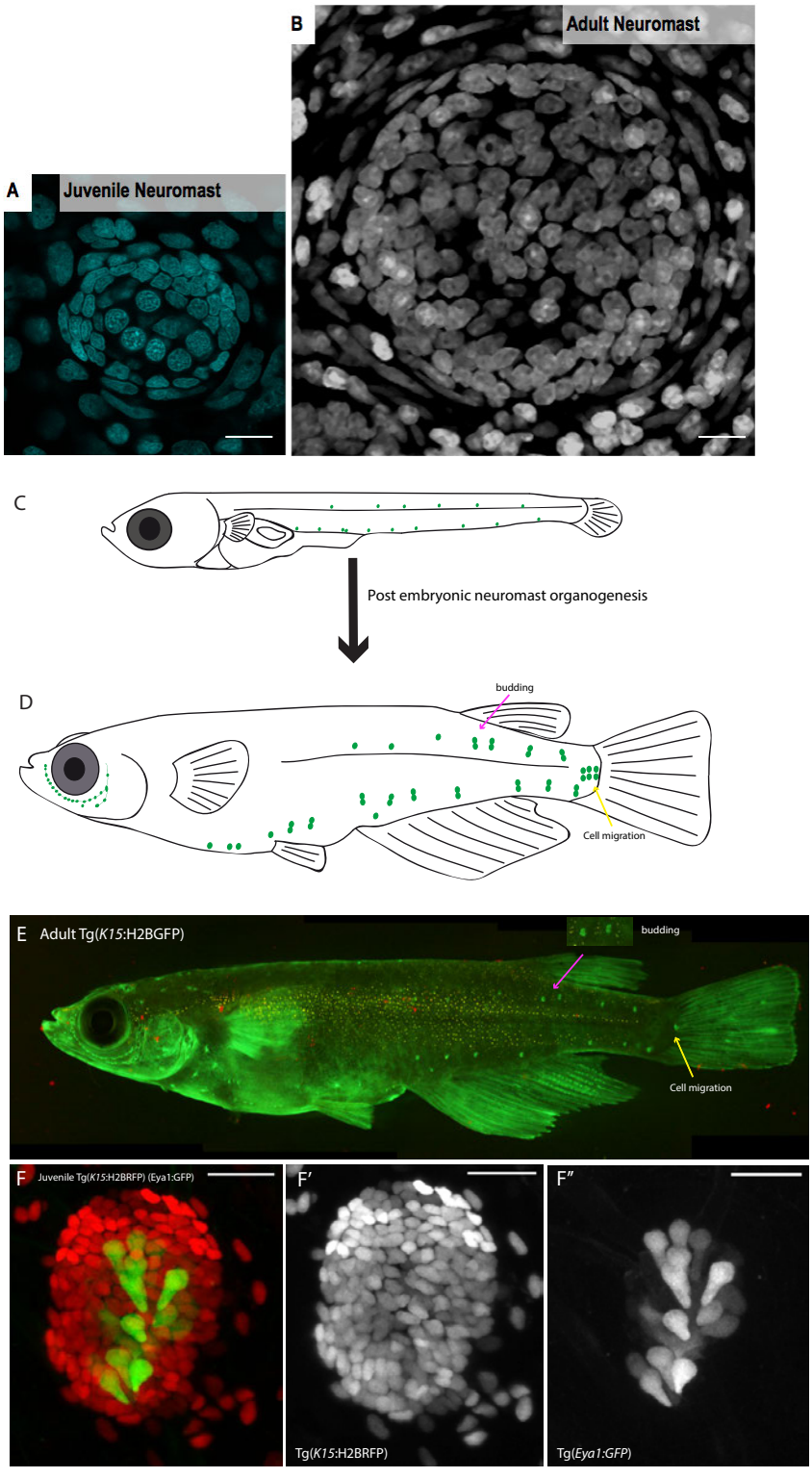

Figure (34) Post-embryonic increase in neuromast size and number of organs (A-B) Size differences between neuromast at hatch and an adult 1 year old neuromast, notice the massive increase in size, pictures taken by Lazaro Centanin and Isabel Kraemer. (C-D) Schemes done by Julian Stolper showing organ addition during post-embryonic stages, magenta and yellow arrows refer to two respective ways of neuromast organogenesis 1- budding/stitching secondary neruomasts the other is individual cell migration CNC(E) an adult Tg(K15 H2BGFP) showing stitches of organs and zoom in patterns. (F-F'') organ budding involves the upregulation of *K15* in all cells of the neuromast, connected neuromast that contain independent sets of hair cells that later off separate to two fully independent organs. Scale bar =20 microns. N=6

Discussion

Teaching old genes new tricks: building the embryonic *pLL* pattern in Medaka

Our understanding of the development of the *pLL* of Zebrafish has been heavily enhanced in the past decade by high resolution imaging, novel transgenic tools and pharmacological and genetic interventions (Aman and Piotrowski, 2008; David et al., 2002; Grant et al., 2005; Haas and Gilmour, 2006; Hernández et al., 2006; Lecaudey et al., 2008; López-Schier and Hudspeth, 2005, 2006; Lush and Piotrowski, 2014; Ma and Raible, 2009; McGraw et al., 2014; Nechiporuk and Raible,2008;Pichon and Ghysen,2004; Sapede et al.,2002; Sánchez et al., 2016). We now have a rather detailed picture on the molecular processes and signals involved in the organized collective cell migration setting the system of neuromasts up during development. What remains unclear is how conserved these findings are across teleosts. Initial insights from other teleosts led to the belief that a similar *pLL* pattern is built at the end of embryogenesis in different fish (Sapede et al., 2002) and published mutants in Medaka argue for the conservation of the chemokine receptors/ligand axis driving primordium migration (Sasado et al., 2008; Yasuoka et al., 2004). Briefly what has been shown in Zebrafish is that the leading edge of the migrating primordium harbours cells with high expression of *cxcr4b* which perceive an *sdf1a* ligand present at the horizontal myoseptum, this interaction drives the migratory potential of the primordium from anterior to posterior up until the tail where the last neuromasts are deposited (David et al., 2002; Haas and Gilmour, 2006; Valentin et al., 2007). A second chemokine receptor *cxcr7* is located primarily at the trailing edge of the migrating primordium and is largely responsible for sequestering the *sdf1* ligand (without

triggering downstream signalling), allowing the leading edge of the primordium to constantly perceive a directional *sdf1a* ligand (Donà et al., 2013; Venkiteswaran et al., 2013). This coordination of chemokine receptors and ligands ensure effective long-distance migration. As soon as the first primordium terminates, a second primordium (primII) travels along the same path and deposits organs in between those deposited by primI (Ghysen and Dambly- Chaudiere, 2007 ; Ledent, 2002 ;Sapede et al.,2002). The existence of primII was validated in all teleosts studied to date (Ghysen et al.,2012, 2010; Pichon and Ghysen, 2004; Sapede et al., 2002).

We have shown that a different *pLL* pattern is built at the end of embryogenesis in Medaka. We have also shown that this depends on the action of one primordium building two parallel sensory lines (making Medaka the first reported teleost with no PrimII). By a series of live-imaging, *in-situ* hybridizations and mutant rescue transplantation assays we were able to show that the same chemokine signals *cxcr4b* and *cxcr7* involved in the initial migration of the primordium are required specifically during secondary organ formation. This reutilization of the same molecular signals to drive different morphogenetic processes (initial collective cell migration of the primordium and then individual cell migration during secondary organ formation) has been uncovered by developmental biologists studying a variety of model organisms and as such constitutes a common principle driving evolutionary novelty (Jiménez-Delgado et al., 2009; Preston et al., 2011; Prud'homme et al., 2006; Rebeiz & Tsiantis, 2017; Rebeiz et al., 2011). It seems that nature has found a way to re-use developmental signals by tinkering with their temporal and spatial expression patterns in new contexts. This in the setting of the

pLL can give rise to new more complex patterns and as thus constitutes an example of teaching old genes new tricks. The work that remains to be done is on the cis-regulatory element evolution of *cxcr4b* and *cxcr7* between Zebrafish and Medaka. Given the existence of vast genomic resources in both species this work can be bio-informatically performed and will contribute to the understanding of how the evolution of cis-regulatory elements can lead to specific morphological novelties. The dream experiment would be to reconstruct the cis-regulatory elements of *cxcr4b* and *cxcr7* of Medaka in Zebrafish and observe whether we can reconstitute a Medaka like *pLL* pattern in Zebrafish (it is highly doubtful that both chemokines would be sufficient for this switch but an intermediate phenotype might be observed).

Probably the most elegant experiment I have come across in the lateral line studies field is that performed by (Haas & Gilmour, 2006) where she was able to rescue primordium migration in a *cxcr4b* mutant by transplanting a few *wildtype* cells that colonized the leading edge of the primordium. While the authors do not go into too much detail over this intriguing colonization, to me it is highly fascinating since it argues clearly for a way in which cells within the same tissue can sense mutant vs non-mutant and organize the tissue in a way to minimize the potential deleterious effects of mosaic loss of function. This level of self-organization is astounding and could be evolutionarily highly conserved and of functional relevance, how it is mediated mechanistically remains unclear. I have performed the same transplantation in Medaka for a different purpose. Not only were the presence of a few *wt* cells sufficient to rescue primordium migration in our model but more importantly secondary organs did form that contained only a fraction of

cells as *wt*. This suggests that as in the case for primordium migration, secondary organ formation requires only a few 'leading cells' to rescue the entire developmental process. This raises the question as to why the entire tissue in both cases expresses the receptor, could this be a form of developmental buffering by ensuring that if some aspect fails other cells can be immediately used to rescue the process? (fail-safe mechanism), alternatively there could be inherent differences in *cxcr4b* expression that get sorted out *in vivo* under physiological conditions where cells with stochastically higher *cxcr4b* expression being positionally preferred for leading positions over others, this remains a theoretical possibility at the moment.

A 'tug-of-war' model for secondary organ formation

The formation of secondary neuromast organs in Medaka represents an excellent avenue to explore individual precursor cell decision-making during organ formation. This is unique to the building of the *pLL* in Medaka since the process of secondary organ formation happens after the end of embryonic development in Zebrafish (Grant et al., 2005; Lopez-Schier & Hudspeth, 2005; Lush & Piotrowski, 2014; Whitfield, 2005) and as thus cannot be easily followed by an *in-vivo* 4D approach. The interneuromast cells (INCs) are laid down during initial primordium migration (Ghysen & Dambly-Chaudiere, 2007; Lecaudey et al., 2008) and connect primary deposited organs together, these precursors were shown to be the source of new neuromast post-embryonically in Zebrafish by proliferation driven organ formation (Grant et al., 2005; Lopez-Schier & Hudspeth, 2005; Lush & Piotrowski, 2014; Whitfield, 2005). Initial steps of secondary organ formation in Medaka lack

any evidence of INC proliferation, as assessed by live-imaging (Seleit et al., 2017a), this suggests that there are fundamental differences in building secondary organs between Medaka and Zebrafish. What occurs instead is a coalescence of INCs connecting primary organs around the mid-point between primary organs, this is followed by a dorsal migration of the forming secondary organ clusters and crucially cell recruitment from the edges of primary organs. This process of cell recruitment is highly intriguing as a method to presumably increase the number of cells contributing to new organ formation. The 4D-data points towards the fact that the process is equivalent to a 'tug-of-war', I usually observed these recruited cells shuttling forward and backward between the older organ and the newer one, indicating that these cells are being 'fought over' by the developing neuromasts. The developmentally younger organs seem to have a stronger 'pull' and most cells do end up joining the newer organ. The struggle over uncommitted progenitors in the context of two identical (but developmentally temporally decoupled) organs has in fact been shown to occur in the context of the planarian eye-field (Peter Reddien, personal communication). There the induction of new eye forming precursor spots in ectopic locations leads to a 'fight' over uncommitted eye progenitors, with the same outcome that most precursors are invariably pulled towards the developmentally younger organs (Peter Reddien, personal communication). The fact that essentially the same process occurs in different neural tissues of a vertebrate and an invertebrate model suggests this might be a highly conserved mechanism. We still largely lack the molecular signals attracting uncommitted cells more strongly towards the developmentally younger organs and we do not know if they are conserved across phyla. However, the way Peter

Reddien describes it is an apt metaphor for the moment; 'gravitational fields' exist around organs that are capable of recruiting uncommitted progenitors, developmentally younger organs have stronger 'gravitational fields' and as such are able to attract uncommitted cells more easily. This idea can be tested in the context of organoids where one can control the developmental age of multiple organoids and add uncommitted progenitors to a defined and controlled space. In our system, it is possible that the two primary organs initiate a 'tug-of-war' over uncommitted progenitors. To escape their pull progenitors will preferentially locate in the mid-point between the two primary organs (point of least 'pull'). This internal logic could ensure a reproducible outcome of the developmental process (only 1 secondary organ in between 2 primaries) without the aid of external signalling or positional accuracy. Our *cxcr4*b and *cxcr7* mutants (Sasado et al., 2008; Yasuoka et al., 2004) that lack secondary organ formation provide some initial insights into the cellular decisions taken by precursor cells. I was able to observe that the reason secondary organ formation fails in *cxcr4b* mutants is that instead of coalescing around the mid-point between two organs, INCs are picked up by the primary organs on both sides (Seleit et al., 2017a). These results suggest that *cxcr4b* is probably required in early steps of secondary organ formation i.e. in preventing INCs from being picked up by primary organs. Indeed, it has been shown that FGF signalling can act as an antagonist of *cxcr4b* signalling in the context the *pLL* in Zebrafish (Breau et al., 2012). There, FGF signalling attracts cells to the primordium while *cxcr4b* forces them to travel away from the primordium (Breau et al., 2012), the lack of *cxcr4b* signalling in our mutants can tilt the balance towards FGF allowing primary organs to integrate the uncommitted

INCs leaving no cellular source for secondary organ formation. With regards to *cxcr7* mutants the process of secondary organ formation fails for a different reason; there INCs remain between primary organs but fail to coalesce and start secondary organ formation (Seleit et al., 2017a). Since mRNA localization suggests *cxcr7* is only expressed in primary organs it is possible that the lack of *cxcr7* prevents the initial pull for uncommitted progenitors from the primary organs. Since this can in turn be the trigger for secondary organ formation, when it does not occur the INCs remain in an uncommitted state with no drive for new organ formation. So far these ideas remain a theoretical model that needs to be validated experimentally, it is in theory possible to think of an *in-vitro* controlled setting where neuromasts can be allowed to develop with controlled distances between them and a defined number of INCs. All in all, the totality of the data suggests that uncommitted progenitors are 'fought over' and that organs have an inherent drive during development towards increasing the number of their constituent cells either by proliferation or cell recruitment. This view sets-up a metaphor of development as a highly dynamic 'battle-field' between different developing organs 'fighting' for space, cells and influence rather than the traditional seamless 'flow' of development metaphor we are used to. The reproducibility of the process points towards the degree of canalization of developmental processes and the ability of the system to buffer noise and reduce variability.

Waddingotnian developmental buffering systems in the context of the *pLL* of Medaka

I report very intriguing aspects of the building of the *pLL* pattern in Medaka fish. These are discussed at more length in the prologue section and rely heavily on

Waddington's theoretical ideas about developmental buffering systems (Waddington 1941, 1942, 1968). Here I would like to briefly summarize the main implications of these findings. It seems clear that the primordium output in terms of numbers of organs in the *pLL* of Medaka is not genetically deterministic but rather plastic. This can be surmised from the differences in output between isogenic Medakas and differences in output between the left and right hand *pLL* of the same fish. In addition, modulating the immediate environment of development (by adjusting the temperature) can impinge directly on the developmental process. Changing the surrounding tissue properties leads to new patterns while maintaining largely *wildtype* average organ numbers (*Da* and *k15* mutants). Interestingly in both mutants the variability in primordium output is wider than what I observed in the *wt*, this higher variability in (any) mutants was realized by Waddington very early on and used as evidence for the existence of developmental buffering systems (Waddington 1941, 1942). All in all the phenotypic plasticity (both in number of organs and their pattern) is not a unique feature of the *pLL* system and has been reported to occur throughout the animal kingdom (Agrawal, 2001). In theory, this makes sense as the environment must have a way of influencing and canalizing developmental traits differentially, it cannot all rely on dry random mutations and infinitesimally small selective pressures on reproductive success. The implications of this low developmental buffering capacity of the *pLL* and strong response to the immediate environment is the possible high (and fast) evolvability of the system as a whole.

Evolution of lateral line patterns in teleosts

A fantastic diversity of lateral lines exists in teleosts (Sapede et al.,2002; Coombs et al., 2014, 1988). The basis of which remains largely unknown. A comparative approach is essential if we are to understand the evolution of lateral line patterns. This was utilized by (Ghysen et al.,2012, 2010; Pichon and Ghysen, 2004; Sapede et al., 2002) and all of the species they characterized have a highly conserved embryonic *pLL* pattern built by two primordia. This led to the idea that most of the diversity observed in *pLL* patterns in the wild must be driven by post-embryonic embellishments on an essentially unified rudimentary pattern (Nuñez et al., 2009; Pichon and Ghysen, 2004). The results I report in Medaka directly challenge this view by showing that differences in *pLL* pattern can have their origin in the unfolding of the developmental process setting up the system during embryogenesis. This led me to carefully characterize a number of different teleost species all of which turned out to have species-specific embryonic *pLL* patterns. This strongly argues that a fast evolution of the developmental module building the *pLL* pattern is one major factor driving the diversity of lateral line patterns in the wild. It also hints towards the plasticity of the system that allows it to very easily adapt and be influenced by its immediate environment. A second unexpected finding was that Medaka unlike all other described teleost species harbours only one *pLL* primordium instead of two. In terms of the overall pattern built by this primordium it highly resembles PrimII in Zebrafish (Nuñez et al., 2009), these findings suggest that medaka might have lost PrimI entirely through the course of its evolution. How widespread this loss is in neighbouring clades and how this can occur remains unclear but recent work suggests that changes in cis-regulatory

elements lead to temporal gene expression changes that in turn can underlie massive changes in morphological traits (Indjeian et al., 2016; O'Brown et al., 2015; Urbansky et al., 2016). A particularly interesting example of embryonic *pLL* patterns is that of *Notobranchius furzeri* where the system seems to be a true intermediate between Zebrafish and Medaka. While it to the best of our knowledge has one *pLL* primordium like Medaka, both organ numbers and positioning resemble Zebrafish. A dream experiment would be to transplant a primordium from one species into the other and observe which pattern will be formed, the plasticity of the system suggests that it will be highly responsive to extrinsic signals. It still remains unclear why the system is evolving so rapidly in fish, but it could be due to the extreme diversity of body plans in teleosts (Coombs et al., 2014, 1988) which would require a peripheral sensory system to be highly adaptable and tuneable (Ghysen & Dambly-Chaudière, 2016). A proper connectomics approach to the *pLL* can also help us understand how the system is connected to the CNS (Lopez-Schier, 2015;Lozano-Ortega et al., 2018) and whether differences in neuromast numbers and patterns between species have any functional relevance.

_k15-/-_ how changing epithelial tissue mechanics leads to new *pLL* patterns

The family of *keratins* are conserved cytoskeletal structural proteins primarily located in skin tissue and are known regulators of skin integrity, mutations in keratin genes lead to diseases of the skin (Haines & Lane, 2012; Chamcheu et al., 2011; Peters et al., 2001). Specifically, *keratin 15* has been shown to be an epithelial stem cell marker in a variety of tissues (Y. Liu et al., 2003; Bose et al., 2013 ;Giroux et al., 2017; Giroux et al., 2018). And a knock-out mouse model has shown impaired esophageal epithelial regeneration, abnormal response to injury

and reduced ability of wound healing with thicker epithelial layers due to 'enhanced basal cell proliferation' (Giroux et al., 2017). We generated a variety of reporter tools based on a partial promoter of the Medaka *k15* driving a variety of fluorescent proteins. Characterization of the expression pattern revealed that k15 localizes to the basal epithelial layer of the skin in addition to being a stable label for mantle cells of the neuromasts. Our CRIPSR knockouts of *k15* show a variety of phenotypes including; epithelial cell extrusion, increased epithelial cell death, epithelial lesions, changes in the morphology and structural integrity of *k15+* basal epithelium cells, a perturbed suprabasal epithelial tissue integrity and most importantly for our purposes a highly perturbed *pLL* pattern in Medaka. By a series of transplantation experiments and *in situ hybridization* data (Karen Gross, unpublished) we were able to show that the defects in the epithelial tissue surrounding the primordium can lead to the *pLL* phenotypes in the *k15* mutants. Those phenotypes included organs 'stuck' at the mid-line, organ mis-orientation and primordium stalling. We hypothesize that the perturbed epithelium directly results in the perturbed lateral line pattern. The data strongly argues that while *k15* might not have an intrinsic role in primordium migration, modulation of the immediate environment (epithelial cell layers) can lead to massive changes in the *pLL* pattern obtained. It seems likely therefore that primordium migration and deposited organ behaviour can be directly affected by sensing and responding to the mechanical tension of the tissue the primordium has to migrate through. This raises the question as to whether nature might have exploited the different mechanical tension properties of the skin epithelium in different teleosts to tinker with the lateral line patterns in these fish. In other words, whether mechanical

tension of the surrounding tissue can directly be involved in the evolution of lateral line patterns. All in all, our *k15* mutant shows perturbed epithelial integrity and recapitulates known expression patterns and functional roles from other model organisms (Y. Liu et al., 2003; Bose et al., 2013; Giroux et al., 2017; Giroux et al., 2018). In addition, it shows strong phenotypes in *pLL* pattern formation that were previously completely unrecognized and that we directly link to the perturbed epithelia in the mutant.

eya1$^{-/-}$ an old mutant with new phenotypes

Conserved from plants to man the *eya* family of transcriptional co-activators have been shown to be involved in a variety of developmental processes (Rebay, 2015; Jemc & Rebay, 2007). The founding member of the family *eya1* was initially isolated and characterized for its role in retinal morphogenesis in flies (Bonini et al., 1993) it quickly became clear that *eya1* plays other major roles including underlying the branchio-oto-renal (BOR) syndrome in humans (Abdelhak et al., 1997). In Zebrafish, an *eya1* mutant isolated by a forward genetic screen has been reported to develop disorganized and smaller otic-vesicles, in addition to slower posterior lateral line migration, higher apoptotic cells within the primordium and missing terminal neuromasts of the *pLL* (Kozlowski et al., 2005). This added to the fact that neuromasts of both the *pLL* and *aLL* have reduced sensory hair cells than their *wt* counterparts (Kozlowski et al., 2005). I generated a new CRISPR *eya1* mutant in Medaka (initially to study effects on *pLL* pattern) but to my surprise the phenotypes were more severe than those described for Zebrafish and in addition mirrored better the known phenotypes from mouse mutants and human BOR

syndrome studies. The *eya* $^{-/-}$ Medakas are not viable and die shortly after hatch from failure of movement and heart edemas (both have not been reported in the Zebrafish mutant). In addition to having smaller otic vesicles as expected from the Zebrafish mutant, the Medaka *eya1* CRISPR mutants showed strong cranio-facial defects. This was compounded by strong sarcomere orientation and morphology defects which have only been reported in the context of drosophila (Y.-H. Liu et al., 2009), relatedly and quite interestingly *eya1* has been also shown to be expressed in tendons of mammalian models (Xu et al., 1997). In the context of the lateral line our *eya1* mutant exhibited very strong phenotypes not reported in Zebrafish. Specifically, *pLL* development was completely disrupted i.e. there were no *pLL* neuromasts. This strongly argues *eya1* is directly involved in initial primordium specification or migration in Medaka. I was also able to report strong phenotypes in the *aLL* where the majority of neuromasts were completely missing. This is the first known mutant to strongly affect both the *aLL* and *pLL* pattern and number of organs. It also seems clear that the role of *eya1* might have been underappreciated in previous studies in Zebrafish either due to hypomorphic alleles, compensatory mechanisms (El-Brolosy et al., 2019) or a different role for the gene between Medaka and Zebrafish. All in all, it is quite useful to generate knockouts of published mutants if they have not yet been characterized in your preferred organism. This is because both the published mutant itself and the organism it was generated in can be caveats that might lead to different results. It certainly helped in this case to define better *eya1*'s promiscuous role in Medaka development and produced some surprises related to *aLL & pLL* pattern formation.

Initial symmetry breaking in *pLL* of Medaka and Zebrafish

The initial difference between the *pLL* pattern building between Zebrafish and Medaka is the fact that Zebrafish clusters are deposited as pre-formed rosettes that stay at the midline (Ghysen & Dambly-Chaudiere, 2007; Lecaudey et al., 2008), while Medaka precursors are both more undifferentiated at deposition (Sapede et al., 2002) and immediately start moving ventrally. I was very interested in this initial difference since it structures the coming divergence in patterns. Theoretically it could be that the movement of the organs ventrally is a passive event (as is suggested for the movement of primary organs ventrally in Zebrafish later on) (Ghysen and Dambly-Chaudiere, 2007; Ledent, 2002; Whitfield, 2005), it could be actively guided by the nerve connections i.e primary organs are passive but the nerve connection drives the organs ventrally. Alternatively, there could be a chemokine signal at the ventral end attracting the primary organs, lastly there could be an exclusionary signal coming from the midline forcing the deposited organs away from it. In the next sections I will discuss how neither the nerve connection or the passive movement theories can account for the behaviour of primary organs. It is therefore most probable that either an exclusionary signal from the midline or an attractive chemokine ligand at the ventral side or a combination of both drive this symmetry breaking event between the *pLL* patterns of Medaka and Zebrafish.

Da mutant reveals plasticity of primordium & autonomous nature of precursor clusters

The *Da* mutant has the strange phenotype of a duplication of the ventral side due to the inactivation of *zic* genes (Ohtsuka et al., 2004; Moriyama et al., 2012), to our purposes this is a very interesting mutation since it essentially alters the immediate environment of the primordium without changing any of the primordium intrinsic properties themselves. I therefore exploited this mutant to understand better the role of modulating the immediate environment on the lateral line pattern. Specifically, I expected that if the ventral movement of the primary organs was a passive event, then we should see a randomization of the primary organs; some will locate to the un-induced ventral side, others will go towards the induced ventral side. While it is possible that *Da* fish have primary organs on both ventral ends, in over 80% of all pLLs what is observed is that there are primary organs that remain 'stuck' in the midline. Combining this with live-imaging one can clearly observe that the stuck organs are being positionally 'fought over', with organs initially specifying to one direction only to be later on moved to the other before returning once more in a 'yo-yo' like movement. These results strongly argue against the passive model of ventral movement since it is clear that primary organs are being actively shuttled between the two ventral sides during development. What is also very interesting is that now within the same fish and the same *pLL* side neuromast precursor clusters behave as autonomous units. They are able to decide independently of the other clusters which side to move to, so that within one *pLL* primary organs can move to the new ventral side, the normal ventral side or stay stuck in the middle. This data suggests that these

clusters are highly sensitive to very local changes in their environment (*e.g.* a different concentration of the proposed chemokine attractant). This sensitivity could in fact also explain the vast diversity of lateral line patterns in the wild, since small local changes can lead to big pattern differences. It is also a possibility that glial cells (Gilmour et al., 2002) are involved in forcing primary organs away from the midline and that this function is duplicated in the *Da* mutant leading to the 'bouncing off' of the neuromast clusters below and above the midline. I will discuss the role of glia below, but all in all the *Da* mutant has been very informative in understanding general design principles of the *pLL* of Medaka. One of which is that the ability to produce one secondary organ in between two primaries is not perturbed even though the positions and orientations of the primary organs are completely unhinged. It therefore seems like the ability to produce one secondary organ between two primaries represents an intrinsic property of the Medaka primordium that cannot be easily altered. So, while certain aspects are more plastic (organ positioning) others are more deterministic (one secondary organ between two primaries) in the *pLL*.

A conundrum: the role of glia in organ numbers & *pLL* pattern in Medaka

Glial cells have been shown to migrate concurrently with the lateral line nerve (Gilmour et al., 2002) during primordium migration. Ablating the *pLL* nerve in Zebrafish prevents glial cells from overshooting, they remain attached to the growing tip of the regenerating nerve (Gilmour et al., 2002). More recently it has been shown that these cells have a unique role in the context of the *pLL* organ number control, as knockouts that perturb glial cell signalling or specification lead

to a massive increase in organ numbers (Lopez-Schier & Hudspeth, 2005; Lush & Piotrowski, 2014; Whitfield, 2005). I attempted to produce ectopic neuromasts in Medaka by generating an *ngn1* CRISPR KO in F0 fish. *ngn1* has been shown in Medaka to lead to a failure of specification of the sensory ganglion that in turn lead to supernumerary neuromasts (Lopez-Schier & Hudspeth, 2005). While I did obtain an increased number of *pLL* organs in *ngn1* crispants in Medaka it was clear that the phenotype also included organ mis-positioning (many organs failed to specify correctly to the ventral side). Intrigued by the effect on *pLL* pattern and not only numbers I targeted other regulators of glial cell development and migration by CRISPR including *foxd3* and *erbb3a/3b* (Lush & Piotrowski, 2014). Interestingly while both produced organs that failed to specify ventrally both did not lead to an increase in neuromast numbers. In addition, *erbb3a/3b* mutants showed primordium migration defects that were unknown before this work and in some cases, complete absence of *pLL* neuromasts, an unexpected phenotype if the role of *erbb3a/3b* was restricted to glial cells. It should be noted however that there is data linking *erbb* signalling to EMTs (Hardy et al., 2010; Appert-Collin et al., 2015) and we know that the primordium must initially undergo an EMT-like state to kick start migration. Additionally, I undertook a different approach where I ablated the *pLL* nerve during primordium migration to observe whether this can lead to a change in the pattern or number of neuromast organs due to the failure of migration of glial cells. To my surprise the Medaka *pLL* nerve did not re-grow or regenerate unlike in Zebrafish (this is yet another new aspect of the regeneration deficiencies well documented in Medaka Lust & Wittbrodt 2018; Ito et al. 2014; Lai et al. 2017). Even more surprisingly neither the neuromast numbers or positions

were affected in the absence of the nerve. This could mean one of two things either Medaka glial cells can migrate without the nerve and are thus unaffected by the nerve ablation or they are dispensable for pattern and organ numbers. I tested both possibilities directly by labelling glial cells with *sox10*:mcherry and ablating the nerve, this led to the same conclusion as reported in Zebrafish, where the glial cells cannot travel further than the tip of the *pLL* nerve (Gilmour et al., 2002). These results are particularly puzzling as they do not fit with the genetic perturbations described above or the data from Zebrafish. The only explanation I could come up with is that the genetic perturbation might affect earlier steps of primordium specification and glial cell type specification (Collazo et al., 1994) and as thus the phenotypes might be different from physically ablating the nerve and preventing glial cell migration. It Is also possible that there are *sox10-ve* glial cells that are able to migrate independently of the *pLL* nerve. I also checked the number and position of glial cells in the *Da* mutant compared to the *wildtype* and while the overall numbers of glia on the *pLL* nerve were similar, the *sox10+* glial cells clustered more intensely in the *Da* mutant, whether this is of any functional relevance remains to be elucidated. In addition, during development I saw that in some cases there is a decoupling of primary organ migration from the presence of glia on their connecting nerves in the *Da* that was not observed in the *wt*, again functional relevance is missing. All in all, the role of glia in *pLL* development in Medaka is highly puzzling and very different from the situation in Zebrafish, it does however seem possible that at least early specification defects of glia can lead to *pLL* pattern difference in Medaka.

Neural stem cells induce the formation of their niche during development

After neuromast deposition and pattern formation organ differentiation takes place. A mature neuromast organ is formed of 3 main cell types (although recent work identifies even more refined sub-populations based on RNA-seq data (Lush et al., 2019). A differentiated cell type known as hair cells (HCs) are the sensing ciliated structures with the primary function of detecting water movement and relaying the information back to the brain (Ghysen and Dambly-Chaudiere, 2007; Williams and Holder, 2000). A supporting cell population directly underneath the hair cells replenish lost hair cells (Ghysen and Dambly-Chaudiere, 2007; Hernandez et al., 2007) and both cell types are surrounded by Mantle cells (MCs) (Jones and Corwin, 1993; Steiner et al., 2014). It has been hypothesized but never proven that mantle cells are the stem cells of neuromasts (Dufourcq et al., 2006; Jones and Corwin, 1993; Stone, 1933; Wada et al., 2013; Ghysen and Dambly-Chaudiere, 2007). Here we prove that mantle cells can act as neural stem cells both during regeneration and under homeostatic conditions (Seleit et al., 2017b). We show that neuromasts of Medaka can regenerate efficiently unlike Medaka hearts and retinas (Lust & Wittbrodt 2018; Ito et al. 2014; Lai et al. 2017) which points to an interesting asymmetry in organ regeneration capacities that is quite different from Zebrafish and more close to the mouse and human conditions. We also report the presence of a new cell type in neuromast organs and we trace its developmental origin to show that the arrival of neural stem cell precursors is sufficient to trigger the induction of normal epithelial cells into nBCs, this is quite similar in overall logic and even molecularly to another induction that happens during development

of the lens from the epithelium by neural retina precursors (Cvekl and Ashery-Padan, 2014; Gunhaga, 2011; Bailey et al., 2006). We show that upon the transformation event nBCs lose key molecular markers of epithelial cell identity in addition to changing their morphology. We show that this fate-change is stable and lifelong and hypothesize based on the evolutionary conservation of nBCs and their role in maintaining the architecture of the neuromasts that they can act as the stem cell niche for mantle cells. Indeed, it has been shown that most stem cell niches have a different lineage than their respective stem cells (Fuchs et al., 2004) this raises a series of fundamental developmental biology questions that remain unanswered those include: do stem cells and their niches form independent during development? If so how do they locate to their respective final locations? Which form first the stem cells or the niche (Ouspenskaia et al., 2016)? And what is the nature of their initial interaction (Tamplin et al., 2015)? The conditions for being a niche in a variety of models is physical contact with the stem cells, displacement away from the niche leads to a loss of stemness (Fuchs et al., 2004; Morrison and Spradling, 2008; Nystul and Spradling, 2006; Scadden, 2014), we observe both criteria in the context of the interaction of mantle cells with nBCs. Our results therefore suggest that during development stem cells are able to induce the formation of their own niches which in turn maintain the stemness of the resident adult stem cells (Tulina and Matunis, 2001; Xie and Spradling, 1998). This concept is new but there is a growing body of experimental evidence from other models that supports the conclusion that this phenomenon could be more widely utilized (Tamplin et al., 2015; Ouspenskaia et al., 2016). This was only elucidated by direct 4D imaging during development which will remain for the time being the gold

standard for understanding the origin and nature of the stem cell-niche interaction during development. I would except that with the tools present at hand in the organoids field this question can be more thoroughly addressed not only by 4D imaging but pharmacological and genetic perturbations. The work that remains to be done is to isolate cell type specific labels for nBCs, FACS sorting them and isolate candidate genes for the signals that maintain the stemness of the neural stem cells of the neuromasts, based on existing evidence it seems that *wnt* ligands could be the sought after signals (Nabhan et al., 2018; Mills, et al., 2017).

Principles of post-embryonic organogenesis in Medaka- How a sensory system copes with a constantly growing body

There are two possible ways a sensory system can cope with a constantly growing body-size. The first is by increasing the size of the organ, as occurs in the retina of Medaka (Tsingos et al., 2019; Centanin & Wittbrodt, 2014) the second is by the constant addition of new functional units which happens in the lateral line of teleosts (Ghysen and Dambly-Chaudiere, 2007; Sapede et al., 2002, Nunez et al., 2009). Surprisingly what I discovered in Medaka is that both strategies are employed in the neuromast system; organs grow massively in size by increasing constituent cell numbers and new neuromasts are also being added. This is in sharp contrast to the situation in Zebrafish where neuromasts do not grow in size as the fish grows (Wada et al., 2013a; Wada et al., 2013b). This organ size regulation is governed by a tight *wnt/dkk* feedback loop that maintains the proportionality of the cell types within the system (Wada et al., 2013b). The fact that in Medaka neuromasts constantly grow argues that this feedback loop might operate under more permissive conditions. This can be experimentally tested first by checking

wnt ligands and receptor expression in Medaka neuromasts, and by forced expression of *dkk* from hair cells of Medaka to observe whether we can force the neuromast to stop growing. I have also analysed in detail the steps involved in building new organs in Medaka, there more surprises were in store. Unlike the situation in Zebrafish where innervation is absolutely required for new organ formation and hair cell development (Wada et al., 2013a), the *pLL* nerve is completely dispensable for both processes in Medaka. This again argues that both systems have evolved different strategies for organogenesis and that they might be operating under differential selective pressures. I have also analysed in detail the steps leading to new organ formation in the CNC of Medaka(Wada et al., 2008). There, stereotypic individual stem cell migration drives organogenesis. This heterogeneity in stem cell behaviour involves the reutilization of molecular players involved in migration and present in precursor cells (upregulation of *eya1* expression), possibly something akin to a highly controlled EMT is occurring (Dongre & Weinberg, 2019). This is particularly important to identify and study the control mechanisms with better detail since it is known that in cancer the EMT process becomes dysregulated and this drives metastasis (Dongre & Weinberg, 2019). This process of post-embryonic organogenesis in the CNC cannot be altered by the loss of the nerve or by ablating the posterior half of the founder neuromast arguing for a highly robust cellular decision making that does not seem to be easily reversible. More organs are added in a similar way in the CNC, what I have also shown is that the same individual cell migration occurs in the *aLL* of Medaka, and there the direction of migration can be from the anterior or posterior end of the founder neuromast. It is possible that the cells are perceiving an attractive signal

from the surrounding tissue that drives the stereotypic nature of organ positioning. Indeed, the *k15* mutant is the only case in which I sometimes observe clear positioning phenotypes in the CNC of Medaka where instead of organs forming first in an anterior-posterior direction they either form or migrate to dorso-ventral ones. This argues that a stable intact epithelium is important for neuromast organ positioning even post-embryonically. This is highlighted even better in Juvenile *k15* mutants that show some 'permissive' neuromast routes that are in the *wt* situation never taken and possibly 'blocked' by an intact epithelium. The modulation of epithelial tissue tension could therefore not only affect embryonic *pLL* patterns but also post-embryonic organ numbers and positioning. At the moment, we cannot exclude that the defect could be intrinsic to mantle cells that express *k15* (however with ongoing and growing transplanted fish we might be able to answer this issue). Another way in which neuromast organs are built is what is known as organ stitching/budding (Nuñez et al., 2009; Wada et al., 2013a; Ghysen & Dambly-Chaudiere, 2007), I have characterized the steps leading to this process in Medaka. This occurs in primary and secondary organs at juvenile stages and involves the upregulation of *k15* expression throughout the existing organ followed by a compartmentalization and the appearance of two connected centres of hair cells, this is in turn followed by organ separation and the down-regulation of *k15* expression to be restricted once more to the mantle cell population. The direction of stitching I observed was usually dorso-ventral even though I have seen cases of anterior posterior stitching also occur. All in all, Medaka neuromasts can be formed by a variety of organogenesis routes; either by cluster deposition from the primordium, individual cell coalescence as occurs during secondary organ

formation, individual cell migration out of a mature organ as occurs in the CNC and *aLL* systems and stitching as occurs in the secondary organs in juvenile and adult stages. This points at the truly astounding plasticity of developmental and organogenesis programs in producing the same exact outcome (neuromasts) by a variety of distinct routes. This organogenesis plasticity is an area that I believe should be explored in more detail by developmental biologists in the future and could benefit a lot from the burgeoning organoid field. Where essentially rudimentary developmental 'recipes' can still produce with a high degree of accuracy organ-like structures. Again, pointing towards the inherent self-organizing properties of cells and their ability to follow even partial and highly fragmented 'instructions.'

Fat1a exploratory cells and heterogeneities of stem cells *in vivo*

Fat1 is a rather large member of the cadherin proteins superfamily and has been shown to be important for a variety of processes including cell adhesion and planar cell polarity (Sopko & McNeill, 2009). Fat1 function has been linked to the hippo pathway (Sopko & McNeill, 2009; Ahmed et al., 2015) with defective expression leading to neuronal differentiation (Ahmed et al., 2015; Helmbacher, 2018) and renal tissue problems (Gee et al., 2016). It has also been shown by RNA-seq data that *fat1a* is highly expressed in mantle cells (Steiner et al., 2014). I confirmed this by generating a transgenic line relying on a partial promoter of the Medaka *fat1a* driving GFP. Indeed, this turned out to be a highly specific label for mantle cells in mature neuromasts. More interestingly however I define a new sub-population of 'exploratory' cells that are attached and part of mature neuromast organs. These

cells are highly dynamic and motile and tend to cluster around the *pLL* nerve connections. The function of these cells remains unknown but I hypothesize that they act as sensing antennas for neuromasts and could participate or kick-start neuromast organogenesis post-embryonically if conditions are favourable. Crucially the expression of *fat1a* is significantly higher in the exploratory cells than in resident mature mantle cells. Indeed previous work on *fat1* in other systems has shown that it is an important regulator of actin dynamics, polarization and migratory potential of cells (Tanoue & Takeichi, 2004; Moeller et al., 2004; Helmbacher, 2018). The higher *fat1a* expression observed in exploratory cells can therefore be linked to their migratory potential. This is further supported by the fact that during post-embryonic organogenesis in the CNC of Medaka individual mantle cells upregulate *fat1a* expression prior to and during their migration to form a new organ. As such *fat1a* heterogeneities in mantle stem cells can lead to a differential behaviour where cells are more likely to escape the organ and start forming a new neuromast if they have higher *fat1a* expression. Every single mantle cell observed undergoing individual cell migration to participate in new organ formation in the CNC upregulated *fat1a*. This raises the spectre that *fat1a* could be functionally important in setting up the heterogeneities in stem cells that would in turn lead to differential behaviours. This is supported by the fact that *fat1* has been shown to act upstream of major signalling networks like the hippo pathway (Ahmed et al., 2015). The role of *fat1a* in the context of the neuromasts can be investigated by functional approaches however I failed to detect any phenotypes probably due to compensatory mechanisms (El-Brolosy et al., 2019) from closely related *fat* proteins or a failure of the targeting approach.

The *pLL* and *aLL*: two contrasting systems building the same organs

The anterior lateral line (*aLL*) is a system of neuromasts located around the head and eyes of teleosts that arises from placodal tissue during development (Ledent, 2002; Piotrowski & Baker, 2014; Ghysen & Dambly-Chaudiere, 2007). In contrast to the plasticity of the *pLL* both within and between species, I report that the *aLL* pattern is highly stable and conserved (Ledent et al., 2002; Owens et al., 2007; Ishikawa et al., 1994; Raible & Kruse 2000). This could be due to the difference in the induction of the placodes forming the *aLL* and *pLL* (Nikaido et al., 2017). Indeed, I have shown that even within the same fish there is a highly ordered and symmetrical *aLL* and a rather disordered *pLL*. My analysis on *k15, Da* and glial cell mutants revealed no obvious modulation of pattern or organ numbers in the *aLL* and a massive effect on the *pLL*. The only mutant that gave a phenotype in both the *aLL* and *pLL* was *eya1*$^{-/-}$ and there again the severity of the mutation was stronger in the *pLL* than the *aLL*. All of this argues for a different developmental trajectory of the *aLL* and possibly a high buffering capacity of this system in contrast the *pLL*. Why this is the case remains unclear, whether there is an evolutionary benefit to this is also unclear but it would be interesting to see which evolved first the *aLL* or the *pLL* or was their evolution in parallel. A commonality between the *aLL* and *pLL* is the building of neuromasts post-embryonically which relies on the same individual cell migration processes in both systems.

How to build a highly evolvable constantly remodelling sensory system

So far I have taken you on a journey from when the initial 120-140 cells started their collective pilgrimage along the horizontal myoseptum setting up the *pLL* of Medaka in the process. We have seen how plastic this system is both in terms of

organ numbers and positioning by the aid of genetic mutants and environmental modulation. And I have argued (hopefully convincingly) that the embryonic *pLL* should be regarded as a system with a low Waddingtonian developmental buffering capacity. This feature might explain the extremely rapid evolvability of the system and its adaptation to the highly dissimilar body plans of teleosts. This can be contrasted to the stability of the *aLL* pattern and organ numbers within and between species. Why both systems are operating with different evolutionary capacities remains unclear but could relate to the different paths of development they undertake (Nikaido et al., 2017). It is however clear that the high evolvability of the *pLL* must have some sort of functional relevance otherwise it would not have been selected for. We then focused on how the neuromast organs differentiate and how the process is inherently self-organizing both in terms of where the organs end up & their induction capacities on neighbouring cells. Next we went into principles of post-embryonic organogenesis only to be confronted once again with the varied strategies utilized to build the same organs. All of this building, growth and rebuilding happens while maintaining the functionality of the system as a whole to guide fish in their sensory perception of the world. Traversing tissue to cellular and even molecular scales I hope I have conveyed my deep sense of wonder at the intricacies & plasticity of this fascinating system. I would end by stressing the importance of taking a systems approach (i.e. trying to distil general principles of operation by studying the totality of a process and its emergent properties at different scales). In addition to the necessity of a comparative-species approach if one wants to gain insights both into the operational logic of a system and to understand its evolution.

Appendix

Sequenced alleles in *k15* (F1) and *eya1* (F2) CRISPR mutants

A

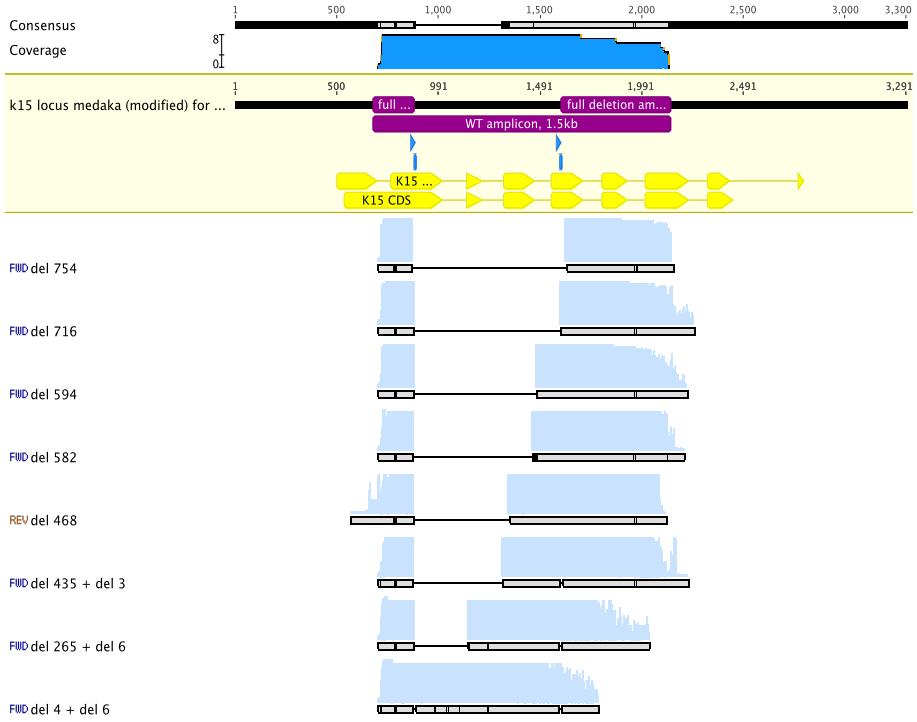

B

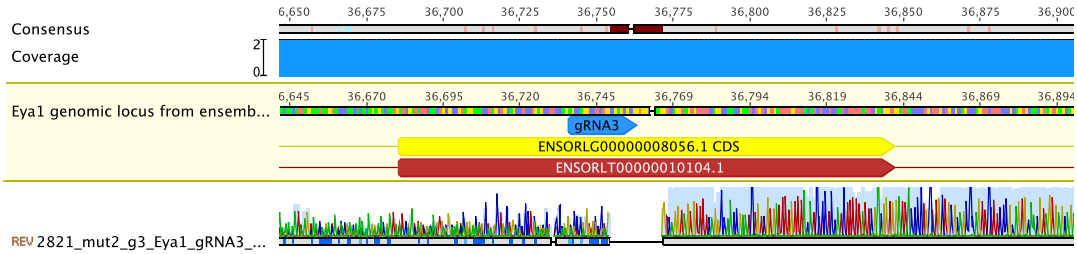

Figure (35) (A)Range of F1 K15 mutant alleles isolated, we focused our efforts on raising a homozygous deletion of 468bp (B) Characterization of stable Eya1 CRIPSR mutant line shows the presence of a small deletion in the region of gRNA3.Illustrations are direct adaptations from GENIOUS and were done with the help of Jonas T.

Symmetry in *aLL* organ numbers and positions

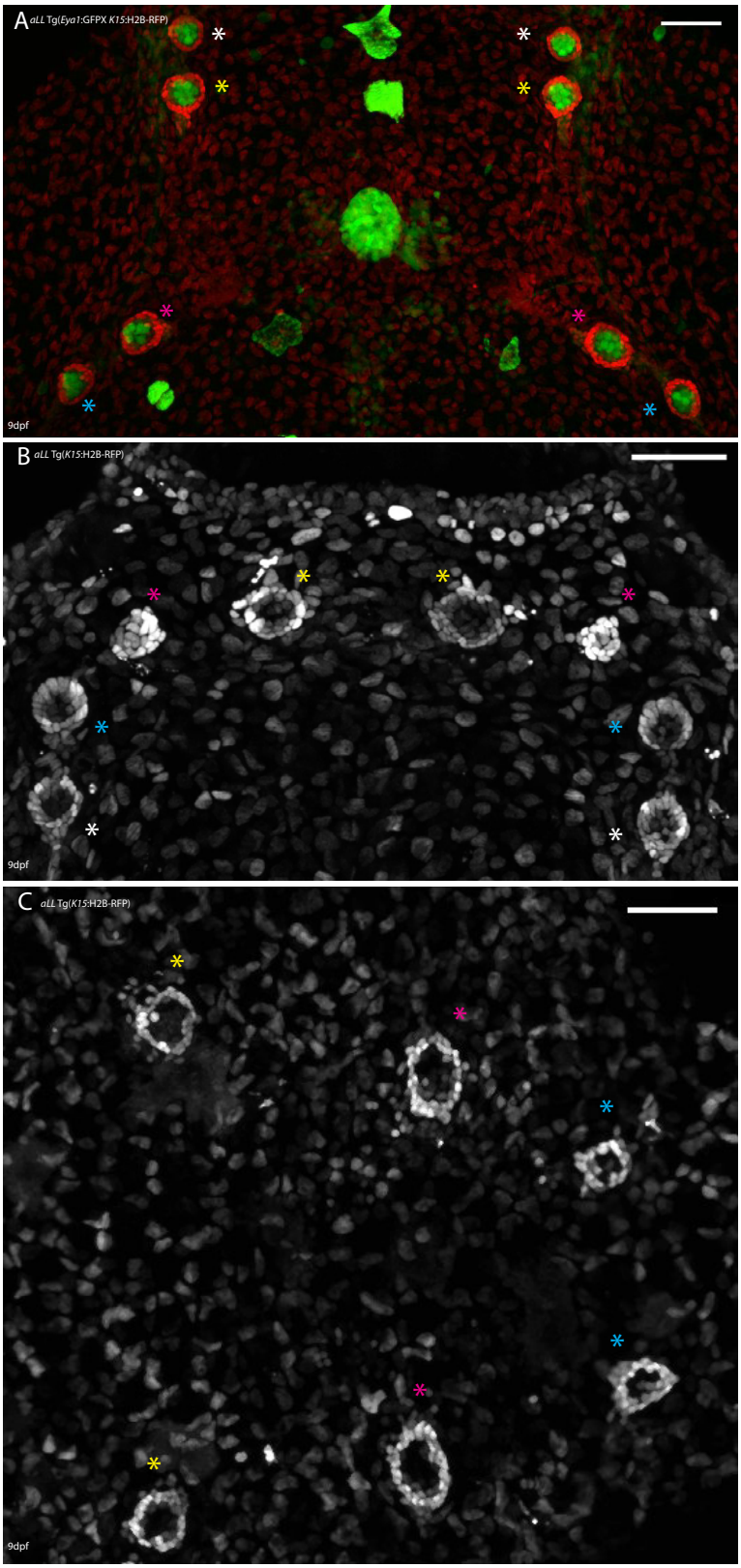

Figure (36) (A) Dorsal view of mid-brain *aLL* pattern in 9dpf double transgenic Tg(Eya1:GFP K15:H2B-RFP) notice that the positions and numbers of organs are symmetrical between the left and right hand sides (organ pairs have same asterisk colors) Scale bar=50 microns N=8 anterior=up posterior=down. (B) Dorsal view of anterior most *aLL* pattern in

9dpf Tg(K15:H2B-RFP) notice that the positions and numbers of organs are symmetrical between the left and right hand sides (organ pairs have same asterisk colors) Scale bar=50 microns N=8 anterior=up posterior=down. (C) Dorsal view of hind-brain *aLL* pattern in 9dpf Tg(K15:H2B-RFP) notice that the positions and numbers of organs are symmetrical between the left and right hand sides (organ pairs have same asterisk colors) Scale bar=50 microns N=8. anterior is to the left posterior is to the right.

The following section involving the results and discussion of the *desmogon* story are entirely written by myself and are currently under review in eLIFE. They will be utilized as is with correct referencing.

While searching for a putative label for neuromast nBCs I came across members of the *desmoglein* family of genes. These are desmosomal cadherins that are an integral part of desmosomes. Since we found desmosomes connecting nBCs to Mantle cells from our EM data I decided to clone a few partial promoters of *desmoglein* family members of Medaka under GFP. After injection, one partial promoter (*desmogon*) gave strong expression not in nBCs but the notochord. Below is how the story developed from there.

“

***desmogon* is a fish-specific desmosomal cadherin expressed in the notochord**

While searching for a stable marker for neuromast border cells (Seleit et al. 2017) we serendipitously came across a novel uncharacterized *desmog-2-like* gene (ENSORLG00000017110), which we named *desmogon*. The 5.3Kb long transcript of *desmogon* is distributed over 14 exons and encodes a protein with at least 3 desmosomal cadherin domains and one cytoplasmic cadherin domain (Supplementary Figure 1). Based on the amino acid sequence the expected sub-cellular localization is plasma membrane and it is predicted to function as a component of the inter-cellular desmosome junctions. A list of all known orthologues of *desmogon* suggests that this gene is fish-specific, as it is absent in all other sequenced chordates (materials and methods for details). Among fish, the *desmogon* locus is conserved in the vast majority of teleost branches although interestingly, it seems to have been lost in Zebrafish and Tetraodon (as evidenced by the syntenic conservation of the surrounding genomic region) (Supplementary Figure 1). *In situ* hybridization showed *desmogon* to be highly expressed in the developing notochord of Medaka (Figure 37A). To gain a better understanding of

the dynamic spatial expression of *desmogon* we generated the Tg(*desmog*:EGFP) (Figure 37B-F) by using a 2.2kb proximal promoter region that contained strong peaks of H3K4 methylation (Supplementary Figure 1). Confocal analysis of mosaic, injected *desmogon*:EGFP and of Tg(*desmogon*:EGFP) medaka embryos revealed EGFP expression in the developing notochord throughout embryogenesis (Figure 37B-F), this expression persists in adult fish in a segmented pattern along the spine (data not shown). Within the notochord, *Desmogon* labels vacuolated cells *(*Figure 37 C, F, arrows in Figure 37E, 1F) and a proportion of covering sheath cells *(*yellow asterisks in Figure 37E, 37F). The expression of a Desmoglein family member in vacuolated and sheath cells suggests the presence of desmosomes in both cell-types, therefore we followed an electron microscopy (EM) approach to characterise the notochord of 10 dpf *wild-type* medaka larvae at the sub-cellular level. Previous studies reported the existence of caveolae in the cellular membrane of vacuolated cells in the zebrafish notochord (Nixon et al., 2007; Lim et. al, 2017), which we confirmed is also present in medaka (Figure 37 G, G'). Additionally, we observed the occurrence of desmosomes mediating the physical association of neighboring vacuolated cells (Figure 37G, G'), presumably to enhance their inter-cellular adhesion capacities. Desmosomes were also found connecting sheath to vacuolated cells (Figure 37H, I), and sheath to sheath cells (Figure 37I). Altogether, our results reveal the expression of an uncharacterised Desmoglein family member in the two cell types of the notochord that concurrently display desmosomes on their cellular membranes." Adapted directly from (Seleit et al., 2019 under review).

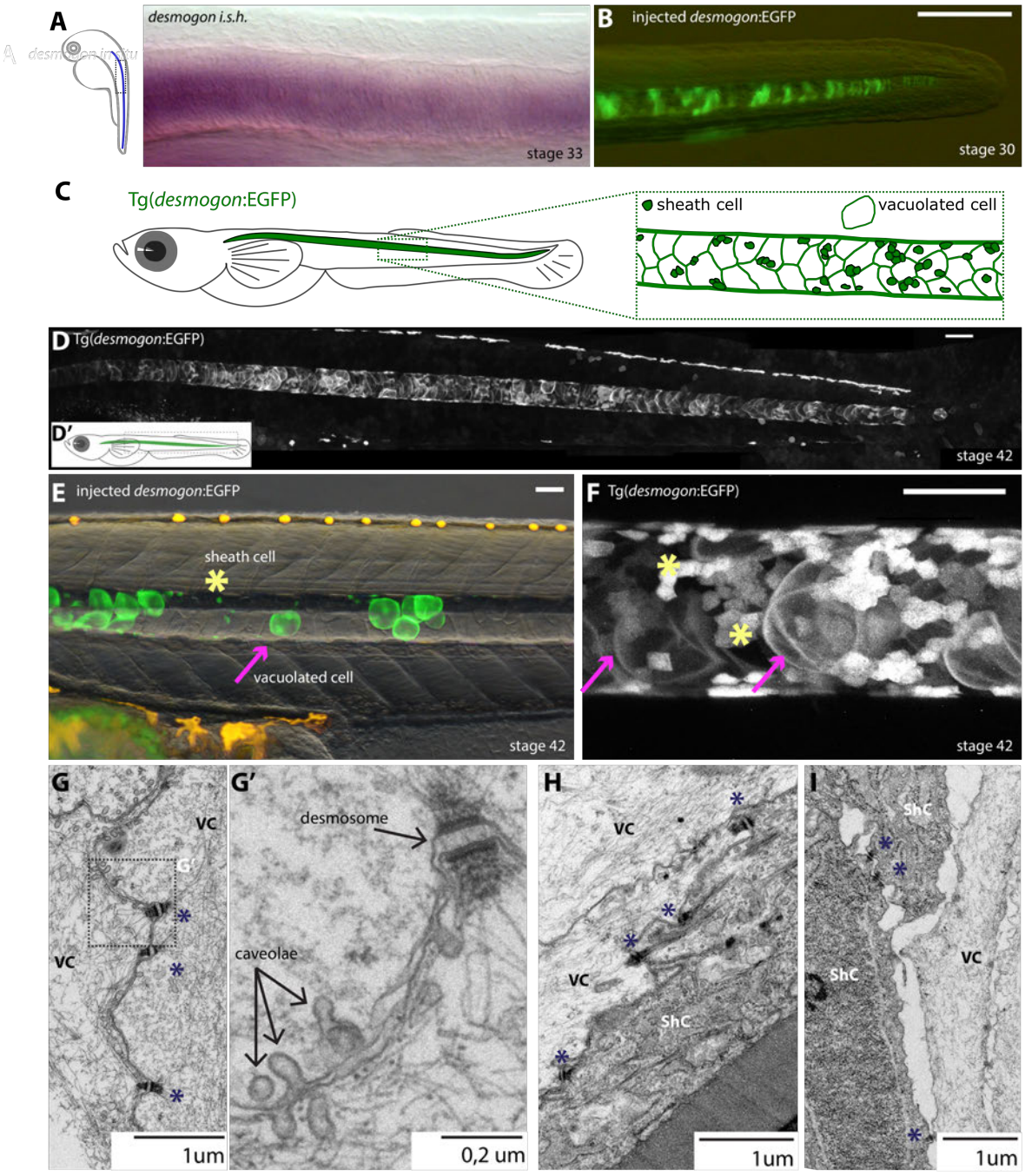

Figure (37) **"**d*esmogon* is a desmosomal cadherin that labels the notochord throughout embryogenesis in Medaka**."** (Seleit et al., 2019 in revision) "(A) *in-situ* hybridization on *desmogon* in stage 33 medaka embryos reveals strong enrichment in the notochord. Scalebar=20 microns (B) mosaic injection of desmogon:EGFP in medaka embryos stage 30, labels the notochord . Scale bar=100um (C-D) Transgenic line *Tg(desmog:EGFP)* labels the notochord in Medaka at stage 42 embryos. Scalebar=100 microns (E-F) Maximum projection of mosaic injected (E) and *Tg(desmog:EGFP)* (F) labelling notochord vacuolated cells and a proportion of covering sheath cells. Magenta arrows indicate vacuolated cells and yellow asterisks sheath cells. Scalebar= 50 microns (G) Longitudinal EM section in between vacuolated cells connected by desmosomes (black asterisk) Scale bar= 1 micron (G') Desmosomal structure and caveolae present between vacuolated cells Scale bar = 0.2

micron. (H) Longitudinal EM section showing desmosomal connections between sheath cells and vacuolated cells scale bar= 1 micron. (I) Cross-section EM showing desmosomal connections between two sheath cells in addition to desmosomes between sheath cells and vacuolated cells scale bar= 1 micron." Figure & legend adapted from (Seleit et al., 2019 in revision) "

Vacuolated cells grow as autonomous units

The Tg(desmog:EGFP) allowed us to follow the axial extension of the notochord as the embryo develops. Notochord expansion was mediated by the growth of vacuolated cells that not only increase in size but also change their circular morphology into a more oblique shape as the notochord matures (Figure 38A, B) (n>10). Using single plane illumination microscopy (SPIM) (Krzic et al., 2012) we observed that vacuolated cells grow anisotropically over time (Figure 38C-E, and Supplementary Figure 2) in a process that appears to be irreversible (N>50 cells). Our 4D data also suggests that desmogon+ vacuolated cells in medaka are post-mitotic, since we have not detected dividing vacuolated cells in any of our imaging (N=3 embryos at 4 dpf, and N=2 embryos at 3dpf image for 24h, N>50 cells). Remarkably, our analysis revealed that vacuolated cells increment their size in a locally uncoordinated manner, where even neighbouring vacuolated cells grow at different rates (Figure 38C-E'). These results demonstrate that vacuolated cells grow as autonomous units. We next wondered whether the Medaka notochord grows in size just by the increase in volume of vacuolated cells, or if in addition new vacuolated cells are being incorporated. We observed desmogon+ precursor cells differentiating into vacuolated cells (Figure 38D-E') in a process that occurred along the notochord. The formation of new vacuolated cells was more frequently observed at the posterior tip of the extending medaka notochord (Figure 38E-E'') (Total N=8 cells in 2 independent embryos). Our data indicates that during axial extension the number of vacuolated cells increases in the notochord, however, this is not the only cell-type that needs to be amplified during notochord extension. We

therefore aimed to better resolve the cellular processes leading to the incorporation of new vacuolated and sheath cells as the notochord grows." Adapted directly from (Seleit et al., 2019 under review).

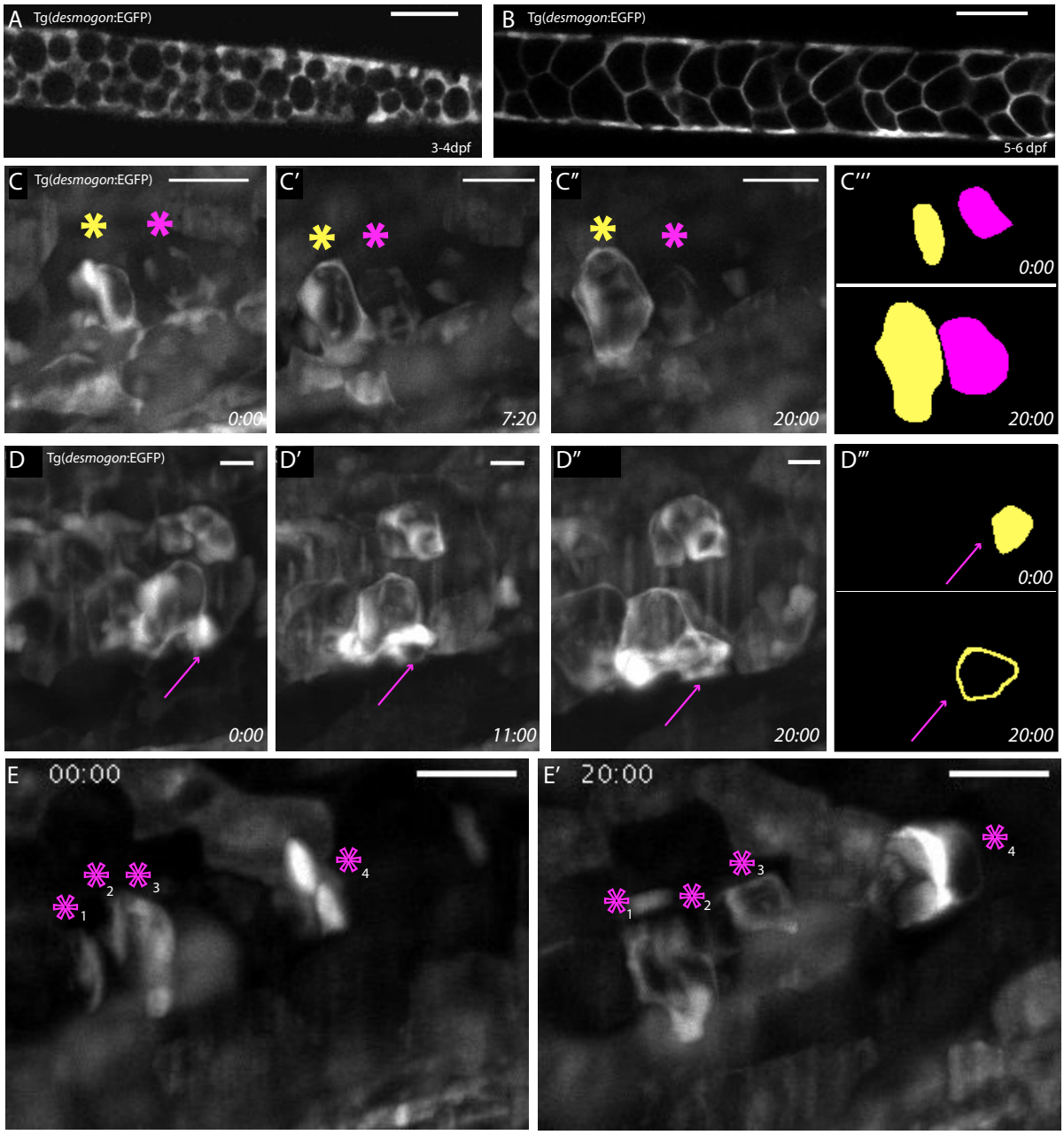

Figure (38) "Live-imaging of *Tg(desmog:EGFP)* reveals Medaka notochord growth dynamics." (Seleit et al., 2019 in revision) "(A) Single plane of 3-4dpf *Tg(desmog:EGFP)* embryo showing vacuolated cells, notice more circular shape and small size compared to (B) 5-6dpf *Tg*Desmogon::EGFP, bigger and oblique vacuolated cells. n>10. Scalebar=50 microns. (C-C‴) SPIM time-lapse imaging *of desmogon+* vacuolated cell growth over time highlighted with yellow and magenta asterisks (n>10 vacuolated cells in 3 embryos at 4-5dpf and n>10 vacuolated cells in 2 embryos at 3-4dpf). Scalebar=20microns. (D-D‴) Differentiation of desmogon+ precursors into vacuolated cells near mid-point of notochord. Arrow labels cell of interest. (E-E') Differentiation of a number of desmogon+ precursors into vacuolated cells near tip of the tail and growing notochord (magenta asterisks). Scalebar=20 microns. Time in hours. Total n=8 sheath cells in 2 independent embryos." Figure and Figure legend adapted from (Seleit et al., 2019 in revision).

“

Behavioural heterogeneity of notochord precursor cells

In addition to labelling vacuolated and sheath cells in medaka, the (desmogon:EGFP) shows expression in early, undifferentiated notochord precursors known as disc-shaped-progenitors (Figure 37B). To gain a finer spatial/temporal resolution on the formation of vacuolated and sheath cells in the notochord, we decided to inject the desmogon:EGFP construct into zebrafish embryos. Even though a desmogon orthologue is not present in this species, we could observe labelled vacuolated and sheath cells in desmogon:EGFP zebrafish injected embryos (Supplementary Figure 3), indicating that the transcriptional machinery driving expression of medaka desmogon is conserved in distantly related teleosts. Live-imaging on embryos with EGFP+ clones in the notochord revealed that the growth of vacuolated cells is incremental but also locally uncoordinated in Zebrafish (n=6 embryos n>10 vacuolated cells). Focusing on earlier stages of notochord development, we were able to clearly observe vacuolated and sheath cell formation from undifferentiated desmogon+ notochord precursor cells. These disc-shaped precursors were located primarily but not exclusively at the growing posterior tip of the notochord. We observed two distinct, mutually exclusive cellular behaviours in desmogon+ precursors. Either they directly generate a single vacuolated cell (Supplementary Figure 3, magenta asterisk) (N=9 cells), or they undergo a dorso-ventral symmetric division leading to the formation of sheath cells (Supplementary Figure 3, yellow asterisk) (n>10 cells). This behavioural heterogeneity does not seem to be temporally controlled or governed by morphogenetic gradients, since both cellular outcomes can occur simultaneously in neighbouring precursors. Our data shows that disc-shaped

desmogon+ precursors can directly differentiate into vacuolated cells that will not undergo mitosis throughout our imaging (n>10 cells in=6 embryos), while the formation of sheath cells necessitates a symmetric division that could be followed by further amplifying rounds of divisions (n>10 cells in n=6 embryos). Interestingly, we consistently observed that disc-shaped precursors contained a detectable vacuole which was expanded during vacuolated cell differentiation, and lost during the maturation of sheath cells. Indeed, directly after the dorso-ventral symmetric division, a proportion of newly formed sheath cells do contain small vacuoles (n>10 cells in n=6 embryos), suggesting that this feature could reflect an earlier developmental state that must be repressed during the maturation of sheath cells. Although phylogenetically distantly related within the teleost branch, the results from Zebrafish mirrored our findings in Medaka, particularly the non-mitotic nature of desmogon+ vacuolated cells. Our results indicate that in both species disc-shaped precursors are exhausted by the end of notochordal development, which raises the question of whether and how vacuolated cells can be replaced after injury of mature Medaka notochords." Adapted directly from (Seleit et al., 2019 under review).

"

Vacuolated cell loss triggers a robust and localized regeneration response in medaka

Spatially targeted and precise multi-photon laser ablation of 6-10 vacuolated cells of 5-6 dpf Tg(desmogon:EGFP) embryos resulted in the specific loss of cells in the area of injury (Figure 39A). Both sheath and vacuolated cells outside the ablated zone retain a normal morphology and the overall integrity of the notochord is

unaffected. We next assessed whether a regeneration response can occur in the ablated area. Indeed, 48-hours post injury we observed the appearance of small desmogon+ vacuolated cells specifically in the area of injury (Figure 39B) (n=8 embryos). Interestingly, the overall morphology, presence of a small vacuole, and EGFP+ expression of these cells was highly reminiscent of the earliest vacuolated sheath cells we observed during development in Zebrafish notochords, suggesting that the source of new vacuolated cells is the same in both species (Garcia et al. 2017). The small vacuolated cells grow in size over time as assessed at 5 days post injury (Figure 39C) (n=8 embryos), this growth followed the same autonomous rationale we observed under physiological conditions in Medaka. Overall, our results indicate that Medaka notochords can mount robust regeneration in response to vacuolated cell loss. This occurs in a highly spatially localized manner that is restricted to the initial injury site." Adapted directly from (Seleit et al., 2019 under review).

"

Peri-notochordal membrane injury triggers a global regeneration response

The perinotochordal membrane is a thick ECM layer that ensheathes the notochord and helps to maintain its integrity. To test the effect of a sudden loss of hydrostatic pressure within the notochordal tube, we ablated the lower lining of the peri-notochordal membrane (Figure 39D). Two days post-injury we observed desmogon+ cells leaking outside of the notochord tube, indicating that the lower lining of the notochordal membrane failed to be repaired. This in turn led to a loss of notochord morphology and the appearance of small vacuolated cells no longer

became restricted to the injury site but were rather spread over the entire tube (Figure 39E). Interestingly, perinotochordal injury and the concomitant lack of repair triggered a global regenerative response even in the absence of vacuolated cell ablation anterior and posterior to the targeted site. Five days post-injury the leakage of notochord vacuolated cells continued and the morphology of the notochord was heavily perturbed. We observed a cluster of desmogonGFP+ vacuolated cells ventral to the notochord tube at the site of the original injury, and small vacuolated cells persisted anterior and posterior to the injury site (Figure 39F) (n=3). Overall, we conclude that injury to the peri-notochordal membrane cannot be repaired efficiently in Medaka. This leads to cell leakage and a perturbed notochord morphology, which in turn triggers a global regeneration response that is not spatially restricted to the initial injury site." Adapted directly from (Seleit et al., 2019 under review).

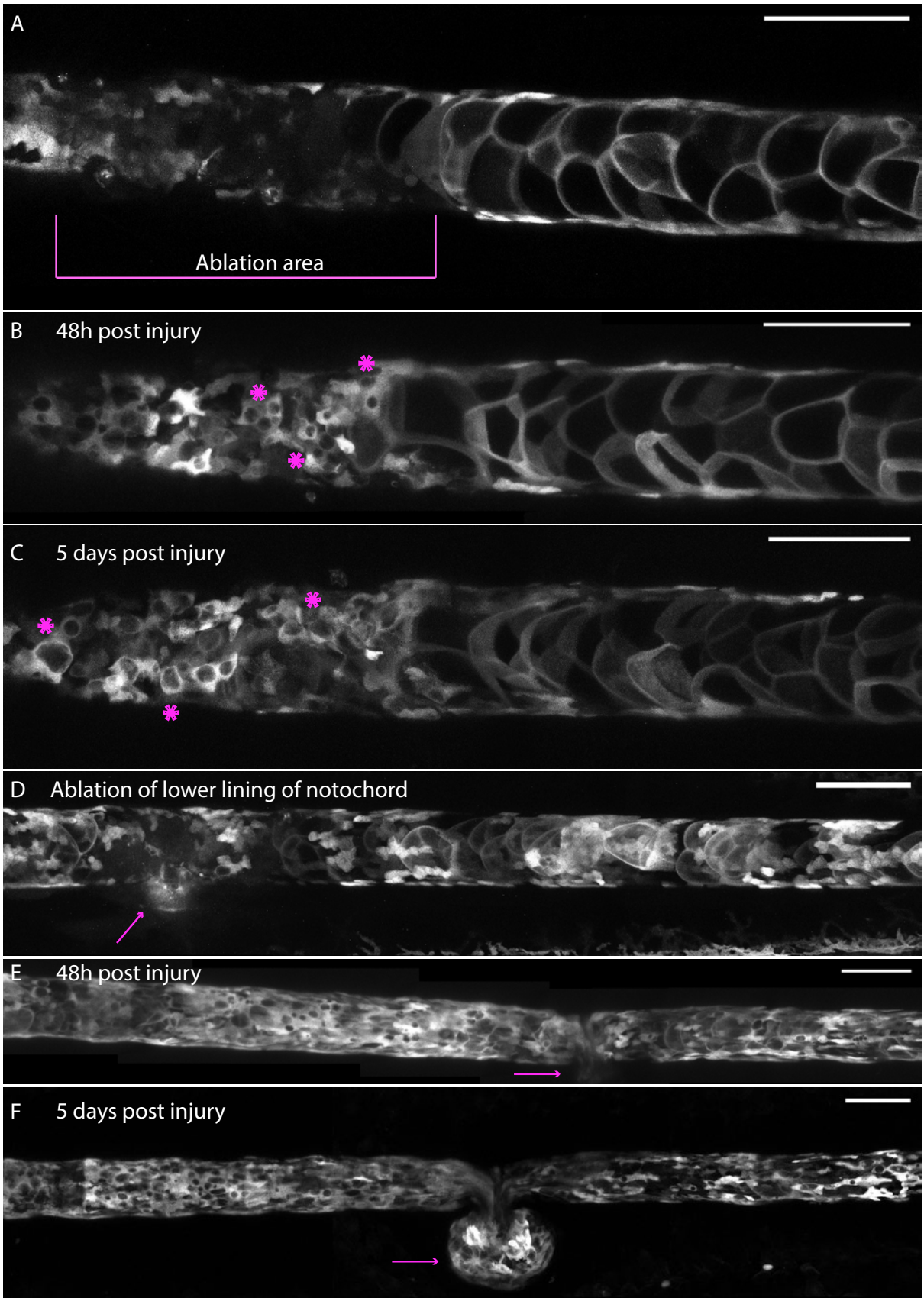

Figure (39) "Local and global regeneration dynamics after notochord injury" (Seleit et al., 2019 in revision)

"(A) *Tg(desmog:EGFP)* 6dpf embryo post ablation. Ablation area indicated by magenta lines. Vacuolated cells in the ablated zone are missing. Vacuolated cells outside ablation zone are intact and morphologically normal. Scalebar= 100 microns. (B) Same embryo 48 hours post injury. Notice the appearance of small vacuolated cells specifically in the ablated zone. Regeneration of injured area is initiated. Vacuolated cells in uninjured area appear normal. Scalebar= 100 microns. (C) Same embryo 5 days post injury vacuolated cells grow in size, notochord is intact. Scalebar= 100 microns. n=8 embryos. (D) Ablation of vacuolated cells and lower lining of notochord tube. (E) 48 hours post injury, magenta arrow highlights position of injury, notice failure to regenerate and leakage of *desmogon+* cells outside of notochord. Overall notochord morphology grossly altered both anterior and posterior to injury site. Notice appearance of small vacuolated cells outside original injury site. Scalebar= 100 microns. (F) 5 days post injury magenta arrow highlights growing leakage of *desmogon+* vacuolated cells outside of the notochord. Failure to repair and correctly regenerate lower tube lining is evident. Gross morphological defects apparent over entire length of notochord. Notice the appearance of small vacuolated cells throughout the notochord. Scalebar= 100 microns. n=3 embryos." Figure and Figure legend adapted from (Seleit et al., 2019 in revision) The experiments shown in the panels of these figures have been performed by Michaela Woelk and Camilla Autorino under my supervision during a 6-week lab practical.

"

Desmogon crispants & stable mutants exhibit notochordal lesions of collapsed vacuolated cells

To test if desmogon has any functional role during notochord morphogenesis we designed 3 gRNAs targeting different exons along its coding sequence. CRISPR/Cas9 injection into Tg(desmogon:EGFP) resulted in lesions containing collapsed vacuolated cells along the length notochord, which were absent in embryos injected with control oca2 gRNAs (Figure 40 A-C) (Lischik et al. 2018). The vast majority of injected embryos survived until stage 42 and no obvious pleiotropic effects were detected, suggesting the effects observed were notochord specific. Importantly, a proportion of F0 injected embryos that survived to adulthood showed strong signs of bending and defective spine formation (data not shown). The described phenotypes for the F0 injected desmogon crispants were consistently recapitulated in desmogon mutants (Figure 40, Supplementary Figure 5). To gain a better understanding of the structural phenotypes we decided to perform electron microscopy (EM) on desmogon mutants. Longitudinal sections on wild-type notochords were characterised by the typical highly ordered array of vacuolated cells (Figure 40E). This contrasts with the structural disorganisation present in lesioned areas of the desmogon mutant notochords (Figure 40F-H). EM

data also showed the presence of vacuolated cells of appreciably different sizes (Figure 40F, arrows), evidence of vacuolated cell collapse (Figure 40F-G'), and invasion of sheath cells into the central notochord tube that indicates the possible triggering of a regenerative response in the lesioned area (Figure 40F asterisk and Figure 40H, Supplementary Figure 4). Stronger desmogon phenotypes included the loss of notochord integrity and shape as revealed by kinking and buckling along the notochord tube (Figure 41A-C). A closer analysis of the phenotypes affecting embryos with collapsed notochords revealed the presence of larger lesions that were consistently filled with *desmogon+* small vacuolated cells. In addition to being a marker for vacuolated cells, we therefore believe that *desmogon* has a functional role in proper notochord development and shape. Its loss leads to vacuolated cell collapse and the appearance of lesions that contain small vacuolated cells, this can in turn lead to gross morphological defects in the notochord." Adapted directly from (Seleit et al., 2019 under review).

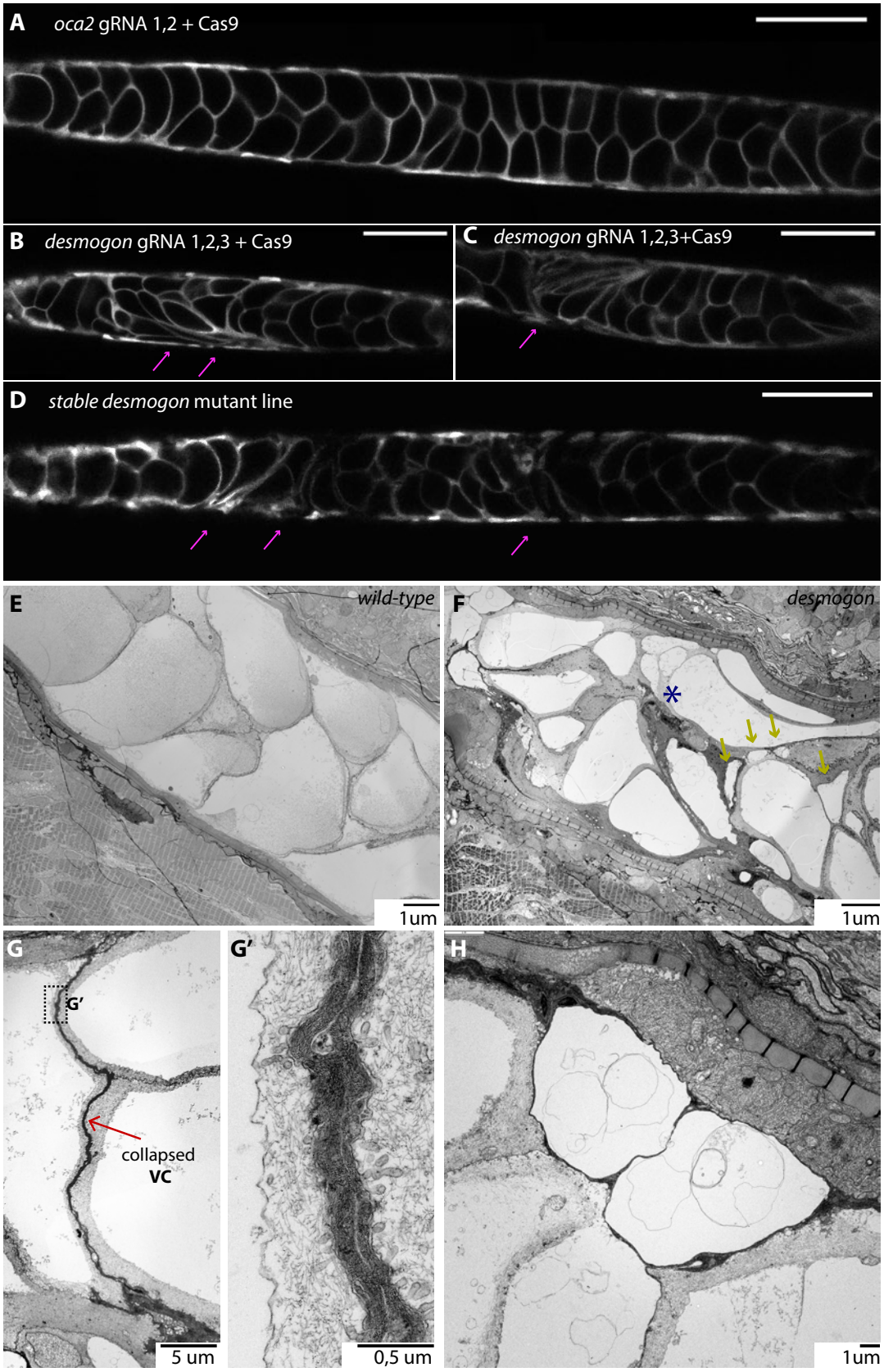

Figure (40) *desmogon* mutants exhibit notochordal lesions and vacuolated cell collapse. (Seleit et al., 2019 in revision) "(A)Control CRISPR injected *Tg(desmog:EGFP)* with o*ca2* gRNA1,2 & Cas9. Single plane. Scalebar=100 microns. (B, C)

desmogon gRNA1, 2, 3 & Cas9 injected into *Tg*Desmogon:E:GFP results in local collapse of vacuolated cells and lesions in the notochord. Single plane. Scalebar=100 microns. (D) Stable desmogon CRISPR mutant line recapitulates phenotypes observed in the injected generation Scalebar=100microns. (E) Longitudinal EM section through wild-type stage 42 medaka notochords with highly ordered vacuolated cell arrangement (F) Longitudinal EM section through lesioned *desmogon* mutant stage 42 notochords, notice the structural disorganization, vacuolated cells with varying sizes (yellow arrows), invading sheath cells (black asterisk) and evidence of collapsed vacuolated cells. (G-G') Longitudinal EM section on *desmogon* mutant notochords reveals the presence of collapsed vacuolated cells. (H) Small vacuolated cells are present in Longitudinal sections of EM in *desmogon* mutants and can be clearly distinguished from the neighboring vacuolated cells and sheath cell." Figure and Figure legend adapted from (Seleit et al., 2019 in revision).

"

Targeted CRISPR screen uncovers novel regulators of notochord integrity

Realizing the concurrence of F0 CRISPR phenotypes with the ones observed for the stable mutant line, as recently reported for other systems (Wu et al. 2018; Lischik et al. 2018; Trubiroha et al. 2018), we decided to use the Tg(desmogon:EGFP) as a fast and straight-forward read-out for notochord defects. We searched for putative regulators of notochord integrity by using the recently generated single-cell transcriptome data from Zebrafish (Briggs et al. 2018; Farrell et al. 2018). We selected a number of well annotated and poorly characterized genes that were conserved across vertebrates and highly expressed during Zebrafish notochord morphogenesis (arrdc3a, kcnk6, pmp22b, si:dkey- 261h17.1 and vgll2b). We then performed a small-scale F0 CRISPR screen (Wu et al. 2018) in Tg(desmogon:EGFP) embryos by targeting each selected gene with 2 gRNAs (for details of selection criteria see materials and methods). For vgll2b this resulted in 55% of injected embryos showing morphological defects in notochord shape and integrity including twisting and bending of the notochord tube (Figure 41D, F and Table 1). Targeting arrdc3a resulted in 30% of injected embryos showing disruption in notochordal integrity, with strong phenotypes including buckling and kinking (Figure 41E, F, and Table 1). Targeting kcnk6, si:dkey- 261h17.1, pmp22b with the same approach resulted in strong phenotypes on the notochord but additionally all three showed significant pleiotropic effects (Stemple et al. 1996), including

general growth retardation, shorter body axes and gross morphological defects (Table 1). It is therefore more difficult to assign causal phenotypes to these genes. It is clear, however, that they directly or indirectly affect correct notochord morphology. In conclusion, using a straight-forward reverse-genetics approach we have uncovered novel and conserved regulators of notochord morphogenesis and maintenance in vertebrates." Adapted directly from (Seleit et al., 2019 under review).

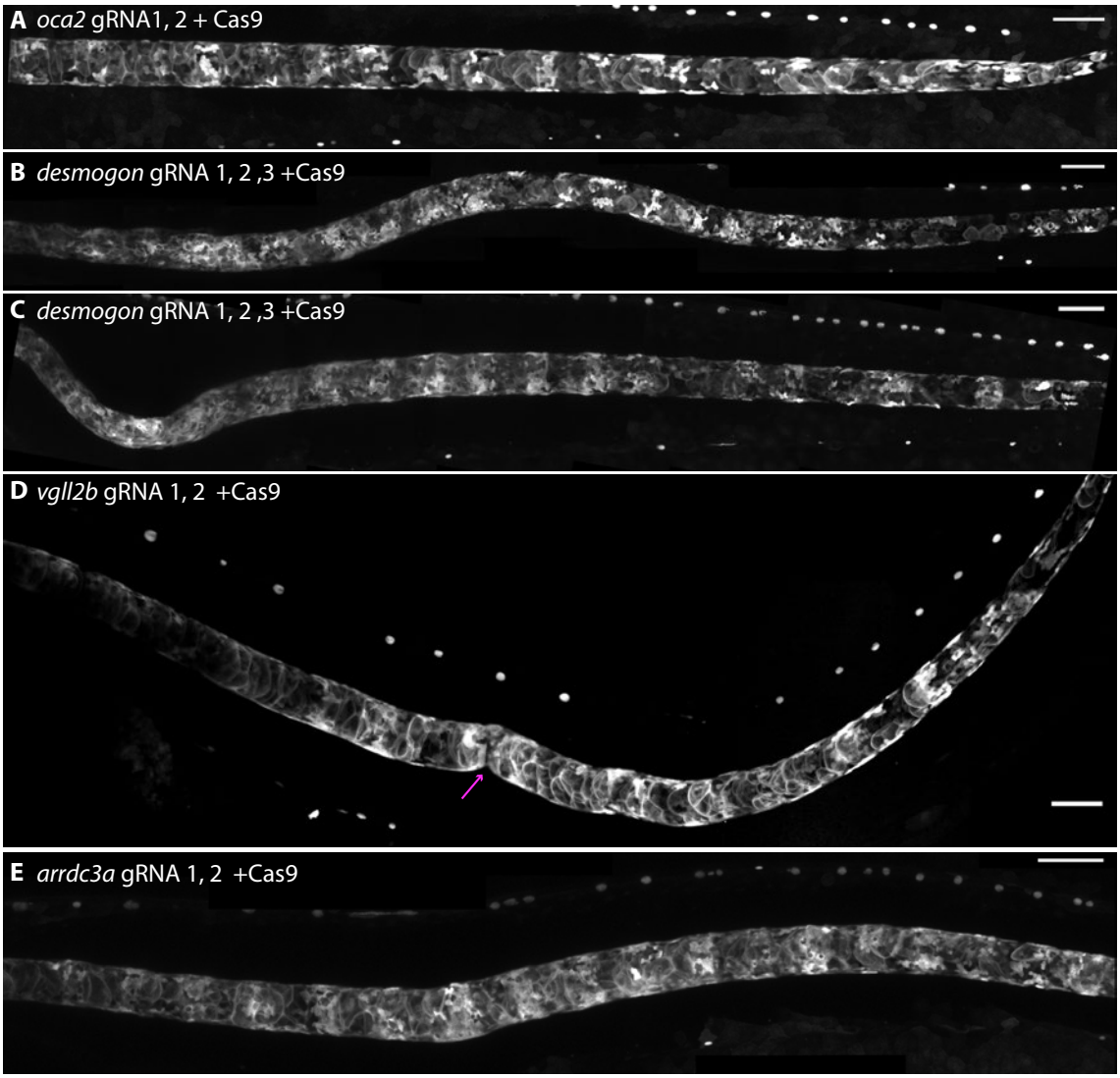

Figure (41) Gross morphological defects in the notochord of *desmogon, vgll2b and arrdc3a* CRISPR injected embryos(Seleitetal.,2019,revision)"(A) Overall morphology of control *oca2* gRNA & Cas9 injected notochord in *Tg(desmogon:EGFP)*(B, C) Strong phenotypes in *desmogon* CRISPR injections results in gross morphological defects in notochord integrity and notochord buckling and bending. maximum projections. Scalebar=100 microns. Embryos with notochord phenotypes 65/160. Over 90% of embryos survive to stage 42. (D, F) *vgll12b* gRNA1,2 & Cas9 injected into

Tg(desmog:EGFP) results in morphological defects in the notochord. Notice magenta arrow where notochord is twisted, overall notochord bending observed. Scale bar=100microns. Embryos with phenotypes in notochord 66/120. 79% of embryos survive to stage 42. (E, F) *arrdc3a* gRNA1,2 & Cas9 injected into *Tg(desmog:EGFP)* results in notochord bending. Scalebar=100microns. Embryos with phenotypes 29/97. 77% of embryos survive to stage 42." Figure and Figure legend adapted from (Seleit et al., 2019 in revision). The panels in this figure have been obtained by injection experiments carried out by Michaela Woelk and Camilla Autorino in the context of a 6 week lab rotation under my supervision.

Gene Name	Full name	proposed roles structure and localization	CRISPR Injected F0 Phenotypes %	Phenotypic description
dsgon	*desmogon*	constituent of desmosomal structures, plasma membrane	40,6	local collapses of vacuolated cells, notochord bending, local notochord collapses, no pleotropic effects, highly specific to notochord, 90% of embryos survive to stage 42
vgll2b	*vestigial-like family member 2b*	predicted transcription factor TF/co-factor, nuclear	55	strong phenotypes in the notochord, bending and twisted notochords, spirals of notochord, notochord tube coiling, local collapses of notochord no big pleotropic effects, 79% of embryos survive to stage 42
arrdc3a	*arrestin domain containing 3a*	regulating signal transduction at G protein-coupled receptors	30	wavy notochords, twisted notochords, no strong pleiotropic effects, 77% of embryos survive to stage 42
kcnk6	*potassium two pore domain channel subfamily K member 6*	ion transport, plasma membrane	44,3	kinks and wavy notochords, shorter axis elongation, general growth retardation 73% survive to stage 42
si:dkey-261h17.1	ENSORLG00000015828	cell adhesion, membrane bound	42,1	notochord spirals and twists, wavy notochord, kinks, perturbed axis elongation, 69% of embryos survive to stage 42
pmp22b	*peripheral myelin protein 22b*	helical transmembarne, integral component of membranes,	31,2	strong pleiotropic effects, growth retardation and developmental delays, heart edemas, smaller eyes, wavy notochords, spiral notochords and twists, short axis/failure of axis extension, patterning defects, 58% survive to stage 42

Table (1) List of genes targeted by CRISPR and quantification of phenotypes in F0 injections. (Seleit et al., 2019 in revision)

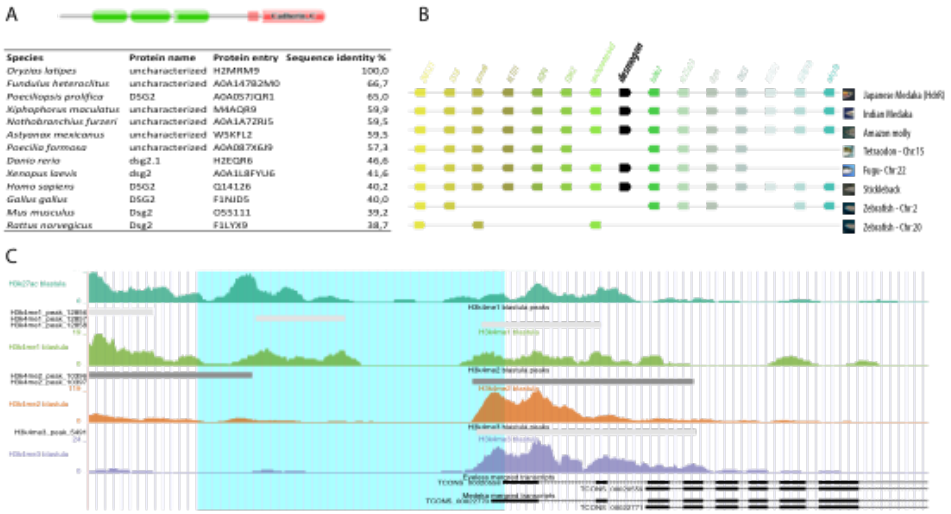

Figure (42) supplementary 1 "(A) Pfam predicted *desmogon* protein domains. In green, 3 cadherin domains and in red, a cytoplasmic cadherin domain. Multiple sequence alignment of 12 selected species to uncharacterized Medaka protein(H2MRM9). Identity score reveals weak amino acid sequence conservation with closest hits (B) Comparative genomic alignment of uncharacterized medaka transcript(ENSORLG00000017110) using GENOMICUS shows conservation of locus in the vast majority of teleost branches, notice the loss of locus in Zebrafish and the Tetraodon. Locus of interest is highlighted by black desmogon label. Scheme modified from Genomicus to highlight syntenic geneomic region (C) Choosing of *desmogon* partial promoter. 2.2kb promoter region (highlighted in blue). H3K27ac, H3K4me1 and H3K4me2 peaks from UCSC genome browser Medaka blastula stage data at 2.2kb upstream of predicted *desmogon* TSS." Figure and Figure legend adaptedfrom(Seleitetal.,2019nrevision)

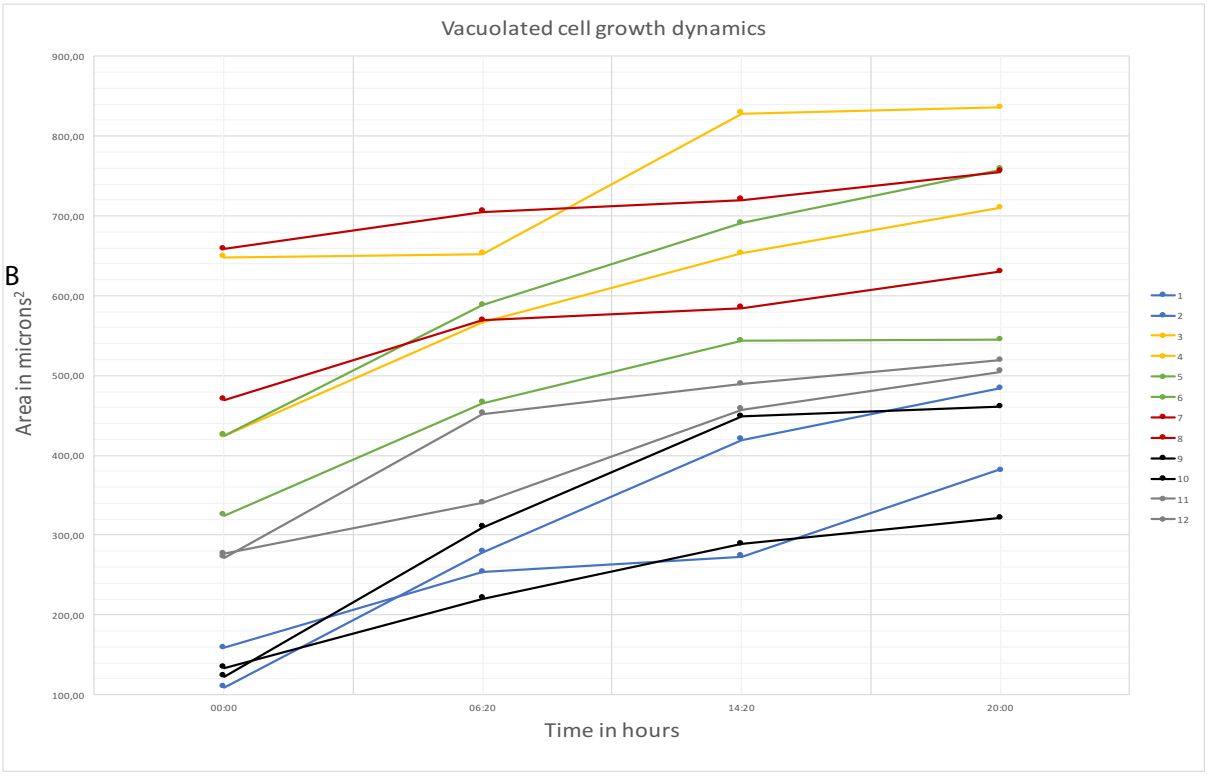

Graph (6) Supplementary 2 (Seleit et al., 2019 in revision) "(A)Area measurement on 12 paired vacuolated cells at 4 different time-point over a 20-hour period reveals the autonomous nature of vacuolated cell growth. Neighbouring vacuolated cells share the same colour code and grow at different rates. Area was calculated on maximum projections using standard Fiji software." Figure and Figure legend adapted from (Seleit et al., 2019 in revision)

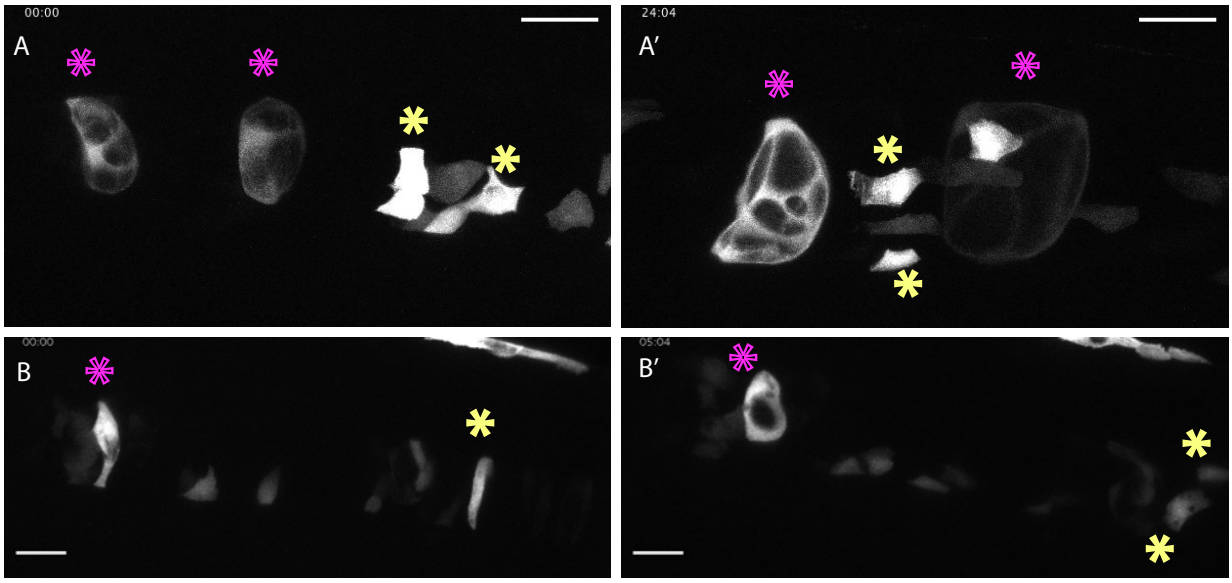

Figure (43) supplementary 3 "(A, A') Time-lapse recording of clones of vacuolated cells (purple asterisks) and sheath cells (yellow asterisks) labelled after injection of desmogonGFP plasmid into Zebrafish embryos. Notice the growth of vacuolated cells over time is asynchronous. (B,B') Time-lapse recording of notochord disc-shaped precursor cells labelled in injected zebrafish embryos. One labelled precursor directly trans-differentiates into vacuolated cell (purple asterisks) while the other undergoes a dorso-ventral division giving rise to two sheath cells (yellow asterisks). Scale bar= 30 microns. Time in hours." Figure and Figure legend adapted from (Seleit et al., 2019 in revision)

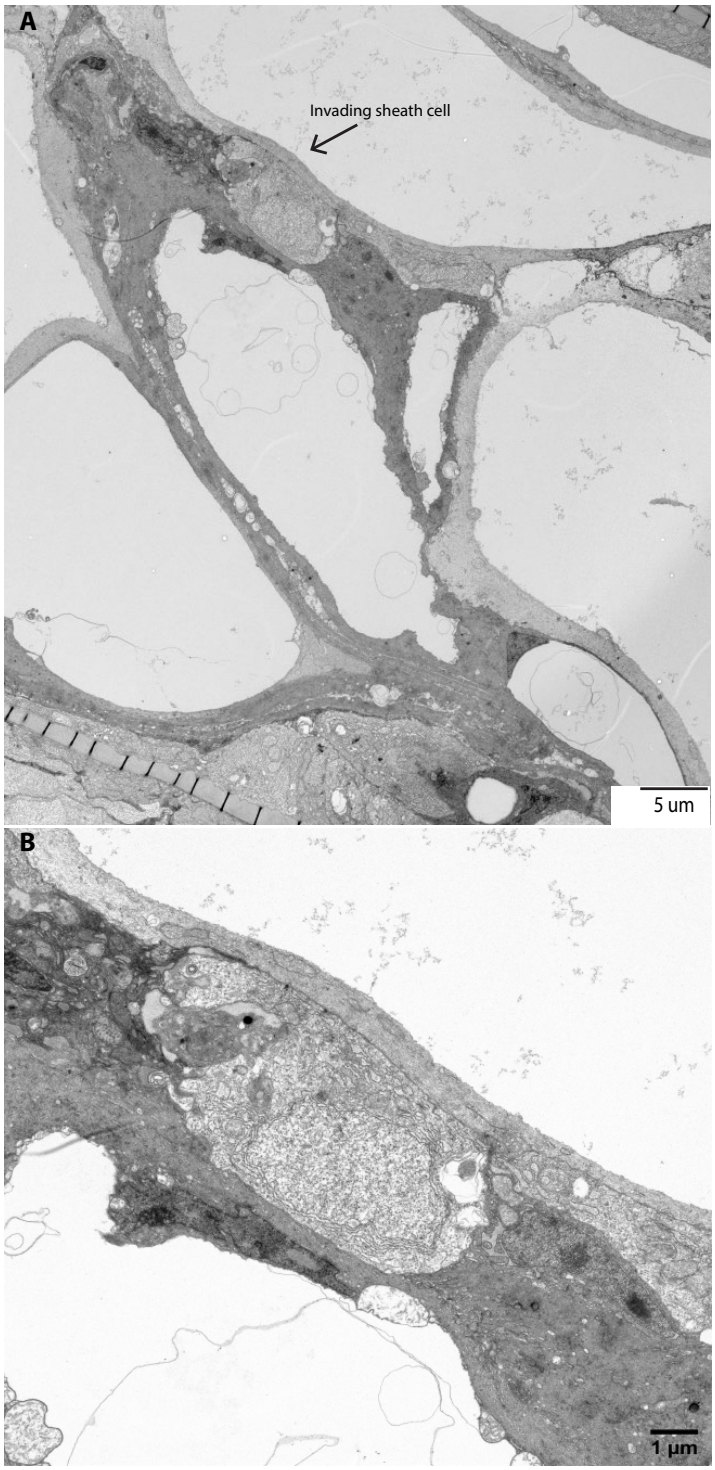

Figure (44) supp. 4 (Seleit et al., 2019 in revision)**"**(A) Longitudinal EM section in *desmogon* mutant notochord. Notice the sheath cell invasion to the center of the lesioned tube Scale bar= 5 microns. (B) High magnification on sheath cell nucleus from (A). Scale bar= 1 micron." Figure and Figure legend adapted from (Seleit et al., 2019 in revision)

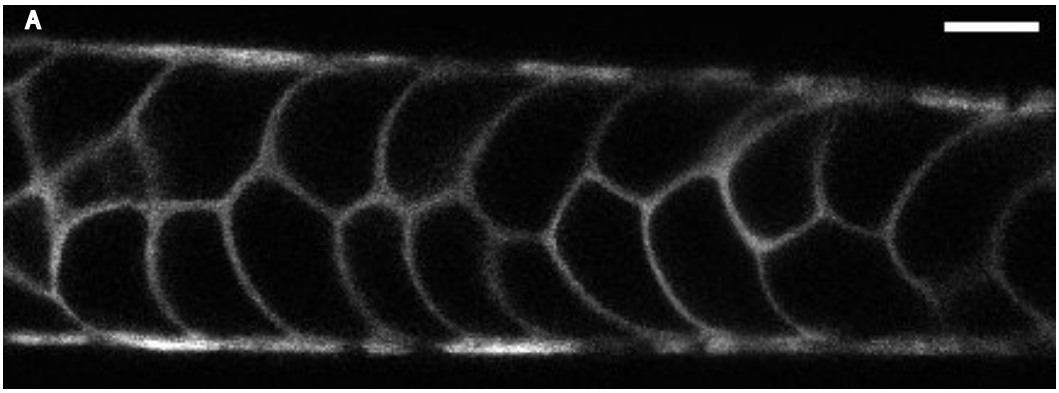

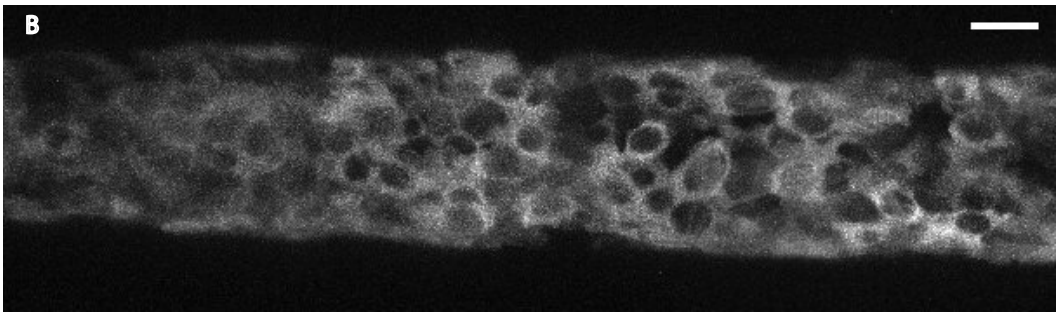

C

Species	Protein name	Protein entry	Sequence identity %
Oryzias latipes	vgll2b	H2MAV4	100
Nothobranchius furzeri	VGLL2B	A0A1A8B070	87,2
Poecilia formosa	uncharacterized	A0A087XF56	78,6
Xiphophorus maculatus	uncharacterized	M4AFN1	77,6
Danio rerio	vgll2b	Q499A6	66
Lepisosteus oculatus	uncharacterized	W5MDI3	57,4
Astyanax mexicanus	uncharacterized	W5KS66	56,5
Gallus gallus	VGLL2	C0KDW3	40,7
Mus musculus	Vgll2	Q8BGW8	38,7
Homo sapiens	VGLL2	Q8N8G2	38

D

Species	Protein name	Protein entry	Sequence identity %
Oryzias latipes	arrdc3a	H2M3K3	100
Oreochromis niloticus	arrdc3	I3K178	96,4
Tetraodon nigroviridis	arrdc3a	H3CX04	95,4
Xiphophorus maculatus	uncharacterized	M4AYA0	93
Poeciliopsis prolifica	ARRD3	A0A0S7HB53	92,7
Astyanax mexicanus	uncharacterized	W5L537	92
Danio rerio	arrdc3a	Q1ECU3	89,9
Gallus gallus	ARRDC3	R4GLF2	85,6
Mus musculus	Arrdc3	Q7TPQ9	85,3
Homo sapiens	ARRDC3	Q96B67	84,8

Figure (45) Supp. 5 (Seleit et al., 2019 in revision) **"**(A) Single Z plane projection in a Tg(desmogon:EGFP) stage 42 embryo, notice the organization and size of vacuolated cells. (B) 3 consecutive Z plane projections in an F1 CRISPR *desmogon* mutant stage 42 embryo, notice the appearance of lesions full of small vacuolated cells (C) Multiple sequence alignment of 9 selected

species to uncharacterized Medaka protein *vgll2b*. Identity score reveals very strong amino acid sequence conservation in vertebrates. (D) Multiple sequence alignment of 10 selected species to uncharacterized Medaka protein *arrdc3a*. Identity score reveals very strong amino acid sequence conservation across vertebrates." Figure and Figure legend adapted from (Seleit et al., 2019 in revision).

The section below was written entirely by myself and is directly adapted from (Seleit et al., 2019 under review)

"

***desmogon* is necessary for correct notochord morphology in Medaka**

The structural demands on teleost notochords are particularly high given that larvae need to swim and feed as soon as embryogenesis concludes (Jiang & Smith 2007; Stemple et al. 1996; Ellis et al. 2014). Significantly, this happens before the ossification and formation of spines (Corallo et al. 2018; Lleras Forero et al. 2018; Wopat et al. 2018; Fleming 2004; Gray et al. 2014). This could explain the specific allocation of this desmoglein family member expression to the notochord. To test whether desmogon has a functional role in the Medaka notochord we targeted it by CRISPR/Cas9 and observed flattened vacuolated cells and lesions along the length of the notochord. This could either be a sign of collapsed vacuolated cells (Lim et al., 2017) or a failure of vacuolated cells to properly form. Our EM data on lesioned mutant notochords strongly suggests that the phenotype results from the local collapse of vacuolated cells. Interestingly, in areas that contained larger lesions (both in injected fish and in stable mutants), we consistently observed the appearance of small vacuolated cells. This is highly reminiscent of results we report from the regeneration experiments and suggests that the collapse of desmogon mutant vacuolated cells can trigger a regenerative response. Indeed EM results on lesioned notochords shows evidence of invading sheath cells. Our results indicate that desmogon is necessary for the maintenance and/or growth, but not the formation, of vacuolated cells. Additionally, we observed a strong correlation between the size of the mutant lesion and the structural integrity of the notochord,

bigger lesions invariably led to buckling and kinking of the notochord tube. Our results are in line with previous observations that have shown that correct vacuolated cell morphology is essential for the notochord to withstand the high mechanical stresses it faces (Lim et al. 2017; Ellis et al. 2013; Garcia et al. 2017; Fleming 2004; Adams et al. 1990). Failure of properly building up and maintaining the high hydrostatic pressure inside the notochord tube leads to bending and buckling along the length of the notochord (Ellis et al. 2013; Corallo et al. 2018). Our results demonstrate that the presence of desmogon in the Medaka notochord is necessary for correct vacuolated cell shape and by extension proper notochord morphology and integrity.

The fact that desmogon is present in the vast majority of teleost branches argues that it has a conserved role in notochord maintenance in fish. However, there are two intriguing exceptions, desmogon has no detectable orthologues in Tetraodon or in Zebrafish. It seems likely that both fish have lost desmogon through the course of their evolution, this interpretation is supported by the fact that we can identify syntenic genomic regions that do not contain desmogon. It remains a formal possibility, however, that an orthologue with a highly divergent nucleotide sequence exists in Zebrafish and Tetraodon. It would be interesting to see whether other desmosomal cadherins have taken over the notochordal role of desmogon in those species. Indeed, other desmosomal cadherin family members have been implicated in notochord integrity in Zebrafish (Goonesinghe et al. 2012), although mutants display earlier gastrulation defects that complicate the proper characterisation of notochordal phenotypes. Interestingly, injecting our medaka

desmogon partial promoter driving GFP in Zebrafish results in vacuolated and sheath cell labelled clones. This suggests that the core transcriptional machinery driving tissue-specific expression of desmogon remains in place and active in Zebrafish. It would be of interest to investigate when the deployment of desmosomal cadherins in notochords arose during evolution and how wide-spread its usage is among the different chordate clades.

Tg(desmogon:EGFP)as a screening tool for genes involved in proper notochord morphology

It has been reported that most biomedical research today focuses heavily on a limited number of genes, leaving behind potentially important genes understudied (Stoeger et al. 2018). Making use of our newly generated transgenic line in combination with the recently published and publicly available single cell transcriptomics data from vertebrate embryos (Briggs et al. 2018; Farrell et al. 2018), we attempted to address this imbalance. To do so we performed a small scale F0 CRISPR screen, the efficacy of which has been recently demonstrated in Zebrafish (Wu et al. 2018) and confirmed in other fish species (own observations and personal communications). Indeed, recent work in Medaka (Lischik et al. 2018), in addition to our results from desmogon mutants, argues for the use of F0 injected embryos as a method to analyse tissue-specific phenotypes. Briefly, we focused on conserved well-annotated genes that were highly and differentially expressed in developing notochords. We addressed whether they might be involved in proper notochord morphology by using the desmogon:GFP line as a fast and straight-forward read-out for notochord shape and integrity. Broadly, the targeted genes fell into two categories. kcnk6, si:dkey- 261h17.1, pmp22b constituted the

first category and showed strong pleiotropic effects in addition to notochordal defects. Delineating the cause of the pleiotropy is difficult given the essential signalling role of the notochord. (Yamada et al. 1991; Yamada et al. 1993; Pourquie et al. 1993; Hebrok et al. 1998; Fouquet et al. 1997; Corallo et al. 2018; Stemple et al. 1996). The observed defects could either arise from the inability of the notochord to correctly pattern adjacent tissue or from notochord independent roles for these genes during embryogenesis. This makes assigning causal phenotypes more difficult. The second group of targeted genes contained the conserved putative co-transcriptional factor vgll2b and the highly conserved membrane bound arrestin arrdc3a. Both genes showed specific defects in notochord morphology and structure when targeted and no overt pleiotropic phenotypes. This argues for functional roles for these genes that are likely to be notochord specific. The precise cellular defects caused by these two genes remain unclear although in both cases vacuolated cells appeared morphologically normal. It is clear, though, that targeted notochords appear unable to withstand the high mechanical strain and buckle under pressure. It remains a challenge for the future to decipher the genetic networks of these genes and to assess whether their roles are functionally conserved in higher vertebrates. All in all, using a simple, targeted, reverse-genetics approach, in combination with publicly available data from single cell transcriptomics (Briggs et al. 2018; Farrell et al. 2018), we believe we have implicated new players in correct vertebrate notochord integrity. This methodology can be easily adapted to other contexts and promises to aid in the study of neglected genes with potentially important functions.

Notochord vacuolated cells during development

We made use of the newly generated *Tg(desmogon:EGFP)* line to address the formation and growth dynamics of notochord vacuolated cells during development. It has previously been reported that one vacuole exists per vacuolated cell under homeostatic conditions (Ellis et al. 2014) and therefore vacuole growth can be used as a proxy for cellular volume growth. Our results confirm that vacuolated cells grow in volume over time as has been reported before (Ellis et al. 2013; Ellis et al. 2014) and reveal that they do so anisotropically, changing their morphology in the process from more roundish to more oblique shapes. This might be due to the increased cellular packing as the notochord expands. While it has been previously shown that notochords extend over time and that this supports axis elongation in vertebrate embryos (Ellis et al. 2014; Garcia et al. 2017; Ellis et al. 2013), it is still unclear exactly how this growth and expansion is coordinated. A possible mechanism could be that a morphogen gradient synchronizes the growth of neighbouring cells in an orderly fashion. Our dynamic data, in both medaka and zebrafish embryos, argues against the presence of such a signal. We reveal that the growth of vacuolated cells in Medaka and Zebrafish is an incremental one-way process that is locally uncoordinated; neighbouring vacuolated cells grow at different rates. This strongly suggests cell-autonomous mechanisms of vacuolated cell growth, how this is coordinated globally to eventually reach an equivalent size remains unclear and constitutes an interesting avenue for future research. It could be that the final size reached is close to the physiological limit as has been previously suggested (Ellis et al. 2014).

In addition to incrementing their size cell-autonomously we report that the number of vacuolated cells increases as the notochord grows. However, in line with previous observations from Zebrafish (Garcia et al. 2017), we have observed no cell division of vacuolated cells. To characterize the initial steps of vacuolated cell formation during notochord development we employed a highly temporally resolved 4-D approach. We observed that vacuolated cells arise from disc-shaped precursors as previously reported (Melby et al. 1996; Dale & Topczewski 2011). Sparse labelling of these *desmogon+* precursors in developing Zebrafish notochords combined with long-term live-imaging revealed a hitherto unrecognized *in vivo* behavioural heterogeneity of the disc-shaped precursors. Either they directly differentiate into vacuolated cells (forgoing any division), or they generate sheath cells by undergoing a dorso-ventral symmetric division, that could be followed by further amplifying rounds of mitosis. When considering the position along the AP axis, the developmental time and the levels of EGFP+ expression, we were unable to reliably predict the output of a precursor cell. It seems plausible therefore that the decision to form a vacuolated or sheath cell is not predetermined nor controlled by tissue-level morphogens, but rather depends on sensing the needs of the growing notochord tube in a local manner. Indeed, it has been previously reported that Notch-Jag1 signalling is important in the balance between vacuolated and sheath cell formation (Yamamoto et al. 2010), suggesting that fate acquisition could be resolved locally among neighbouring cells. Complementarily, it is possible that local mechanical forces that arise during the expansion of the tube could operate on inherently plastic disc-shaped precursors and contribute to adopting vacuolated or sheath cell identity.

Notochord vacuolated cells in regeneration

It has been recently shown that Medaka hearts and retinas have a vastly reduced regenerative potential as compared to Zebrafish (Lust & Wittbrodt 2018; Ito et al. 2014; Lai et al. 2017). However, we have previously reported that Medaka neuromasts are able to regenerate efficiently (Seleit, et al. 2017), and the same happens after mechanical amputations on the caudal fin (Katogi et al. 2004) and injuries to the liver (Van Wettere et al. 2013). It therefore seems that Medaka has a highly variable tissue-specific regenerative capacity (Kang et al. 2016). We wondered whether Medaka can regenerate lost notochord vacuolated cells. It has been shown in Zebrafish that loss of caveolae mutant vacuolated cells in response to mechanical strain triggers an efficient regeneration response (Garcia et al. 2017). This is mediated by sheath cells that invade the inside of the notochord tube and trans-differentiate into vacuolated cells (Garcia et al. 2017). Localized laser-ablation of vacuolated cells in Medaka leads to a very similar process as in Zebrafish where small vacuolated cells specifically invade the injury site. Interestingly, these invading cells start growing in size cell-autonomously mirroring the un-coordinated nature of growth that we observe for vacuolated cells during development. The appearance of small vacuolated cells during regeneration is another reminiscent feature of what we report during notochord development. Indeed, a proportion of sheath cells formed from dividing precursors do initially contain small vacuoles that highly resemble the cells participating in the regenerative response. This suggests two things; a) the presence of sub-populations of sheath cells that display distinct behaviours both during

development and regeneration (Lopez-Baez et al. 2018), b) sheath cells participating in the regenerative response most likely re-acquire a small vacuole and could thus be reverting to an earlier state in their developmental history. Reactivation of developmental programs has been a hallmark of efficient regeneration in a variety of models (Tanaka & Galliot 2009; Rodrigo Albors et al. 2015; Kaloulis et al. 2004) and it seems likely that this takes place in the notochord of Medaka after vacuolated cell loss.

The highly specific spatially localized response to vacuolated cell injury we observe in Medaka indicates that there are mechanisms in place that can sense injured tissue without the need to activate a global regeneration program (LoCascio et al. 2017). Indeed, it has been shown that the release of vacuolated cell contents upon apoptosis can trigger a local regenerative reaction from neighboring sheath cells (Garcia et al. 2017). A similar process can therefore be occurring in Medaka. Interestingly, when we ablated a small part of the peri-notochordal membrane this led to vacuolated cell leakage at the injury site. As the vacuolated cell leakage continued we witnessed the activation of a global regenerative response anterior and posterior to the original injury site. This could be observed by the presence of small vacuolated cells along the entire length of the notochord. It therefore seems likely that sheath cells can also respond to injury without specific vacuolated cell death, suggesting that sheath cells might be able to sense other stresses like tissue tension. It has recently been reported in Zebrafish that a wilms+ subpopulation of sheath cells gets activated in response to a coarse needle injury to the notochord (Lopez-Baez et al. 2018). This sub-population mainly forms scar-tissue that acts as

a stopper to maintain notochordal integrity (Lopez-Baez et al. 2018). In Medaka, leakage of vacuolated cells at the site of injury indicates that the peri-notochordal membrane was not efficiently repaired. It is tempting to speculate that this is due to the absence or delayed activation of the *wilms+* subpopulation of sheath cells. Overall, our results strongly argue for the presence of distinct injury-sensing mechanisms in sheath cells (dependent and independent of vacuolated cell death). We also report the existence of two regenerative responses in Medaka notochords, one spatially localized and the other global, that depend on the type of injury sustained. Our data positions vacuole re-acquisition by sheath cells as the key step for replenishing vacuolated cells regardless of the type of injury sustained. Identifying the molecular trajectories sheath cells traverse will allow a better understanding of the existing heterogeneities among and plasticity of sheath cells both during development and regeneration. This will in turn allow a more targeted exploitation of the potential of sheath cells in treating notochordal and by extension spinal cord defects in vertebrates."

The above section was directly adapted from (Seleit et al., 2019 under review) and is written entirely by myself.

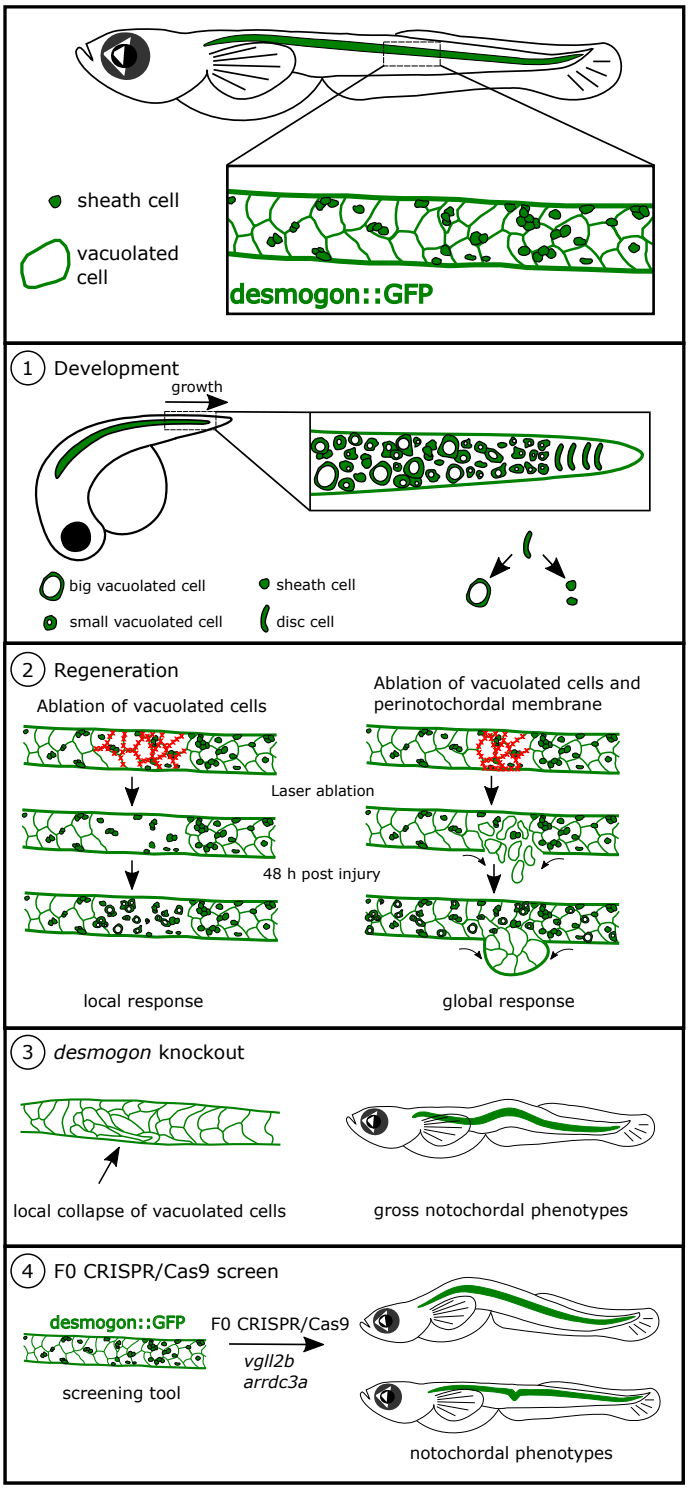

Figure (46) schematic summary of main findings from Desmogon story. Schemes done by Karen Gross.

Gaudi^{NSG} an improved lineaging tool in Medaka

I have created an optimized version of the *Gaudi*^{RSG} lineage tracing tool in Medaka (Centanin et al., 2014). Briefly the *Gaudi*^{RSG} relies on a ubiquitous or tissue-specific heat-shock or tamoxifen activated CRE that allows the recombination event to occur switching a ubiquitously expressed floxed red fluorescent protein (default un-induced) into green fluorescent nuclei. Depending on the strength of the induction the number of recombined cells differs. Recombined cells in green allow the following of clonal output of stem cells in a variety of tissues (Centanin et al., 2014). A major problem of the system is the default DS-red signal before induction that remains even in strongly induced fish (Figure 47 A-D). This prevents using the red channel either for tissue-specific markers or for another red based lineage tracing of recombined cells or for immunohistochemistry in red (as some DS-red signal remains even after fixation). I solved this problem by designing 2-gRNAs against the DS-red locus and injecting them into *Gaudi*^{RSG} fish. I raised a stable CRISPR line that does not contain any DS-red signal before or after recombination and is able to recombine effectively (Figure 47 E-G). This improvement will broaden the range of possible experiments to be performed in live fish as explained below.

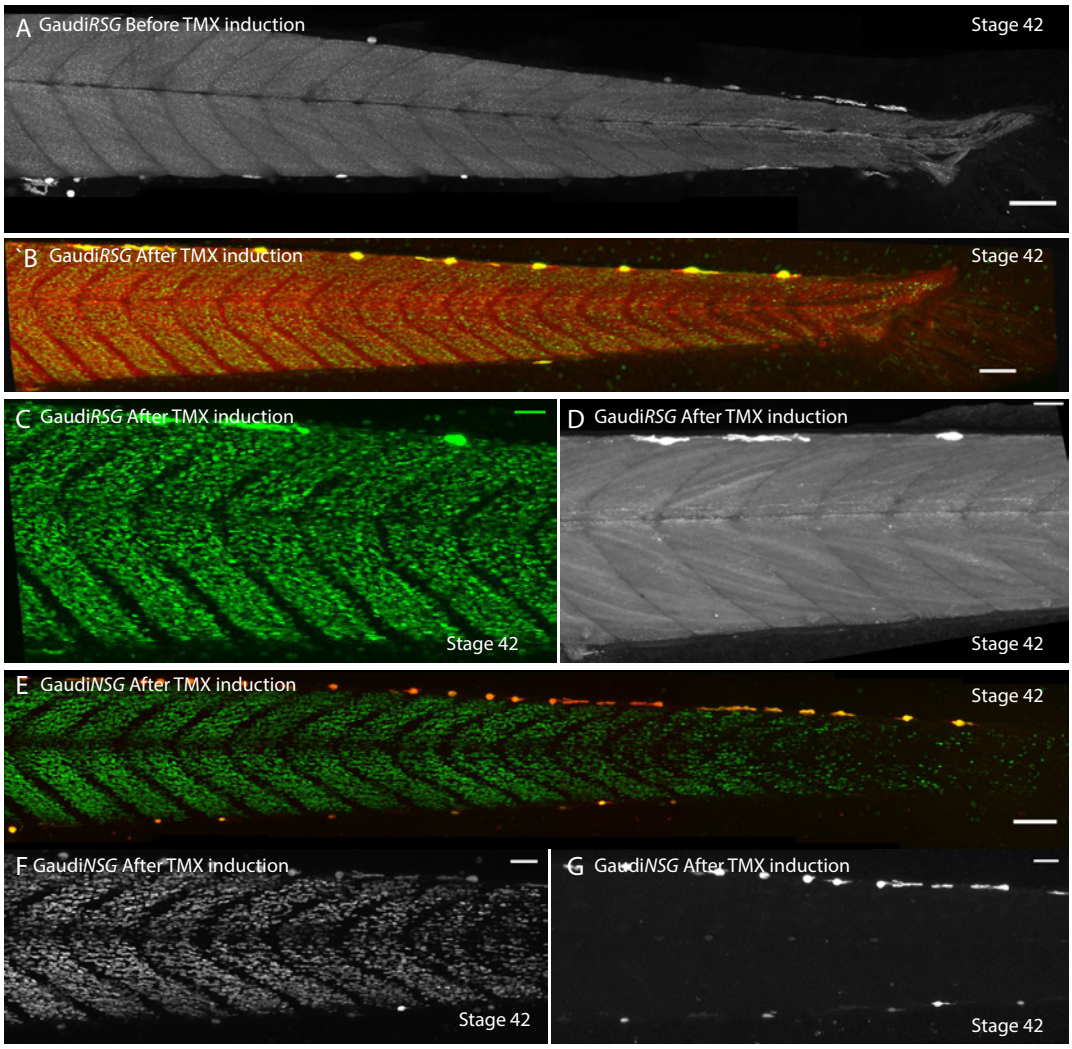

Figure (47) Stable *Gaudi$^{(NSG)}$* line shows complete loss of DS-red signal (A)DS-red signal clear in normal Gaudi(RSG) before induction scale bar 100 microns.(B) Gaudi(RSG) after tamoxifen induction, notice the presence of green nuclei in addition to the remaining DS-red signal scale bare 100 microns(C &D) Individual channel panels of section of (B) notice the strong presence still of DS-red even after recombination Scale bars= 50 microns. (E) Gaudi (NSG) after tamoxifen induction, notice the complete absence of the DS-red signal scale bar =100microns.(F and G) zoom in panels from (E) showing complete lossof Ds-red signal after recombination in the stable CRISPR line. Scale bars=50 microns.

Gaudi^{NSG} combining lineage tracing with cell-type specific marker analysis

The *Gaudi^{NSG}* allowed the exploitation of existing tissue specific markers in combination with a lineage tracing approach, something that was not possible in the regular *Gaudi^{RSG}* in the red channel. Using the Tg(*ccl25a*:RFP) which labels a subset of hair cells in mature neuromasts, in addition to a ring of cells directly around the sensory organs, in combination with the *Gaudi^{RSG}* tool prevents the observation of the tissue specific expression of the Tg(*ccl25a*:RFP) before or after

tamoxifen induction (Figure 48 A-B). This can be contrasted to the ease of combining and observing both lineaging and tissue-specific expression in the *Gaudi*^{NSG} tool (Figure 48 C). In addition, what the tool now offers is the possibility of further modification of the locus by inserting one or more floxed fluorescent proteins in the DS-red area which will allow multi-color lineaging. Furthermore, the *Gaudi*^{NSG} line can be crossed to other lineage tracing tools. Finding a truly ubiquitously expressed FP can be a tedious process that involves a variety of laborious screening and maintaining steps. By exploiting the CRISPR methodology to directly shape transgenic lines even further one can ensure that the advantages of established lines are exploited.

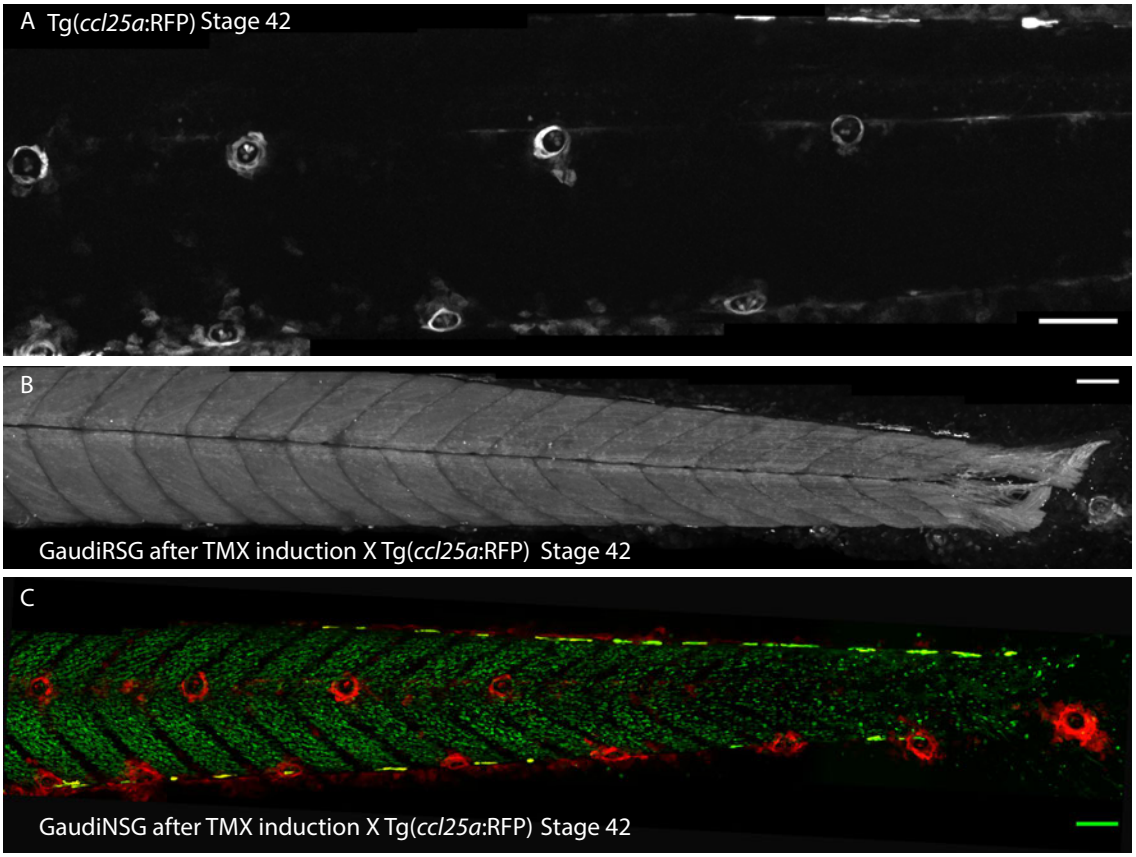

Figure (48) Practical application of GaudiNSG (A)Tg (ccl25a-RFP) shows expression specifically in a ring of cells around the developing neuromasts. Scale bar 100 microns (B) Crossing Tg (ccl25a-RFP) to GaudiRSG and inducing recombination, notice the bright DS-red signal that precludes any useful analysis of cell lineage. Scale bar 100 microns (C) Gaudi (NSG) X Tg (ccl25a-RFP) after TMX induction, notice the complete loss of DS-red signal and the presence of induced nuclei, lineaging is possible in this setting of the ccl25a-RFP positive cells. Scale bar 100 microns.

Epilogue

The biologist is the most romantic figure on earth at the present day. At first sight he seems to be just a poor little scrubby underpaid man, groping blindly amid the mazes of the ultra-microscopic, engaging in bitter and lifelong quarrels over the nephridia of flatworms, waking perhaps one morning to find that someone whose name he has never heard has demolished by a few crucial experiments the work which he had hoped would render him immortal. There is real tragedy in his life, but he knows that he has a responsibility which he dare not disclaim, and he is urged on, apart from all utilitarian considerations, by something or someone which he feels to be higher than himself- JBS Haldane

The state of modern biological research is in dire straits. Not only is there a massive gap between academic positions and the number of people graduating with degrees that want tenure but the way we do research itself has been thoroughly commercialized. This is not a problem of the group or institute or even country this is a global phenomenon. Graduate students have been relegated to stressed 'data-collectors', PIs have become 'marketing experts' and whole departments have been turned into nothing more than 'spin-doctors' and 'gadget acquisition' committees. All in service of the publishing gods, who can in turn based on largely vacuous and self-serving metrics, define success and by extension the amount of funding crumbs one can hope to receive to stay afloat. What gets lost in all this is the spirit of curiosity and drive for knowledge that sustains meaningful discovery. This is a sort of 'science without science', where we discuss in lab meetings data collection efforts and 'progress' but there is no time to really engage with, question and critique the theoretical underpinnings of the work we are doing, the bigger picture and our position in it does not exist any longer, there is no time for it. We are there to collect and curate data, more data, better data. The current structure does not breed creativity in graduate students; it actively kills it. Whether it is through the sheer amount of work expected or inane argumentation about feasibility or by a genuine fear of failure of students or active distancing from more 'crazy' ideas or lack of funds or simple bureaucracy one gets inundated over time with a spirit that can best be described with 'we have limited time, let's stick to what is known and something that might work and could be publishable.' Naïve ideas that might be incorrect but are still the right way to approach certain questions are ignored. It is ludicrous to suggest for example that a G-coupled protein receptor might have functions not directly linked to being activated by its known ligand, or that "Lamarckianism" might not be as thoroughly wrong as it is made out to be, you will simply not be taken seriously. This is how dogmas operate.

This atmosphere is compounded by an obsession with techniques over meaningful biological questions. The amount of data generated by RNA-sequencing with all its forms over the past few years (while extremely powerful) will take years to go through and thoroughly make sense of, during which new and fancier techniques with even higher accuracy will be invented making the old data essentially obsolete. This pace of technique refinement while good in the sense of more accurate quantitative measurements of extremely minute materials obfuscates the need for a meaningful biological question to be addressed. Even if new

techniques are not invented, there is already a huge standardization problem that is rife in the field, which could explain the reproducibility crisis we are having. And without reproducibility science is not too much better than alchemy. This situation also creates strong power-asymmetries where young inexperienced groups with limited funding simply cannot compete with behemoth institutes with all the latest equipment, specializations and essentially unlimited core funding. And the vicious cycle continues. While the problems presented above are systemic and hard to change, it is still important to recognize and talk openly about them. The private sector requires PhD degrees now for many entry-level jobs and Universities are happy to take in more students as it justifies their *raison d'etre*. This means that the army of PhD holders will continue to grow while positions in academia stagnate. One solution could be to have a two-tiered PhD system in all biological sciences; one more technical and the other more theoretical, where students can pick which suits their interest more. The technical will prepare students for a life in industry and will be more techniques-based while a theoretical one will give more leeway to experimentation and less data-accumulation burdens and prepare one for an academic life.

I would like to end with a metaphor and an anecdote to highlight why I think we are sometimes not asking the right questions or taking the right approach in biology today.

The Metaphor

Imagine an alien species descended on earth and decided to try to understand a game of football. Being highly sentient and understanding the primacy of mathematics and quantitative methods they decide to begin their quest by observing a game of football.

One approach they could take is to immediately identify the individual entities on the field and assign names based on position, movement, interactions colors etc. from there they can spend months developing techniques that would allow them to quantify to the minutest detail the movement of each individual player in every femtosecond of the game from start to end. They are very proud of their achievements and their highly sensitive quantitative methods. Thousands of games are analysed in parallel and this generates a huge amount of 'big-data' needing an ever-expanding number of aliens and more and more machines to analyse it all. Not knowing what to look for the aliens toil for meaning in their vast data mines and try to link behaviours to outcomes. But because at any given moment most players on a field of football are not directly involved in the play, and most of their movements are essentially idiosyncratic a lot of data is in essence meaningless in trying to understand what the game is about and why individual entities behave the way they do at the time they do. The aliens end up with a backlog of contradictory data that is waiting to be analysed so that it can be added to "the list" and they are no closer to understanding what the game is about than when they began. They do have a lot of nice names for the players though, and they

believe they understand what these entity 'heterogeneities' are about, but they are confusing understanding with observing and recording.

A second approach is to just observe a game of football in its totality and come up with intuitive un-proven theoretical frameworks that can be formally tested with simple experiments. What is an entity? Are all entities equal? What are the causal relationships between the entities? What is the game about? is it a game? is there cooperation? are there factions? how many? are there leaders and followers? Are certain interactions more favoured than others? are certain movements over-represented than others? are certain behaviours more consequential than others? From this the aliens quickly notice that certain interactions seem to be more pertinent than others at particular times and they can predict long sequences that lead to certain outcomes. They begin to notice the primacy of rare events. They do not know in detail what each entity is doing at every femtosecond during the game but they quickly begin to grasp the broad causal relationships and from this they go on to try and decipher what governs those causal relationships. Before long they arrive at an approximation of a very broad understanding of what the game is about. And then they watch a game for FC Barcelona and it is back to square one!

The Anecdote

During a meeting I had in the beginning of my PhD a couple of graduate students were 'shocked' that I had presented unproven hypotheses and argued for one over the other based on incomplete data and gut-feeling. In science, one of them mentioned, 'we should not have opinions we should be focused solely on collecting data and then let the data speak for itself once enough of it is accumulated.' This I think encapsulates quite well the problem of modern biological research today, first we confuse being opinionated with being dogmatic and/or biased. Second we fail to realize that we are a hypothesis driven endeavour, if you don't have a testable hypothesis and you are just collecting data you are nothing more than a data collecting android. Useless, meaningless data because there is no theoretical framework to try to make sense of it. What is evident from the history of science is that the theoretical frameworks we have are in a process of constant refinement and evolution (as we ourselves are!) but they are nonetheless an essential inseparable part of our understanding of the world we live in, its mysteries, its beauties and more importantly how it works. Be opinionated but don't be dogmatic. Science needs bravery, don't be afraid to be wrong. I will end with words from Aristotle 'the sign of an enlightened mind is the ability to entertain a thought without necessarily accepting it' Let's entertain thoughts!

Materials and Methods

Materials

Antibiotics

Ampicillin: stock solution 50 mg/ml Ampicillin (Sigma), working concentration 100 μg/ml.

Kanamycin: stock solution 30 mg/ml Kanamycin (Roth) working concentration of 50 μg/ml.

Antibodies

Primaries
Anti-eGFP rabbit (Invitrogen) 1:500 dilution
Anti-DSred rabbit (Clontech) 1:500 dilution
Anti-tRFP rabbit (Evrogen) 1:250 dilution

Secondaries
AlexaFluor anti-rabbit 488 from goat (Invitogen) diluted 1:500
AlexaFluor anti-rabbit 546 from goat (Invitrogen) diluted 1:500
AlexaFluor anti-rabbit 647 from goat (Invitrogen) diluted 1:500

In-situ
Digoxigenin-11-UTP 10mM (Roche) coupled to anti-Digoxigenin-AP Fab fragment from (Roche), 1:2000 in 5% sheep serum in PTW.

Chemicals and reagents

Chemicals	*Company*
4',6-Diamidin-2-phenylindole Dilactate (DAPI)	Sigma
4-Di-2-ASP	Invitrogen
Acetone	Sigma
Agar	Gibco
Agarose	Biozym
Agarose low melting	Biozym
Ampicillin	Sigma
ATP	Thermo
Bacto-Tryptone	Gibco
BCIP	Roche
BSA (10 mg/ml)	NEB
Trisodium citrate	Sigma
Calcium chloride dehydrate	Sigma
Chloroform	Merck
DMSO	NEB
dNTPs	Sigma
dATPs	Thermo
Doxycycline hyclate	Sigma
DTT	Thermo Scientific

EDTA	Roth
Ethidium Bromide	Sigma
Ethanol	Merck
Ethanol 70%	Roth
Ethanol 99%	Sigma
Fetal calf serum	Sigma
Formamide	Sigma
GeneRuler mix	Thermo
Glacial acetic acid	Merck
Glucose	Sigma
Glycerol	Applichem
H_2O_2	Sigma
HCl	Merck
Isopropanol	Sigma
Magnesium Chloride	Merck
MachT1 chem comp.	Life Tech.
Methylene blue trihydrate	Sigma
Methanol	Roth
Methylcellulose	Sigma
Magnesium Sulphate Heptahydrate	Grussing
Natural goat serum NGS	Sigma
NBT	Roche
PGEMTeasy	Promega
Paraformaldehyde PFA	Roth
Phenol	Roth
Potassium hydrogen phosphate	Merck
Potassium chloride	Applichem
Potassium dihydrogen phosphate	Merck
Potassium acetate	Sigma
Potassium hydroxide	Merck
Proteinase K	Roche
Ribolock	Thermo Scientific
rNTP Mix	Roche
Sodium Chloride	Sigma
Sodium hydroxide	Merck
Sodium Hydrogen phosphate	Applichem
Sodium dodecyl sulphate SDS	Serva
(4-OH) tamoxifen	Sigma
Trans tamoxifen	Sigma
Tricaine mesylate	Sigma
Tris base	Sigma
Triton X-100	Roth
Tween-20	Sigma
X-Gal	Thermo Scientific
Yeast extract	Roth

Consumables

Cell saver tips 200l Roth, FEP tubes 1mm Karl Schupp AG, Filter paper Whatman, Filter Tips Starlab, Glass beads Roth, Glass Petri dishes STERIPLAN® 9cm Roth, Glass vials Roth, Injection needles GC100F-10 Harvard Apparatus, Latex Gloves Semperguard, Micro pestles 1.5/2.0 ml Eppendorf, Nitrile Gloves Starlab, Petri dishes greiner, Pipette tips Steinbrenner, Reaction tubes 1.5 ml, 2 ml Sarstedt Sandpaper 1000 grit Bauhaus, Tubes 15 ml, 50 ml Sarstedt, Well plates (6 well) böttger, Whatman® Cellulose Filter Paper Whatman.

Enzymes and buffers

Restriction Enzyme	Company
SalI-FD	Thermo Scientific
ApaI-FD	Thermo Scientific
KpnI-FD	Thermo Scientific
HindIII-FD	Thermo Scientific
EcoRI	Thermo Scientific
EcoRV	Thermo Scientific
BamHI	Thermo Scientific
Eco31I-FD	Thermo Scientific
DraI-FD	Thermo Scientific
BsaI-HF	NEB
NcoI-HF	NEB
NotI-HF	NEB
XhoI	NEB
BssHII	NEB
SpeI-HF	NEB
NdeI-HF	NEB
XmaI	NEB

Enzyme	Company
T4 Ligase (5U/μl)	Thermo Scientific
T4 ligase (30U/μl)	Thermo Scientific
Alkaline Phosphatase (2U/μl)	NEB
I-SceI Meganuclease (5U/μl)	NEB
Q5 High-Fidelity DNA Polymerase (2U/μl)	NEB
Sp6 polymerase (20U/μl)	Roche
T7 polymerase (20U/μl)	Roche
T3 polymerase (20U/μl)	Roche
Turbo DNaseI (2U/μl)	Ambion
RiboLock RNase Inhibitor 40u/μl	Thermo Scientific
Taq Roboklon	NA
Hatching Enzyme	Lab-made

Buffer	Company
FastDigest green buffer	Thermo Scientific
T4 ligase buffer (10×)	Thermo Scientific
Q5 reaction buffer (5X)	NEB
Cutsmart buffer	NEB
I-SceI buffer	NEB
10× transcription buffer	Roche

Equipment

Description	*Company*

Axio microscope connected to an HRC camera	Zeiss
Bacterial Shaker INNOVA 44	New Brunswick scientific
Borosilicate glass capillaries GC100T(F)	ClarcElectromedical Instruments
Centrifuge 5417C	Eppendorf
Centrifuge 5430 R	Eppendorf
Centrifuge 5810 R	Eppendorf
Fish incubators	Heraeus instruments and RuMed
FemtoJet express	Eppendorf
Forceps5	Dumont
Freezer -20 C	Bosch
Freezer -80	Thermo
Glass Bottom Dishes	MatTek
InjectMan NI2	Eppendorf
Leica TCS SPE	Leica
Leica TCS SP5 II	Leica
Leica TCS SP8	Leica
Microinjector 5242	Eppendorf
Microwave	Sharp
Microscope slide temperature controller	Biotronix (Univeristy of Cambridge)
Mini-Centrifuge	Starstedt
MuVi-SPIM	EMBL
NanoDrop ND-1000 Spectrophotometer	Thermo Fisher Scientific
Needle puller P-30	Sutter Instrument Co USA
Nikon AZ100 Multizoom	Nikon
Olympus MVX10	Olympus
Power-Supply Power-PAC Basic	BioRAD
Pipettes	Eppendorf
Scale	Saturius
Shaker CAT S 20	NeoLab
Shaker GFL 3005	HILAB
Stereomicroscope Nikon SMZ18	Nikon
Stereomicroscope Olympus SZX7	Olympus
Stereomicroscope Zeiss Stemi 2000	Zeiss
Thermocycler	Bio Rad
LaVision Biotec TriM Scope multi photon microscope	Nikon imaging Center

Kits

Name	*Company*
innuPREP DOUBLEpure Kit	Analytik Jena
RNeasy Kit	Qiagen
Plasmid Midi Kit	Qiagen
Megashortscript T7	Ambion
mMessage Sp6 Transcription	Invitorgen
innuPREP DNA Mini Kit	Analytic Jena

pGEM-Teasy	Promega
RNeasy Mini Kit	Qiagen
Qiagen Plasmid Midi	Qiagen

Media and buffers

Name	Ingredients	Composition
ERM (1X)	Sodium chloride	17 mM
	Potassium chloride	0.4 mM
	Calcium chloride dihydrate Magnesium	0.27mM
	SulphateHeptahydrate	0.66mM
	pH 7	
P1	Glucose	50 mM
	Tris-HCl	25 mM
	EDTA	10 mM
	pH 8, stored at 4 °C	
P2	Sodium hydroxide	0.2 N
	SDS	1%
P3	Potassium acetate	5 M
	Stored at 4 °C	
PBS	Sodium chloride	137 mM
	Potassium chloride	2.7 mM
	Potassium dihydrogen phosphate	240 mg/l
	Sodium hydrogen phosphate	1.44 g/l
	pH 7.4	
PTW 1X	Sodium chloride	137 mM
	Potassium chloride	2.7 mM
	Potassium dihydrogen phosphate	240 mg/l
	Sodium hydrogen phosphate	1.44 g/l
	Tween 20	0.1%
	pH 7.4	
Finclip Buffer	TrisHCl pH8	400 mM
	EDTA pH 8	5 mM
	NaCl	150 mM
	Tween 20	0.10%
	Proteinase K stored at 4 °C	1 mg/ml
TE	Tris-HCl	10 mM
	EDTA	1 mM
	pH 8.0	
TAE	Tris base	242 g/l
	Glacial acetic acid	5.71%
	EDTA	50 mM
	pH 8.5	
Hatching medium	Sodium chloride	17 mM
	Potassium chloride	0.4 mM
	Calcium chloride dihydrate Magnesium	0.27 mM
	Sulphate Heptahydrate Methylene blue	0.66 mM
	pH 7.2	0.0001%

Yamamoto 10X	Sodium chloride Potassium chloride Calcium chloride dihydrate Sodium hydrogen carbonate pH 7.3	7.5 g/ml 0.2 g/ml 0.2 g/ml 0.02 g/ml
Blocking buffer	Sheep serum Triton X-100 BSA PTW DMSO Natural goat serum or fetal calf serum	10% 0.8% 1% 1% 0.01% 4%
Oligo-annealing Buffer	Tris NaCl	10 mM 30 mM
Terrific Broth (TB)-Medium	Bacto-Tryptone Yeast Extract Glycerin Potassium dihydrogen phosphate Potassium hydrogen phosphate	12 g/l 24 g/l 0.4% 2.13 g/l 12.54 g/l
LB-Medium	Bacto-Tryptone Yeast Extract Sodium chloride	10 g/l 5 g/l 10 g/l
Lb-Plates	Bacto-Tryptone Yeast Extract Sodium chloride Agar	10 g/l 5 g/l 10 g/l 15 g/l
SB buffer	TrisCl, PH 9.5 NaCl MgCl2 Tween20 H20	100mM 100mM 50mM 0.1%
20x SCC	Sodium chloride Sodium citrate	3M 0.3M
4x SCCT	Dilute 20x SCC to 4xSCC Tween 20	 0.1%
Hybridization mix	Formamide 20xSCC 50mg/ml Heparin Torula-RNA Tween 20	50% 4x 0.15 mg/ml 5mg/ml 0.1%
75% MeOH/PTw, 50% MeOH/PTw, 25% MeOH/PTw	Methanol PTW	Each adjusted accordingly
Zebrafish medium 1X	Red sea salt	
20X Tricane	Tricane $Na_2HPO_4.2H_2O$	4g/l 10 g/l
50mmol Tamoxifen	Trans-tamoxifen	18.5 mg/ml

Miscellaneous materials

Material	Source
Mach1TM T1 Phage-resistant Chemically Competent E. coli	Lab-made
Glass bottom microwell dishes	Matek

Slides and cover slips	Roth
GeneRuler™ 1 kb Plus DNA Ladder	Thermo Scientific
GeneRuler™ DNA Ladder Mix	Thermo Scientific
6x DNA loading dye	Thermo Scientific
RNA loading dye	Life Technologies
87% Glycerol	Grussing
Sheep serum	NA

Plasmids used

Name
I-SceI/Eya::GFP
Adgene DR274
K15::mYFP
Kremen:GFP

Plasmids generated

Number	*Name*
4668	Eya1::moGFP-NTR
4689	IsceI/K15::iCRE cmlc2::eCFP
4690	Eya1::H2BGFP PolyA
4691	Eya1::H2BRFP PolyA
4694	K15::H2B-GFP
4733	ISceI/Cxcr4b::GFP
4788	Cxcr4b::d2-GFP
4838	Fatla::GFP
5172	K15::Lifeact-tRFP
5191	Desmog::GFP
5192	TERT::GFP
5193	VCAM::GFP
5332	Atohl::EGFP
5345	Sox10::mcherry

Primers

Number	*Name*	*Sequence*
JW6169	DSred_gRNA1_fwd	TAGGCTCGAACTCGTGGCCGTTCA
JW6170	DSred_gRNA1_rev	AAACTGAACGGCCACGAGTTCGAG
JW6171	DSred_gRNA2_fwd	TAGGCGGCGGCCACTACGACGCTG
JW6172	DSred_gRNA2_rev	AAACCAGCGTCGTAGTGGCCGCCG
JW6727	sdf1b_gRNA1_fwd	TAGGAGCAGCTTGGCGTCCATGGT
JW6728	sdf1b_gRNA1_rev	AAACACCATGGACGCCAAGCTGCT
JW6729	sdf1b_gRNA2_fwd	TAGGCACCGCTCCACCAGGCTGAT
JW6730	Sdf1b_gRNA2_rev	AAACATCAGCCTGGTGGAGCGGTG
JW6732	cxcr4a_grna1_fwd	TAGGACTATGACTTAAATGATA
JW6733	cxcr4a_grna1_rev	AAACTATCATTTAAGTCATAGT
JW6734	cxcr4a_grna2_fwd	TAGGTATGGCAGCGTTCTTATCC
JW6735	cxcr4a_gRNA2_rev	AAACGGATAAGAACGCTGCCATA
JW7255	Lifeact_RFP_fwd_wAge1	CTTTCTTTACCGGTCGCCA
JW7256	Lifeact_tagRFP_rev_wnot1	GCGGCCGCACCAGATCCTAGTCAGCCAC
JW7257	GCaMPs_fwd_wAgeI	CTTTCTTTACCGGTCGCCAC
JW7258	GCaMP6s_rev_Not1	TAGTCAGTCACTAGTCGCGG

JW7259	k15gRNA1_oligo_fwd	TAGGTGACCGGCTTGCCAGCTACC
JW7260	k15gRNA1_oligo_rev	AAACGGTAGCTGGCAAGCCGGTCA
JW7261	k15gRNA2_oligo_fwd	TAGGCACTGGTCAGGTCAACGTTG
JW7262	k15gRNA2_oligo_rev	AAACCAACGTTGACCTGACCAGTG
JW7263	k15_HF_fwd_NOoverhang	GATCTCCGACCACACTGCAC
JW7264	k15_HF_rev_NOoverhang	AAGCCGGTCATTGAGGTTCT
JW7265	k15_HF_fwd_withEV2overhang	GCCGGTCTCAGGCTCCGATCTCCGACCACACTGCAC
JW7266	k15_HF_rev_wEV2overhang	GCCGGTCTCAAGGTAAGCCGGTCATTGAGGTTCT
JW7267	fatla_gRNA1_oligo_fwd	TAGGCTGTAACCTTGGCACCCTC
JW7268	fatla_gRNA1_oligo_rev	AAACGAGGGTGCCAAGGTTACAG
JW7269	fatla_gRNA2_oligo_fwd	TAGGTTTGCCATTGACTCAAGCAC
JW7270	fatla_gRNA2_oligo_rev	AAACGTGCTTGAGTCAATGGCAAA
JW7271	fatla_gRNA3_oligo_fwd	TAGGAATACCCCGGAGGCGTTCT
JW7272	fatla_gRNA3_oligo_rev	AAACAGAACGCCTCCGGGGTATT
JW7273	fatla_HF_gRNA1_fwd_NOoverhang	ATGGGGAAGCAAATGATACCACT
JW7274	fatla_HF_gRNA1_rev_NOoverhang	TGCCAAGGTTACAGCGGTAA
JW7275	fatla_HF_gRNA2_fwd_nooverhangs	ACGCCACCATTGTCTACCAC
JW7276	fatla_HF_gRNA2_rev_nooverhangs	GTCAATGGCAAAATAGTTATGAGCA
JW7277	fatla_HF_gRNA1_fwd_EV2overhangs	GCCGGTCTCAGGCTCCATGGGGAAGCAAATGATACCACT
JW7278	fatla_HF_gRNA1_rev_EV2overhangs	GCCGGTCTCAAGGTTGCCAAGGTTACAGCGGTAA
JW7279	fatla_HF_gRNA2_fwd_EV2overhangs	GCCGGTCTCAGGCTCCACGCCACCATTGTCTACCAC
JW7280	fatla_HF_gRNA2_rev_EV2overhangs	GCCGGTCTCAAGGTGTCAATGGCAAAATAGTTATGAGCA
JW7281	HF_fatla_gRNA1_fwd(number2)_EVOH	GCCGGTCTCAGGCTCCCCAACATCCTACAGCATCTCCA
JW7291	Lifeact_tagRFP_rev_withNotIOH	ATAAGCGGCCGCACCAGATCCTAGTCAGCCAC
JW7292	gRNA1_fatla_promoter_oligo_fwd	TAGGTACTGCCATACTGAACCGAG
JW7293	gRNA1_fatla_promoter_oligo_rev	AAACCTCGGTTCAGTATGGCAGTA
JW7294	gRNA2_fatla_promoter_fwd_oligo	TAGGTAGATAATAGCGTATCGTTG
JW7295	gRNA2_promoter_oligo_rev	AAACCAACGATACGCTATTATCTA
JW7296	desmo_promoter_fwd	ACCCAAACTACAAGGCTGCT
JW7297	desmo_promoter_rev	CATTGGCGCAGTGATTTGAA
JW7298	desmo_gRNA1_oligo_fwd	TAGGCCCATATGGTGTGTTCAGCG
JW7299	desmo_gRNA1_oligo_rev	AAACCGCTGAACACACCATATGGG
JW7300	desmo_gRNA2_oligo_fwd	TAGGTTGGTGCCAGCTCTTCAGCG
JW7301	desmo_gRNA2_oligo_rev	AAACCGCTGAAGAGCTGGCACCAA
JW7302	desmo_gRNA3_oligo_fwd	TAGGATCTATGACTATGAAGGTCG
JW7303	desmo_gRNA3_oligo_rev	AAACCGACCTTCATAGTCATAGAT
JW7310	MCM5_oligo_fwd_sacII_OH	GCGGGCTCCAGCTTTTGTTCCCTG
JW7311	MCM5_oligo_rev_withEcorIOH	AATTCAGGGAACAAAAGCTGGAGCCC
JW7312	Mcm5_oligo(2)_fwd_wsacIIOh	GGGCTCCAGCTTTTGTTCCCTG
JW7313	Mcmc_oligo(2)_rev_EcorIOH	AATTCAGGGAACAAAAGCTGGAGCCCGC
JW7494	foxm1_fwd	CTCCTCCACGTCACCTTCAC
JW7495	foxm1_rev	GGTTCAAATCATCCAAAGGGCC
JW7496	tertfwd	GACGTCTGAGTACTGTGGACG
JW7497	tertrev	TCTGCACGGACTCAGTCAAG
JW7498	VCAM_fwd	GGGATAATTCTGGCGCATTG
JW7499	VCAM_rev	TGTGATTTGTCACCCTAATTACACTG
JW7500	epcam_fwd	GATGTATGCCGGCATTTGGG

JW7501	epcam_rev	GGTGTAGAAATCCAGAAAAACAGT
JW7512	desmo_fwd_2	TCGCTGCTTGTTGTGTAGGT
JW7594	Eya1_gRNA1_oligo_fwd	TAGGTCCCAAAACATGGCGGCGTA
JW7595	Eya1_gRNA1_oligo_rev	AAACTACGCCGCCATGTTTTGGGA
JW7596	Eya1_gRNA2_oligo_fwd	TAGGAGTTATCCAGGCTTTGGCCA
JW7597	gRNA2_eya1_oligo_rev	AAACTGGCCAAAGCCTGGATAACT
JW7598	Eya1_gRNA3_oligo_fwd	TAGGTGCCTGGCCACAGGCGTGCG
JW7599	Eya1_gRNA3_oligo_rev	AAACCGCACGCCTGTGGCCAGGCA
JW7602	Kremen_gRNA1_oligo_fwd	TAGGTCTGTAGTCCTCGCCGTTGG
JW7603	Kremen_gRNA1_oligo_rev	AAACCCAACGGCGAGGACTACAGA
JW7604	Kremen_gRNA2_oligo_fwd	TAGGCACGGCTGCACGTCTCCGTC
JW7605	Kremen_gRNA2_oligo_rev	AAACGACGGAGACGTGCAGCCGTG
JW7606	Kremen_gRNA3_oligo_fwd	TAGGAAGGATCCGGGTGCCTGGA
JW7607	Kremen_gRNA3_oligo_rev	AAACTCCAGGCACCCGGATCCTT
JW7608	sox10_gRNA1_oligo_fwd	TAGGCTTCCCGCGTTGACGCGCA
JW7609	sox10_gRNA1_rev_oligo	AAACTGCGCGTCAACGCGGGAAG
JW7610	sox10_gRNA2_oligo_fwd	TAGGCCATAGCCGTATGGCGAGCT
JW7611	sox10_gRNA2_oligo_rev	AAACAGCTCGCCATACGGCTATGG
JW7622	H2B-RFP_SVpolyA_fwd	ATCGATATGCCAGAGCCAGC
JW7623	H2B-RFP_SVpolyA_rev	AAAGGGAACAAAAGCTGGAGC
JW7624	LoxP_fwd	GCATTCTAGTTGTGGTTTGTCCA
JW7625	LoxP_rev	GGTGGATCCGTCGAGGGG
JW7626	inverted_eCFP_fwd_EV20H	GCCGGTCTCAGGCTCCCAATCCTCCCCCTTGCTGTC
JW7627	inverted_eCFP_rev_EV20H	GCCGGTCTCAAGGTAACATGGTGAGCAAGGGC
JW7692	LoxP_correctOri_fwd_EV50H	GCCGGTCTCACTGCTGCGCGGGAATTCGATGCATT
JW7693	LoxP_correctOri_rev_EV50H	GCCGGTCTCACTGAGCCGCGAATTCACTAGTGATG
JW7694	H2B-RFP_correctOri_fwd_EV60H	GCCGGTCTCATCAGGCGCCGCGGGAATTCGATATCG
JW7695	H2B-RFP_correctOri_rev_EV6'0H	GCCGGTCTCACTTAGCCGCGAATTCACTAGTGAT
JW7696	Inverted_LoxP_fwd_EV30H	GCCGGTCTCAACCTCTGCGGGAATTCGATGGTGGA
JW7697	inverted_loxp_rev_EV30H	GCCGGTCTCATAGTCCGCGAATTCACTAGTGATGC
JW7698	Inverted_CFP_EV2_fwd	GCCGGTCTCAGGCTCCCAATCCTCCCCCTTGCTGTC
JW7699	invertedCFP_EV2_rev	GCCGGTCTCAAGGTAACATGGTGAGCAAGGGC
JW7718	oligo_gRNA(mCFP HDR++)_fwd	TAGGTTTCCTCATTTTATTAGGAA
JW7719	oligo_gRNA(mCFP HDR ++)_rev	AAACTTCCTAATAAAATGAGGAAA
JW7720	oligo_gRNA(3167 linearizer)_fwd	TAGGAGATCGCCGCCACCGCGGT
JW7721	oligo_gRNA(3167 linearizer)_rev	AAACACCGCGGTGGCGGCGATCT
JW7722	oligo_gRNA(NucBow Ali)_fwd	TAGGAATGGGCTCGCGATAATGTC
JW7723	oligo_gRNA(NucBowALI_linearizer)_rev	AAACGACATTATCGCGAGCCCATT
JW7754	col12a1a_p2a_cerulean_fwd_mfeI_oh	GCCCAATTGGGCCACCATGAAGATCAGGT
JW7755	col12a_rev	GCCATACCACATTTGTAGAGGT
JW7756	inverted_mCFP_fwd_ApaI_oh	GCCGGGCCCCAATCCTCCCCCTTGCTGTC
JW7757	inverted_mCFP_rev_ncoI_oh	GCCCCATGGAACATGGTGAGCAAGGGC
JW7758	loxp_fwd_SpeI	GCCACTAGTGCATTCTAGTTGTGGTTTGTCCA
JW7759	Loxp_rev_SalI_oh	GCCGTCGACGGTGGATCCGTCGAGGGG
JW7760	H2BRFP_fwd_NdeI_oh	GCCCATATGATCGATATGCCAGAGCCAGC
JW7761	H2BRFP_rev_MIuI	GCCACGCGTAAAGGGAACAAAAGCTGGAGC
JW7772	atoh1_promoter_fwd	AGGCGTGACCAATGGAACAT

JW7773	atoh1_promoter_rev	ACCATTGCTCCAATCCTCCAG
JW7804	xma1_OH_mfeisite_fwd_4082	GCCCCCGGGATAGTGTCAATTGCAGATGAAAGAT
JW7805	NcoI_mfeisite_4082_rev	GCCCCATGGTTCATCATTGGTCTACGACAGC
JW7806	4082_sapI_rev	GCCGAAGAGCTTCATCATTGGTCTACGACAGC
JW7807	k15_CRISPRcheck_fwd	GGGACCAGAGTCTCTGTTTCC
JW7808	k15_CRISPRcheck_rev	TCGTACCACTCTTGAAGTTCTT
JW7813	loxp_fwd_sal1 OH	GCCGTCGACGCATTCTAGTTGTGGTTTGTCCA
JW7816	dkk2CS2_wada_SVpolyA_rev_sal1OH	GCCGTCGACCCCGGCCGCGAATTAAAAA
JW7817	dkk2_Pcs2_wada_fwd_sal1OH	GCCGTCGACTGCAGGATCCTGGTGCCTTT
JW7818	Ubi_promoter_3167_ApaI_OH_fwd	GCCGGGCCCTCGCCCTTAAAACTCGAGACC
JW7819	Ubi_promoter_rev_3167	GCCCAAGCTGATCCTCTAGAG
JW7820	sapI_oh_rev_4082	GCCTTGAAGAGCTTCATCATTGGTCTACGACAGC
JW7834	Ubi_promoter_rev_3167_not1OH	GCCGCGGCCGCGCCCAAGCTGATCCTCTAGAG
JW7852	H2B-RFP_rev_seqlox	GCCTTAGTCACCGCCTTCTT
JW7857	k15crisprcheck_1.5kb_rev	TTGGTGTTCCATGTCGTTGC
JW7858	K15_fulllength_sal1_oh_fwd	GCCGTCGACCAGCTCGTCCTGTCAGAAGG
JW7859	k15fulllength_sal1OH_rev	GCCGTCGACAATCTGAACATTTTAGTTGCCGTG
JW7860	k15fulllength_rev_xba1OH	GCCTCTAGAAATCTGAACATTTTAGTTGCCGTG
JW7862	LoxP_fwdorientation_revprimer_Nde1OH	GCCCATATGGGTGGATCCGTCGAGGGG
JW7975	Loxp_fwdorientation_NdeI_oh	GCCCATATGTCACTATAGGGCGAATTGGGC
JW7976	Loxp_fwdorientation_revprimerndeI	CTCAAGCTATGCATCCAACGC
JW7986	p2a_cerulean_fwd_xba1OH	GCCTCTAGACGGAGCTACAAACTTCAGCC
JW7987	p2a_cerulean_rev_xbaI	TCTGGCTAGAATCTTACTTGAGTAA
JW8143	vgll2b_gRNA1_oligo_fwd	TAGGTGGGCCCCCAGACATTCCTT
JW8144	vgll2b_gRNA1_rev	AAACAAGGAATGTCTGGGGGCCCA
JW8145	vgll2b_gRNA2_fwd	TAGGGTGCGCCCGTTTCACAGT
JW8146	vgll2b_gRNA2_rev	AAACACTGTGAAACGGGCGCAC
JW8147	si:dkey_gRNA1_fwd	TAGGAGCTTGCTGTCACAAGCCT
JW8148	si_dkey_gRNA1_rev	AAACAGGCTTGTGACAGCAAGCT
JW8149	si:dkey_gRNA2_fwd	TAGGCTGAGTCACTTCAATCTGCC
JW8150	si:dkey_gRNA2_rev	AAACGGCAGATTGAAGTGACTCAG
JW8151	pmp22b_gRNA1_fwd	TAGGCCTGCTGCACATTGCTGCAC
JW8152	pmp22b_gRNA1_rev	AAACGTGCAGCAATGTGCAGCAGG
JW8153	pmp22b_gRNA2_fwd	TAGGCAGCTCTTCACCTTGCAGAA
JW8154	pmp22b_gRNA2_rev	AAACTTCTGCAAGGTGAAGAGCTG
JW8155	ntd5_gRNA1_fwd	TAGGAGAAAGACTTGTGGGAGCGG
JW8156	ntd5_gRNA1_rev	AAACCCGCTCCCACAAGTCTTTCT
JW8157	ntd5_gRNA2_fwd	TAGGATCCATGGAGATGCCTCAGT
JW8158	ntd5_gRNA2_rev	AAACACTGAGGCATCTCCATGGAT
JW8159	kcnk6_gRNA1_fwd	TAGGTTCTCCAGCATCGAGCGGC
JW8160	kcnk6_gRNA1_rev	AAACGCCGCTCGATGCTGGAGAA
JW8161	kcnk6_gRNA2_fwd	TAGGTGTATTGTAGTCGCCGGGCG
JW8162	kcnk6_gRNA2_rev	AAACCGCCCGGCGACTACAATACA
JW8163	cox6a2_gRNA1_fwd	TAGGAGCGGCGAGGACTCGACGAG
JW8164	cox6a2_gRNA1_rev	AAACCTCGTCGAGTCCTCGCCGCT
JW8165	cox6a2_gRNA2_fwd	TAGGAATACGGCACAAACTCCGGC
JW8166	cox6a2_gRNA2_rev	AAACGCCGGAGTTTGTGCCGTATT

JW8167	chstl1_gRNA1_fwd	TAGGAGATTACAATCTATCGCTCT
JW8168	chstl1_gRNA1_rev	AAACAGAGCGATAGATTGTAATCT
JW8169	chstl1_gRNA2_fwd	TAGGTTACTGCTATGTTCCCAAGG
JW8170	chstl1_gRNA2_rev	AAACCCTTGGGAACATAGCAGTAA
JW8171	ardc33a_gRNA1_fwd	TAGGAAGTTCGTTGGACGGAATCG
JW8172	ardc33a_gRNA1_rev	AAACCGATTCCGTCCAACGAACTT
JW8173	arrdc3a_gRNA2_fwd	TAGGATCCCGCATGGTGGTCCCAA
JW8174	arrdc3a_gRNA2_rev	AAACTTGGGACCACCATGCGGGAT
JW8202	guideRna1 multicolor new FWD	TAGGCGCCCTTGCTCACCATCTCG
JW8203	guideRna 1 multicolor REV	AAACCGAGATGGTGAGCAAGGGCG
JW8204	guideRna2 NucBowmulticolor FWD	TAGGCTTCGCCCGCGCCCGCTAGA
JW8205	guideRna2 NucBowmulticolor REV	AAACTCTAGCGGGCGCGGGCGAAG
JW8285	mbpa_gRNA1_fwd	TAGGATGCACCACAGCGTTCTCGT
JW8286	mbpa_gRNA1_rev	AAACACGAGAACGCTGTGGTGCAT
JW8287	mbpa_gRNA2_fwd	TAGGCAGTTTCAAAGTCATCCAGA
JW8288	mbpa_gRNA2_rev	AAACTCTGGATGACTTTGAAACTG
JW8289	krox20_gRNA1_fwd	TAGGAGGAGAAAGCGTGTACTCGG
JW8290	krox20_gRNA1_rev	AAACCCGAGTACACGCTTTCTCCT
JW8291	krox20_gRNA2_fwd	TAGGCCCATCATCCCCGATTACAC
JW8292	krox20_gRNA2_rev	AAACGTGTAATCGGGGATGATGGG
JW8293	foxd3_gRNA1_fwd	TAGGACAGCGACTGCGACAGTCCG
JW8294	foxd3_gRNA1_rev	AAACCGGACTGTCGCAGTCGCTGT
JW8295	foxd3_gRNA2_fwd	TAGGTACAGCCTCGGGAGTCCCTA
JW8296	foxd3_gRNA2_rev	AAACTAGGGACTCCCGAGGCTGTA
JW8297	erbb3b_gRNA1_fwd	TAGGAAAGTGGTTCATCGCAAT
JW8298	erbb3b_gRNA1_rev	AAACTATTGCGATGAACCACTTT
JW8299	erbb3b_gRNA2_fwd	TAGGTCAGACTGTTGACTCGAACT
JW8300	erbb3b_gRNA2_rev	AAACAGTTCGAGTCAACAGTCTGA
JW8301	erbb3a_gRNA1_fwd	TAGGGCATACTGGTCCTCATAG
JW8302	erbb3a_grna1_rev	AAACCTATGAGGACCAGTATGC
JW8303	erbb3a_gRNA2_fwd	TAGGCTGCAGCGATCGGAACCCCA
JW8304	erbb3a_gRNA2_rev	AAACTGGGGTTCCGATCGCTGCAG
JW8305	erbb2_gRNA1_fwd	TAGGCCGACCCCCGGAGTATAGAT
JW8306	erbb2_GRNA1_rev	AAACATCTATACTCCGGGGGTCGG
JW8307	erbb2_gRNA2_rev	TAGGTCTGGCTGTCAGCGATGTAA
JW8308	erbb2_gRNA2_fwd	AAACTTACATCGCTGACAGCCAGA
JW8458	eya1_genotyping_fwd_1	CTTCAGCCCAAGACAAACGC
JW8459	eya1_genotyping_fwd_2	AAAGTAGCAACACCGGTGCA
JW8460	eya1_genotying_reverse_2	GGAGGGTGTAAGTGGTGGTG
JW8461	eya1_genotyping_rev_3	TATGGAGGCGAGCAAAACGT
JW8500	xirp2a_insitu_fwd	TTCAGGGGAGATGCTGGAGA
JW8501	xirp2a_rev_inistu	CAGATCCACTTGTGACGCCT
JW8570	desmogon_insituprobe_fwd	TTCTGCGAGATCAGGCTCAC
JW8571	desmogon_insituprobe_rev	AAGGCCCCTCCTCTGTAACT
JW8572	desmogon_gRNA1_fwd_genotyping	ACTGGATTGTAGCCCCCAGA
JW8573	desmogon_gRNA2_rev_genotyping	TCGTACCTGACATTGGTGGC
JW8574	desmogon_gRNA3_rev_genotyping	GTACAGCGTCTGGTTGGGAA

JW8609	fwd_fullCDS_desmogon	ATGTCTCTCCTGCTGAAATCCAG
JW8610	desmogon_fulllengthCDS_rev_nostop	GCAAGATGCATCACAAAACTCT
JW8639	vgll2b_fwd_insitu	TTCTTTTTGCGCTCACCAGC
JW8640	vgll2b_rev_insituprobe	CATGAAGAGGTCTCGGTGGG
JW8641	arddc3a_fwd_insituprobe	TCAGGGAGGGTGATCATCGA
JW8642	arddc3a_rev_insituprobe	GCGAGACAGGTGGGATCTTC
JW8644	desmogon_fwd_bamH1_site_halfCDS	AAGTGGTGACGGTGTCTGAG
JW8645	desmogon_rev_bamH1_halfCDS	GCAGCGTGTCACTGTCAATG
JW8646	desmogon_fulllength_reverse_STOPincluded	CCTCTGCGGACAGGCTAAAT
JW8647	desmogon_rev_fulllength+10aamissing	AGTAACAACCCTCTGCCTGC
JW8660	desmogon_gRNA1_rev_genotping	GGTCGAGATCGTCTTCAGCC
JW8661	desmogon_gRNA2_fwd_genotyping	GCTGGCAGCCTTTGAAATTG
JW8662	Desmogon_gRNA3_fwd_genotyping	TGACAGGACAAGAGATGGGC
JW8683	fwd_fulllength_CDS_desmog_NCOI_OH	AGGCCATGGATGTCTCTCCTGCTGAAATCCAG
JW8684	fulllength_desmogon_REV_NCOI_oh+1bp	AGGCCATGGCATCTATGTTTCTCTCAGT
JW8719	desmogon_full_CDS_reverse_OHproline_NCO1	AGGCCATGGGATCTATGTTTCTCTCAGTTACTGAGATTTTTTTGTGCTGAGTAACAACCCTCTGCCTGC
JW8863	desmogon_promoter_SalI_OH_rev	GAGGTCGACGTGATCATTGGCGCAGTGAT
JW8864	desmogon promorter_KPN1_OH_fwd	AGGGGTACCTTCGATTCGCTGCTTGTTGTG

RNA

RNA	Supply
Cas9 mRNA	Lab-made
Cxcr4b gRNA1	Lab-made
Cxcr4b gRNA2	Lab-made
Cxcr4a gRNA1	Lab-made
Cxcr4b gRNA2	Lab-made
K15 gRNA1	Lab-made
K15 gRNA2	Lab-made
Desmog gRNA1	Lab-made
Desmog gRNA2	Lab-made
Desmog gRNA3	Lab-made
Erbb3a gRNA1	Lab-made
Erbb3a gRNA2	Lab-made
Erbb3b gRNA1	Lab-made
Erbb3a gRNA2	Lab-made
Foxd3 gRNA1	Lab-made
Foxd3 gRNA2	Lab-made
Vgll2b gRNA1	Lab-made
Vgll2b gRNA2	Lab-made
Arrdc3a gRNA1	Lab-made
Arrdc3a gRNA2	Lab-made
Pmp22b gRNA1	Lab-made
Pmp22b gRNA2	Lab-made
Sox10 gRNA1	Lab-made
Sox10 gRNA2	Lab-made
Kcnk6 gRNA1	Lab-made
Kcnk6 gRNA2	Lab-made
Ngn1 gRNA1	Lab-made
Ngn1 gRNA2	Lab-made
Fat1a gRNA1	Lab-made
Fat1a gRNA2	Lab-made
Si:dkey-261h17.1	Lab-made
Si:dkey-261h17.1	Lab-made
Eya1 gRNA1	Lab-Made

Eya1 gRNA2	Lab-Made
Eya1 gRNA3	Lab-Made
DS-red gRNA1	Lab-Made
DS-red gRNA2	Lab-Made
Sdf1b gRNA1	Lab-Made
Sdf1b gRNA2	Lab-Made

Fish transgenic and mutant lines used or generated

Cab (wild-type population), kazura (cxcr4b mutant), yanagi (cxcr7 mutant) (Sasado et al., 2008; Yasuoka et al., 2004), DA mutant, Gaudi^{LoxPOUT} (ubiquitous H2B-EGFP expression) (Centanin et al., 2014). Gaudı $^{Ubiq.iCre}$ Gaudı^{RSG} (Centanin et al., 2014), Tg(cxcr4b:Cxcr4b-EGFP) (Dona et al., 2013). Tg (neurom^{K8}:H2B-EGFP) Tg(Eya1:EGFP)Tg(K15:mYFP),Tg(Fli1:EGFP), Tg(Ccl25a-RFP).

Tg(Eya1:mECFP), Tg(Eya1: H2B-EGFP), Tg(K15:H2B-EGFP), Tg(K15:LifeAct-tRFP), Tg(K15:H2B-RFP), Tg(olK15:H2B-EGFP) in zebrafish, Tg(Desmog::GFP), Tg(cxcr4b:EGFP), Tg(Sox10:mCherry), Tg(Fat1a:GFP), Gaudı^{NSG}, K15 (-/-)' , Eya1(-/-) (+/-), Desmogon(-/-) (+/-)For generation of Eya1 and K15 injected plasmids details available as described in (Seleit et al., 2017a, b).

Methods

Animal ethics statement and standard fish maintenance

Medaka and Zebrafish were maintained as closed stocks at the Centre of Organismal Studies of the University of Heidelberg (Tierschutzgesetz §11, Abs. 1, Nr. 1). Medaka and Zebrafish husbandry and experiments were performed according to local animal welfare standards (Tierschutzgesetz 111, Abs. 1, Nr. 1, Haltungserlaubnis) and in accordance with European Union animal welfare guidelines. The fish facility is under the supervision of the local representative of the animal welfare agency. The fish colony was maintained under standard recirculating aquaculture conditions, 14 hours of light and 10 hours of darkness.

Antibodies and staining

IHC was performed as described (Centanin et al., 2014). Primary antibodies rabbit anti-GFP, rabbit anti-DsRed. Secondary antibodies Alexa 488 anti-Rabbit, Alexa 546 anti-Rabbit, Alexa 647 anti-Rabbit. DAPI was used in a final concentration of 5 ug/l.

Bacterial transformation

MACHT1 chemically competent cells were thawed on ice. 3-8µl of DNA construct was added to 50µl of the MACHT1 cells, incubate for 20 minutes on ice, transferred to 42°C

for 45-60 seconds then on ice for 2 minutes. 300µl TB medium added and bacterial culture incubated for 1h at 37°C with shaking (180rpm). 100µl of transformed solution was then added to plates with respective antibiotics (100 µg/ml ampicillin, 50 µg/ml kanamycin). The plates were left overnight at 37°C.

CRISPR/Cas9

All gRNAs were generated using CCtop CRISPR/Cas9 target online predictor (Stemmer et al., 2015). Steps for gRNA synthesis were performed as previously described (Stemmer e al., 2015). In-vitro transcription proceeded using the MEGAshortscript™ T7. The gRNAs were purified and extracted using phenol/chloroform or an RNeasy-Kit. List of guides used available from publications material and methods section (Seleit et al., 2017a,b). Lab-made xCas9 mRNA was transcribed by mMachine Sp6 Transcription Kit (Thermo Fisher).

DiAsp staining

Hair cells in living embryos were detected by using the vital dye 4-Di-2-ASP (Sigma-Aldrich) as previously described (Collazo et al., 1994; Sapeđ e et al., 2002; Seleit et al., 2017a). Briefly, live samples were incubated for 5-10 min in a 5 mM DiAsp solution, washed three times in ERM and observed under a fluorescent binocular.

Dechorionation

Embryos were rolled on commercially available sand-paper, ten washed in ERM at least 5 times to remove residual dirt then transferred to a small petri-dish with 1 spot covered in hatching enzyme for 45 minutes to 2 hours at 28 °C. Then they were washed repeatedly with ERM to remove residual hatching enzyme.

DNA A-tailing and pGEM-T cloning

15µl of clean PCR product, 1.5µl 2mM dATPs, 1.5µl 10Xpol Buffer (EURx), 0.5µl 5µ/µl Taq Roboklon (EURx) remainder by to 15µl by water. This mixture was then incubated for 35 minutes at 72°C in a PCR machine. 3.5µl of fresh A-tailed PCR product, 0.5µl pGEM-T vector, 5µl of 2X ligase buffer, 1µl of T4 ligase left ON at 4°C. 5µl of the product were used for the transformation.

DNA ligations and restriction digests

1µl T4 DNA Ligase, 1µl 10x T4 DNA Ligase Buffer, as a general rule 3 microliters of 15ng/µl of insert were added to 2 microliters of 20ng/ µl in a reaction volume of 10µl, incubate for 1 hour at RT or overnight at 4°C. For digests 1X FD or HF (or appropriate) buffer were added to 0.5µl restriction enzyme and 3-5µg DNA with the rest up to 10µl with H_2O. For FD or HF cuts, usually 1 hour was sufficient for more tricky restrictions ON at 37 degrees was utilized.

Fish mating and micro-injections
Male fish were separated overnight from females. After mating (20–30 min) eggs were collected in Petri dishes in 1x embryo rearing medium ERM. Injections were performed as previously described (Rembold et al., 2006) The injection mix was as follows 12.5µl Yamamato buffer, 1.25µl IsceI buffer, 1µl meganuclease enzyme, 7.75µl H_2O, 2.5µl of DNA construct (100ng/µl). Transgenic fish were created using I-SceI meganuclease protocols described by (Thermes et. al, 2002). For gRNA injections, final concentrations of 15ng/µl of each gRNA approximately 200ng/µl mRNA xCas9 were used.

Genomic DNA extraction
Quick genomic DNA extraction was performed as previously described in (Hammouda et al.,2018). For Genomic DNA extraction from stage 42 embryos, body part was cut and placed into 50 microlitres of Fin clip buffer overnight at 60 degrees Celsius this was followed by addition of 200 microliters of water and heating to 95 degrees for 10 minutes which was followed by centrifugation for 10 minutes at maximum speed. The supernatant contained the gDNA and 2 microliters were usually sufficient for running a standard PCR.

Tamoxifen induction of Gaudi(N)SG
Cre Induction was performed as previously described in (Seleit et al., 2017b). Briefly, 5 mM tamoxifen solution was used overnight on stage 42 or earlier embryos, embryos were kept in the dark and recombination was checked the next day.

Image analysis and stitching
All Image analysis FIJI and ImageJ. Image stitching utilized 2D and 3D stitching plug-ins on ImageJ or using Photoshop to manually align images. All registration of imaging time-stamping manual tracking segmentation of cells and quantification of areas was done using standard FIJI plug-ins. Pseudocolouring of pigments and/or $eya1^+$ spinal cord neurons was achieved using Fiji software. All graphs were done on excel or R and all boxplots were done using PlotsOfData on R from Joachim G.

Live-imaging sample preparation
All live-imaging was done as previously described in (Seleit et al., 2017a, b). Briefly dechorionated embryos or hatchlings were anaesthetised in 1x Tricaine in 1x ERM and then mounted in 0.6% low melting agarose in 1xERM containing 1x Tricaine at 42°C on Matek dishes.

Oligonucleotide annealing
Primers were diluted to a working concentration of 10µM. 10µl of each diluted oligo was mixed with 20µl annealing buffer (10mM Tris, 30mM NaCl). Annealing conditions: 95°C for 5 minutes, ramp down to 70°C (0.1°C/sec), hold for 10min,

ramp down to 65°C, hold for 10min (0.1°C/sec), ramp down to 60°C (0.1°C/sec), hold for 10min, ramp down to 10°C (0.1°C/sec).

PCR

PCR conditions were used as described by the supplier of the reagents NEB. 10µl Q5 buffer, 4µl 10mM dNTPs and 0.5µl Q5-HF DNA polymerase. 1µl of 1-10ng/µl DNA and 2.5µl of 10µM forward and reverse primers + 29.5µl H_2O = final volume of 50µl. Conditions for each PCR vary according to parameters like primer length and GC content.

Plasmid generation (mini and midi preparations)

4 ml LB medium + antibiotic (100 µg/ml ampicillin, 50 µg/ml kanamycin) was inoculated grown 5–20 h at 37°C at 180rpm. 2ml of the bacterial culture centrifuged for 2 minutes then supernatant was removed. Resuspend pallet in in 250µl cold P1 buffer, 250µl P2 buffer added and tubes inverted 4-6 times. 250µl cold P3 buffer was added and tubes were inverting and centrifuged at 14,000rpm for 10 minutes. Add 600µl isopropanol and supernatant and vortex followed by centrifugation at maximum speed for 10 minutes. Isopropanol was removed and the DNA pellet washed in 400µl 70% ethanol in dH_2O and centrifuged at maximum speed for 5 minutes. Ethanol was removed and pellets dried at 37°C for 30 mins. DNA put in 30µl dH_2O. Big minis were done using the Qiagen kit instructions

Screening and imaging

All screening and imaging was done as previously described in detail in (Seleit et al., 2017a,b). This involved binocular, confocal and SPIM imaging. For the SPIM imaging the MuVi-SPIM (Krzic et al., 2012) with two illumination objectives (10x Nikon Plan Fluorite Objective, 0.30 NA) and two detection objectives (16X Nikon CFI LWD Plan Fluorite Objective, 0.80 NA) were used. Embryos were placed in glass capillaries using 0,6% low melting agarose. Embryo screening was performed using either the Olympus MVX10 macrofluorescence binocular or the Nikon AZ100 multizoom macrofluorescence binocular. Live-imaging was done using the confocal laser-scanning microscope Leica TCS SPE (40x oil objective) or Leica TCS SP5 II (10X dry, 40x dH_2O objectives). Samples were placed in the Microscope Slide Temperature Controller from Biotronix to control temperature. In-situ hybridization pictures were acquired by an Axio microscope connected to an HRC camera (Zeiss).

Two-photon laser ablations

A LaVision Biotec TriM Scope multi photon microscope on a Nikon Eclipse FN-1 upright microscope was used to ablate the lateral line primordium as previously described in (Seleit et al., 2017a). For cellular ablations of mantle cells the same set-up was used as described in (Seleit et al., 2017b). For cellular ablations of nBCs and vacuolated cells the multi-photon laser coupled to a Leica TCS SP5 II

microscope was used. Conditions varies depending on type and severity of injury in general I used 'point ablations' and used 880 nm wavelength with a laser power ranging from 25–50% for 250–850 ms.

Whole-mount antibody staining

Done as previously described in (Seleit et al., b) Embryos were anesthetised and fixed in 2ml 4% paraformaldehyde (PFA) in PBS +Tween (PTW). Fixed samples were then washed 5 X 5 minutes each in PTW. Then acetone for 10 mins at -20°C. Embryos were then washed for a number of times in dH_2O and PTW. Blocking solution: 1% PTW, 1% BSA, 100 µl DMSO and 4% natural goat serum NGS in 10 ml dH_2O. Samples were incubated 1 hour in blocking solution at RT on rotating wheel. First antibody (rabbit anti-GFP) with a dilution of 1:500. Incubate ON at 4°C with rotation. The samples were then rinsed with PTW, and then washed 6x in PTW. The secondary antibody (anti-rabbit 488 for example) and DAPI were then applied in block solution (1:500 dilution both). The mixture was incubated for 5 hours at RT on rotating wheel. The samples were then washed repeatedly with PTW.

Whole mount *in-situ hybridization*

Probe generation and in situ hybridisations were performed as previously reported (Stemmer et al., 2015a). Briefly, partial eya1, desmogon, cxcr4b, cxcr7 and cxcl12a cDNA clones were linearized to generate an anti-sense and sense probe. The fragments were purified with InnuprepPCRpure (Analytic Jena), and used in reactions with T7, SP6 (antisense) or T3 (sense) RNA polymerases and Dig-UTP. Hybridisations were performed overnight at 65°C and samples were incubated afterwards with an antibody against anti-digoxigenin conjugated with AP Fab fragments (1:2000; Roche, 11093274910). Staining was performed using NBT/BCIP (Roche) (Seleit et al., 2017 a, b).

Bioinformatics tools

The following bioinformatics tools were used ENSEMBL(www.ensembl.org), GENOMICUS (www.genomicus.biologie.ens.fr/). Uniprot (www.uniprot.org). UCSC (https://genome.ucsc.edu/). Pfam and PRINTS (https://pfam.xfam.org/) (http://130.88.97.239/PRINTS/index.php). Single cell transcriptomics data was visualized using (https://kleintools.hms.harvard.edu/paper_websites/wagner_zebrafish_timecourse2018/springViewer.html?coarse_grained_tree)

Electron microscopy on neuromast and notochord

For details on EM methodology followed for neuromasts (Seleit et al., 2017b). For EM on notochords, we received the following protocol from the EM facility at the Univeristy of Heidelberg: "10 dpf fish from Medaka wt Cab strain and stable Desmogon mutants were placed in a fixative consisting of 2.5% glutaraldehyde and 4% paraformaldehyde in 0.1M PHEM buffer. The fluorescing part of the notochord in mutant fish and equally small pieces of the wt fish was cut out in the fixative and fixation was continued for 30 min at room temperature and at 4° C overnight. The samples were further fixed in 1% osmium in 0.1M PHEM buffer, washed in water, and incubated in 1% uranylacetate in water overnight at 4° C. Dehydration was done in 10 min steps in an acetone gradient followed by stepwise Spurr resin infiltration at room temperature and polymerization at 60° C. The blocks were trimmed to get longitudinal sections of the notochord. 70nm thick sections were obtained using a leica UC6 ultramicrotome (Leica Microsystems, Vienna) and the sections were collected on Formvar-coated, copper slot grids and thereafter post-stained with uranyl acetate and Reynold's lead citrate. Imaging was done using a JEOL JEM-1400 electron microscope (JEOL, Tokyo) operating at 80 kV and equipped with a 4K TemCam F416 (Tietz Video and Image Processing Systems GmBH, Gautig)."

List of figures

List of Tables

References

Abdelhak, S., Kalatzis, V., Heilig, R., Compain, S., Samson, D., Vincent, C., et al. (1997). A human homologue of the Drosophila eyes absent gene underlies branchio-oto-renal (BOR) syndrome and identifies a novel gene family. Nature Genetics, 15(2), 157–164. http://doi.org/10.1038/ng0297-157

Agrawal, A. A. (2001). Phenotypic plasticity in the interactions and evolution of species. Science, 294(5541), 321–326. http://doi.org/10.1126/science.1060701

Ahmed, A. F., de Bock, C. E., Lincz, L. F., Pundavela, J., Zouikr, I., Sontag, E., et al. (2015). FAT1 cadherin acts upstream of Hippo signalling through TAZ to regulate neuronal differentiation. Cellular and Molecular Life Sciences : CMLS, 72(23), 4653–4669. http://doi.org/10.1007/s00018-015-1955-6

Aman, A., & Piotrowski, T. (2008). Wnt/β-Catenin and Fgf Signaling Control Collective Cell Migration by Restricting Chemokine Receptor Expression. Developmental Cell, 15(5), 749–761. http://doi.org/10.1016/j.devcel.2008.10.002

Andermann, P., Ungos, J., & Raible, D. W. (2002). Neurogenin1 defines zebrafish cranial sensory ganglia precursors. Developmental Biology, 251(1), 45–58.

Appert-Collin, A., Hubert, P., Crémel, G., & Bennasroune, A. (2015). Role of ErbB Receptors in Cancer Cell Migration and Invasion. Frontiers in Pharmacology, 6(17), 283. http://doi.org/10.3389/fphar.2015.00283

Bailey, A.P., Bhattacharyya, S., Bronner-Fraser, M., Streit, A., 2006. Lens specification is the ground state of all sensory placodes, from which FGF promotes olfactory identity. Dev. Cell 11, 505–517. doi:10.1016/j.devcel.2006.08.009

Bonini, N. M., Leiserson, W. M., & Benzer, S. (1993). The eyes absent gene: genetic control of cell survival and differentiation in the developing Drosophila eye. Cell, 72(3), 379–395.

Bose, A., Teh, M.-T., Mackenzie, I. C., & Waseem, A. (2013). Keratin k15 as a biomarker of epidermal stem cells. International Journal of Molecular Sciences, 14(10), 19385–19398. http://doi.org/10.3390/ijms141019385

Breau, M. A., Wilson, D., Wilkinson, D. G., & Xu, Q. (2012). Chemokine and Fgf signalling act as opposing guidance cues in formation of the lateral line primordium. Development, 139(12), 2246–2253. http://doi.org/10.1242/dev.080275

Boldajipour, B., Mahabaleshwar, H., Kardash, E., Reichman-Fried, M., Blaser, H., Minina, S., Wilson, D., Xu, Q.

and Raz, E. (2008). Control of chemokine-guided cell migration by ligand sequestration. Cell 132, 463–473.Centanin, L., & Wittbrodt, J. (2014). Retinal neurogenesis. Development, 141(2), 241–244. http://doi.org/10.1242/dev.083642

Centanin, L., Ander, J.-J., Hoeckendorf, B., Lust, K., Kellner, T., Kraemer, I., et al. (2014). Exclusive multipotency and preferential asymmetric divisions in post-embryonic neural stem cells of the fish retina. Development, 141(18), 3472–3482. http://doi.org/10.1242/dev.109892

Centanin, L., Hoeckendorf, B., Wittbrodt, J., 2011. Fate Restriction and Multipotency in Retinal Stem Cells. Cell Stem Cell 9, 553–562. doi:10.1016/j.stem.2011.11.004

Chamcheu, J. C., Siddiqui, I. A., Syed, D. N., Adhami, V. M., Liovic, M., & Mukhtar, H. (2011). Keratin gene mutations in disorders of human skin and its appendages. Archives of Biochemistry and Biophysics, 508(2), 123–137. http://doi.org/10.1016/j.abb.2010.12.019

Chitnis, A. B., Dalle Nogare, D., & Matsuda, M. (2012). Building the posterior lateral line system in zebrafish. Developmental Neurobiology, 72(3), 234–255. http://doi.org/10.1002/dneu.20962

Cruz, I.A., Kappedal, R., Mackenzie, S.M., Hailey, D.W., Hoffman, T.L., Schilling, T.F., Raible, D.W., 2015. Robust regeneration of adult zebrafish lateral line hair cells reflects continued precursor pool maintenance. Developmental Biology 402, 229–238. doi:10.1016/j.ydbio.2015.03.019

Cvekl, A., Ashery-Padan, R., 2014. The cellular and molecular mechanisms of vertebrate lens development. Development 141, 4432–4447. doi:10.1242/dev.107953

Cox, B.C., Chai, R., Lenoir, A., Liu, Z., Zhang, L., Nguyen, D.-H., Chalasani, K., Steigelman, K.A., Fang, J., Rubel, E.W., et al. (2014). Spontaneous hair cell regeneration in the neonatal mouse cochlea in vivo. Development 141, 816–829.

Collazo, A., Fraser, S. E. and Mabee, P. M. (1994). A dual embryonic origin for vertebrate mechanoreceptors. Science 264, 426–430.

Coombs, S., Bleckmann, H., Fay, R. R. and Popper, A. N. eds. (2014). The Lateral Line System. New York, NY: Springer New York.

Coombs, S., Janssen, J. and Webb, J. F. (1988). Diversity of Lateral Line Systems: Evolutionary and Functional Considerations. In Sensory Biology of Aquatic Animals, pp. 553–593. New York, NY: Springer New York.

Dambly-Chaudière, C., Cubedo, N. and Ghysen, A. (2007). Control of cell migration in the development of the posterior lateral line: antagonistic interactions between the chemokine receptors CXCR4 and CXCR7/RDC1. BMC Dev. Biol. 7, 23.

David, N. B., Sapède, D., Saint-Etienne, L., Thisse, C., Thisse, B., Dambly-Chaudière, C., Rosa, F. M. and Ghysen, A. (2002). Molecular basis of cell migration in the fish lateral line: role of the chemokine receptor CXCR4 and of its ligand, SDF1. Proc. Natl. Acad. Sci. U.S.A. 99, 16297–16302.

Doitsidou, M., Reichman-Fried, M., Stebler, J., Köprunner, M., Dörries, J., Meyer, D., Esguerra, C. V., Leung, T. and Raz, E. (2002). Guidance of primordial germ cell migration by the chemokine SDF-1. Cell 111, 647–659.

Dongre, A., & Weinberg, R. A. (2019). New insights into the mechanisms of epithelial-mesenchymal transition and implications for cancer. Nature Reviews Molecular Cell Biology, 20(2), 69–84. http://doi.org/10.1038/s41580-018-0080-4

Donà, E., Barry, J.D., Valentin, G., Quirin, C., Khmelinskii, A., Kunze, A., Durdu, S., Newton, L.R., Fernandez-Minan, A., Huber, W., Knop, M., Gilmour, D., 2013. Directional tissue migration through a self-generated chemokine gradient. Nature 503, 285–289. doi:10.1038/nature12635

Dufourcq, P., Roussigné, M., Blader, P., Rosa, F., Peyrieras, N., Vriz, S., 2006. Mechano-sensory organ regeneration in adults: the zebrafish lateral line as a model. Mol. Cell. Neurosci. 33, 180–187. doi:10.1016/j.mcn.2006.07.005

Dercum, F. (1880). The lateral sensory apparatus of fishes. Proceedings of the Academy of Natural Sciences of Philadelphia, 1879, pp. 152-154

Dijkgraaf, S. (1963). The functioning and significance of the lateral line organs. Biol Rev 38: 51-105.

El-Brolosy, M. A., Kontarakis, Z., Rossi, A., Kuenne, C., Gunther, S., Fukuda, N., et al. (2019). Genetic compensation triggered by mutant mRNA degradation. Nature, 568(7751), 193–197. http://doi.org/10.1038/s41586-019-1064-z

Friedl, P., & Gilmour, D. (2009). Collective cell migration in morphogenesis, regeneration and cancer. Nature Reviews Molecular Cell Biology, 10(7), 445–457. http://doi.org/10.1038/nrm2720

Furness, D.N. (2015). Molecular basis of hair cell loss. Cell Tissue Res. http:// dx.doi.org/10.1007/s00441-015-2113-z. Gee, H. Y., Sadowski, C. E., Aggarwal, P. K., Porath, J. D., Yakulov, T. A., Schueler, M., et al. (2016). FAT1 mutations cause a glomerulotubular nephropathy. Nature Communications, 7(1), 10822. http://doi.org/10.1038/ncomms10822

Fuchs, E., Tumbar, T., Guasch, G., 2004. Socializing with the neighbors: stem cells and their niche. Cell 116, 769–778.

Ghysen, A., & Dambly-Chaudiere, C. (2007). The lateral line microcosmos. Genes & Development, 21(17), 2118–2130. http://doi.org/10.1101/gad.1568407

Ghysen, A., & Dambly-Chaudière, C. (2016). Development vs. behavior: a role for neural adaptation in evolution? The International Journal of Developmental Biology, 60(4-5-6), 77–84. http://doi.org/10.1387/ijdb.160097ag

Ghysen, A., Dambly-Chaudière, C., Coves, D., la Gandara, de, F. and Ortega, A. (2012). Developmental origin of a major difference in sensory patterning between zebrafish and bluefin tuna. Evol Dev 14, 204–211.

Ghysen, A., Schuster, K., Coves, D., la Gandara, de, F., Papandroulakis, N. and Ortega, A. (2010). Development of the posterior lateral line system in Thunnus thynnus, the Atlantic blue-fin tuna, and in its close relative Sarda sarda. Int. J. Dev. Biol. 54, 1317–1322.

Gilmour, D. T., Maischein, H.-M., & Nüsslein-Volhard, C. (2002). Migration and function of a glial subtype in the vertebrate peripheral nervous system. Neuron, 34(4), 577–588.

Giroux, V., Lento, A. A., Islam, M., Pitarresi, J. R., Kharbanda, A., Hamilton, K. E., et al. (2017). Long-lived keratin 15+ esophageal progenitor cells contribute to homeostasis and regeneration. The Journal of Clinical Investigation, 127(6), 2378–2391. http://doi.org/10.1172/JCI88941

Giroux, V., Stephan, J., Chatterji, P., Rhoades, B., Wileyto, E. P., Klein-Szanto, A. J., et al. (2018). Mouse Intestinal Krt15+ Crypt Cells Are Radio-Resistant and Tumor Initiating. Stem Cell Reports, 10(6), 1947–1958. http://doi.org/10.1016/j.stemcr.2018.04.022

Grant, K. A., Raible, D. W., & Piotrowski, T. (2005). Regulation of Latent Sensory Hair Cell Precursors by Glia in the Zebrafish Lateral Line. Neuron, 45(1), 69–80. http://doi.org/10.1016/j.neuron.2004.12.020

Gunhaga, L., 2011. The lens: a classical model of embryonic induction providing new insights into cell determination in early development. Philos. Trans. R. Soc. Lond., B, Biol. Sci. 366, 1193–1203. doi:10.1098/rstb.2010.0175

Gudipaty, S. A., Lindblom, J., Loftus, P. D., Redd, M. J., Edes, K., Davey, C. F., et al. (2017). Mechanical stretch triggers rapid epithelial cell division through Piezo1. Nature, 543(7643), 118–121. http://doi.org/10.1038/nature21407

Haas, P., & Gilmour, D. (2006). Chemokine Signaling Mediates Self-Organizing Tissue Migration in the Zebrafish Lateral Line. Developmental Cell, 10(5), 673–680. http://doi.org/10.1016/j.devcel.2006.02.019

Hardy, K. M., Booth, B. W., Hendrix, M. J. C., Salomon, D. S., & Strizzi, L. (2010). ErbB/EGF signaling and EMT in mammary development and breast cancer. Journal of Mammary Gland Biology and Neoplasia, 15(2), 191–199. http://doi.org/10.1007/s10911-010-9172-2

Herpin, A., Fischer, P., Liedtke, D., Kluever, N., Neuner, C., Raz, E. and Schartl, M. (2008). Sequential SDF1a and b-induced mobility guides Medaka PGC migration. Developmental Biology 320, 319–327

Haines, R. L., & Lane, E. B. (2012). Keratins and disease at a glance. Journal of Cell Science, 125(Pt 17), 3923–3928. http://doi.org/10.1242/jcs.099655

Hernández, P.P., Olivari, F.A., Sarrazin, A.F., Sandoval, P.C., Allende, M.L., 2007. Regeneration in zebrafish lateral line neuromasts: expression of the neural progenitor cell marker sox2 and proliferation-dependent and-independent mechanisms of hair cell renewal. Devel Neurobio 67, 637–654. doi:10.1002/dneu.20386

Helmbacher, F. (2018). Tissue-specific activities of the Fat1 cadherin cooperate to control neuromuscular morphogenesis. PLOS Biology, 16(5), e2004734. http://doi.org/10.1371/journal.pbio.2004734

Ito, K., Morioka, M., Kimura, S., Tasaki, M., Inohaya, K., Kudo, A., 2014. Differential reparative phenotypes between zebrafish and medaka after cardiac injury. Dev. Dyn. 243, 1106–1115. doi:10.1002/dvdy.24154

Indjeian, V. B., Kingman, G. A., Jones, F. C., Guenther, C. A., Grimwood, J., Schmutz, J., Myers, R. M. and Kingsley, D. M. (2016). Evolving New Skeletal Traits by cis-Regulatory Changes in Bone Morphogenetic

Proteins. Cell 164, 45–56.

Ishikawa, Y. (1994). Innervation of lateral line system in the medaka, Oryzias latipes. The fish biology journal Medaka 6, 17–24.

Jessen, K. R., & Mirsky, R. (2005). The origin and development of glial cells in peripheral nerves. Nature Reviews. Neuroscience, 6(9), 671–682. http://doi.org/10.1038/nrn1746

Jemc, J., & Rebay, I. (2007). The eyes absent family of phosphotyrosine phosphatases: properties and roles in developmental regulation of transcription. Annual Review of Biochemistry, 76(1), 513–538. http://doi.org/10.1146/annurev.biochem.76.052705.164916

Jiménez-Delgado, S., Pascual-Anaya, J., & Garcia-Fernàndez, J. (2009). Implications of duplicated cis-regulatory elements in the evolution of metazoans: the DDI model or how simplicity begets novelty. Briefings in Functional Genomics & Proteomics, 8(4), 266–275. http://doi.org/10.1093/bfgp/elp029

Jones, J.E., Corwin, J.T., 1993. Replacement of lateral line sensory organs during tail regeneration in salamanders: identification of progenitor cells and analysis of leukocyte activity. J. Neurosci. 13, 1022–1034.

Knutsdottir, H., Zmurchok, C., Bhaskar, D., Palsson, E., Dalle Nogare, D., Chitnis, A. B., & Edelstein-Keshet, L. (2017). Polarization and migration in the zebrafish posterior lateral line system. PLoS Computational Biology, 13(4), e1005451. http://doi.org/10.1371/journal.pcbi.1005451

Kimmel, C. B., Ballard, W. W., Kimmel, S. R., Ullmann, B. and Schilling, T. F. (1995). Stages of embryonic development of the zebrafish. Dev. Dyn. 203, 253–310.

Knaut, H., Werz, C., Geisler, R., Nüsslein-Volhard, C.Tübingen 2000 Screen Consortium (2003). A zebrafish homologue of the chemokine receptor Cxcr4 is a germ-cell guidance receptor. Nature 421, 279–282.

Knutsdottir H, Zmurchok C, Bhaskar D, Palsson E, Dalle Nogare D, Chitnis AB, et al. (2017) Polarization and migration in the zebrafish posterior lateral line system. PLoS Comput Biol 13(4): e1005451. https://doi.org/10.1371/journal.pcbi.1005451

Kniss, J.S., Jiang, L., Piotrowski, T., 2016. Insights into sensory hair cell regeneration from the zebrafish lateral line. Curr. Opin. Genet. Dev. 40, 32–40. doi:10.1016/j.gde.2016.05.012

Krzic, U., Gunther, S., Saunders, T.E., Streichan, S.J., Hufnagel, L., 2012. Multiview light-sheet microscope for rapid in toto imaging. Nature Methods 9, 730–733. doi:10.1038/nmeth.2064

Kozlowski, D. J., Whitfield, T. T., Hukriede, N. A., Lam, W. K., & Weinberg, E. S. (2005). The zebrafish dog-eared mutation disrupts eya1, a gene required for cell survival and differentiation in the inner ear and lateral line. Developmental Biology, 277(1), 27–41. http://doi.org/10.1016/j.ydbio.2004.08.033

Lecaudey, V., Cakan-Akdogan, G., Norton, W. H. J., & Gilmour, D. (2008). Dynamic Fgf signaling couples morphogenesis and migration in the zebrafish lateral line primordium. Development, 135(16), 2695–2705. http://doi.org/10.1242/dev.025981

Ledent, V. (2002). Postembryonic development of the posterior lateral line in zebrafish. Development, 129(3), 597–604.

Lee, F. S. (1898). The functions of the ear and the lateral line in fishes. American Journal of Physiology, vol. 1, no. 1, pp. 128-144.

Liu, Y., Lyle, S., Yang, Z., & Cotsarelis, G. (2003). Keratin 15 promoter targets putative epithelial stem cells in the hair follicle bulge. The Journal of Investigative Dermatology, 121(5), 963–968. http://doi.org/10.1046/j.1523-1747.2003.12600.x

Liu, Y.-H., Jakobsen, J. S., Valentin, G., Amarantos, I., Gilmour, D. T., & Furlong, E. E. M. (2009). A systematic analysis of Tinman function reveals Eya and JAK-STAT signaling as essential regulators of muscle development. Developmental Cell, 16(2), 280–291. http://doi.org/10.1016/j.devcel.2009.01.006

López-Schier, H., Hudspeth, A.J., 2006. A two-step mechanism underlies the planar polarization of regenerating sensory hair cells. Proc. Natl. Acad. Sci. U.S.A. 103, 18615–18620. doi:10.1073/pnas.0608536103

López-Schier, H., Starr, C. J., Kappler, J. A., Kollmar, R. and Hudspeth, A. J. (2004). Directional cell migration establishes the axes of planar polarity in the posterior lateral-line organ of the zebrafish. Dev. Cell 7, 401–412.

Lopez-Schier, H. (2015). Developmental and architectural principles of the lateral-line neural map, 1–9. http://doi.org/10.3389/fncir.2013.00047/abstract

Lopez-Schier, H., & Hudspeth, A. J. (2005). Supernumerary neuromasts in the posterior lateral line of zebrafish lacking peripheral glia. Proceedings of the National Academy of Sciences, 102(5), 1496–1501. http://doi.org/10.1073/pnas.0409361102

Lozano-Ortega, M., Valera, G., Xiao, Y., Faucherre, A., & Lopez-Schier, H. (2018). Hair cell identity establishes labeled lines of directional mechanosensation. PLOS Biology, 16(7), e2004404. http://doi.org/10.1371/journal.pbio.2004404

Lush, M. E., & Piotrowski, T. (2014). ErbB expressing Schwann cells control lateral line progenitor cells via non-cell-autonomous regulation of Wnt/β-catenin. eLife, 3, 323–27. http://doi.org/10.7554/eLife.01832

Lush, M. E., Diaz, D. C., Koenecke, N., Baek, S., Boldt, H., St Peter, M. K., et al. (2019). scRNA-Seq reveals distinct stem cell populations that drive hair cell regeneration after loss of Fgf and Notch signaling. eLife, 8, 365. http://doi.org/10.7554/eLife.44431

Lust, K., Sinn, R., Pérez Saturnino, A., Centanin, Wittbrodt, J., 2016. De novo neurogenesis by targeted expression of atoh7 to Müller glia cells. 143, 1874–1883. doi:10.1242/dev.135905

Lust, K., & Wittbrodt, J. (2018). Activating the regenerative potential of Müller glia cells in a regeneration-deficient retina. eLife, 7, 7028. http://doi.org/10.7554/eLife.32319

Lyons DA, Talbot WS. Glial cell development and function in zebrafish. Cold Spring Harb Perspect Biol. ;7(2):a020586. Published . doi:10.1101/cshperspect.a020586

Lyons, D. A., Pogoda, H.-M., Voas, M. G., Woods, I. G., Diamond, B., Nix, R., et al. (2005). erbb3 and erbb2 are essential for schwann cell migration and myelination in zebrafish. Current Biology, 15(6), 513–524. http://doi.org/10.1016/j.cub.2005.02.030

Ma, E.Y., Rubel, E.W., Raible, D.W., 2008. Notch signaling regulates the extent of hair cell regeneration in the zebrafish lateral line. J. Neurosci. 28, 2261–2273. doi:10.1523/JNEUROSCI.4372-07.2008

Morrison, S.J., Spradling, A.C., 2008. Stem cells and niches: mechanisms that promote stem cell maintenance throughout life. Cell 132, 598–611. doi:10.1016/j.cell.2008.01.038

Mills, K. M., Szczerkowski, J. L. A., & Habib, S. J. (2017). Wnt ligand presentation and reception: from the stem cell niche to tissue engineering. Open Biology, 7(8), 170140. http://doi.org/10.1098/rsob.170140

Moeller, M. J., Soofi, A., Braun, G. S., Li, X., Watzl, C., Kriz, W., & Holzman, L. B. (2004). Protocadherin FAT1 binds Ena/VASP proteins and is necessary for actin dynamics and cell polarization. The EMBO Journal, 23(19), 3769–3779. http://doi.org/10.1038/sj.emboj.7600380

Moriyama, Y., Kawanishi, T., Nakamura, R., Tsukahara, T., Sumiyama, K., Suster, M. L., et al. (2012). The medaka zic1/zic4 mutant provides molecular insights into teleost caudal fin evolution. Current Biology : CB, 22(7), 601–607.

Meyers, J. R. (2018). Zebrafish: Development of a vertebrate model organism.Current Protocols Essential Laboratory Techniques e19http://doi.org/10.1016/j.cub.2012.01.063

McGraw, H. F., Culbertson, M. D. and Nechiporuk, A. V. (2014). Kremen1 restricts Dkk activity during posterior lateral line development in zebrafish. 141, 3212–3221.

Nechiporuk, A. and Raible, D. W. (2008). FGF-dependent mechanosensory organ patterning in zebrafish. Science 320, 1774–1777

Nabhan, A. N., Brownfield, D. G., Harbury, P. B., Krasnow, M. A., & Desai, T. J. (2018). Single-cell Wnt signaling niches maintain stemness of alveolar type 2 cells. Science, 359(6380), 1118–1123. http://doi.org/10.1126/science.aam6603

Nikaido, M., Navajas Acedo, J., Hatta, K., & Piotrowski, T. (2017). Retinoic acid is required and Fgf, Wnt, and Bmp signaling inhibit posterior lateral line placode induction in zebrafish. Developmental Biology, 431(2), 215–225. http://doi.org/10.1016/j.ydbio.2017.09.017

Nuñez, V. A., Sarrazin, A. F., Cubedo, N., Allende, M. L., Dambly-Chaudière, C., & Ghysen, A. (2009). Postembryonic development of the posterior lateral line in the zebrafish. Evolution & Development, 11(4), 391–404. http://doi.org/10.1111/j.1525-142X.2009.00346.x

Nicolson, T. (2005). The genetics of hearing and balance in zebrafish. Annu. Rev. Genet. 39, 9–22.

Nelson, J. (2006). Fishes of the World, Fourth Edition (New York: Wiley).

Nystul, T.G., Spradling, A.C., 2006. Breaking out of the mold: diversity within adult stem cells and their niches. Curr. Opin. Genet. Dev. 16, 463–468. doi:10.1016/j.gde.2006.08.003

Ouspenskaia, T., Matos, I., Mertz, A.F., Fiore, V.F., Fuchs, E., 2016. WNT-SHH Antagonism Specifies and Expands Stem Cells prior to Niche Formation. Cell 164, 156–169. doi:10.1016/j.cell.2015.11.058

O'Brown, N. M., Summers, B. R., Jones, F. C., Brady, S. D. and Kingsley, D. M. (2015). A recurrent regulatory change underlying altered expression and Wnt response of the stickleback armor plates gene EDA. Elife 4, e05290.

Ohtsuka, M., Kikuchi, N., Yokoi, H., Kinoshita, M., Wakamatsu, Y., Ozato, K., et al. (2004). Possible roles of zic1 and zic4, identified within the medaka Double anal fin (Da) locus, in dorsoventral patterning of the trunk-tail region (related to phenotypes of the Da mutant). Mechanisms of Development, 121(7-8), 873–882. http://doi.org/10.1016/j.mod.2004.04.006

Owens, K. N., Cunningham, D. E., MacDonald, G., Rubel, E. W., Raible, D. W., & Pujol, R. (2007). Ultrastructural analysis of aminoglycoside-induced hair cell death in the zebrafish lateral line reveals an early mitochondrial response. The Journal of Comparative Neurology, 502(4), 522–543. http://doi.org/10.1002/cne.21345

Parker G. H. (1905) The function of the lateral-line organs in Fishes. February 18, 1905 DEPARTMENT OF COMMERCE AND LABOR BUREAU OF FISHERIES Extracted from BULLETIN OF THE BUREAU OF FISHERIES for 1904,Vol, XHV. Pages 183 to 207

Peters, B., Kirfel, J., Büssow, H., Vidal, M., & Magin, T. M. (2001). Complete cytolysis and neonatal lethality in keratin 5 knockout mice reveal its fundamental role in skin integrity and in epidermolysis bullosa simplex. Molecular Biology of the Cell, 12(6), 1775–1789. http://doi.org/10.1091/mbc.12.6.1775

Piotrowski, T., & Baker, C. V. H. (2014). The development of lateral line placodes_ Taking a broader view. Developmental Biology, 389(1), 68–81. http://doi.org/10.1016/j.ydbio.2014.02.016

Preston, J. C., Hileman, L. C., & Cubas, P. (2011). Reduce, reuse, and recycle: developmental evolution of trait diversification. American Journal of Botany, 98(3), 397–403. http://doi.org/10.3732/ajb.1000279

Prud'homme, B., Gompel, N., Rokas, A., Kassner, V. A., Williams, T. M., Yeh, S.-D., et al. (2006). Repeated morphological evolution through cis-regulatory changes in a pleiotropic gene. Nature, 440(7087), 1050–1053. http://doi.org/10.1038/nature04597

Pinto-Teixeira, F., Viader-Llargués, O., Torres-Mejía, E., Turan, M., González-Gualda, E., Pola-Morell, L., López-Schier, H., 2015. Inexhaustible hair-cell regeneration in young and aged zebrafish. Biol Open 4, 903–909. doi:10.1242/bio.012112

Pichon, F. and Ghysen, A. (2004). Evolution of posterior lateral line development in fish and amphibians. Evol Dev 6, 187–193.

Raible, D. W., & Kruse, G. J. (2000). Organization of the lateral line system in embryonic zebrafish. The Journal of Comparative Neurology, 421(2), 189–198.

Rembold, M., Lahiri, K., Foulkes, N.S., Wittbrodt, J., 2006. Transgenesis in fish: efficient selection of transgenic fish by co-injection with a fluorescent reporter construct. Nat Protoc 1, 1133–1139. doi:10.1038/nprot.2006.165

Romero-Carvajal, A., Navajas Acedo, J., Jiang, L., Kozlovskaja-Gumbrienė, A., Alexander, R., Li, H., Piotrowski, T., 2015. Regeneration of Sensory Hair Cells Requires Localized Interactions between the Notch and Wnt Pathways. Dev. Cell 34, 267–282. doi:10.1016/j.devcel.2015.05.025

Rebay, I. (2015). Multiple Functions of the Eya Phosphotyrosine Phosphatase. Molecular and Cellular Biology, 36(5), 668–677. http://doi.org/10.1128/MCB.00976-15

Rebeiz, M., & Tsiantis, M. (2017). Enhancer evolution and the origins of morphological novelty. Current Opinion in Genetics & Development, 45, 115–123. http://doi.org/10.1016/j.gde.2017.04.006

Rebeiz, M., Jikomes, N., Kassner, V. A., & Carroll, S. B. (2011). Evolutionary origin of a novel gene expression pattern through co-option of the latent activities of existing regulatory sequences. Proceedings of the National Academy of Sciences of the United States of America, 108(25), 10036–10043. http://doi.org/10.1073/pnas.1105937108

Sapède, D., Gompel, N., Dambly-Chaudière, C. and Ghysen, A. (2002). Cell migration in the postembryonic development of the fish lateral line. Development 605–615.

Sasado, T., Yasuoka, A., Abe, K., Mitani, H., Furutani-Seiki, M., Tanaka, M. and Kondoh, H. (2008). Distinct contributions of CXCR4b and CXCR7/RDC1 receptor systems in regulation of PGC migration revealed by medaka mutants kazura and yanagi. Developmental Biology 320, 328–339.

Sánchez, M., Ceci, M. L., Gutiérrez, D., Anguita-Salinas, C. and Allende, M. L. (2016). Mechanosensory organ regeneration in zebrafish depends on a population of multipotent progenitor cells kept latent by Schwann cells. BMC Biol. 14, 27.

Santos, A.C., Lehmann, R., 2004. Germ cell specification and migration in Drosophila and beyond. Curr. Biol. 14, R578–89. doi:10.1016/j.cub.2004.07.018

Scadden, D.T., 2014. Nice neighborhood: emerging concepts of the stem cell niche. Cell 157, 41–50.

doi:10.1016/j.cell.2014.02.013

Schartl, M., Walter, R.B., Shen, Y., Garcia, T., Catchen, J., Amores, A., Braasch, I., Chalopin, D., Volff, J.-N., Lesch, K.-P., Bisazza, A., Minx, P., Hillier, L., Wilson, R.K., Fuerstenberg, S., Boore, J., Searle, S., Postlethwait, J.H., Warren, W.C., 2013. The genome of the platyfish, Xiphophorus maculatus, provides insights into evolutionary adaptation and several complex traits. Nat. Genet. 45, 567–572. doi:10.1038/ng.2604

Seleit, A., Krämer, I., Ambrosio, E., Dross, N., Engel, U., Centanin, 2017. Sequential organogenesis sets two parallel sensory lines in medaka dev.142752. doi:10.1242/dev.142752

Seleit, A., Gross, K., Woelk, M., Autorino, C., & Centanin, L. (2019). The desmosomal cadherin Desmogon is necessary for the structural integrity of the Medaka notochord. bioRxiv, 620070.

Seleit, A., Krämer, I., Riebesehl, B. F., Ambrosio, E. M., Stolper, J. S., Lischik, C. Q., et al. (2017). Neural stem cells induce the formation of their physical niche during organogenesis. eLife, 6, 505. http://doi.org/10.7554/eLife.29173

Schofield, R., 1978. The relationship between the spleen colony-forming cell and the haemopoietic stem cell. Blood Cells 4, 7–25.

Steiner, A.B., Kim, T., Cabot, V., Hudspeth, A.J., 2014. Dynamic gene expression by putative hair-cell progenitors during regeneration in the zebrafish lateral line. Proceedings of the National Academy of Sciences 111, E1393–401. doi:10.1073/pnas.1318692111

Stemmer, M., Schuhmacher, L.-N., Foulkes, N.S., Bertolucci, C., Wittbrodt, J., 2015. Cavefish eye loss in response to an early block in retinal differentiation progression. 142, 743–752. doi:10.1242/dev.114629

Stemmer, M., Thumberger, T., Del Sol Keyer, M., Wittbrodt, J. and Mateo, J. L. (2015b). CCTop: An Intuitive, Flexible and Reliable CRISPR/Cas9 Target Prediction Tool. PLOS ONE 10, e0124633.

Stone, L.S., 1933. The development of lateral-line sense organs in amphibians observed in living and vital-stained preparations. J. Comp. Neurol. 57, 507–540. doi:10.1002/cne.900570307

Streisinger, G., Walker, C., Dower, N., Knauber, D., & Singer, F. (1981). Production of clones of homozygous diploid zebra fish (Brachydanio rerio). Nature, 291, 293–296.

Sopko, R., & McNeill, H. (2009). The skinny on Fat: an enormous cadherin that regulates cell adhesion, tissue growth, and planar cell polarity. Current Opinion in Cell Biology, 21(5), 717–723. http://doi.org/10.1016/j.ceb.2009.07.001

Steiner, A. B., Kim, T., Cabot, V., & Hudspeth, A. J. (2014). Dynamic gene expression by putative hair-cell progenitors during regeneration in the zebrafish lateral line. Proceedings of the National Academy of Sciences, 111(14), E1393–E1401. http://doi.org/10.1073/pnas.1318692111

Tanoue, T., & Takeichi, M. (2004). Mammalian Fat1 cadherin regulates actin dynamics and cell-cell contact. The Journal of Cell Biology, 165(4), 517–528. http://doi.org/10.1083/jcb.200403006

Tamplin, O.J., Durand, E.M., Carr, L.A., Childs, S.J., Hagedorn, E.J., Li, P., Yzaguirre, A.D., Speck, N.A., Zon, L.I., 2015. Hematopoietic stem cell arrival triggers dynamic remodeling of the perivascular niche. Cell 160, 241–252. doi:10.1016/j.cell.2014.12.032

Tulina, N., Matunis, E., 2001. Control of stem cell self-renewal in Drosophila spermatogenesis by JAK-STAT signaling. Science 294, 2546–2549. doi:10.1126/science.1066700

Thermes, V., Grabher, C., Ristoratore, F., Bourrat, F., Choulika, A., Wittbrodt, J. and Joly, J.-S. (2002). I-SceI meganuclease mediates highly efficient transgenesis in fish. Mechanisms of Development 118, 91–98.

Tsingos, E., Höckendorf, B., Sütterlin, T., Kirchmaier, S., Grabe, N., Centanin, L., & Wittbrodt, J. (2019). Retinal stem cells modulate proliferative parameters to coordinate post-embryonic morphogenesis in the eye of fish. eLife, 8, 3470. http://doi.org/10.7554/eLife.42646

Urbansky, S., González Avalos, P., Wosch, M. and Lemke, S. (2016). Folded gastrulation and T48 drive the evolution of coordinated mesoderm internalization in flies. Elife 5, e18318.

Valentin, G., Haas, P. and Gilmour, D. (2007). The chemokine SDF1a coordinates tissue migration through the spatially restricted activation of Cxcr7 and Cxcr4b. Curr. Biol. 17, 1026–1031.

Venkiteswaran, G., Lewellis, S. W., Wang, J., Reynolds, E., Nicholson, C. and Knaut, H. (2013). Generation and dynamics of an endogenous, self-generated signaling gradient across a migrating tissue. Cell 155, 674–687.

Van Keymeulen, A., Rocha, A.S., Ousset, M., Beck, B., Bouvencourt, G., Rock, J., Sharma, N., Dekoninck, S., Blanpain, C., 2011. Distinct stem cells contribute to mammary gland development and maintenance.

Nature 479, 189–193. doi:10.1038/nature10573
Wada, H., Ghysen, A., Satou, C., Higashijima, S.-I., Kawakami, K., Hamaguchi, S. and Sakaizumi, M. (2010). Dermal morphogenesis controls lateral line patterning during postembryonic development of teleost fish. Developmental Biology 340, 583–594.

Wada, H., Dambly-Chaudière, C., Kawakami, K., & Ghysen, A. (2013a). Innervation is required for sense organ development in the lateral line system of adult zebrafish. Proceedings of the National Academy of Sciences of the United States of America, 110(14), 5659–5664. http://doi.org/10.1073/pnas.1214004110
Wada, H., Ghysen, A., Asakawa, K., Abe, G., Ishitani, T., & Kawakami, K. (2013b). Wnt/Dkk Negative Feedback Regulates Sensory Organ Size in Zebrafish. Current Biology, 23(16), 1559–1565. http://doi.org/10.1016/j.cub.2013.06.035
Wada, H., Hamaguchi, S., & Sakaizumi, M. (2008). Development of diverse lateral line patterns on the teleost caudal fin. Developmental Dynamics, 237(10), 2889–2902. http://doi.org/10.1002/dvdy.21710
Waddington, CH 1941, Evolution of developmental systems. 1941. Nature

Waddington, CH 1942, Canalization of development and the inheritance acquired characters. 1942. Nature

Waddington, CH 1968, Towards a theoretical biology. 1968. Nature

Waddington CH, Towards a Theoretical Biology, Vol. 1, Prolegomena, International Union of Biological Sciences & Edinburgh University Press, 1968, pp. 1–32.

Waddington CH, Towards a Theoretical Biology, Vol. 2, Sketches, International Union of Biological Sciences & Edinburgh University Press, 1969, pp. 106–123.

Whitfield, T. T. (2005). Lateral Line: Precocious Phenotypes and Planar Polarity. Current Biology, 15(2), R67–R70. http://doi.org/10.1016/j.cub.2004.12.059
Whitfield, T.T. (2002). Zebrafish as a model for hearing and deafness. J. Neurobiol. 53, 157–171.

Wittbrodt, J., Shima, A. and Schartl, M. (2002). Medaka--a model organism from the far East. Nat. Rev. Genet. 3, 53–64.

Wibowo, I., Pinto-Teixeira, F., Satou, C., Higashijima, S.-I., López-Schier, H., 2011. Compartmentalized Notch signaling sustains epithelial mirror symmetry. 138, 1143–1152. doi:10.1242/dev.060566

Williams, J.A., Holder, N., 2000. Cell turnover in neuromasts of zebrafish larvae. Hear. Res. 143, 171–181.

Xie, T., Spradling, A.C., 1998. decapentaplegic is essential for the maintenance and division of germline stem cells in the Drosophila ovary. Cell 94, 251–260.
Xu, P. X., Cheng, J., Epstein, J. A., & Maas, R. L. (1997). Mouse Eya genes are expressed during limb tendon development and encode a transcriptional activation function. Proceedings of the National Academy of Sciences, 94(22), 11974–11979. http://doi.org/10.1073/pnas.94.22.11974

Yasuoka, A., Hirose, Y., Yoda, H., Aihara, Y., Suwa, H., Niwa, K., Sasado, T., Morinaga, C., Deguchi, T., Henrich, T., et al. (2004). Mutations affecting the formation of posterior lateral line system in Medaka, Oryzias latipes. Mechanisms of Development 121, 729–738.

Specific references for *desmogon*

Adams, D.S. & Keller, R.E., Koehl, M.A.R 1990. Mechanical Development of the Notochord in Xenopus Early Tail-Bud Embryos. In Biomechanics of Active Movement and Deformation of Cells. Berlin, Heidelberg: Springer Berlin Heidelberg, pp. 471–485.

Briggs, J.A. et al., 2018. The dynamics of gene expression in vertebrate embryogenesis at single-cell resolution. Science, 360(6392), pp.eaar5780–17.

Corallo, D., Trapani, V. & Bonaldo, P., 2018. The notochord: structure and functions. Cellular and Molecular Life Sciences, pp.1–20.

Dale, R.M. & Topczewski, J., 2011. Identification of an evolutionarily conserved regulatory element of the zebrafish col2a1a gene. Developmental Biology, 357(2), pp.518–531.

Delva, E., Tucker, D.K. & Kowalczyk, A.P., 2009. The desmosome. Cold Spring Harbor Perspectives in Biology, 1(2), pp.a002543–a002543.

Ellis, K., Bagwell, J. & Bagnat, M., 2013. Notochord vacuoles are lysosome-related organelles that function in axis and spine morphogenesis. The Journal of Cell Biology, 200(5), pp.667–679.

Ellis, K., Hoffman, B.D. & Bagnat, M., 2014. The vacuole within. BioArchitecture, 3(3), pp.64–68.

Farrell, J.A. et al., 2018. Single-cell reconstruction of developmental trajectories during zebrafish embryogenesis. Science, 360(6392), pp.eaar3131–15.

Fleming, A., 2004. A central role for the notochord in vertebral patterning. Development, 131(4), pp.873–880.

Fouquet, B. et al., 1997. Vessel Patterning in the Embryo of the Zebrafish: Guidance by Notochord. Developmental Biology, 183(1), pp.37–48.

Garcia, J. et al., 2017. Sheath Cell Invasion and Trans-differentiation Repair Mechanical Damage Caused by Loss of Caveolae in the Zebrafish Notochord. Current Biology, 27(13), pp.1982–1989.e3.

Garrod, D. & Chidgey, M., 2008a. Desmosome structure, composition and function. Biochimica et Biophysica Acta (BBA) - Biomembranes, 1778(3), pp.572–587.

Garrod, D. & Chidgey, M., 2008b. Desmosome structure, composition and function. Biochimica et Biophysica Acta (BBA) - Biomembranes, 1778(3), pp.572–587.

Goonesinghe, A. et al., 2012. Desmosomal cadherins in zebrafish epiboly and gastrulation. BMC Developmental Biology, 12(1), p.1.

Gray, R.S. et al., 2014. Loss of col8a1a function during zebrafish embryogenesis results in congenital vertebral malformations. Developmental Biology, 386(1), pp.72–85.

Hebrok, M., Kim, S.K. & Melton, D.A., 1998. Notochord repression of endodermal Sonic hedgehog permits pancreas development. Genes & Development, 12(11), pp.1705–1713.

Ito, K. et al., 2014. Differential reparative phenotypes between zebrafish and medaka after cardiac injury. Developmental Dynamics, 243(9), pp.1106–1115.

Jiang, D. & Smith, W.C., 2007. Ascidian notochord morphogenesis. Developmental Dynamics, 236(7), pp.1748–1757.

Kaloulis, K. et al., 2004. Reactivation of developmental programs: the cAMP-response element-binding protein pathway is involved in hydra head regeneration. Proceedings of the National Academy of Sciences, 101(8), pp.2363–2368.

Kang, J. et al., 2016. Modulation of tissue repair by regeneration enhancer elements. Nature, 532(7598), pp.201–206.

Katogi, R. et al., 2004. Large-scale analysis of the genes involved in fin regeneration and blastema formation in the medaka, Oryzias latipes. Mechanisms of Development, 121(7-8), pp.861–872.

Koehl, M.A.R., Quillin, K.J. & Pell, C.A., 2000. Mechanical Design of Fiber-Wound Hydraulic Skeletons: The Stiffening and Straightening of Embryonic Notochords. American Zoologist, 40(1), pp.28–041.

Krzic, U., Gunther, S., Saunders, T.E., Streichan, S.J. & Hufnagel, L., 2012a. Multiview light-sheet microscope for rapid in toto imaging. Nature methods, 9(7), pp.730–733.

Krzic, U., Gunther, S., Saunders, T.E., Streichan, S.J. & Hufnagel, L., 2012b. Multiview light-sheet microscope for rapid in toto imaging. Nature methods, 9(7), pp.730–733.

Lai, S.-L. et al., 2017. Reciprocal analyses in zebrafish and medaka reveal that harnessing the immune response promotes cardiac regeneration. eLife, 6, p.1382.

Lim, Y.-W. et al., 2017. Caveolae Protect Notochord Cells against Catastrophic Mechanical Failure during Development. Current Biology, 27(13), pp.1968–1981.e7.

Lischik, C.Q., Adelmann, L. & Wittbrodt, J., 2018. Enhanced in vivo-imaging in fish by optimized anaesthesia, fluorescent protein selection and removal of pigmentation.

Lleras Forero, L. et al., 2018. Segmentation of the zebrafish axial skeleton relies on notochord sheath cells and not on the segmentation clock. eLife, 7, p.15.

LoCascio, S.A., Lapan, S.W. & Reddien, P.W., 2017. Eye Absence Does Not Regulate Planarian Stem Cells during Eye Regeneration. Developmental Cell, 40(4), pp.381–391.e3.

Lopez-Baez, J.C. et al., 2018. Wilms Tumor 1b defines a wound-specific sheath cell subpopulation associated with notochord repair. eLife, 7, p.239.

Lust, K. & Wittbrodt, J., 2018. Activating the regenerative potential of Müller glia cells in a regeneration-deficient retina. eLife, 7, p.7028.

Melby, A.E., Warga, R.M. & Kimmel, C.B., 1996. Specification of cell fates at the dorsal margin of the zebrafish gastrula. Development, 122(7), pp.2225–2237.

Nixon, S.J. et al., 2007. Caveolin-1 is required for lateral line neuromast and notochord development. Journal of Cell Science, 120(13), pp.2151–2161.

Pourquie, O. et al., 1993. Control of dorsoventral patterning of somitic derivatives by notochord and floor plate. Proceedings of the National Academy of Sciences, 90(11), pp.5242–5246.

Rembold, M. et al., 2006. Transgenesis in fish: efficient selection of transgenic fish by co-injection with a fluorescent reporter construct. Nature protocols, 1(3), pp.1133–1139.

Rodrigo Albors, A. et al., 2015. Planar cell polarity-mediated induction of neural stem cell expansion during axolotl spinal cord regeneration. eLife, 4, p.664.

Satoh, N., Tagawa, K. & Takahashi, H., 2012. How was the notochord born? Evolution & Development, 14(1), pp.56–75.

Seleit, A., Krämer, I., Ambrosio, E., et al., 2017. Sequential organogenesis sets two parallel sensory lines in medaka. Development, 144(4), pp.687–697.

Seleit, A., Krämer, I., Riebesehl, B.F., et al., 2017. Neural stem cells induce the formation of their physical niche during organogenesis. eLife, 6, p.505.

Stemmer, M., Schuhmacher, L.N., et al., 2015. Cavefish eye loss in response to an early block in retinal differentiation progression. Development, 142(4), pp.743–752.

Stemmer, M., Thumberger, T., et al., 2015. CCTop: An Intuitive, Flexible and Reliable CRISPR/Cas9 Target Prediction Tool. S. Maas, ed. PloS one, 10(4), p.e0124633.

Stemple, D.L., 2005. Structure and function of the notochord: an essential organ for chordate development. Development, 132(11), pp.2503–2512.

Stemple, D.L., 2004. The notochord. Current Biology, 14(20), pp.R873–R874.

Stemple, D.L. et al., 1996. Mutations affecting development of the notochord in zebrafish. Development, 123, pp.117–128.

Stoeger, T. et al., 2018. Large-scale investigation of the reasons why potentially important genes are ignored. T. Freeman, ed. PLOS Biology, 16(9), p.e2006643.

Tada, M. & Heisenberg, C.P., 2012. Convergent extension: using collective cell migration and cell intercalation to shape embryos. Development, 139(21), pp.3897–3904.

Talbot, W.S. et al., 1995. A homeobox gene essential for zebrafish notochord development. Nature, 378(6553), pp.150–157.

Tanaka, E. & Galliot, B., 2009. Triggering the regeneration and tissue repair programs. In Development (Cambridge, England). pp. 349–353.

Trubiroha, A. et al., 2018. A Rapid CRISPR/Cas-based Mutagenesis Assay in Zebrafish for Identification of Genes Involved in Thyroid Morphogenesis and Function. Scientific Reports, pp.1–19.

Van Wettere, A.J. et al., 2013. Immunohistochemical characterization of the hepatic progenitor cell compartment in medaka (Oryzias latipes) following hepatic injury. Journal of comparative pathology, 149(4), pp.434–445.

Wopat, S. et al., 2018. Spine Patterning Is Guided by Segmentation of the Notochord Sheath. CellReports, 22(8), pp.2026–2038.

Wu, R.S. et al., 2018. A Rapid Method for Directed Gene Knockout for Screening in G0 Zebrafish. Developmental Cell, 46(1), pp.112–125.e4.

Yamada, T. et al., 1991. Control of cell pattern in the developing nervous system: Polarizing activity of the floor plate and notochord. CELL, 64(3), pp.635–647.

Yamada, T. et al., 1993. Control of cell pattern in the neural tube: Motor neuron induction by diffusible factors from notochord and floor plate. CELL, 73(4), pp.673–686.

Yamamoto, M. et al., 2010. Mib-Jag1-Notch signalling regulates patterning and structural roles of the notochord by controlling cell-fate decisions. Development, 137(15), pp.2527–2537

Publications

The desmosomal cadherin Desmogon is necessary for the structural integrity of the Medaka notochord. Seleit, A., Gross, K., Woelk, M., Autorino, C., & Centanin, L. (2019). bioRxiv, 620070

Neural stem cells induce the formation of their physical niche during organogenesis. (2017) Seleit A, Krämer I, Riebesehl BF, Ambrosio EM, Stolper JS, Lischik CQ, Dross N, Centanin L Elife, doi: 10.7554/eLife.29173

Sequential organogenesis sets two parallel sensory lines in medaka. (2017) Seleit A, Krämer I, Ambrosio E, Dross N, Engel U, Centanin L Development, doi:10.1242/dev.142752

Acknowledgments

This work is dedicated to Omar El Shazly & Khaled Ghalab. I would like to thank my family for their constant support and sacrifices that made this possible Khalda & Mohsen I am eternally grateful for your love and selflessness. Ismail & Lamia, Hassan & Farida thank you for always being there and for the great memories whenever we meet. My extended family in Egypt (and all over the world now) I miss you all so much I hope we meet soon. I would like to thank my boss Lazaro for his belief in me and the freedom I was given to pursue my interests (I hope it paid off). Jochen for always being a larger than life character and a mentor, your impact on me (and many others) cannot be overstated. Baubi and Virginie for their constant encouragement and positivity and advice over the years. I would like to thank Isa, Liz and Maria for their friendship and a wonderful and extremely enjoyable environment in and out of the lab (and the great costumes always), I will never forget these memories. Julian for all the fun and for his wit, for always being on the same level and for his priceless friendship and advice. Omnya for endless Soban dinners and talks and for being through it all. Anne-Laure for her care craziness and honesty. Karen for her kindness and for making this last year as fun and as enjoyable and for all her help throughout the process. Cami for her big heart and authenticity. Omar, Shaymaa and Sherif for always always being there. Frederike for help with navigating German bureaucracy and visa bullshit. All the people on the 5th floor and in COS for a great time and spirit. Teju Cole for the playlists that inspired the writing of this work. Abdo for some crazy nights, Roshdi for Berlin, Sameih for the road-trips and bad luck, Brolosy for his friendship and intellect, Hussein and the Bob for their timeless friendship, Boro2 for financial wizardry and deep intellectual conversations, Badr for his positivity, actually the entire swimming team all over the world now for all the memories. And Esther, for adding so much colour in such a short time.